VOL. 107 NO. HY7. JULY 1981

JOURNAL OF THE HYDRAULICS DIVISION

PROCEEDINGS OF
THE AMERICAN SOCIETY
OF CIVIL ENGINEERS

VOL. 107 NO. HY7. JULY 1981

JOURNAL OF THE HYDRAULICS DIVISION

PROCEEDINGS OF
THE AMERICAN SOCIETY
OF CIVIL ENGINEERS

ISSN 0044-796X

Melvin W. Anderson, Editor
University of South Florida

AMERICAN SOCIETY OF CIVIL ENGINEERS

CONTENTS

The Journal of the Hydraulics Division (ISSN 0044-796X) is published monthly by the American Society of Civil Engineers. Publications office is at 345 East 47th Street, New York, N.Y. 10017. Address all ASCE correspondence to the Editorial and General Offices at 345 East 47th Street, New York, N.Y. 10017. Allow six weeks for change of address to become effective. Subscription price to members is $16.50. Nonmember subscriptions available; prices obtainable on request. Second-class postage paid at New York, N.Y. and at additional mailing offices. HY.

POSTMASTER: Send address changes to American Society of Civil Engineers, 345 East 47th Street, New York, NY 10017.

DISCUSSION

Proc. Paper 16357

---

*Discussion period closed for this paper. Any other discussion received during this discussion period will be published in subsequent Journals.

INFORMATION RETRIEVAL

The key words, abstract, and reference "cards" for each article in this Journal represent part of the ASCE participation in the EJC information retrieval plan. The retrieval data are placed herein so that each can be cut out, placed on a 3 × 5 card and given an accession number for the user's file. The accession number is then entered on key word cards so that the user can subsequently match key words to choose the articles he wishes. Details of this program were given in an August, 1962 article in CIVIL ENGINEERING, reprints of which are available on request to ASCE headquarters.

*Discussion period closed for this paper. Any other discussion received during this discussion period will be published in subsequent Journals.

16380 RELIABILITY AND HYDRAULIC ENGINEERING

KEY WORDS: Earthwork; Failure; **Hydraulic design; Hydraulic engineering; Hydraulic structures;** Hydrology; Levee failures; **Levees; Probability theory; Reliability;** Simulation; Uncertainty principle

ABSTRACT: The reliability of two hydraulic engineering systems with random resistance and/or loading is estimated. The first system is a flood levee reach that is subject to four failure modes: overtopping, boiling, slope sliding and wind wave erosion. The second system is a flood levee system along a confluence reach. For this levee, failure by overtopping depends on the bivariate distribution of water stages in the tributary and the main river, linked by a backwater curve. The failure probability, which is the complement of reliability, is estimated analytically for the first system, and then by hydraulic calculations and simulation for the second system. In each case, estimated reliabilities agree well with experimental observations.

REFERENCE: Duckstein, Lucien (Prof., Dept. of Systems and Industrial Engrg., Univ. of Arizona, Tucson, Ariz. 85721), and Bogardi, Istvan, "Application of Reliability Theory to Hydraulic Engineering Design," *Journal of the Hydraulics Division,* ASCE, Vol. 107, No. HY7, **Proc. Paper 16380**, July, 1981, pp. 799-815

16381 RELIABILITY OF UNDERGROUND FLOOD CONTROL SYSTEM

KEY WORDS: Failure; **Flood control;** Ground water; **Hydraulic structures;** Hydrology; **Mine water;** Mining; Probability theory; **Reliability;** Simulation; Tunneling; **Underground structures;** Waterproofing

ABSTRACT: The reliability of an underground hydraulic engineering system, which is characterized by both resistance and loading being random, is estimated. This system consists of a mine water control system in which failure may be caused either by excessive underground inrushes (or floods) or by equipment breakdown. The failure probability, which is the complement of reliability, is estimated by a combination of failure tree analysis and simulation. The estimated reliabilities appear to agree well with experimental observations.

REFERENCE: Duckstein, Lucien (Prof., Dept. of Systems and Industrial Engrg., Univ. of Arizona, Tucson, Ariz. 85721), Bogardi, Istvan, and Szidarovzky, Ferenc, "Reliability of Underground Flood Control System," *Journal of the Hydraulics Division,* ASCE, Vol. 107, No. HY7, **Proc. Paper 16381**, July, 1981, pp. 817-827

16372 MODELING GRADUAL DAM BREACHES

KEY WORDS: Channel erosion; **Channels; Dam breaches;** Dam stability; Earth dam performance; **Earth dams; Flood control;** Mathematical models; Models; Numerical analysis; Open channel flow; Sediment transport; **Simulation models**

ABSTRACT: A simulation model of the gradual failure of an earth dam has been formulated, developed and tested with real-life data. A significant feature of the model is its ability to account for the growth of the breach and the eventual draining of the reservoir. Concepts of water and sediment routing are used in conjunction with a channel geometry descriptor to arrive at a self-contained mathematical model of the breach enlargement and the ensuing flood wave. Unsteady flow elements of the simulation are an implicit numerical solution of the complete Saint Venant equations coupled with a sequential sediment routing technique. This approach provides an increased rational basis for determining outflow hydrographs from postulated earth dam breaches.

REFERENCE: Ponce, Victor Miguel (Assoc. Prof. of Civ. Engrg., San Diego State Univ., San Diego, Calif. 92182), and Tsivoglou, Andrew J., "Modeling Gradual Dam Breaches," *Journal of the Hydraulics Division,* ASCE, Vol. 107, No. HY7, **Proc. Paper 16372**, July, 1981, pp. 829-838

16364 BOUNDARY SHEAR IN CHANNELS

KEY WORDS: Beds under water; **Boundary shear; Channels (waterways);** Depth; Flow measurement; **Flumes; Friction; Open channel flow;** Rivers; **Roughness (hydraulic);** Shear stress

ABSTRACT: A series of flume experiments are reported in which the walls and bed were differentially roughened, normal depth flow set, and measurements made of the boundary shear stress distribution. An empirically derived equation is presented giving the percentage of the shear force carried by the walls as a function of the breadth/depth ratio and the ratio between the Nikuradse equivalent roughness sizes for the bed and the walls. The results are compared with other available data for the smooth channel case and some disagreements noted. The systematic reduction in the shear force carried by the walls with increasing breadth/depth ratio and bed roughness is illustrated. Further equations are presented giving the mean wall and bed shear stress variation with apsect ratio and roughness parameters. Although the experimental data is somewhat limited, the equations are novel and thought to indicate the general behavior of such open channel flows with some success.

REFERENCE: Knight, Donald W. (Lect., Civ. Engrg. Dept., Univ. of Birmingham, P.O. Box 363, Birmingham, B15 2TT, England), "Boundary Shear in Smooth and Rough Channels," *Journal of the Hydraulics Division,* ASCE, Vol. 107, No. HY7, **Proc. Paper 16364**, July, 1981, pp. 839-851

16368 STREAMFLOW STOCHASTIC MODELS

KEY WORDS: Ground water; Hydrologic data; **Hydrologic models;** Hydrologic properties; **Models;** Precipitation (meteorology); **Statistical analysis; Stochastic models; Stream flow;** Time factors

ABSTRACT: The identification of streamflow stochastic models is explored. The identification of the type of stochastic model is made, based on a conceptual physical representation of natural watershed. The identification of the form of the model is made, based on the recently developed R-functions and S-functions. ARMA is the autoregressive moving average. For a ARMA(p,q) precipitation input, the ground-water storage is an ARMA(p+1, q) process, and the streamflow is an ARMA(p+1, q+1) process. In general, such ground-water and streamflow processes belong to the class of restricted ARMA processes in the sense that their parameter space is a subspace of that corresponding to the general ARMA models. The form or order of the ground-water and streamflow ARMA processes for given historical time series can be uniquely identified by using the R-functions and S-functions. An example is given as a application of such techniques.

REFERENCE: Salas, Jose D. (Assoc. Prof., Dept. of Civ. Engrg., Colorado State Univ., Fort Collins, Colo. 80523), Obeysekera, Jayantha T.B., and Smith, Ricardo A., "Identification of Streamflow Stochastic Models," *Journal of the Hydraulics Division,* ASCE, Vol. 107, No. HY7, **Proc. Paper 16368**, July, 1981, pp. 853-866

16384 PREDICTING LAKE LEVELS

KEY WORDS: **Exponential functions; Forecasting; Lakes;** Mathematical models; Observation; **Predictions;** Statistical analysis; Statistical distributions; Time factors; **Time series analysis; Water levels; Water resources management**

ABSTRACT: A statistical univariate forecasting technique called Exponentially Weighted Moving Average (EWMA) is used to obtain the estimates of future water levels of a large lake. The characteristics of the time series data consisting of average monthly lake levels is examined, and the parameters of the EWMA model are determined. The ex-post forecasts generated by this model are compared with the actual observations of lake water levels and with results obtained earlier with other stochastic methods. EWMA yields forecasts which are statistically indistinguishable from the actual observations.

REFERENCE: Koppula, Sivajogi D. (Section Head, Design and Construction Div., Alberta Environment, 16403-102 Street Edmonton, Alberta, T5X 2G9, Canada), "Predicting Lake Levels by Exponential Smoothing," *Journal of the Hydraulics Division,* ASCE, Vol. 107, No. HY7, **Proc. Paper 16384**, July, 1981, pp. 867-878

16365 THREE HYDRAULIC VARIABLES

KEY WORDS: **Alluvial channels; Boundary shear;** Erosion; Mathematical models; **Open channel flow;** Scour; **Secondary flow;** Sediments; **Sediment transport; Shear stress;** Simulation; **Three dimensional flow**

ABSTRACT: A mathematical modeling and computational technique is presented which is capable of treating and dealing with interactions among hydraulic variables is open channel flows, such as the distribution of primary flow velocity, channel cross section, discharge rate, secondary flow, shear stress, and sediment concentration. A shear stress formula is presented that can include the effect of secondary flow. The formula gives peak values of boundary shear that occur on the channel bottom near the corners and on the side walls. Such peak values of boundary shear are owing to the momentum transfer to the region by secondary flow. The simulation technique can be used as a decision-making tool in selecting engineering designs and controls for channel protections. The main role of secondary flow in sediment transport seems to be to transport sediments in the transverse direction, whereas the gravity brings sediments downward and the diffusion brings sediment particles upward. The vertical component of secondary flow seems to help gravity bring sediment down in most of the area in a transverse cross section of a channel.

REFERENCE: Chiu, Chao-Lin (Prof. of Civ. Engrg., Univ. of Pittsburgh, Pittsburgh, Pa.), and Hsiung, David E., "Secondary Flow, Shear Stress and Sediment Transport," *Journal of the Hydraulics Division,* ASCE, Vol. 107, No. HY7, **Proc. Paper 16365**, July, 1981, pp. 879-898

16363 FLOW RESISTANCE IN GRAVEL BED RIVERS

KEY WORDS: **Boulders; Boundary shear; Channels (waterways);** Cross sections; **Field tests;** Flow resistance; Geometry; **New Zealand; Rivers; Roughness (hydraulic);** Sediments; **Velocity distribution**

ABSTRACT: Flow resistance relations are deduced from data on coarse gravel bed reaches of New Zealand rivers. Measurements of hydraulic variables were made during reasonably uniform subcritical flows at cross sections regular in confirmation. Channel bed and bank roughness are not distinguished, and surface bedmaterial is characterized by the median size. When the channel boundary is rigid the Darcy-Weisbach friction factor is only a statistically significant function of the ratio of hydraulic radius to median size of surface bedmaterial. A model of this form explained 60 percent of the friction factor variance inherent in the field data set. With active bedload transport conditions and changing bed topography, the Froude Number based on median surface bedmaterial size was statistically significant, and 40 percent of friction factor variance was explained by this latter model.

REFERENCE: Griffiths, George A. (Scientist, Water and Soil Div., Ministry of Works and Development, P.O. Box 1479, Christchurch, New Zealand), "Flow Resistance in Coarse Gravel Bed Rivers," *Journal of the Hydraulics Division,* ASCE, Vol. 107, No. HY7, **Proc. Paper 16363**, July, 1981, pp. 899-918

16385 STANDARDS FOR COMPUTER-BASED DESIGN STUDIES

KEY WORDS: **Computer applications; Computer models;** Computer systems hardware; **Engineering education;** Model studies; **Municipal engineering; Project planning;** Standards; Storm water; Water management (applied); Water resources

ABSTRACT: As a result of the large variety of computer-based studies available, their rapid evolution and their complex structures, these programs are becoming increasingly difficult to manage. The following activities could be specified in detail when study bids are requested: problem review, requisite accuracy, review of available programs, program selection criteria, model verification, data preparation and output interpretation, and documentation of the modified program actually used. Many of these activities will be implemented by a reputable engineer in any case, but by including these terms of reference, all consultants proposing services will be assured that their estimates will be met, and clients will be ensuring their investment. Each of these points is explored in general terms; the examples used are appropriate to stormwater management modeling studies; however, the principles could be applied to any computer-based design study.

REFERENCE: James, William (Prof., Dept. of Civ. Engrg. and Engrg. Mech., McMaster Univ., 1280 Main Street West, Hamilton, Ontario, Canada, L8S 4L7), and Robinson, Mark A., "Standards for Computer-Based Design Studies," *Journal of the Hydraulics Division,* ASCE, Vol. 107, No. HY7, **Proc. Paper 16385**, July, 1981, pp. 919-930

U.S. Customary-SI Conversion Factors

In accordance with the October, 1970 action of the ASCE Board of Direction, which stated that all publications of the Society should list all measurements in both U.S. Customary and SI (International System) units, the following list contains conversion factors to enable readers to compute the SI unit values of measurements. A complete guide to the SI system and its use has been published by the American Society for Testing and Materials. Copies of this publication (ASTM E-380) can be purchased from ASCE at a price of $3.00 each; orders must be prepaid.

All authors of *Journal* papers are being asked to prepare their papers in this dual-unit format. To provide preliminary assistance to authors, the following list of conversion factors and guides are recommended by the ASCE Committee on Metrication.

To convert	To	Multiply by
inches (in.)	millimeters (mm)	25.4
feet (ft)	meters (m)	0.305
yards (yd)	meters (m)	0.914
miles (miles)	kilometers (km)	1.61
square inches (sq in.)	square millimeters (mm^2)	645
square feet (sq ft)	square meters (m^2)	0.093
square yards (sq yd)	square meters (m^2)	0.836
square miles (sq miles)	square kilometers (km^2)	2.59
acres (acre)	hectares (ha)	0.405
cubic inches (cu in.)	cubic millimeters (mm^3)	16,400
cubic feet (cu ft)	cubic meters (m^3)	0.028
cubic yards (cu yd)	cubic meters (m^3)	0.765
pounds (lb) mass	kilograms (kg)	0.453
tons (ton) mass	kilograms (kg)	907
pound force (lbf)	newtons (N)	4.45
kilogram force (kgf)	newtons (N)	9.81
pounds per square foot (psf)	pascals (Pa)	47.9
pounds per square inch (psi)	kilopascals (kPa)	6.89
U.S. gallons (gal)	liters (L)	3.79
acre-feet (acre-ft)	cubic meters (m^3)	1,233

APPLICATION OF RELIABILITY THEORY TO HYDRAULIC ENGINEERING DESIGN

By Lucien Duckstein[1] and Istvan Bogardi[2]

INTRODUCTION

Reliability models for two hydraulic engineering systems are presented. The first system consists of a flood levee reach where various phenomena (overtopping, boiling, slope sliding, wind wave erosion) may cause failure. The second system considered is a confluence reach of a tributary where different flooding conditions (flood in the main river or the tributary, or both) may result in a failure.

During the last two decades, there has been a rapid development in the probabilistic methods of safety analysis of engineering structures. It was realized that structures designed by using deterministic (fixed) values of load and resistance may often not be safe enough; in other words, they were underdesigned. On the contrary, other structures may have been overdesigned to compensate for uncertainties. As a consequence, statistical analyses of the load and resistance were undertaken to estimate the failure probability. Two approaches to this problem can be distinguished. The first one is characterized by the work of Freudenthal (16,17), who used classical probability computations to determine the distribution function (DF) or the probability density function (pdf) of the safety factor if the pdf of load and resistance are known. Since failure occurs when load is greater than resistance, i.e., when the safety factor $\nu < 1$, the probability of failure P_F can be calculated by taking the value of the DF for which $\nu = 1$. Since the structure generally consists of more than one element, and each element generally has different properties, several modes of failure are possible. The resistances to these various modes are not independent random variables. As a consequence, the usage of probability analyses as previously described (16,17), has been restricted to simple structures; the safety analysis of complex structures, or systems, has received relatively little attention (27).

The second approach to investigating failures statistically is exemplified by

[1]Prof., Dept. of Systems and Industrial Engrg., Univ. of Arizona, Tucson, Ariz. 85721.
[2]Sr. Systems Analyst, Mining Development Inst., 1037 Budapest III, Mikoviny u. 2-4, Hungary.

Note.—Discussion open until December 1, 1981. Separate discussions should be submitted for the individual papers in this symposium. To extend the closing date one month, a written request must be filed with the Manager of Technical and Professional Publications, ASCE. Manuscript was submitted for review for possible publication on July 18, 1980. This paper is part of the Journal of the Hydraulics Division, Proceedings of the American Society of Civil Engineers, ©ASCE, Vol. 107, No. HY7, July, 1981. ISSN 0044-796X/81/0007-0799/$01.00.

the work of Cornell (10) and Lind (23). These methods keep intact the principle inherent in present design codes but suggest introduction of probabilistic considerations into the codes. This approach is of great practical importance in the design of concrete and steel structures where the relatively small randomness of resistance and load moderates the distorting effect of the deterministic assumptions. On such probabilistic grounds, Misteth (25) analyzed the safety of complex hydraulic structures, such as river dams. The present paper represents an effort to combine both approaches.

Reliability of Flood Levee Systems

Problem Description.—The probability of failure, P_F, of a levee reach is investigated. The reach refers to a levee line of several kilometers that protects a given area in the flood plain. The levee reach behaves as a structure. If there is a levee rupture at any point of the reach, the structure fails and the whole area under protection becomes inundated.

The load on the levee reach is the flood wave, whose different parameters (peak level, duration, volume, etc.) can be used as load characteristics. This load is a random variable whose distribution may be estimated using observations taken at a gaging station along the reach. If there is no effect from backwater or wind waves along the reach, this load is the same in every cross section of the levee. Otherwise, there is a spatial change in load conditions, and for every cross section a different pdf of load should be estimated (4,30). The pdf of load is estimated by known probabilistic or stochastic methods. Naturally, the pdf parameters bear the uncertainty imposed by finite samples (18).

The approach of Freundethal (16,17) cannot be applied in a simple case like slope stability analysis of earthworks because the simplest earth structure should be regarded as a system subject to other modes of failure (11). The assumptions generally used in earthworks analysis are: (1) The load is assumed to be constant; (2) the load and resistance are independent, i.e., statistically rigid structures are assumed; (3) relatively simple, often approximate methods of soil mechanics are used to estimate resistance; and (4) spatial changes of soil properties are described by linear regression models. In the case of hydraulic earthworks, especially along natural waterways, the assumption of constant load cannot be made.

In the case of large flat rivers, failure of the levee reach in any cross section can be caused by one of the following effects (Fig. 1): (1) Overtopping caused by a flood level higher than the levee crest; (2) sand boiling or subsoil failure due to adverse soil conditions; (3) failure of the levee slope due to seepage and wetting; and (4) wind wave effects (e.g., erosion). The resistance or the protection in one cross section should be determined for each of the four effects and should be expressed in terms of the flood parameter that triggers the failure effect.

Generally, there is no single flood parameter governing all four effects: the maximum flood level, the duration of the flood, the intensity and duration of levee soaking, characterized by the value of the so-called flood exposure (3), or another parameter may trigger the adverse phenomena.

Resistance values can be determined by direct measurements (e.g., levee crest height, or soil properties), computations (e.g., seepage and slope stability analyses)

or on the basis of observations during flood occurrences (information on the location and time of adverse phenomena and on the corresponding flood load).

Specifically, resistance values were estimated in the following way.

Resistance against Overtopping, $\underline{H}_1$.—The triggering flood parameter is the peak flood level, and the resistance is the levee height minus 30 cm–80 cm reflecting a spongy layer under the crest. This resistance, $\underline{H}_1$, is a random variable for at least two reasons: (1) There could be a random fluctuation in the levee height; and (2) both the measurement of $\underline{H}_1$ and the estimation of $\underline{H}_1$ from one common gaging station within the reach have random errors. However, the variance of $\underline{H}_1$ is generally quite small as compared to that of other resistances.

Resistance against Sand Boiling or Subsoil Failure, $\underline{H}_1$.—This value can also be expressed by the peak flood level or alternatively by the flood exposure or duration. Theoretical methods and empirical equations (34) generally consider the flood level as the triggering value. However, there have been data showing that given values of flood exposure or duration may cause sand boiling (29). Since the mechanism of this failure phenomenon is rather complicated and there is no model generally acceptable for practical cases, the resistance $\underline{H}_2$ should

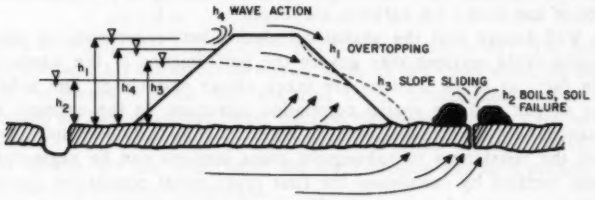

FIG. 1.—Modes of Levee Failure

be a random variable with considerable variance (5,6). The variance of $\underline{H}_2$ can only be estimated in a systematic way if historical data are available on the actual flood levels at the time when boiling started; otherwise, only the expected value of $\underline{H}_2$ can be estimated.

A Bayesian approach (12) offers a way to connect in-situ practical experience on boiling with regional boiling data. In that case, regional boiling data can be regarded as prior information (28,35) and observation data of past floods can serve for the likelihood function. The Bayes formula yields a posterior pdf using the prior information and likelihood function mentioned. Foloyan, Hoeg, and Benjamin (14) used such a Bayesian approach to determine a posterior pdf of soil settlement.

Resistance against Slope Failure, $\underline{W}_3$, $\underline{H}_3$.—As a consequence of high level or long duration floods, or both, the land slide slope of the levee is saturated and slope sliding may occur. Experience shows that this failure phenomena is influenced not only by the peak flood level but also by the flood duration. This complex load can be fairly well characterized by the flood exposure $\underline{w}$ (3) which is the area of the stage hydrograph ($m \times$ day) above bankful stage. Classical methods of slope stability analysis cannot regard this flood exposure as a load on the levee; therefore, experience from past flood data is used

to estimate the resistance values $\underset{\sim}{W}_3$. It is also a general observation that there is a lower threshold water level $\underset{\sim}{H}_3$ below which no sliding occurs regardless of the magnitude of the flood exposure. This value, $\underset{\sim}{H}_3$, may correspond to the height of a very old levee core or to the pressure necessary to wet the landslide slope from the bottom up. Theoretically, there exists some function between the geometry and soil properties of the levee, on the one hand, and the resistances, $\underset{\sim}{W}_3$ and $\underset{\sim}{H}_3$, on the other hand. The approach applied to determine the DF of resistance $\underset{\sim}{H}_2$ can be used to estimate the DF of $\underset{\sim}{W}_3$ and $\underset{\sim}{H}_3$, considered as random variables. A Bayesian approach provides again an appropriate way to estimate $\underset{\sim}{W}_3$ and $\underset{\sim}{H}_3$ by combining prior information and observation data.

Resistance against Wind Wave Failure.—This dynamic failure is triggered by the sum of the flood level and wave effect (wave height and run-up) (4). In the case of flat, large rivers, the distance between the levees can be as great as 5 km–8 km. Naturally, adverse wind conditions (large fetch) during floods may give rise to huge waves which attack the top of the levee. The resistance against this composite effect can be taken as the levee height minus 20 cm–30 cm. The stochastic model of levee system failure also considers this failure mode (30). However, the example presented in that paper deals with a levee reach where wave action is negligible because of the relatively short distance of less than 1 km between the levees.

It is well known that the spatial correlation between resistance values of subsequent cross sections may govern the performance of the whole system (11). In fact, as cross sections are taken closer and closer, the subreaches become shorter and the spatial correlation increases. In the example shown, the distances between cross sections are large enough so that the spatial correlation between the resistances of subsequent cross sections can be neglected. This has been verified by calculating the first order serial correlation coefficients between the estimated resistances. No significant correlation has been found according to the Durbin-Watson test (19) on the 5% level of significance. However, in other cases, the spatial correlation might take on significant values and cannot be neglected. The proposed model can also be used in such cases as it was shown by Szidar (33) in a paper examining the effect of random errors in subsequent values of economic loss and cost functions. Between subsequent errors, a strong correlation exists, as it might between neighboring regions in soil systems.

Reliability Model.—The proposed method takes into consideration: (1) The stochastic character of flood load; (2) the various degrees of protection offered along the levee reach; and (3) the different modes of failure. The model is presented in two parts: (1) P_F in a given cross section; and (2) P_F of a levee reach.

P_F in Given Cross Section.—There is a failure in the cross section if either: (1) $\underset{\sim}{h} > \underset{\sim}{H}_1$: overtopping; (2) $\underset{\sim}{h} > \underset{\sim}{H}_2$: subsoil failure; (3) $(\underset{\sim}{h} > \underset{\sim}{H}_3) \cap (\underset{\sim}{w} > \underset{\sim}{W})$: slope stability failure; and (4) $\underset{\sim}{h} + \underset{\sim}{x} > \underset{\sim}{X}$: wind wave attack, erosion in which the random loads are $\underset{\sim}{h}$ = peak flood level; $\underset{\sim}{w}$ = flood exposure, i.e., the area of the stage hydrograph ($m \times$ day) above bankful capacity; and $\underset{\sim}{x}$ = wave height and run-up (5). The random resistances are:

1. $\underset{\sim}{H}_1$: the highest flood level allowable with respect to overtopping.
2. $\underset{\sim}{H}_2$: the highest flood level allowable with respect to boiling.

3. $\underline{H}_3$, $\underline{W}_3$: respectively, the smallest necessary flood level and the highest allowable flood exposure with respect to slope sliding. This threshold value H_3 is needed since a flood exposure W_3 might pertain to a low flood level $h < H_3$, say 10 cm above bankful level for a few weeks, which certainly causes no sliding.

4. $\underline{X}$: the highest dynamic water level (peak static level + wave + run-up) allowable with respect to erosion failure.

Thus, a failure event in a cross section is defined by

$$T = [(\underline{h} + \underline{x}) > \underline{X}] \cup (\underline{h} > \underline{H}_1) \cup (\underline{h} > \underline{H}_2) \cup [(\underline{H}_3 < \underline{h}) \cap (\underline{w} > \underline{W})] \quad . \quad . \quad . \quad (1)$$

The probability of T, that is, the probability of failure, can be computed by dividing the right side of Eq. 1 into disjoint events. As a result, the following expression for P_F can be reached under the assumptions that $\underline{x}$ and $(\underline{h}, \underline{w})$ are independent, and $\underline{H}_3 \leq \underline{H}$ (31).

The foregoing relations may be transformed into the following expression for P_F

$$\underline{P}_F = 1 - F(\underline{H}) + \int_{H_3}^{H} \int_{W}^{\infty} f(h, w)\, dw\, dh + g \quad . \quad . \quad . \quad . \quad . \quad . \quad . \quad . \quad . \quad . \quad . \quad . \quad . \quad . \quad . \quad . \quad . \quad (2)$$

in which $g = (\int_{-\infty}^{H} \int_{-\infty}^{W} + \int_{-\infty}^{H} \int_{W}^{\infty})[1 - F_{\underline{X}}(X - h) f(h, w)\, dw\, dh]$. The last term of Eq. 2 accounts for the effect of waves. Thus, in the cases when the distance between the levees is small, say less than 1 km, considerable waves cannot be generated for lack of enough fetch, the first three terms of Eq. 2 are sufficient to calculate P_F. Such will be the case for the practical example presented in the next section. On the other hand, the wave erosion can be a critical factor in large flat-land rivers or reservoirs.

P_F of Levee Reach.—For each failure mode, the levee reach is divided into subreaches, within which the mean value and variance of resistance for each failure mode is constant. Assuming that every subreach is characterized by one cross section, the failure event for the whole reach is the union of the failure events T_i of the subreaches $i = 1, \ldots, n$:

$$T = T_1 \cup T_2 \cup T_i \ldots \cup T_n$$

Let $\underline{H} = \min_{1 \leq i \leq n} (\underline{H}_{1i}, \underline{H}_{2i})$; $\underline{H}_3 = \min_{1 \leq i \leq n} \underline{H}_{3i}$; $t(\underline{h}) = \min_{H_{3i} < \underline{h} < H} \underline{W}_i$

in which $\underline{H}_{1i}$, $\underline{H}_{2i}$, $\underline{H}_{3i}$, and $\underline{W}_i$ are the resistances of subreach i. The system $\underline{P}_F$, without considering wind wave attack, can be calculated as:

$$\underline{P}_F = 1 - F(\underline{H}) + \int_{H_3}^{H} \int_{t(h)}^{\infty} f(h, w)\, dw\, dh \quad . \quad . \quad . \quad . \quad . \quad . \quad . \quad . \quad . \quad . \quad . \quad . \quad . \quad . \quad . \quad . \quad . \quad (3)$$

Note that $\underline{P}_F$ is considered as a random variable itself because of the uncertainties in the resistances, $\underline{H}_1$, $\underline{H}_2$, $\underline{H}_3$ and $\underline{W}$.

It is assumed that the resistances follow normal distributions with means equal to the deterministic values H_1, H_2, N_3, and W and standard deviations estimated as described in Ref. 7.

Often there is a spatial dependence between subsequent resistances. This spatial dependence can be characterized by a significant first order correlation

coefficient. Naturally in such cases, Eq. 3 would not hold and the system resistance for each failure mode should be represented with an n-dimensional normal distribution as in Ref. 7.

Eq. 3 can be solved in four different cases depending on the various uncertainties considered.

1. No uncertainty in the resistances is assumed. Estimated mean values of resistances are substituted into Eq. 3 which yields a single P_F.
2. Uncertainty in the resistances is assumed. Based on estimated means, variances and assumed normal distributions of the resistances, a large number of possible system $\underset{\sim}{P}_F$s are calculated using Eq. 3. An expected value and variance of system $\underset{\sim}{P}_F$ can be computed; also a discrete or continuous distribution can be fitted to the simulated values of $\underset{\sim}{P}_F$.
3. Uncertainties in the estimated stochastic properties of the load are considered; namely, parameters of the joint pdf $f(h, w)$ are estimated from a finite sample size. From a Bayesian viewpoint, these parameters may be regarded as random variables (2); on this basis, equally likely samples and parameters can be generated. Again, with the help of Eq. 3, possible values of $\underset{\sim}{P}_F$ can be calculated using the generated parameters. Statistical properties of the random values of $\underset{\sim}{P}_F$ can be determined as in the preceding case.
4. Uncertainties in the resistances and in the load parameters are considered; then one generates simultaneous independent sets of resistances and load parameters.

A practical example is presented in the next section to illustrate the difference between the four cases.

Numerical Example and Consideration.—The probability of failure of a levee reach, 14 km in length, of the Sebes-Koros River, Hungary, is sought. A flood event occurs each time the stage climbs above 500 cm. For each event, flood load is given in terms of peak stage and flood exposure data taken in the period 1901–1970 at the Korosladany gaging station, which is located in the reach under study. During this period, 81 events have occurred. The hypothesis that $\underset{\sim}{h}$ is lognormally distributed cannot be rejected on the basis of a Kolmogorov-Smirnov test at the 0.05 level. A similar result is found for $\underset{\sim}{w}$. The sample mean M and standard deviation D of $\underset{\sim}{h}$ and $\underset{\sim}{w}$, respectively, are as follows: (1) $M(\underset{\sim}{h}) = -0.5132$; (2) $D(\underset{\sim}{h}) = 1.1683$; (3) $M(\underset{\sim}{w}) = 0.7197$; and (4) $D(\underset{\sim}{w}) = 1.8417$. The correlation coefficient between $\underset{\sim}{h}$ and $\underset{\sim}{w}$ is $r = 0.97$, which is a fairly high value. As a result of this high correlation, the difference between the P_F of the system and that of the weakest section is expected to be small, since failure caused only by $\underset{\sim}{h}$ also causes failure by $\underset{\sim}{w}$, and vice-versa. Note that this strong linear correlation between h and w cannot be taken for granted in other examples.

Resistance values H_{1i}, H_{2i}, H_{3i}, and W_{3i} are presented in Table 1 and have been determined as follows:

1. H_{1i} is a geometric measurement, taken as the height of the levee crest minus 40 cm; these 40 cm account for a layer of spongy soil just under the crest. On the basis of the existing record, the coefficient of variation V of $\underset{\sim}{H}_1$ has been taken as 2% for every cross section.

TABLE 1.—Resistance Values H_1, H_2, L_3 and H_3 of Subreaches with Associated Failure Probability

Number (1)	Subreach limits, in kilometers (2)	H_1,[a] in centimeters (3)	H_2,[b] in centimeters (4)	H_3,[b] in centimeters (5)	W_3,[b] in meters × day (6)	P_F without soil uncertainties (7)
1	0–0.5	816				0.0485
2	0–1.0	782	782			0.0571
3	0–1.5	834				0.0446
4	0–2.0	789	774			0.0571
5	0–2.5	826				0.0465
6	0–3.0	784				0.0560
7	0–3.5	807				0.0505
8	0–4.0	754		600	47	0.0022
9	0–4.5	800				0.0516
10	0–5.0	778				0.0571
11	0–5.5	839				0.0505
12	0–6.0	781				0.0571
13	0–6.5	846				0.0428
14	0–7.0	818				0.0485
15	0–7.5	780				0.0571
16	0–8.0	769				0.0606
17	0–8.5	830	800	530	44	0.0603
18	0–9.0	766				0.0606
19	0–9.5	803				0.0516
20	0–10.0	765				0.0618
21	0–10.5	855	785	550	40	0.0611
22	0–11.0	769				0.0606
23	0–11.5	762				0.0618
24	0–12.0	847				0.0428
25	0–12.5	850				0.0428
26	0–13.0	832				0.0455
27	0–13.5	835				0.0446
28	0–14.0	771				0.0594

[a]Coefficient of variation = 2%.
[b]Coefficient of variation = 10%.

Note: P_F for the levee reach without soil-mechanical uncertainties = 0.0643; Mean value of P_F for the subreaches = 0.0520; $E(P_F)$ for the levee reach with soil-mechanical uncertainties = 0.0865; $D(P_F)$ for the levee reach with soil-mechanical uncertainties = 0.0161; $E(P_F)$ for the levee reach with parameter uncertainties = 0.0676; $D(P_F)$ for the levee reach with parameter uncertainties = 0.0276; $E(P_F)$ for the levee reach with soil-mechanical and parameter uncertainties = 0.0887; and $D(P_F)$ for the levee reach with soil-mechanical and parameter uncertainties = 0.0395.

2. The resistance against boiling H_2 is a quantity computed by the formulas developed for the Mississippi River levees (34), and verified experimentally during those flood events which actually caused boiling. The coefficient of variation V of $\underline{H}_2$, based on existing data, is taken as 10% for every cross section.

3. The resistance against sliding W_3 and the corresponding H_3 are taken as the flood exposure and the peak stage of the flood wave observed at the time of the critical phenomenon, namely, sliding during the 1970 flood (36). The coefficients of variation V of $\underline{W}_3$ and $\underline{H}_3$, which reflect the variability of soil parameters, have been taken as 10% for every cross section.

As shown in Table 1, there are four subreaches, numbered 2, 4, 17, and 21, where dangerous boiling has occurred and three subreaches, numbered 8, 17 and 21, where slope sliding has happened. No entries have been made for the values of H_2 and H_3 that exceeded the value of H_1 for any given subreach. In this example, the reach is divided into the same equispaced subreaches for every failure mode. For the estimation of P_F of the system, the value of min $[H_1, H_2]$ was found at subreach 8 (3.5 km–4 km), while W_3 and H_3 were located at subreach 21 (10 km–10.5 km). Table 1 also contains the system P_F values.

Results of the calculations may be summarized as follows:

1. Without soil-mechanical uncertainties, the system P_F of 0.0643 is greater than the mean value of the P_Fs of the subreaches, found to be 0.052, but it is also greater than the P_F of 0.0622 for the "weakest link" (subreach 8). If the stochastic dependence, measured in this case by linear correlation r between loads $\underline{h}$ and $\underline{w}$, were weaker, then the difference between system P_F and "weakest link" P_F would be even greater. This statement can be justified by replacing $f(h, w)$ in Eq. 3 by a joint lognormal DF, which contains r explicitly.

2. With soil-mechanical uncertainties, the mean and standard deviation of system $\underline{P}_F$ estimated from 100 samples are, respectively: $E(\underline{P}_F) = 0.0865$ and $D(\underline{P}_F) = 0.0161$. Note the considerable change in $\underline{P}_F$; in fact, the soil-mechanical uncertainties increase the expected $\underline{P}_F$ result in a non-negligible variance of $\underline{P}_F$.

3. With load parameter (or hydrologic) uncertainties, the mean and standard deviation of system $\underline{P}_F$, also estimated from 100 samples are, respectively: $E(\underline{P}_F) = 0.0676$ and $D(\underline{P}_F) = 0.0276$. Note in this case the large variance of $\underline{P}_F$ but also a smaller change in the mean of $\underline{P}_F$ than in case 2.

4. With both soil-mechanical and hydrological uncertainties, there is a larger change in the mean value of $\underline{P}_F$ (0.0887) than in case 2, and the standard deviation of $\underline{P}_F$ (0.0395) is also larger than in case 3.

System Reliability Along Confluence Reach

Problem Description.—One of the most complicated problems in water resources engineering is to design a hydraulic structure under uncertain beckwater effect, i.e., in the case of random headwater, $\underline{h}$, or tailwater $\underline{H}$, or both. A typical example of this situation is the levee system of a tributary along the confluence reach with the main river.

The purpose herein is to develop a methodology to account for the effect of uncertain backwater curves on the reliability of a structural system. The structural system consists of a levee along the tributary reach just adjacent to the main river. Note that the methodology can be used for estimating the reliability of any system operating under similar conditions. Other hydraulic engineering examples where backwater effects may strongly influence the reliability of the system may be found in the design of irrigation channels and of urban or land drainage systems.

Steady flow conditions are assumed in both the main river and the tributary while a flood flows down from the tributary. This is a common working hypothesis especially justifiable for flat rivers where the duration of peak flow may be as much as several days (35).

The differential equation governing the nonuniform steady flow in the tributary has been given by Kuiper (21):

$$\frac{dz}{dx} + \frac{\bar{u}}{g}\frac{d\bar{u}}{dx} = \frac{Q^2}{K^2(z,x)} \quad \ldots\ldots\ldots\ldots\ldots\ldots\ldots\ldots\ldots\ldots\ldots\ldots\ldots\ldots (4)$$

in which z = the height of the water level; x = the horizontal distance; $\bar{u}$ = the average flow velocity through a cross section located at x; Q = the discharge of the tributary; and $K(z,x)$ = the water carrying capacity of the tributary. Eq. 4 can be solved by a common step method, such as a finite difference scheme (9).

Available data include time series at a gaging station on the main river near the confluence and at another station in the tributary just upstream of the end of the backwater curve; also known is the stage-discharge relationship at the tributary observation point. From the two time series, partial duration series can be constructed and simultaneous peak stages $\underline{h}$ and $\underline{H}$ can be calculated. Generally, the random variables, $\underline{h}$ and $\underline{H}$, are not independent; statistical analysis is used to determine a best-fit joint DF. The proposed methodology to estimate flood protection reliability can be applied when this fitted DF is either of the normal or lognormal type.

Reliability Model.—The reliability model is presented in two parts: (1) The P_F of a given levee cross section is obtained by partitioning the set of backwater curves into two subsets, i.e., the curves passing above the existing levee and those not passing above it; and (2) the P_F of the whole levee system is calculated by combining failure events in a finite number of cross sections. In this section, only levee failure by overtopping is considered; the parameter of the flood wave that triggers this phenomenon is the peak height. If other modes of failure were considered, then other flood parameters (e.g., flood exposure or duration of the flood wave) must be brought into the picture (see the section "Reliability of Flood Levee Systems"), but the assumption of steady condition would no longer be valid. Dynamic routing would have to be used to determine the variation of discharge in time and space along both the tributary and the main river. For simple situations, different routing methods have been elaborated (1,15,22,26), however, in general, dynamic routing is rather complicated, even for the case of a single flood moving down a rectangular channel of constant width; then, in the present case, many floods (h, H) are considered.

Probability of Failure in One Levee Cross Section.—Given joint sample elements

(h_i, H_i) for the main river and the tributary ($i = k, 2, ..., m$), backwater curves can be computed using Eq. 8 and water stage sample elements z_{ki} are obtained for each cross section. Let Z_k and R_k denote, respectively, the levee height and DF of the water level in cross section k; then the probability of failure of section k is

$$P_{Fk} = P(\underset{\sim}{z}_k > Z_k) = 1 - R_k(Z_k) \quad \text{(5)}$$

On the other hand, the reliability of any given cross section means the probability that all backwater curves in that cross section fall lower than the height of the levee. Dropping the index k for sake of brevity, this reliability may be determined in the following way.

A sample value of h is taken and, knowing the height, Z, in the cross section, discharge Q and stage H can be computed by Eq. 4. Repeating this procedure, pairs of values of h and H can be determined, which yield a function, $H(h)$. To each pair $[h, H(h)]$, there belongs a backwater curve which has a height, Z, in the cross section. The reliability of the cross section is then by definition:

$$R = P(\underset{\sim}{z} \le Z) = \int_{-\infty}^{+\infty} \left[\int_{-\infty}^{H(h)} f(h, H)\, dH \right] dh \quad \text{(6)}$$

in which $f(h, H)$ = the joint density function of the pair $(\underset{\sim}{h}, \underset{\sim}{H})$.

Probability of Failure of Whole Levee System.—The probability of failure of the system means the probability that in at least one cross section along the reach considered the water level z_k is greater than the levee height, Z_k. Using the union-intersection principle of probability theory yields (24):

$$P_F = P\left[\bigcup_k (\underset{\sim}{z}_k > Z_k) \right] = 1 - P\left[\bigcap_k (\underset{\sim}{z}_k \le Z_k) \right] \quad \text{(7)}$$

Since there are several cross sections along the reach, the procedure previously outlined for one cross section cannot be used. A direct method to compute P_F will now be developed. The joint sample elements (h_i, H_i) and the values of $\underset{\sim}{z}_k$ given by Eq. 4 are used to calibrate a predictive model of $\underset{\sim}{z}_k$ for each cross section. The following linear regression model is used to estimate this variation of z_k as a function of $\underset{\sim}{h}$ and $\underset{\sim}{H}$:

$$\underset{\sim}{z}_k = a_k \underset{\sim}{h} + b_k \underset{\sim}{H} + c_k \quad \text{(8)}$$

in which the coefficients of a_k, b_k, and c_k are least-squares estimates. Note that, for the first cross section, $z_1 = h$, and for the last one, $z_n = H$, so that $a_1 = b_n = 1$ and $b_1 = c_1 = a_n = c_n = 0$. Eq. 8 can be substituted into Eq. 7 to obtain

$$P_F = 1 - P\left[\bigcap_k (a_k \underset{\sim}{h} + b_k \underset{\sim}{H} + c_k \le Z_k) \right] \quad \text{(9)}$$

Consider the region of the $(\underset{\sim}{h}, \underset{\sim}{H})$ plane defined by the inequalities $a_k \underset{\sim}{h} + b_k \underset{\sim}{H} + c_k \le Z_k$. This region is bounded by the piecewise linear function $T(h)$ defined by the set of n segments

$$\underset{\sim}{H} = \frac{Z_k - c_k - a_k \underset{\sim}{h}}{b_k}; \quad k = 1, 2, ..., n \quad \text{(10)}$$

Thus the probability of failure for the whole system is

$$P_F = 1 - \int_{-\infty}^{Z_n} \int_{-\infty}^{T(h)} f(h,H)\,dHdh \quad \ldots \ldots \ldots \ldots \ldots \ldots \ldots \quad (11)$$

in which f = the joint pdf of $(\underset{\sim}{h}, \underset{\sim}{H})$.

The integral in Eq. 11 is readily computed when the pdf $f(h,H)$ is a joint normal pdf. In case of lognormal variates, a logarithmic transformation of all values is used.

The proposed methodology recognizes the existence of the uncertainties that are generally present in engineering design, i.e., natural, sample, and model uncertainty (20).

1. The natural uncertainty caused by the double randomness of floods is taken into consideration by using the joint pdf $f(h,H)$ for the reliability calculation.

2. Sample or parameter uncertainty originates from the fact that the joint pdf $f(\underset{\sim}{h}, \underset{\sim}{H})$ is estimated from a finite sample, i.e., if another historical sample were at hand, the value of P_F would be different. A Bayesian method (2) may be used to analyze the effect of this sample uncertainty on the value of P_F as follows. The possible parameters $\mathbf{a}$ of the joint pdf $f(h,H)$ are regarded as random variables and a pdf of the probability of failure P_F is estimated. For this purpose, let $p(\mathbf{a}\,|\,\mathbf{a}_0)$ denote the pdf $f(h,H)$ given sample parameters $\mathbf{a}_0$. Then the value of P_F is a function of the parameters $\mathbf{a}$:

$$P_F(\mathbf{a}) = 1 - \int_{-\infty}^{Z_n} \int_{-\infty}^{T(h\,|\,\mathbf{a})} f(h,H\,|\,\mathbf{a})\,dHdh \quad \ldots \ldots \ldots \ldots \ldots \quad (12)$$

in which $T(h\,|\,\mathbf{a})$ = the function $\underset{\sim}{H} = T(\underset{\sim}{h})$ corresponding to the parameter, $\mathbf{a}$; and $f(h,H\,|\,\mathbf{a})$ = the joint density function of the pair $(\underset{\sim}{h}, \underset{\sim}{H})$ given parameter $\mathbf{a}$.

The right-hand side of Eq. 12 defines P_F as a function of the parameter, $\mathbf{a}$, whose pdf is known. Random values of $\mathbf{a}$ are simulated and introduced into Eq. 12 to compute random values of P_F. An empirical distribution of P_F is thus obtained and may then be fitted to a continuous pdf using standard statistical procedures. Using this empirical pdf with an appropriate objective function, Bayes decision theory may be applied to account for sample uncertainty and obtain an optimum design value of P_F (12,13).

3. Model uncertainty stems from several assumptions in the hydrological model [type of the joint pdf $f(h,H)$], hydraulic computations (steady flow, lumped friction parameters), and system definition (finite number of cross sections, fixed values of levee height Z_k).

It may be noted that simulation is an alternative procedure for finding the optimum levee design, as shown in Ref. 32 for the same case study problem. Results are about the same as with the analytical method.

Numerical Example and Consideration.—The method is now applied to estimate the reliability of the levee system along the confluence reach of the Zagyva River, in Hungary. A levee reach of 37.5 miles (60.4 km) between the Jasztelek gaging station and the mouth in the Tisza River at Szolnok is analyzed (Fig. 2). Along this reach, wetted cross-sectional areas and hydraulic radii for both

the river bed and the flood plain have been determined in 49 cross sections. Moreover, the stage-discharge relationship, $H - Q$, for the Jasztelek gaging

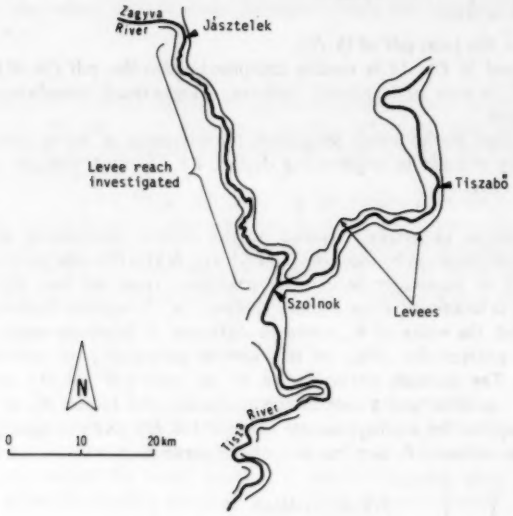

FIG. 2.—Geographic Sketch of Confluence Levee Reach Investigated

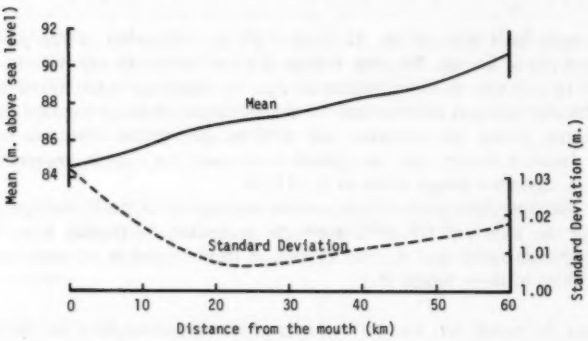

FIG. 3.—Variation of Mean and Standard Deviation of Peak Stages along Confluence Reach

station is also known. The roughness coefficients for the bed and the flood plain has been determined by a special calibration algorithm (30).

Statistical samples for $\underline{h}$ and $\underline{H}$ were obtained from observation data of peak

stages at the duo gaging stations and of the simultaneous stage at the other station. Between the years of 1932 and 1967, the number of sample pairs (h, H) is 68; thus 68 surface curves can be computed. The hypothesis that $f(h, H)$ is joint normal cannot be rejected by the Kolmogorov-Smirnov test at the 5% level. Parameters of the pdf are $E(h) = 33.33$ in. (850 mm); $D(h) = 1.05$ in. (30 mm); $E(H) = 35.78$ in. (910 mm); $D(H) = 0.54$ in. (14 mm); and $r = 0.4889$. The use of Eq. 12 to calculate the reliability of cross section $k = 6$ yields:

$$R_6 = P(z \leq Z) = 0.986 \quad \text{or} \quad P_F(6) = 1.4 \times 10^{-2} \ldots\ldots\ldots\ldots\ldots (13)$$

Next, the probability of failure of the whole levee system is determined. The linear regression model of Eq. 8 was estimated for every cross section. The variation of the mean and standard deviation of z along the confluence reach is shown in Fig. 3. A minimum of the standard deviation occurs between 12.4 miles (20 km) and 18.6 miles (30 km). The maximum residual variance among linear regression equations for the cross sections is 0.256 and the smallest multiple correlation coefficient in the same cross section is 0.821; however, 90% of

TABLE 2.—Effect of Sample Uncertainty on P_F

$E(h)$, in meters (1)	$D(h)$, in meters (2)	$E(H)$, in meters (3)	$D(H)$, in meters (4)	r (5)	$P_F \times 10^2$ (6)	Remark (7)
84.67	2.67	90.88	1.37	−0.4889	3.61	sample values
84.35	3.03	91.05	1.62	−0.5784	6.35	highest P_F[a]
85.03	2.62	91.00	1.22	−0.5151	1.19	lowest P_F[a]

[a]45 samples were simulated; the mean P_F was 3.79×10^{-2}, and the standard deviation, 1.91×10^{-2}.

Note: Convert meters to feet by dividing by 0.305.

the correlation coefficients are greater than 0.90, which shows the applicability of this form of regression.

Function T is composed in this case of 49 line segments (49 cross sections). Eq. 11 yields a probability of failure of 3.61×10^{-2} for the whole system.

The effect of sample uncertainty is then evaluated using 45 simulated joint normal samples of the pair (h, H) of size 68—the same size as the historical data. For each of the 45 samples, a P_F is obtained from Eq. 12, which was integrated numerically by a simulation method. Runs resulting in the highest and lowest P_F values are shown in Table 2. The mean P_F with sample uncertainty is found to be 3.79×10^{-2}, which is somewhat higher than 3.61×10^{-2} without sample uncertainty, but the remarkable feature is a non-negligible variance of P_F of 1.91×10^{-2}.

Conclusions and Recommendations

1. In the case of earth works such as flood levees, statistical approximations must be used to estimate the reliability because of the complexity of the failure phenomenon.

2. Both load and resistance should be considered as random variables; the probability of failure is then a function of the ratio of two random variables.

3. The stochastic model of levee failure may yield fairly high values of the probability of failure P_F; these high values are in agreement with experimental observations.

4. A stochastic approach can also be used in the case of bivariate hydraulic uncertainty. The reliability of a structure under backwater effect, with both ends of backwater curve being at a random stage, is used as an example. In this bivariate case, both sample and model uncertainty are high.

5. Model uncertainty in hydraulic systems can be handled by use of either sensitivity analysis or Bayesian methods.

Acknowledgment

Part of this research was performed within the framework of two cooperative research projects between the University of Arizona and the Institute of Cultural Relations in Budapest under, respectively, National Science Foundation Grants #GF 38183, "Decision Making Under Uncertainty in Hydrologic and Other Resource Systems," and INT 78-12184, "Decision-Making in Natural Resources Management." Hungarian funds were provided, respectively by the National Water Authority and the Ministry of Heavy Industry. This research is the product of teamwork between members of the American and Hungarian research team working under the auspices of the aforementioned grants; in particular, the indispensable contribution of Ferenc Szidarovszky to both theoretical and numerical phases of the project is gratefully acknowledged.

Appendix I.—References

1. Baltzer, R. A., and Lai, C., "Computer Simulation of Unsteady Flows in Waterways," *Journal of the Hydraulics Division*, ASCE, Vol. 94, No. HY4, Proc. Paper 6048, July, 1968, pp. 1083–1117.
2. Benjamin, J. R., and Cornell, C. A., *Probability, Statistics and Decision for Civil Engineers*, McGraw-Hill Book Co., New York, N.Y., 1970.
3. Bogardi, I., "Flood Exposure Recommended as a Parameter for Describing the Fatigue Loading on Flood Control Structures," *Bulletin of the International Association of Hydrological Sciences*, Vol. 3, 1968.
4. Bogardi, I., "Hydrological, Hydraulic, Soil Mechanical and Meteorological Aspects of Models for Determining the Degree of Protection Offered by Flood Levees," *Bulletin of the International Association of Hydrological Sciences*, Vol. 9, 1971.
5. Bogardi, I., *Flood Control*, Series of Subject Notes, UNESCO Postgraduate Training Course in Water Management, Budapest, Hungary, 1972.
6. Bogardi, I., "The Load and Resistance of Flood Levees," (in Hungarian), thesis presented in 1974 for a Candidacy in Science, Budapest, Hungary.
7. Bogardi, I., Duckstein, L., Schmieder, A., and Szidarovszky, F., "Stochastic Forecasting of Mine Water Inrushes," *Advances in Water Resources*, Vol. 3, Mar., 1980, pp. 3–8.
8. Bogardi, I., Duckstein, L., and Szidarovszky, F., "On the Reliability of Flood Levee Systems," *Proceedings*, 2nd International Conference on Statistics and Probability, 1975.
9. Chow, V. T., *Open-Channel Hydraulics*, McGraw-Hill Book Co., New York, N.Y., 1959.

10. Cornell, C. A., "A Probability-Based Structural Code," *American Concrete Institute Journal*, Dec., 1969.
11. Cornell, C. A., "First Order Uncertainty Analysis of Soils Deformation and Stability," *Proceedings*, First International Conference on Applications of Statistics and Probability to Soil and Structural Engineering, Sept., 1971.
12. Davis, D., Kisiel, C., and Duckstein, L., "Bayesian Decision Theory Applied to Design in Hydrology," *Water Resources Research*, Vol. 8, No. 1, Feb., 1972, pp. 33–41.
13. Duckstein, L., Krzysztofowicz, R., and Davis, D., "To Build or Not to Build: a Bayesian Analysis," *Journal of Hydrological Sciences*, Vol. 5, No. 1, 1978, pp. 55–68.
14. Foloyan, I., Höeg, K., and Benjamin, I., "Decision Theory Applied to Settlement Predictions," *Journal of the Soil Mechanics Division*, Vol. 96, No. SM4, Proc. Paper 7390, July, 1970, pp. 1127–1141.
15. Fread, D. L., "Technique for Implicit Dynamic Routing in Rivers with Tributaries," *Water Resources Research*, Vol. 9, No. 4, 1972, pp. 913–926.
16. Freudenthal, A. M., "Safety, Reliability and Structural Design," *Journal of the Structural Division*, ASCE, Vol. 87, No. ST3, Proc. Paper 2764, Mar., 1961, pp. 1–16.
17. Freudenthal, A. M., Carrelts, J. M., and Schinozuka, M., "The Analysis of Structural Safety," *Journal of the Structural Division*, ASCE, Vol. 92, No. ST1, Proc. Paper 4682, Feb., 1966, pp. 267–325.
18. Haan, C. T., "Adequacy of Hydrologic Records for Parameter Estimation," *Journal of the Hydraulics Division*, ASCE, Vol. 98, No. HY8, Proc. Paper 9128, Aug., 1972, pp. 1387–1393.
19. Johnston, J., *Econometric Methods*, 2nd ed., McGraw-Hill Book Co., New York, N.Y., 1972.
20. Kisiel, C., and Duckstein, L., eds., *Proceedings of the International Symposium on Uncertainty in Hydrologic and Water Resource Systems*, 3 Volumes, University of Arizona, Dec., 1972.
21. Kuiper, E., *Water Resources Development*, Butterworths, London, England, 1965.
22. Larson, D., Wei, C. T., and Bowers, C. E., "Numerical Routing of Flood Hydrographs through Open Channel," *Bulletin 40*, Water Resources Research Center, University of Minneapolis Graduate School, Minneapolis, Minn., Aug., 1971.
23. Lind, N. C., "Deterministic Formats for the Probabilistic Design of Structures," *An Introduction to Structural Optimization, SM Study No. 1*, Solid Mechanics Division, University of Waterloo, Waterloo, Ontario, Canada, 1969.
24. Lindgren, B. W., *Statistical Theory*, 3rd ed., The MacMillan Co., New York, N.Y., 1968.
25. Misteth, E., "Some Safety Problems," presented at the Sept., 1968, International Association for Bridge and Structural Engineering, Eighth Congress, held at New York, N.Y.
26. Pinkayan, S., "Routing Storm Water Through a Drainage System" *Journal of the Hydraulics Division*, ASCE, Vol. 98, No. HY1, Proc. Paper 8642, Jan., 1972, pp. 123–135.
27. Ravindra, M. K., Heaney, A. C., and Lind, N. C., "Probabilistic Evaluation of Safety Factors, Final Report," presented at the 1969, Symposium on Concepts of Safety of Structures and Methods of Design, International Association for Bridge and Structural Engineering, held at London, England.
28. Rodriguez-Iturbe, I., and Vicens, G. I., "On the Combined Use of Regional and Historical Hydrologic Information," presented at the Dec., 1974, Fall Annual Meeting, American Geophysical Union, held at San Francisco, Calif.
29. Szepessy, I., "Investigation of the Time of Occurrence of Failure Phenomena Along Levees," (in Hungarian), Report of the Research Institute of Water Resources Development, Budapest, Hungary, 1973.
30. Szidarovszky, F., Duckstein, L., and Bogardi, I., "Levee System Reliability Along a Confluence Reach," *Journal of the Engineering Mechanics Division*, ASCE, Vol. 101, No. EM5, Proc. Paper 11621, Oct., 1975, pp. 609–622.
31. Szidarovszky, F., Duckstein, L., and Bogardi, I., "A Stochastic Model of Levee Failure," *Mathematical Models for Environmental Problems*, C. A. Brebbia, ed., Pentech Press, London, England, 1976, pp. 129–141.

32. Szidarovszky, F., and Yakowitz, S., "Analysis of Flooding for an Open Channel Subject to Random Inflow and Blockage," *Journal of Hydrological Sciences*, Vol. 3, No. 3-4, 1976, pp. 93–103.
33. Szidarovszky, F., Bogardi, I., Duckstein, L., and Davis, D., "Economic Uncertainties in Water Resources Project Design," *Water Resources Research*, Vol. 12, No. 4, Aug., 1976, pp. 573–580.
34. Turnbull, W. J., and Mansur, C. I., "Investigation of Underseepage—Mississippi River Levees," *Journal of the Soil Mechanics and Foundations Division*, Vol. 85, No. SM4, Proc. Paper 2217, Aug., 1959, pp. 129–159.
35. Vicens, J. G., Rodriguez-Iturbe, I., and Schaake, Jr., J. C., "A Bayesian Framework for the Use of Regional Information in Hydrology," *Water Resources Research*, Vol. 11, No. 3, June, 1975, pp. 405–414.
36. Vizugyi Kozlemenyek, (Hydraulic Engineering) "Tisza Valley Flood 1970," Special number in Hungarian with English summaries, Budapest, Hungary, 1971.

Appendix II.—Notation

The following symbols are used in this paper:

a_k, b_k, c_k = regression coefficients;
a_0 = parameters of f estimated from sample;
D = sample standard deviation;
DF = (cumulative) distribution function;
$E(\cdot)$ = expected value;
F = DF;
f = joint pdf of $(\underline{h}, \underline{w})$ and $(\underline{h}, \underline{H})$;
g = acceleration of gravity;
$\underline{H}$ = stage at end of backwater curve;
$\underline{H}_1$ = resistance against overtopping;
$\underline{H}_2$ = resistance against sand boiling or subsoil failure;
$\underline{H}_3$ = lower threshold water level for slope failure;
$\underline{h}$ = peak flood level and stage at beginning of backwater curve;
i = sample element index;
K = water carrying capacity;
k = cross section index;
M = sample mean;
m = number of sample elements;
n = number of cross sections;
P = probability of event;
P_F = probability of failure;
pdf = probability density function;
Q = discharge in tributary;
$R = 1 - P_F$ = reliability;
T = boundary in plane $(\underline{h}, \underline{H})$;
t = time;
$\bar{u}$ = mean velocity;
$\underline{W}_3$ = resistance against slope failure;
$\underline{w}$ = flood exposure;
x = horizontal distance;
$\underline{z}$ = wave height and run-up;
Z = levee height;

z = water level;
ϵ = error term;
Φ = distribution function of standard normal distribution;
ϕ = pdf of standard normal distribution;
$\cup$ = union of sets;
$\cap$ = intersection of sets; and
$\sim$ = random variable.

RELIABILITY OF UNDERGROUND FLOOD CONTROL SYSTEM

By Lucien Duckstein,[1] Istvan Bogardi,[2] and Ferenc Szidarovszky[3]

INTRODUCTION

The reliability model of an underground hydraulic engineering system is presented. Specifically, the case of a system designed to protect underground spaces (such as mines) against inflows or inrushes is considered. This paper may be viewed as a complement of the companion paper (5), which deals with reliability models of surface hydraulic systems. In that paper, a brief review of approaches to reliability investigations of civil engineering structures is given. A more thorough review of the reliability of complex systems may be found in Ref. 9. The importance of investigating risk and reliability at the design stage has been pointed out in Ref. 13.

Mining operations, construction of underground spaces such as subways, tunnels, must often be undertaken under water hazard. In case of karstic aquifers, the forecasting of inflows or inrushes into the underground spaces can only be given in a statistical sense (1) since the fault structure of the aquifer exhibits random variations. If the underground space to be constructed or operated is located under karstic water level, some inflow control, called heretofore an underground flood control system, should be provided. The elements of this system are the drainage equipment, artificial sealing facilities, the water conveyance, sediment settling and removal equipment, and the pumping station(s). Since the system load and also its resistance or capacity are likely to be stochastic, methods for estimating system reliability will be used.

Kesseru (8) has pointed out the necessity of using reliability theory in mine water control systems in Hungary, where mining operations generally take place under water hazard.

[1]Prof., Dept. of Systems and Industrial Engrg., Univ. of Arizona, Tucson, Ariz. 85721.
[2]Sr. Systems Analyst, Mining Development Inst., 1037 Budapest III, Mikoviny u. 2-4, Hungary.
[3]Prof., Dept. of Computer Sciences, Univ. of Agric., H-1113 Budapest XI, Villanyi ut 29-35, Hungary.

Note.—Discussion open until December 1, 1981. Separate discussions should be submitted for the individual papers in this symposium. To extend the closing date one month, a written request must be filed with the Manager of Technical and Professional Publications, ASCE. Manuscript was submitted for review for possible publication on March 9, 1981. This paper is part of the Journal of the Hydraulics Division, Proceedings of the American Society of Civil Engineers, ©ASCE, Vol. 107, No. HY5, July, 1981. ISSN 0044-796X/81/0007-0817/$01.00.

It is appropriate to distinguish between the analyses for protection of human life and for protection of the facilities of a mine. In this paper, only the protection of facilities is considered; in other words, equipment and structures for life protection, such as rescue routes, are outside of the scope of the present reliability analysis.

In summary, an estimate will be found for the probability that the underground flood control system fulfills its facility protection task within a given time interval.

Problem Description

As a case study, a commonly used protection system against karstic water hazard has been selected. The structure of this system, which is shown in Fig. 1, is composed of six principal elements: (1) Protection of faces; (2) water cut of faces; (3) block water cut; (4) mine water cut; (5) sediment settler and removal equipment; and (6) central pumping station. The protection of faces (element 1) against inrushes can be effected in several ways, such as grouting,

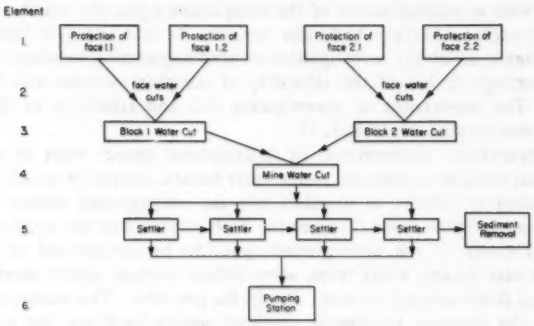

FIG. 1.—Elements of Underground Flood Control System

the "INSTANTAN" protection method, which provokes inrushes before full-mining scale starts (7), or else, preliminary or posterior sealing. Water collected or drained in the faces is conveyed through water cuts (element 2) to the block water cut (element 3). In other systems there may be special sediment settlers and booster pumps in every block, but gravitational conveyance of water and sediment is predominant in recently designed facilities. Water and sediment from block water cuts travel to the mine water cut (element 4) which leads to the central sediment settler (element 5), and the central pumping station (element 6). Sediment is removed from the settler by special equipment and pumped to the surface by hydraulic means. The number of faces and blocks increases as the exploitation of the mine proceeds; the amount of inrushes and sediment also increases as new underground spaces are opened. There are several uncertainties in the estimation of the load, i.e., the amount of water and sediment to be removed by the control system. A stochastic model developed earlier (1) is used to estimate the statistical characteristics of inflow quantities

which constitute the input for the reliability analysis. This stochastic model is summarized in the next section for ease of reference.

Reliability Model

System Failure Events.—The failure of an underground flood control system can be caused by a complex set of natural and engineering factors. It is necessary to single out those failure events which are critical as far as the design and operation is concerned. More precisely, "disturbance of operation" and "flooding" are distinguished. The disturbance of operation corresponds to a failure event which disrupts or decreases mining production but does not stop it. On the other hand, flooding is defined as a failure which stops production altogether. Depending on the location of the failure, the following top events are defined: (1) Disturbance of operation because of flooding in faces; (2) disturbance of operation because of flooding in blocks; (3) disturbance of operation in the mine with simultaneous disturbances in several blocks; and (4) flooding of mines. In the next section, the stochastic model of loading due to inrush events is summarized.

System Load.—System loading as a result of inrushes can be characterized by the following three quantities: (1) $\underset{\sim}{q}$ = magnitude or yield of inrush events; (2) $q_{\max}$ = maximum inrush event yield over area A; and (3) $\underset{\sim}{Q}(A)$ = total yield of inrush events over area A. The pdf of these variates can be estimated as follows (1).

1. Yield of inrush events.—In a reasonable hypothesis based on physical reasoning $\underset{\sim}{q}$ follows a lognormal distribution. Observation data tend to support this assumption.

2. Maximum inrush event yield over area A.—Let $\underset{\sim}{N}(A)$, the number of inrush events occurring over an area A, follow a Poisson distribution with mean λA, which is a second hypothesis based on phenomenological reasoning and supported by observation data. Then the distribution of $q_{\max}$ is derived from the distributions of $\underset{\sim}{N}(A)$ and $\underset{\sim}{q}$ as follows:

$$P(\underset{\sim}{q}_{\max} \leq x) = F_{q_{\max}}(x) = \exp\left[-\lambda A\,(1 - F_{\underset{\sim}{q}}(x))\right] \quad \ldots\ldots\ldots\ldots\ldots\ldots (1)$$

3. Total yield of inrush events $\underset{\sim}{Q}(A)$.—The total yield for area A is the sum of inrush event yields, and is thus calculated as the sum of a Poisson number $\underset{\sim}{N}$ of lognormal inrushes $\underset{\sim}{q}$

$$\underset{\sim}{Q}(A) = \sum_{i=1}^{\underset{\sim}{N}(A)} \underset{\sim}{q}(i) \quad \ldots\ldots\ldots\ldots\ldots\ldots\ldots\ldots\ldots\ldots\ldots\ldots\ldots\ldots (2)$$

The DF of $\underset{\sim}{Q}$ must be determined from the DF of $\underset{\sim}{q}$ and $\underset{\sim}{N}$, since direct observation data on $\underset{\sim}{Q}$ are rarely available. There are three possible approaches to estimate the stochastic properties of $\underset{\sim}{Q}$: the analytic method, the first-order analysis and the simulation method.

The analytic method is straightforward but fraught with numerical difficulties. The first-order analysis consists essentially in calculating directly the expected value and variance of $\underset{\sim}{Q}$, but leads to large errors of estimation of small

probabilities. Thus, as stated in Ref. 1, a simulation method such as the one used in Ref. 11 appears to provide the only practical method to estimate the pdf of $\underset{\sim}{Q}$. The statistical dependence in space of inrush events should be examined as shown in Ref. 1.

The yield of inrush events can be controlled by various methods such as sealing, grouting, and freezing (10). In fact, element 1 of the system, the protection of faces, includes such yield control. The impact of the control method on inrush yield should be considered in the reliability analysis. A decision rule or impact function expressing the effect of control strategy on a given inrush can be defined as:

$$\underset{\sim}{q}'_{ij} = f_{ij}(\underset{\sim}{q}_{ij}, a_{1ij}, a_{2ij}, a_{3ij}) \quad \ldots\ldots\ldots\ldots\ldots\ldots\ldots\ldots\ldots\ldots\ldots\ldots (3)$$

in which $\underset{\sim}{q}'_{ij}$ = controlled yield of inrush in face (i,j); $f_{ij}(\cdot)$ = impact function in face (i,j); $\underset{\sim}{q}_{ij}$ = natural yield of event; and a_{1ij}, a_{2ij}, a_{3ij} = parameters of the impact function.

As an example, consider the control method of sealing with a decision rule as follows:

1. If $\underset{\sim}{q}_{ij} < a_{1ij}$ do not seal; then $\underset{\sim}{q}'_{ij} = q_{ij}$.
2. If $a_{1ij} < \underset{\sim}{q}_{ij} < a_{3ij}$ seal a portion of the inrush yield: $\underset{\sim}{q}'_{ij} = a_{2ij}\,\underset{\sim}{q}_{ij}$.
3. If $\underset{\sim}{q} > a_{3ij}$ seal the total inrush: $\underset{\sim}{q}'_{ij} = 0$.

The impact function is considered in the following reliability model although notation $\underset{\sim}{q}'$ is not used. Also, uncertainty of the control can be accounted for by introducing a random error with a known distribution into the impact function.

To sum up, the calculation of system loading, based on a stochastic model, leads to the calculation of the DF of inrush yield, the DF of the maximum yield of inrushes, and that of the total yield of inrushes. The effect of the decision rule of control on the inrush yield can be accounted for by an impact function having three parameters.

Simulation which appears to be a practical method for implementing the model, calculates the block yield of inrushes, given block i with number n of faces, as:

$$\underset{\sim}{Q}_i = \sum_{j=1}^{n} \underset{\sim}{Q}(A_{ij}) \quad \ldots\ldots\ldots\ldots\ldots\ldots\ldots\ldots\ldots\ldots\ldots\ldots (4)$$

in which $\underset{\sim}{Q}(A_{ij})$ = the total yield of inrushes for face (i,j), characterized by $\mu(\underset{\sim}{q}_{ij})$, $s^2(\underset{\sim}{q}_{ij})$, λ_{ij}; and A_{ij}.

Similarly, the total yield of inrushes for a mine having m blocks is:

$$\underset{\sim}{Q}^* = \sum_{i=1}^{m} \underset{\sim}{Q}_i \quad \ldots\ldots\ldots\ldots\ldots\ldots\ldots\ldots\ldots\ldots\ldots\ldots (5)$$

Reliability Calculation.—Reliability models for each event defined in the section "Systems Failure Events" is given in Ref. 3. As an example, the reliability of mine flooding is now calculated. Flooding of the mine occurs when any of the following six events occurs:

1. Event E.—There is flooding in every block of the mine:

$$E: \quad D_1 \cap D_2 \cap \ldots \cap D_i \cap \ldots \cap D_m \quad \ldots \ldots \ldots \ldots \ldots \ldots \ldots \ldots \quad (6)$$

in which $D_i = (\underset{\sim}{Q}_i > a_i)$ = the event of flooding in block i; Cv_i is the capacity of block water cut (element 3).

2. Event F.—The sediment removal capacity CH of the mine is smaller than the maximum amount of sediment inrush $\underset{\sim}{s}$. Empirical evidence shows that a linear statistic relationship between this sediment volume and the yield $\underset{\sim}{q}_{max}$ may be assumed:

$$\underset{\sim}{s} = \max_{ij} (k_0 \underset{\sim}{q}_{max_{ij}} + \underset{\sim}{\epsilon}) \quad \ldots \ldots \ldots \ldots \ldots \ldots \ldots \ldots \ldots \ldots \quad (7)$$

in which k_0 = a specific sediment yield (in tons of sediment per cubic meter of water); and $\underset{\sim}{\epsilon}$ = an error term assumed to be distributed normally

$$F: \quad (\underset{\sim}{s} > CH) \quad \ldots \ldots \ldots \ldots \ldots \ldots \ldots \ldots \ldots \ldots \quad (8)$$

3. Event FR.—A failure of the mine sediment removal equipment occurs:

$$FR: \quad (\underset{\sim}{\beta} < t) \quad \ldots \ldots \ldots \ldots \ldots \ldots \ldots \ldots \ldots \ldots \quad (9)$$

in which $\underset{\sim}{\beta}$ = the first failure time of the mine sediment removal equipment;

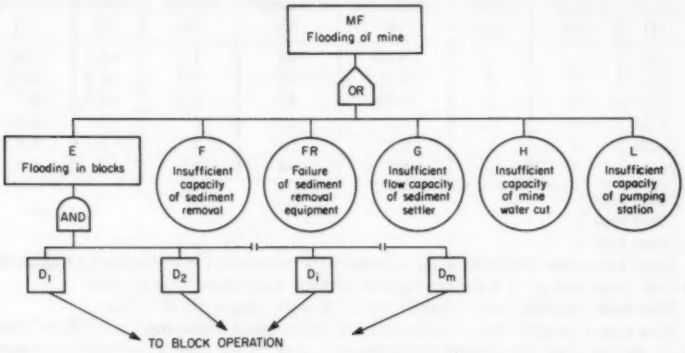

FIG. 2.—Failure Tree for Mine Flooding

and t = the time considered. The variable $\underset{\sim}{\beta}$ is an exponential variate which is characterized by λ_2, the average number of failures within unit time interval.

4. Event G.—The total yield of mine inrushes, $\underset{\sim}{Q}^*$, is greater than the capacity CQ of the central sediment settler (element 5):

$$G: \quad (\underset{\sim}{Q}^* > CQ) \quad \ldots \ldots \ldots \ldots \ldots \ldots \ldots \ldots \ldots \ldots \quad (10)$$

5. Event H.—The total mine water yield, $\underset{\sim}{Q}^*$, is larger than the capacity CV of the mine water cut (element 4):

$$H: \quad (\underset{\sim}{Q}^* > CV) \quad \ldots \ldots \ldots \ldots \ldots \ldots \ldots \ldots \ldots \ldots \quad (11)$$

6. Event L.—The actual capacity $\underset{\sim}{y}$ of the central pumping station (element 6) is smaller than the total yield of mine water, $\underset{\sim}{Q}^*$:

L: $(\underset{\sim}{y} < \underset{\sim}{Q}^*)$ . . . . . (12)

This event may be caused by an excessive flooding in the mine, or failure of some of the pumps; in either case the real capacity, $\underset{\sim}{y}$ of the pumping station decreases. The pump failure event is assumed to be exponentially distributed with parameter λ_3 (the average failure rate of one pump). The number of pumps remaining in operation is a binomially distributed variate and $\underset{\sim}{y}$ is the product of this binomial variate and the nominal capacity of one pump.

TABLE 1.—Data for Estimation of System Reliability Mine Mányi, Hungary

Time period, in years[a] (1)	Number of blocks[b] (2)	Number of faces in block[b] (3)	Area of a face, A, in square kilometers[a] (4)	Specific number of inrushes, λ, per square kilometer[c] (5)	DATA ON INRUSH EVENTS[c]		
					Average yield, in cubic meters per minute (6)	Statistics of Lognormal Distribution	
						In meters (7)	In seconds (8)
0–2	1	1	0.10	40	1.2	−0.3	0.64
2–3	2	2	0.15	40	1.2	−0.3	0.64
3–6	4	2	0.25	40	1.2	−0.3	0.8
6–16	5	2	0.6	60	2	0	0.8
16–26	5	2	0.6	60	2	0	0.8
26–30	5	1	0.2	40	2	0	0.8

[a]Data type 1.
[b]Data type 2.
[c]Data type 3.

Note: Data type 4 includes $q_0(0)$ = inrush yield threshold for disturbance of operation = 5 m^3/min; and cf_0 = water conveyance capacity from faces = 60 m^3/min.

Data type 5 includes Cv_i = capacity of block water cuts = 550 m^3/min.

Data type 6 includes Q_{kM} = maximum amount of block water (Eq. 5) = 180 m^3/min; k_0 = specific yield of sediment = 0.1 ton/m^3; $S^2(\xi)$ = variance of sediment estimation = 0; CH = sediment removal capacity = 3 tons/min; CQ = water capacity of the control sediment settler = 170 m^3/min; CV = water conveyance capacity of the mine water cut = 550 m^3/min; n = number of pumps = 16; C = nominal capacity of a pump = 11 m^3/min; λ_2 = specific number of failures of a pump: 0.11/yr; λ_3 = specific number of failures of the sediment removal equipment = 0.03/yr; and ΣQ_{kM} = maximum total amount of mine water 300 m^3/min.

Since all possible failure events have been defined, the event MF of mine flooding can be written as:

MF: $E \cup F \cup FR \cup G \cup H \cup L$ . . . . . (13)

The failure-tree of mine flooding is shown in Fig. 2.

The probabilities of failure events are estimated by a Monte Carlo simulation method. Input data for this simulation method should be given according to Table 1.

Numerical Example and Consideration

Let the reliability model be applied to the Manyi mine to be located in the Transdanubian region of Hungary at a depth of 300 m below the karstic water level. Two alternative mine water strategies are considered: the first alternative is the application of "INSTANTAN" protection combined with artificial sealing, while the second alternative consists in a passive control method. Passive control means that inrushes may enter the facilities in which a drainage system has been provided, but added costs emerge as a result of production slowdown.

Fig. 3 shows the effect of the artificial sealing strategy on inrush yield probability. The upper distribution, Fig. 3, (*a*) reflects original inrushes; distributions, Figs. 3 (*b*) and (*c*), refer to two different sealing strengths. Input data

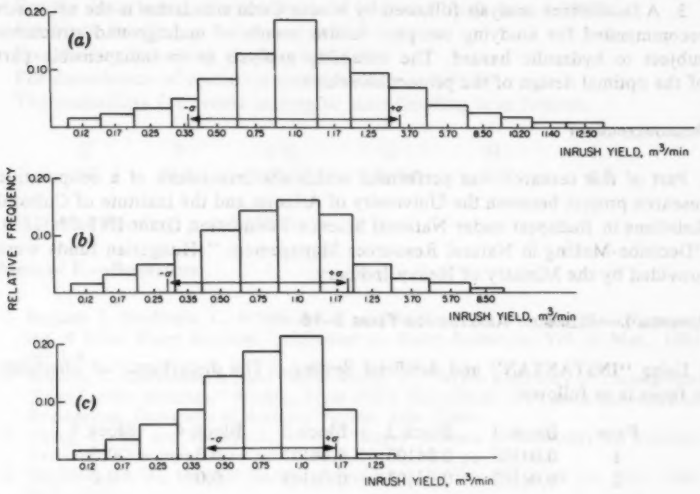

FIG. 3.—Effect of Sealing on Probability Distribution of Inrush Yield: (*a*) No Sealing; (*b*) Moderate Sealing; (*c*) High Sealing

are given in Table 1. Appendix I gives sample simulation results using the indicated protection methods.

Generally speaking, system reliability of engineering structures is very sensitive to the accuracy of loading statistics because the numerical value of reliability is generally found in the upper tail of the distribution, where probability estimates are most uncertain. In the present case, the mean and variance of inrush yields and the specific number of inrushes are parameters that strongly affect the numerical value of reliability. At the same time, these statistics are themselves uncertain, since they are based on regional data, experience or at best small samples. A Bayes approach can be used to account for this parameter uncertainty (2,3,4,12). The use of Bayesian distributions for the pdf of different loading

quantities accounts for the effect of this parameter uncertainty. Another approach would be to establish confidence limits for reliability (6).

The reliability of the systems considered can be augmented in a number of ways, such as redundancy, maintenance, and standby. It is possible to include these factors in the reliability model shown in the present study.

Conclusions and Recommendations

1. To investigate the reliability of underground works such as mines, statistical approximations must be used because of the complexity of the failure phenomenon.
2. Both load and resistance should be considered as random variables: the probability of failure is then a function of the ratio of two random variables.
3. A failure tree analysis followed by Monte Carlo simulation is the approach recommended for studying complex failure events of underground structures subject to hydraulic hazard. The reliability analysis is an indispensible part of the optimal design of the protection scheme.

Acknowledgment

Part of this research was performed within the framework of a cooperative research project between the University of Arizona and the Institute of Cultural Relations in Budapest under National Science Foundation Grant INT 78-12184, "Decision-Making in Natural Resources Management." Hungarian funds were provided by the Ministry of Heavy Industry.

Appendix I.—Reliability Analysis for Years 6–16

Using "INSTANTAN" and Artificial Sealing.—The disturbance of operation in faces is as follows:

Face	Block 1	Block 2	Block 3	Block 4	Block 5
1	0.04103	0.04103	0.04103	0.0	0.0
2	0.04103	0.04103	0.04103	0.0	0.0

For the flooding of faces, the probability, $p = 0.0$ everywhere.

For disturbance of operation in blocks, p is as follows:

Block 1	Block 2	Block 3	Block 4	Block 5
0.00168	0.00168	0.00168	0.0	0.0

For the disturbance of operation in at least one block, $p = 0.00504$.

For block flooding, $p = 0.0$ everywhere.

For flooding in at least one block, $p = 0.0$.

For disturbance of operation in the mine, $p = 0.00001$.

The probabilities for events leading to mine flooding is as follows:

E	F	FR	G	H	L
0.0	0.0	0.24270	0.0	0.0	0.0

For mine flooding, $p = 0.24270$.

Using Passive Protection in Faces.—The disturbance of operation in faces is as follows:

Face	Block 1	Block 2	Block 3	Block 4	Block 5
1	0.99904	0.99904	0.99904	0.54905	0.54905
2	0.99904	0.99904	0.99904	0.54905	0.54905

For the flooding of faces, $p = 0$ everywhere.
For the disturbance of operation in blocks:

Block 1	Block 2	Block 3	Block 4	Block 5
0.99809	0.99809	0.99809	0.30146	0.30146

For the disturbance of operation in at least one block, $p = 1.00000$.
For block flooding, $p = 0.0$ everywhere.
For flooding in at least one block, $p = 0.0$.
For disturbance of operation in the mine, $p = 0.99999$.
The probability for events leading to mine flooding is as follows:

E	F	FR	G	H	L
0.0	0.0	0.24270	1.00000	0.0	0.0

For mine flooding, $p = 1.00000$.

Appendix II.—References

1. Bogardi, I., Duckstein, L., Schmieder, A., and Szidarovszky, F., "Stochastic Forecasting of Mine Water Inrushes," *Advances in Water Resources*, Vol. 3, Mar., 1980, pp. 3–8.
2. Bogardi, I., Duckstein, L., and Szidarovszky, F., "Bayes Reliability of Underground Water Control Systems," *Working Paper #80-6*, Department of Systems and Industrial Engineering, University of Arizona, Tucson, Ariz., 1980.
3. Chang, E. Y., and Thompson, W. E., "Bayes Analysis of Reliability for Complex Systems," *Operations Research*, Vol. 24, No. 1, 1976, pp. 156–168.
4. De Groot, M. H., *Optimal Statistical Decisions*, McGraw-Hill Book Co., New York, N.Y., 1970.
5. Duckstein, L., and Bogardi, I., "Application of Reliability Theory to Hydraulic Engineering Design," *Journal of the Hydraulics Division*, ASCE, Vol. 107, No. HY7, Proc. Paper 16380, July, 1981, pp. 799–815.
6. Easterling, R. G. "Approximate Confidence Limits for System Reliability," *JASA*, Vol. 67, 1972, pp. 220–222.
7. Kapolyi, L., "New Trends in Mine Water Protection," *VII International Conference on Mine Water Protection*, Vol. 1, Budapest, Hungary, 1976.
8. Kesseru, Zs., "Some Remarks on Mining Decision Analysis," *Mining and Metallurgical Journal*, (in Hungarian) Vol. 101, No. 3, 1968.
9. Metler, W., "The Estimation of Large Scale Complex System Reliability," dissertation presented to the University of Arizona, at Tucson, Ariz., in 1980 in partial fulfillment for the degree of Doctor of Philosophy.
10. Schmieder, A., Kesseru, Zs., Juhasz, J., Willems, T., and Martos, F., *Water Hazard and Water Management in Mining* (in Hungarian), Muszaki Konyvkiado, Budapest, Hungary, 1975.
11. Szidarovszky, F., Duckstein, L., and Bogardi, I., "A Stochastic Model of Levee Failure," *Mathematical Models for Environmental Problems*, C. A. Brebbia, ed., Pentech Press, London, England, 1976, pp. 129–141.

12. Vicens, J. G., Rodriguez-Iturbe, I., and Schaake, Jr., J. C., "A Bayesian Framework for the Use of Regional Information in Hydrology," *Water Resources Research*, Vol. 11, No. 3, June, 1975, pp. 405–414.
13. Yevjevich, V., "Systematization of Flood Control Measures," *Journal of the Hydraulics Division*, ASCE, Vol. 100, No. HY11, Proc. Paper 10943, Nov., 1974, pp. 1537–1548.

Appendix III.—Notation

The following symbols are used in this paper:

A = area;
$\underline{a}$ = parameters of f;
a_1, a_2, a_3 = parameters of impact function;
a_0 = parameters of f estimated from sample;
CH = sediment removal capacity;
CQ = sediment settler capacity;
CV = capacity of mine water cut;
D = sample standard deviation;
D_i = flooding event in block i;
DF = (cumulative) distribution function;
E = flooding event in every block;
$E(\cdot)$ = expected value;
F = event element of mine flooding;
$F(\cdot)$ = DF;
FR = failure event of sediment removal;
f_{ij} = impact function in face (i,j);
G = event element of mine flooding;
$\underline{H}$ = event element of mine flooding;
i = sample element index;
k_0 = specific sediment yield;
L = event element of mine flooding;
M = sample mean;
MF = event of mine flooding;
m = number of sample elements or number of mining blocks;
n = number of cross sections or subreaches or mining faces;
P = probability of event;
P_F = probability of failure;
p = pdf of $\underline{a}$;
pdf = probability density function;
Q = total yield of inrush events;
q = yield of inrush event;
q' = yield of controlled inrush event;
$q_{\max}$ = maximum yield of inrush events;
$R = 1 - P_F$ = reliability;
$\underline{s}$ = amount of sediment inflow;
T = failure event;
t = time;
y = capacity of pumping station;
z = water level;

β = first failure time;
$\underset{\sim}{\varepsilon}$ = error term;
λ = specific number of inrush events;
λ_2 = average failure rate of sediment removal equipment;
λ_3 = average failure rate of one pump; and
$\underset{\sim}{\cdot}$ = random variable.

MODELING GRADUAL DAM BREACHES

By Victor Miguel Ponce,[1] M. ASCE and Andrew J. Tsivoglou,[2] A. M. ASCE

INTRODUCTION

There are approx 50,000 dams in the United States, 40% of which have been classified as potentially dangerous to life and property in the event of a failure (23). The majority of these dams are earth embankments, and failure of earth embankments is usually associated with some type of breaching. Despite these impressive statistics, very little is known about the breach itself—its inception, shape, and rate of development.

The few documented earth dam failures have shown one striking common denominator: the failure is anything but sudden. For instance, in the overtopping case a breach will form and grow gradually under the erosive action of the waters. This gradual failure of an earth dam is of particular interest to disaster relief planners, because the rate of growth of the breach strongly influences the peak and shape of the ensuing flood wave. Gradual failure here should be contrasted with the commonly assumed sudden (or instantaneous) failure, although the former probably amounts to only a few hours in most cases.

The objective of this paper is to present a mathematical model of the gradual failure of an earth dam. The main body of the paper contains a review of the pertinent literature and a description of the model formulation. The mathematical model is tested using data from the Huaccoto dam failure, which occurred in central Peru in June, 1974.

At this stage of the model development, the overall objective is to achieve a physically realistic simulation of the gradual failure of an earth embankment caused by an overtopping flood event. To the writers' knowledge, the approach presented herein is the first attempt to attack this problem within the framework of an implicit numerical solution technique. The implicit technique solves for water elevations simultaneously at all cross sections over the full channel length by successive time steps. Principles of unsteady open channel flow, sediment transport mechanics, and channel morphology were successfully combined to simulate the embankment failure. Further model improvements, specifically in the description of the breach morphology will be the subject of additional research.

[1]Assoc. Prof. of Civ. Engrg., San Diego State Univ., San Diego, Calif. 92182.
[2]Hydr. Engr., United States Army Corps of Engineers, Mobile District, Mobile, Ala.

Note.—Discussion open until December 1, 1981. To extend the closing date one month, a written request must be filed with the Manager of Technical and Professional Publications, ASCE. Manuscript was submitted for review for possible publication on September 25, 1980. This paper is part of the Journal of the Hydraulics Division, Proceedings of the American Society of Civil Engineers, ©ASCE, Vol. 107, No. HY7, July, 1981. ISSN 0044-796X/81/0007-0829/$01.00.

Related Studies

Considerable research is available for the case of instantaneous failure of a dam. Reference is made to papers by Ritter (16), Dressler (5), and Whitham (25), to name a few. Instantaneous failure causes a positive wave in the downstream direction and a negative wave in the upstream direction. As evidenced by recent work of Brown and Rogers (1), such an assumption is likely to be far from reality in the case of a gradual breach. In their investigation of the Teton Dam failure, Brown and Rogers documented a control section that formed just upstream of the breach, and described how the reservoir level dropped uniformly upstream of this section, preventing the negative wave from propagating upstream. The duration of the Teton breach was approx 3 h.

Cristofano's work is perhaps the first attempt to simulate the growth of a breach in an earth dam. Using geotechnical principles, Cristofano equated force of water flowing through the breach to resistive shear strength acting on the bottom surface of the overflow channel. Thus, he was able to relate rate of change of erosion to rate of change of water flowing through the overflow channel. This analysis led to an algebraic equation relating amount of eroded material to flow of water through the breach.

Cristofano assumed that the breach top width would remain constant over time, and that the breach would maintain a trapezoidal shape throughout the failure process. In addition, he fixed side slopes of the breach equal to angle of repose of the bank material, and bottom slope of overflow channel equal to angle of friction of bed material. However, the use of an arbitrary constant in Cristofano's formula renders it, in effect, empirical. In spite of this limitation, the formula has been used in preliminary estimates of dam breach potential, as evidenced by TVA (Tennessee Valley Authority) practice (13).

In the late 50's, the United States Army Corps of Engineers Waterways Experiment Station (WES) used physical models to conduct an extensive investigation into floods resulting from suddenly breached dams (21,22). A correlation was found between peak outflow from a suddenly breached dam and a shape factor describing the geometry of the breach. The WES findings support the conclusion that the Froude number based on peak flow would reach a value of 0.29, which verifies the Schoklitsch equation (19) for peak outflow from a sudden dam failure.

The WES findings do not apply to the case of a gradual breach of an earth dam. The experiments were carried out in a laboratory flume of specified bed slope, cross section, and roughness characteristics, and the failure was simulated by an almost instantaneous removal of part or all of the dam. Therefore, while the tests were representative of sudden failure case, the results cannot be associated with gradual failures because the hydraulics of the two cases are in fact quite different.

Prince, et al. (15) of the TVA have reported on models that use the relations for sudden dam breaches developed by WES. They do not apply their models to earth dams, but rather to sudden failure of large gravity dams. Su and Barnes (20) studied geometric and frictional effects of sudden releases, and concluded that both resistance and cross-sectional shape were significant in determining behavior of waves caused by sudden releases.

Brown and Rogers (1) developed a computational model based on earlier

work by Harris and Wagner (9), in which the Schoklitsch formula was used to compute suspended sediment. They considered the failure of an earth dam immediately upon overtopping, degradation of the breach, and erosion to datum level.

Brown and Rogers make several rather lucid statements regarding the mechanics of breach development. They point out the need for incorporating lateral erosion into the model simulation. They also address some of the differences in modes of failure for exceptionally high earth dams as opposed to long, low embankments. In addition, they point out that the bulk of the material eroded from the breach is deposited almost immediately downstream of the dam, thus affecting tailwater depths and outflow hydrograph.

Fread (7) has substantially contributed to modeling of dam breach phenomena in recent years. His doctoral dissertation dealt with a dam breach model which used the method of characteristics as its numerical solution scheme. The most current version of Fread's model uses the four-point implicit finite difference scheme (8).

Fread assumes the rate of growth of the breach to be time-dependent, with either rectangular, triangular, or trapezoidal shape. He accomplishes this by considering vertical erosion to take place at a constant, predetermined rate. This assumption is convenient because it allows the time scale of the phenomena to be fixed *a priori*. However, it renders the model incapable of predicting the breach-induced flood wave properties. It can produce a range of flood events for a given range of vertical erosion rates, but which flood event is likely to occur is not discernible. Fread does indicate that the outflow hydrograph is extremely sensitive to the chosen rate of vertical erosion, but assumes any errors in prediction to be dampened as the sharp wave moves downstream.

Fread's main concern is the downstream valley routing of the flood wave from a breached earth dam, which is the ultimate goal of any investigation of potential dam breaches. However, it should be emphasized that rate of erosion and mode of failure of dam determine to a large extent the shape and duration of the flood wave. Until this mechanism is better understood and properly described by mathematical modeling, Fread's approach can be considered only as an approximation giving a range of probable events.

For a useful description of dam incidents in the United States, reference is made to an ASCE-USCOLD publication (24). This report contains a well documented chronological listing of dam incidents involving major dams dating back to the late 1800's. In striking contrast to the general concern for dam safety, this book actually documents a superb safety record for United States dams.

Theoretical Development

The model described herein has five major components: (1) Numerical scheme; (2) channel resistance; (3) sediment routing; (4) breach morphology; and (5) initial and boundary conditions.

Numerical Scheme.—Extensive literature on unsteady flow and numerical models justifies using an implicit solution of the dynamic wave to simulate a gradual breach. The rate of rise of the outflow hydrograph is fast compared with the usual stream channel flood waves. Therefore, its adequate description

should consider the inertia terms in the equation of motion, i.e., a dynamic wave model.

The four-point implicit scheme, also referred to as Preissmann's scheme (11), is used in the simulation. In theory, this scheme is unconditionally stable. In practice, however, it is often necessary to introduce a weighting factor to damp out disturbances of the same scale as the grid size. In addition, proper specification of initial and boundary conditions is crucial to the stability and convergence of the numerical solution. The success of the Preissmann scheme is well documented in the literature.

Channel Resistance.—No closed form expression for channel resistance is available, and empirical equations continue to be used in practice. These equations have been derived for equilibrium flow conditions, and their application to unsteady flow is justified on practical grounds.

The model uses the Manning equation to describe the resistance of the channel bottom. For simplicity, the Manning coefficient is kept invariant in time and space. An improvement which may hold some promise is to relate the resistance coefficient to the hydraulic and sediment characteristics of the overflow channel.

Sediment Routing.—The sediment routing component has two major features: (1) Numerical solution of the sediment continuity equation (the Exner equation); and (2) computation of bed material transport using a bedload formula suitable for application to high Froude number flows. In this particular application, the time scale of water and sediment waves is likely to be the same because the channel bed changes are taking place at a rate comparable to the changes in water surface elevation. Therefore, the same time step is used for water and sediment routing.

The choice of a suitable bed load function applicable to high Froude number flows remains primarily one of computational convenience. Phenomenological models such as that of Einstein (6) are attractive, considering the physical detail that can be incorporated into the simulation. However, the complexity and associated expense of these models is a definite limitation. On practical grounds, a simpler and yet reliable equation such as that of Meyer-Peter and Müller was selected. This equation can be expressed as follows:

$$q_s = a(\tau - \tau_c)^b \quad \ldots \quad (1)$$

in which q_s = bed material transport rate by weight, per unit of channel width; τ = bottom shear stress; τ_c = critical shear stress (shear stress at incipient motion); and a and b = coefficient and exponent, respectively. A value of $b = 1.5$ is widely recognized in connection with high Froude number flows, while the value of a is based on experience.

The bottom shear stress is expressed by the following formula:

$$\tau = \gamma d S_f \quad \ldots \quad (2)$$

in which γ = density of water; d = flow depth; and S_f = friction slope. The critical shear stress is expressed as follows:

$$\tau_c = 0.047(\gamma_s - \gamma) D_{50} \quad \ldots \quad (3)$$

in which γ_s = density of solids; and D_{50} = median grain size of solid particles. For steep slopes and high sediment transport rates such as in the dam breach case, the bottom shear stress is likely to be several orders of magnitude larger

than the critical shear stress. Therefore, Eq. 1 can be simplified to the following:

$$q_s = a\tau^{1.5} \quad \ldots \quad (4)$$

Breach Morphology.—The model includes a component to tie the cross-sectional geometry of the breach to the outflow from the failing dam. This relation must function as an additional degree of freedom to represent the vertical and lateral development of the breach in a physically realistic way. At its present stage of development, the breach morphology component consists of a relation between top width and flow rate. The existence of such a relation is rooted in the work on regime channels. It is used here for nonequilibrium channels for lack of a rigorous theory of breach morphology. This aspect of the modeling can be readily improved as additional research helps clarify the governing morphological principles. The recent works of Parker (14) and Chang (3) are important steps in this direction.

Initial and Boundary Conditions.—Correct specification of initial and boundary conditions is a crucial aspect of modeling. Computational convenience dictates that initial values of hydraulic variables be finite, i.e., nonzero. Therefore, a small but finite flow is specified as initial condition on the downstream side of the dam. Hydraulic conditions are determined using steady flow principles.

The upstream boundary condition is the reservoir water surface level. In addition, the elevation of the top of dam is specified. Outflow at start of the computation is a function of the specified size of the rivulet. Progressive erosion widens and deepens the rivulet, increasing outflow and erosion rate in a self-generating manner. The upper cross section on the sloping downstream face "creeps" upstream across the dam top until it reaches the upstream face, whereby rate of flow and erosion increase at a faster rate.

If outflow increases enough to lower the reservoir level faster than the channel bed erodes, both outflow and erosion gradually diminish. Of course, outflow will eventually decrease even if the breach bed erodes all the way down to the stream bed. This mode of failure creates the outflow hydrograph in the shape of a sharp but nevertheless gradual flood wave.

Model Description

The mathematical model assumes an overtopping failure of an earth embankment, whereby a breach begins to grow at some low or weak point of the crest and downstream face. This is a likely form of small embankment failure. The actual task of modeling by computational means can be quite demanding. Many calculations must be assembled in a logical and stable framework to achieve a workable numerical solution.

The model has the following major parts: (1) Input data and initial conditions; (2) cross-sectional characteristics; (3) matrix coefficients and double sweep solution; (4) breach geometry descriptor; (5) sediment transport; and (6) reservoir routing. The model simulates spatial and temporal variations of hydraulic and cross-sectional characteristics along the breach channel, from inception until either the reservoir has drained completely or the breach has stopped eroding. Additional details on the various parts of the mathematical model are given in the following.

Input Data and Initial Conditions.—Subroutines are used to input data such

as initial area, width, depth and flow rate; dam and breach geometry; soil characteristics; roughness coefficients; spatial and temporal resolution; etc.

Cross-Sectional Characteristics.—The cross-sectional characteristics are described by the following algebraic relations:

$$y = \alpha A^{\beta} \quad \ldots \quad (5)$$

and $$P = a_1 A^{b_1} \quad \ldots \quad (6)$$

in which y = stage; A = cross-sectional area; P = wetted perimeter; and α and a_1, β and b_1 are coefficients and exponents, respectively. A least square fit is used to determine the coefficients and exponents of Eqs. 5 and 6 as a function of distance (along the breach channel) and time (achieved by updating the cross-sectional parameters after every time step).

Matrix Coefficients and Double Sweep Solution.—These model components calculate the coefficients of the discretized Saint Venant equations and solve the resulting matrix by the double sweep solution technique. For a detailed treatment of the discretization following the Preissmann scheme, reference is made to Liggett and Cunge (11).

Breach Geometry Descriptor.—To properly describe the gradual breaching of an earth dam, the geometry of the breach must be related to the hydraulics of the flow and bed material properties. According to Johnson and Illes (10), the breach geometry is directly related to the duration and shape of the overtopping flood wave. They state that the typical breach is between one and three times as wide as it is deep. However, no documented research exists to relate breach geometry to breach hydraulics. For the sake of simplicity, the writers initially assumed the breach top width to remain constant. After a stable and physically realistic simulation was achieved, the constant width assumption was relaxed, and instead, a relation between the breach width and flow rate was specified. This relation was applied from inception to peak flow, after which the breach width was kept constant and equal to the peak flow width.

This descriptor of breach geometry provided satisfactory results and allowed greater flexibility and an altogether better simulation. Future model upgrading should focus on identifying the underlying erosional mechanisms and incorporating them into the simulation scheme.

Sediment Transport.—The model uses the equation of sediment continuity (the Exner equation) to describe the erosive processes at the channel bed. The Exner equation is given as follows:

$$\frac{\partial Q_s}{\partial x} + (1-p)\gamma_s B \frac{\partial z}{\partial t} = 0 \quad \ldots \quad (7)$$

in which Q_s = sediment transport rate, by weight; p = porosity of material forming the bed; B = average channel width; and z = bed elevation. Eq. 7 enables the calculation of change in bed elevation as a function of prevailing sediment transport rate and bed material properties.

To describe sediment transport rate, the Meyer-Peter and Müller equation is used. On this basis, a simple yet reliable relation between sediment transport rate and mean velocity can be postulated. Consequently, breach erosion rate can be related to breach hydraulics.

Reservoir Routing.—This model component determines the upstream boundary

condition, i.e., the upstream stage and flow depth. This is accomplished by computing the rise/drop in reservoir level within one time step as follows:

$$\Delta H = \frac{(Q_{out} - Q_{in})\,\Delta t}{A_n} \quad \ldots\ldots\ldots\ldots\ldots\ldots\ldots\ldots\ldots\ldots\ldots\ldots\ldots\ldots (8)$$

in which ΔH = rise/drop in reservoir level from time level n to time level $n + 1$; Q_{out} = flow rate at upstream section of breach at time level n; Q_{in} = inflow to the reservoir at time level n; Δt = time step; and A_n = reservoir surface area at time level n. Eq. 8 amounts to a local linearization of the upstream boundary condition; its accuracy is contingent upon its use with reasonably small time steps.

The aforementioned upstream boundary condition computed as indicated provides the mechanism that triggers the development of the breach. As the upstream flow depth increases, the flow rate and velocity also increase, leading to the breach enlargement. The process is halted when the reservoir is depleted to the point where the upstream flow depth and velocity can no longer sustain any further erosive action.

Case Study: Huaccoto Natural Dam, Peru

The Huaccoto natural dam was formed as a result of a landslide that occurred in Cochacay Creek, a tributary of the Mantaro River in Central Peru, in April, 1974. The embankment created behind it a huge reservoir which took approx 60 days to fill. The failure occurred by overtopping, whereby a breach developed and grew progressively under the erosive action of the waters. The large volume of material encompassing the embankment made this particular failure somewhat unusual—Rodriguez (17) has stated that there was enough material to build an engineered dam about three times as high in the same location. First, the breach did not erode to datum, but rather, erosion stopped when the available water in the reservoir was insufficient to sustain further breach growth. Second, the duration of the failure was approx 48 h, including breach development and reservoir depletion. This is in sharp contrast to documented failure times for engineered dams, which usually take at most a few hours to erode to datum. Of course, the dam thickness, and thus, the amount of material to be eroded

TABLE 1.—Comparison between Estimated Actual and Simulated Flood Characteristics, Huaccoto Dam Failure, June, 1974, Mantaro River, Peru

Description (1)	Estimated actual (2)	Simulated (3)
Peak discharge, in cubic meters per second	13,700	13,200
Maximum crest erosion, in meters	35	37
Maximum flow depths, in meters	15–20	12–22
Time from 0 m^3 s–100 m^3/s, in hours	16	16
Time from 100 m^3/s to peak discharge, in hours	10	10
Hydrograph duration, from 100 m^3/s rising–400 m^3/s receding, in hours	32	34

in an engineered dam would be much less than that of the Huaccoto dam.

The overall characteristics of the Huaccoto embankment and reservoir are (18): (1) Reservoir capacity = 665 millions of m^3; (2) maximum height of embankment = 170 m; (3) lateral length of embankment = 3,800 m; (4) approximate crest elevation = 2,630 m above mean sea level; (5) representative bed material size = 11 mm; and (6) percentage of material finer than 200 sieve size = 15%. These characteristics and other auxiliary data were used to perform a hindcast simulation of the Huaccoto embankment failure. Eleven cross sections were used, each 300 m apart; the simulation was carried on for 72 h using a time step of 5 min. The channel friction, sediment transport, and channel geometry parameters were adjusted within physically realistic bounds.

Table 1 shows a comparison of estimated actual versus simulated flood characteristics. It should be emphasized that the estimated actual values shown are by no means exact, considering the strenuous circumstances under which they were made. The simulated results agree reasonably well with the estimated actual values, further demonstrating the potential of this modeling tool in the assessment of postulated embankment failures.

Summary and Conclusions

A simulation model of the gradual failure of an earth embankment has been formulated, developed, and tested with real-life data. A significant feature of the model is its ability to account for the growth of the breach and the eventual draining of the reservoir behind the embankment. Concepts of water and sediment routing are used in conjunction with a channel geometry descriptor to arrive at a self-contained mathematical model of the breach enlargement and the ensuing flood wave. Unsteady flow elements of the simulation are an implicit numerical solution of the complete Saint Venant equations coupled with a sequential sediment routing technique. This approach provides an increased rational basis for determining outflow hydrographs from postulated earth dam breaches.

The model is tested on the failure of the natural embankment which formed in April, 1974 on the Mantaro River in central Peru, as a result of an earthquake-generated landslide. Agreement between estimated actual and simulated flood characteristics is remarkable, considering the coarseness of the physical detail incorporated at this early stage of model development.

The need for this type of analysis is supported by recent findings of a National Science Foundation-sponsored workshop which convened to delineate priorities in hydraulic and hydrologic research. According to the workshop report (2), government regulations are now requiring that embankments be analyzed against potential failure due to overtopping. At present, such evaluations are primarily based on scant data available from a few documented failures. With mathematical models becoming more widely available, there is a definite trend toward the use of these improved ways of analyzing gradual embankment failures.

Acknowledgments

The writers are indebted to J. D. Salas, who provided the data on the Huaccoto dam failure, and to the anonymous reviewers for their constructive criticism of the original manuscript.

Appendix I.—References

1. Brown, R. J., and Rogers, D. C., "A Simulation of the Hydraulic Events During and Following the Teton Dam Failure," *Proceedings of the Dam-Break Flood Routing Workshop*, Water Resources Council, Oct., 1977.
2. "Research Needs: Hydraulics, Coastal Engineering and Irrigation," *Civil Engineering*, ASCE, Vol. 52, No. 4, Apr., 1980, pp. 83–87.
3. Chang, H. H., "Geometry of Gravel Streams," *Journal of the Hydraulics Division*, ASCE, Vol. 106, No. HY9, Proc. Paper 15678, Sept., 1980, pp. 1443–1456.
4. Cristofano, E. A., "Method of Computing Erosion Rate for Failure of Earthfill Dams," United States Bureau of Reclamation, Denver, Colo., 1965.
5. Dressler, R. F., "Hydraulic Resistance Effects Upon the Dam-Break Functions," *Journal of Research*, National Bureau of Standards, Vol. 49, No. 3, Washington, D.C., 1952, pp. 217–225.
6. Einstein, H. A., "The Bed-Load Function for Sediment Transportation in Open Channel Flow," *Technical Bulletin No. 1026*, United States Department of Agriculture Soil Conservation Service, Washington, D.C., 1950.
7. Fread, D. L., "The Development and Testing of a Dam-Break Flood Forecasting Model," *Proceedings of the Dam-Break Flood Routing Workshop*, Water Resources Council, Oct., 1977.
8. Fread, D. L., "Capabilities of NWS Model to Forecast Flash Floods Caused by Dam Failures," *Proceedings of the Second Conference on Flash Floods*, American Meteorological Society, Mar., 1980.
9. Harris, G. W., and Wagner, D. A., "Outflow from Breached Earth Dams," University of Utah, Salt Lake City, Utah, 1967.
10. Johnson, F. A., and Illes, P., "A Classification of Dam Failures," *Water Power and Dam Construction*, Dec., 1976, pp. 43–45.
11. Liggett, J. A., and Cunge, J. A., "Numerical Methods of Solution of the Unsteady Flow Equations," in *Unsteady Flow in Open Channels*, K. Mahmood and V. Yevyevich, eds., Water Resources Publications, Fort Collins, Colo., 1975.
12. Meyer-Peter E., and Müller, R., "Formulas for Bed Load Transport," *Proceedings, Second Meeting of the International Association for Hydraulic Research*, 1948.
13. Newton, D. W., and Cripe, M. W., "Flood Studies for Safety of TVA Nuclear Plants—Hydrologic Embankment Breaching Analysis," Tennessee Valley Authority, Knoxville, Tenn., Nov., 1973.
14. Parker, G., "Hydraulic Geometry of Active Gravel Beds," *Journal of the Hydraulics Division*, ASCE, Vol. 105, No. HY9, Proc. Paper 14841, Sept., 1979, pp. 1185–1201.
15. Price, J. T., Lowe, G. W., and Garrison, J. M., "Hydraulic Transients Generated by Partial and Total Failure of Large Dams," presented at the Aug., 1974, ASCE Hydraulics Division Specialty Conference, held at Knoxville, Tenn.
16. Ritter, A., "The Propagation of Water Waves," *Ver Deutsch Ingenieure Zeitschr*, Vol. 36, Part 2, No. 33, Berlin, Germany, 1892, pp. 947–954.
17. Rodríguez, R., "Represamiento del Mantaro por el Deslizamiento de Cochacay," *Symposium*, Colegio de Ingenieros del Perú, July, 1974.
18. Salas, J. D., "Modelo Matemático del Proceso de Erosión de la Represa Natural del Mantaro," *Symposium*, Colegio de Ingenieros del Perú, July, 1974.
19. Schoklitsch, A., "Uber Dammbuchwellen," *Sitzber. Akad. Wiss. Wien*. 126, 1917.
20. Su, S., and Barnes, A. H., "Geometric and Frictional Effects on Sudden Releases," *Journal of the Hydraulics Division*, ASCE, Vol. 96, No. HY11, Proc. Paper 7650, Nov., 1970, pp. 2185–2200.
21. "Floods Resulting from Suddenly Breached Dams—Conditions of Minimum Resistance," *Miscellaneous Paper No. 2-374*, Report 1, United States Army Engineer Waterways Experiment Station, Vicksburg, Miss., Feb., 1960.
22. "Floods Resulting from Suddenly Breached Dams—Conditions of High Resistance," *Miscellaneous Paper No. 2-374*, Report 2, United States Army Engineer Waterways Experiment Station, Vicksburg, Miss., Nov., 1961.
23. "National Program of Inspection of Dams," Vol. I–V, United States Army Corps of Engineers, Department of the Army, Office of the Chief of Engineers, Wash., D.C., 1975.

24. "Lessons from Dam Incidents—USA," United States Committee on Large Dams, ASCE/USCOLD Publication, New York, N.Y., 1975.
25. Whitham, G. B., "The Effect of Hydraulic Resistance on the Dam—Break Problem," *Proceedings, Royal Society of London*, No. 1170, Jan., 1955.

Appendix II.—Notation

The following symbols are used in this paper:

A = cross-sectional area;
A_n = reservoir surface area;
a = coefficient, Eqs. 1 and 4;
a_1 = coefficient, Eq. 6;
B = average channel width;
b = exponent, Eq. 1;
b_1 = exponent, Eq. 6;
D_{50} = median grain size;
d = flow depth;
P = wetted perimeter;
p = porosity;
Q_{in} = inflow to the reservoir;
Q_{out} = flow rate at upstream section of breach;
Q_s = sediment transport rate, by weight;
q_s = sediment transport rate, by weight, per unit of channel width;
S_f = friction slope;
t = time;
x = longitudinal distance;
y = stage (or water surface elevation);
z = channel bottom level (or bed elevation);
α = coefficient, Eq. 5;
β = exponent, Eq. 5;
γ = density of water;
γ_s = density of solids;
ΔH = rise/drop in reservoir level;
Δt = time step;
τ = bottom shear stress; and
τ_c = critical shear stress.

BOUNDARY SHEAR IN SMOOTH AND ROUGH CHANNELS

By Donald W. Knight[1]

INTRODUCTION

The boundary shear stress is a particularly important parameter in open channel flow. It is also one of the most difficult to analyse from a purely theoretical point of view. The influence of secondary flow (1,5,9), cross-sectional shape (7,8), and nonuniform roughness distribution around the wetted perimeter (4) all combine to make the prediction of the boundary shear stress distribution impossible, even for simple cases. Recourse thus has to be made to empirical methods. It is of interest to note that in striving to solve the 'turbulence closure' problem, new interest has been expressed in 'simple cases' such as rectangular duct flow (6).

This lack of data is unfortunate in the light of the importance of the boundary shear stress or velocity in resistance, sediment, and dispersion studies. This paper therefore presents a method whereby the mean wall or bed shear stress may be calculated for flows in a rectangular channel over a wide range of differential roughness and breadth to depth ratios. The experimental data has been contained in two previous papers by the writer (see Refs. 3 and 4), but is now presented in a more useful form that will be particularly helpful for those engaged in flume studies.

EXPERIMENTAL PROCEDURE

Experimental Apparatus.—The experiments were conducted in a 15-m flume, 460 mm wide, set at a constant bed slope of 9.58×10^{-4}. Artificial strip roughness was used on the bed of the flume at varying wavelengths, λ, in order to differentially roughen the channel bed in comparison with the smooth flume walls. Uniform depth flow was obtained for each roughness spacing at breadth to depth ratios, B/h, of 1.5, 2, 3, 5, 7.5, 10, and 15. For each depth and roughness intensity, the wall and bed shear stresses were measured by a Preston tube or by semilogarithmic plotting of the velocity profiles. The percentage

[1]Lect., Civ. Engrg. Dept., Univ. of Birmingham, P.O. Box 363, Birmingham, B15 2TT, England.

Note.—Discussion open until December 1, 1981. To extend the closing date one month, a written request must be filed with the Manager of Technical and Professional Publications, ASCE. Manuscript was submitted for review for possible publication on May 27, 1980. This paper is part of the Journal of the Hydraulics Division, Proceedings of the American Society of Civil Engineers, ©ASCE, Vol. 107, No. HY7, July, 1981. ISSN 0044-796X/81/0007-0839/$01.00.

TABLE 1.—Summary of Experimental Data

Experiment number (1)	Discharge, Q, in liters per second (2)	Depth, h, in millimeters (3)	k_{s_b}/k_{s_w} (4)	Shear Stresses: $\bar{\tau}_w$, in Newtons, per square meter (5)	Shear Stresses: $\bar{\tau}_b$, in Newtons, per square meter (6)	Shear Forces: SF_w, in Newtons per meter (7)	Shear Forces: SF_b, in Newtons per meter (8)	Shear Forces: SF_p, in Newtons per meter (9)	$\%SF_w$ (10)
01	4.3	31.1	1.0	0.187	0.267	0.011	0.123	0.134	8.3
02	7.7	45.9	1.0	0.266	0.389	0.024	0.179	0.203	12.0
03	11.8	60.5	1.0	0.382	0.440	0.046	0.202	0.248	18.5
04	22.6	91.2	1.0	0.604	0.608	0.110	0.280	0.390	28.2
05	47.6	152.3	1.0	0.945	0.816	0.208	0.375	0.663	43.4
06	79.0	230.0	1.0	1.218	0.988	0.560	0.454	1.014	55.2
07	110.5	304.4	1.0	1.152	1.043	0.701	0.480	1.181	59.4
12	6.6	45.3	322	0.242	0.316	0.022	0.145	0.167	13.2
14	20.0	91.6	262	0.482	0.632	0.086	0.291	0.379	23.2
16	74.5	222.1	90	0.973	1.081	0.432	0.497	0.929	46.5
21	3.0	30.7	1,214	0.117	0.290	0.007	0.133	0.140	5.0
22	5.8	45.1	1,056	0.193	0.343	0.019	0.158	0.177	10.7
23	9.5	61.4	906	0.294	0.453	0.036	0.208	0.244	14.8
24	18.5	92.2	666	0.566	0.594	0.104	0.273	0.377	27.6
25	38.5	154.4	296	0.676	0.864	0.209	0.397	0.606	34.5
26	73.8	224.9	162	1.083	0.968	0.487	0.445	0.932	52.3
27	113.6	306.7	70	1.234	1.291	0.757	0.594	1.351	56.0
32	5.0	45.0	2,280	0.206	0.343	0.019	0.158	0.177	10.7
34	16.5	92.8	1,762	0.391	0.636	0.073	0.293	0.366	19.9
36	68.0	227.8	702	0.810	1.360	0.369	0.626	0.995	37.1
42	3.7	46.1	—	0.256	0.343	0.024	0.158	0.182	13.2
43	6.8	62.6	7,880	0.240	0.571	0.030	0.263	0.293	10.2
44	13.6	92.1	5,260	0.382	0.624	0.071	0.287	0.358	19.8
45	30.9	156.7	4,160	0.470	0.931	0.147	0.428	0.575	25.6
46	57.7	227.8	3,500	0.612	1.350	0.279	0.621	0.900	31.0
47	86.9	303.9	3,080	0.819	1.658	0.498	0.763	1.261	39.5
52	3.4	46.0	—	0.183	0.375	0.017	0.172	0.189	9.0
54	11.5	92.6	—	0.210	0.795	0.039	0.366	0.405	9.6
56	52.0	235.2	9,300	0.548	1.657	0.258	0.762	1.020	25.3
63	5.4	62.4	—	0.184	0.549	0.023	0.253	0.276	8.3
64	10.4	92.2	—	0.236	0.757	0.044	0.348	0.392	11.2
65	24.5	152.4	15,420	0.410	1.097	0.125	0.505	0.630	19.8
66	48.5	230.1	11,620	0.520	1.484	0.239	0.683	0.922	25.9
67	80.0	308.4	7,380	0.778	1.904	0.480	0.876	1.356	35.4
74	10.0	91.7	—	0.238	0.725	0.044	0.334	0.378	11.6
76	48.0	229.0	17,120	0.478	1.350	0.219	0.621	0.840	26.1
83	5.2	62.0	—	0.140	0.498	0.017	0.229	0.246	6.9
84	10.0	91.7	—	0.151	0.777	0.028	0.357	0.385	7.3
85	25.5	155.6	14,840	0.335	1.338	0.104	0.615	0.719	14.5
86	47.9	231.4	13,040	0.503	1.691	0.233	0.779	1.012	23.0
87	84.6	310.7	5,220	0.708	2.065	0.440	0.950	1.390	31.7
92	3.4	44.6	—	0.177	0.418	0.016	0.174	0.190	8.4
94	11.6	91.0	3,280	0.239	0.877	0.043	0.403	0.446	9.6
96	48.7	223.7	3,320	0.600	1.700	0.268	0.782	1.050	25.5
102	4.2	43.9	1,296	0.215	0.396	0.019	0.182	0.201	9.5
103	6.8	57.9	1,154	0.231	0.521	0.027	0.240	0.267	10.1
104	13.0	89.0	1,522	0.381	0.587	0.068	0.270	0.338	20.1

TABLE 1.—*Continued*

(1)	(2)	(3)	(4)	(5)	(6)	(7)	(8)	(9)	(10)
105	30.5	149.6	1,170	0.493	1.085	0.148	0.499	0.647	22.9
106	58.6	223.6	814	0.750	1.484	0.335	0.683	1.018	32.9
107	98.5	305.6	284	0.995	1.714	0.608	0.788	1.396	43.6

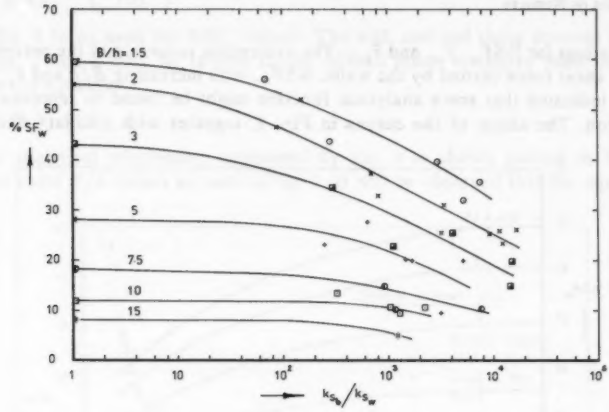

FIG. 1.—Percentage Shear Force Carried by Walls vs B/h and k_{s_b}/k_{s_w}

of the shear force carried by either the walls or bed was then calculated and correlated with roughness intensity and aspect ratio. The Nikuradse equivalent sand roughness size, k_{s_b}, for the bed was also determined. Further details of the experimental technique and results may be found in the earlier papers (3,4).

Experimental Results.—A summary of the shear stress data is given in Table 1. The individual experiment numbers are the same as those used previously. Values of the depth and discharge are given for each experiment together with the mean values of the measured wall and bed shear stresses, $\bar{\tau}_w$ and $\bar{\tau}_b$. The corresponding values of the shear force acting on the walls, SF_w (= $2h\bar{\tau}_w$), the bed SF_b (= $B\bar{\tau}_b$), and the wetted perimeter, SF_p (= $\bar{\tau}_0 P = \rho g A S_f$) are also tabulated, in which $\bar{\tau}_0$ = mean boundary shear stress; P = wetted perimeter; ρ = density; g = gravitational acceleration; A = cross-sectional area; and S_f = energy gradient. The percentage of the shear force carried by the walls, $\%SF_w$(= $SF_w \times 100/SF_p$) and bed, $\%SF_b$(= $SF_b \times 100/SF_p$) are also given. Values of the Nikuradse roughness size for the bed, k_{s_b}, were determined from values of the bed friction factor and Reynolds number and are shown in dimensionless form by dividing by the wall roughness size, k_{s_w}, taken to be equal to the 'smooth' value of 0.0015 mm. The ratio k_{s_b}/k_{s_w} is then a measure of the differential roughness between the bed and the walls.

The results are presented graphically in Fig. 1 in which the $\%SF_w$ values are shown plotted against k_{s_b}/k_{s_w} for different B/h values. Although there

is a certain amount of scatter, due to the difficulty in determining k_{s_b} accurately, the overall trend is systematic. This diagram essentially represents an entirely new way of looking at Figs. 10 and 7 in the writer's earlier papers (Refs. 3 and 4, respectively). It should be noted that although the results were obtained by using artificial strip roughness, the use of the Nikuradse roughness size makes it applicable to other kinds of roughness pattern.

Analysis of Results

Equations for $\%SF_w$, $\bar{\tau}_w$, and $\bar{\tau}_b$.—The systematic reduction in the percentage of the shear force carried by the walls, $\%SF_w$, with increasing B/h and k_{s_b}/k_{s_w} ratios indicated that some analytical function might be found to represent this variation. The shape of the curves in Fig. 1, together with ancillary data for

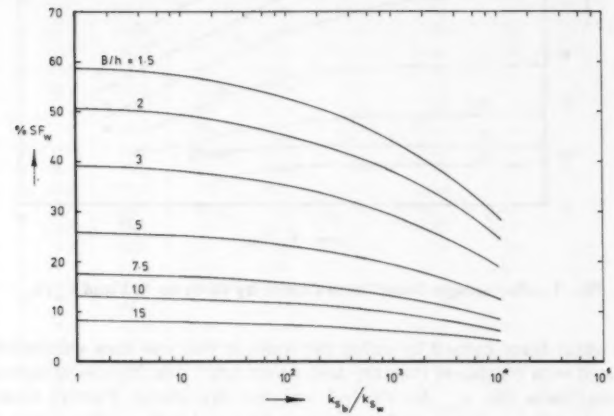

FIG. 2.—Values of $\%SF_w$ Predicted by Eq. 1

smooth channel flow, suggested an equation of the form

$$\%SF_w = e^{\alpha} [\tanh \pi\beta - 0.5 \{\tanh \pi\beta - \beta\}^2] \quad \ldots\ldots\ldots\ldots\ldots\ldots (1)$$

in which $\alpha = -3.264 \log (B/h + 3) + 6.211$; $\beta = 1 - \gamma/5$; and $\gamma = \log (k_{s_b}/k_{s_w})$.

Eq. 1 resulted from a curve fitting exercise using the basic function $y = \tanh (\pi - x)$ with a correction term $-0.5 \{\tanh (\pi - x) - (1 - x/\pi)\}^2$ added to it to fit the mean of the data points for all B/h values. Having obtained the relationship $y = \tanh (\pi - x) - 0.5 \{\tanh (\pi - x) - (1 - x/\pi)\}^2$, the variation in the parameter y for different B/h values was accounted for by assuming a relationship between y and B/h for the smooth wall/bed data (i.e., $x = 0$) in the form given by the equation for α, and the coefficients obtained by linear regression. Eq. 1 results if the substitutions $y = \%SF_w$ and $x = \pi\gamma/5$ are made. The choice of $\gamma = 5$ as an arbitrary end point was made on the basis of the shape of the majority of the curves.

The corresponding equations for the mean wall and bed shear stresses are then

$$\frac{\bar{\tau}_w}{\rho g h S_f} = \left\{\frac{\%SF_w}{100}\right\}\left[\frac{B}{2h}\right] \quad \ldots\ldots\ldots\ldots\ldots\ldots\ldots\ldots\ldots\ldots (2)$$

and $$\frac{\bar{\tau}_b}{\rho g h S_f} = \left\{\frac{\%SF_b}{100}\right\} = 1 - 0.01\,(\%SF_w) \quad \ldots\ldots\ldots\ldots\ldots\ldots (3)$$

with Eq. 1 being used for $\%SF_w$ values. The wall and bed shear stresses given by Eqs. 2 and 3 may be related to the overall mean boundary shear stress, $\bar{\tau}_0$, by the equation

$$\bar{\tau}_0 P = 2h\bar{\tau}_w + B\bar{\tau}_b \quad \ldots\ldots\ldots\ldots\ldots\ldots\ldots\ldots\ldots\ldots\ldots\ldots (4)$$

The analytical relationship expressed by Eq. 1 is shown plotted in Fig. 2 for the same B/h values as used in Fig. 1. It will be observed that the equation

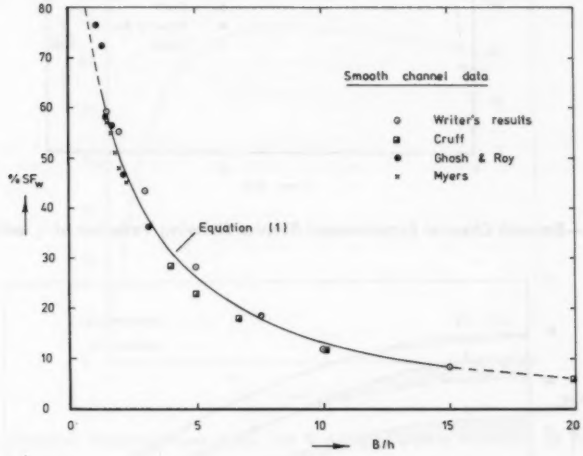

FIG. 3.—Smooth Channel Experimental Results Showing Variation of $\%SF_w$ with B/h

predicts the same kind of systematic reduction in $\%SF_w$ with increasing B/h and k_{s_b}/k_{s_w} as shown by the experimental data in Fig. 1. However the precise form of Eq. 1 has been chosen in the light of additional data relating to smooth channels, i.e., $k_{s_b}/k_{s_w} = 1$.

Figs. 3 and 4 show some of the available data on mean wall shear stresses in smooth open channel flow in which $k_{s_b}/k_{s_w} = 1$. The writer's data is taken from Table 1, the Myers and Cruff data from Figs. 7 and 8 in Ref. 7, and the Ghosh and Roy data from Fig. 13 Ref. 2. Where precise numerical results are not available the writer has estimated the numerical values and computed the $\%SF_w$ and $\bar{\tau}_w$ values accordingly. The main purpose in concentrating upon

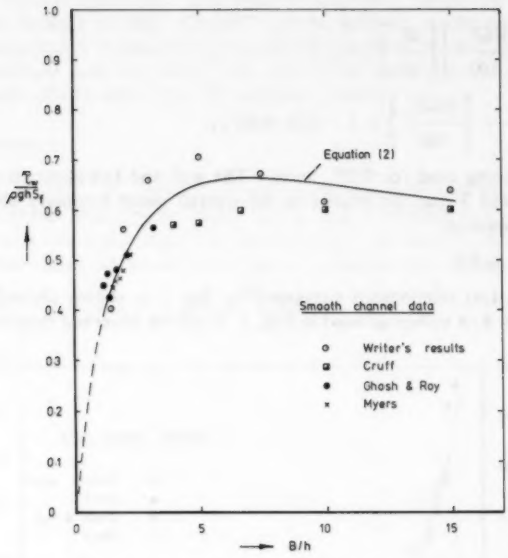

FIG. 4.—Smooth Channel Experimental Results Showing Variation of $\bar{\tau}_w$ with B/h

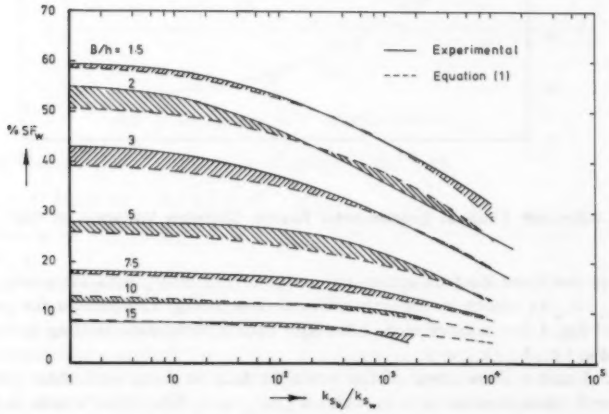

FIG. 5.—Comparison of Experimental and Analytical Results

smooth channel data is because the form of Eq. 1 distinguishes between the influence of roughness (values of β), and the influence of B/h (values of α). For $k_{s_b}/k_{s_w} = 1$, $\gamma = 0$, $\beta = 1$, and the term in square brackets becomes 0.9963. The equation for α thus governs the numerical values given by Eq. 1 for different values of γ. It is therefore particularly important that any equation for α should fit the available smooth channel data well. Figs. 3 and 4 indicate that Eqs. 1 and 2 fit the data reasonably well although there appears to be some difference between the writer's data and that of other investigators. The line drawn through the data in both is a compromise between the conflicting

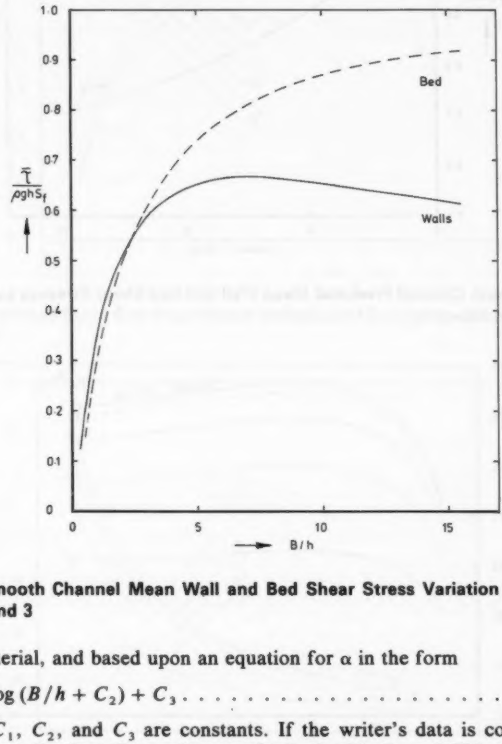

FIG. 6.—Smooth Channel Mean Wall and Bed Shear Stress Variation as Predicted by Eqs. 2 and 3

source material, and based upon an equation for α in the form

$$\alpha = -C_1 \log (B/h + C_2) + C_3 \quad (5)$$

in which C_1, C_2, and C_3 are constants. If the writer's data is considered on its own, then the best fit results are obtained with $C_1 = 3.775$, $C_2 = 4$, and $C_3 = 6.909$. In the interests of trying to fit the expression to as many results as possible, the coefficients in the equation for α given by Eq. 1 are to be preferred.

The overall agreement between Eq. 1 and the data is shown in Fig. 5, which is a composite of Figs. 1 and 2. The reduction in the $\%SF_w$ values appears to be well simulated over a wide range of B/h and k_{s_b}/k_{s_w} values. The discrepancies at low values of k_{s_b}/k_{s_w} for B/h values of 2, 3, and 5 may

be attributed to the choice of coefficients in the equation for α, since it was felt that all available data and not just the writer's should be incorporated in the analysis. If the writer's data is considered on its own, then the correlation

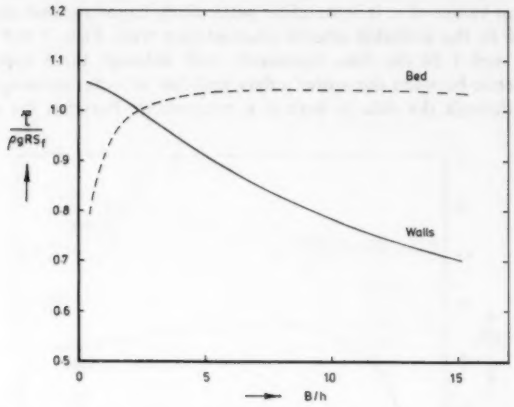

FIG. 7.—Smooth Channel Predicted Mean Wall and Bed Shear Stresses as Proportion of Total Mean Stress, τ_0

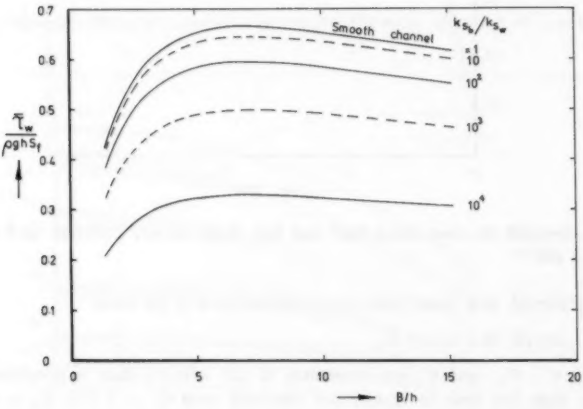

FIG. 8.—Predicted Mean Wall Shear Stress Variation for Smooth and Rough Channels, Using Eq. 2

is improved provided that the coefficients in Eq. 5 are changed to those values given in the preceding paragraph.

Mean Boundary Shear Stresses in Smooth and Rough Channels.—Having

obtained an equation for the percentage of the shear force carried by the walls, and demonstrated its general limitations and validity, it is instructive to use it in Eqs. 2 and 3, to obtain the mean wall and bed shear stress variation with B/h and k_{s_b}/k_{s_w}.

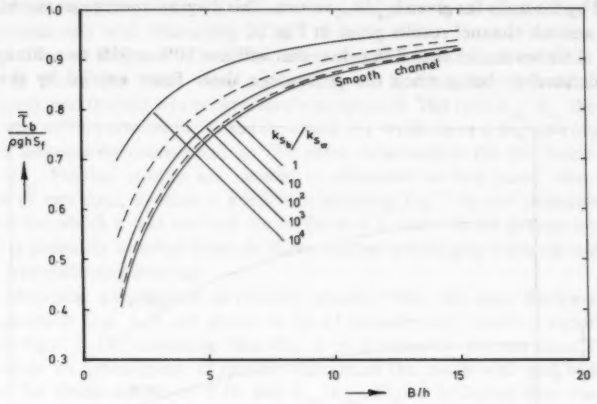

FIG. 9.—Predicted Mean Bed Shear Stress Variation for Smooth and Rough Channels, Using Eq. 3

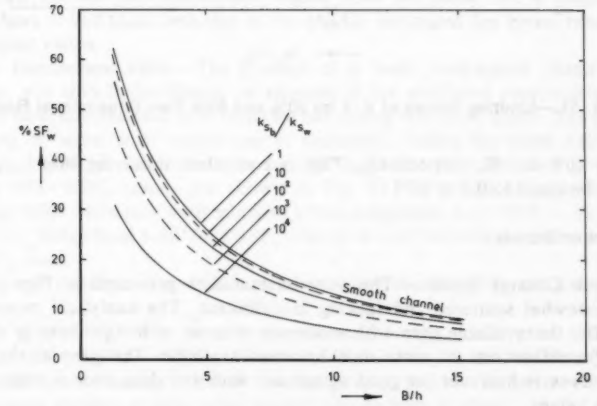

FIG. 10.—Predicted %SF_w Values for Smooth and Rough Channels Using Eq. 1

Figs. 6 and 7 show how the mean wall and bed shear stresses vary with B/h for the smooth channel case. The shear stress is nondimensionalized by the two-dimensional shear ($= \rho g h S_f$) in Fig. 6, and by the overall mean shear

($= \rho g R S_f$) in Fig. 7, in which R = hydraulic radius. Figs. 8 and 9 show the variation of mean stresses for channels with roughened beds in the same dimensionless format as Fig. 6. Diagrams corresponding to the format of Fig. 7 could also be produced for the rough channel case.

Fig. 10 shows the variation with B/h in the percentage of the shear force carried by the walls for given k_{s_b}/k_{s_w} values. This diagram represents an extension of the smooth channel results given in Fig. 3.

Fig. 11 shows the limiting B/h values that will give 90% or 95% two-dimensional flow, defined as being when the percentage shear force carried by the walls

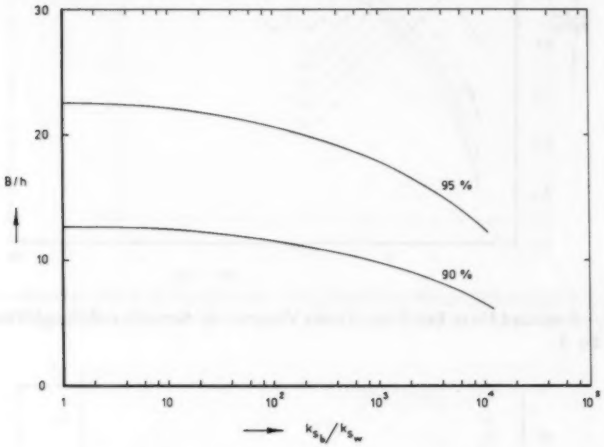

FIG. 11.—Limiting Values of B/h for 90% and 95% Two-Dimensional Flow

is only 10% or 5%, respectively. This is equivalent to saying that $\bar{\tau}_b/\rho g h S_f$ should be equal to 0.9 or 0.95.

Analysis of Results

Smooth Channel Results.—The experimental data presented in Figs. 3 and 4 is somewhat scattered and lacking in definition. The analytical expression for α fits the available data with moderate success, although there is clearly room for refinement as more data becomes available. The general shape of both curves is however, in good agreement with the data over a wide range of B/h values.

The analytical relationships for the mean wall and bed shear stresses shown in Figs. 6 and 7, shows the complexity of boundary shear stresses in open channels. The mean wall shear stress, $\bar{\tau}_w$, is higher than the mean bed shear stress, $\bar{\tau}_b$, for low B/h values, is equal to $\bar{\tau}_b$ at $B/h = 2.4$, and lower than $\bar{\tau}_b$ at higher B/h values. When nondimensionalized by $\rho g h S_f$, as in Fig. 6, the mean wall shear stress reaches a maximum at $B/h = 7.2$. Different analytical

expressions for α however, will yield maxima at widely differing B/h values owing to the flatness of the curve. All the available data suggests that the maximum stress is likely to be reached in the region of $5 < B/h < 8$.

The ratio between the mean bed shear stress and the overall mean shear stress shown in Fig. 7 is remarkably constant at around 1.04 for $B/h > 6$. The ratio between the mean wall shear stress and the overall mean shear stress falls continuously with increasing B/h.

Rough Channel Results.—The data presented in Fig. 1 was derived from flume studies in which the walls were assumed to be hydraulically smooth (k_{s_w} = 0.0015 mm), and the bed was progressively roughened. The ratio k_{s_b}/k_{s_w} therefore refers only to this condition. Cases in which the walls have a higher roughness will not necessarily correspond to the same relationship for the same value of k_{s_b}/k_{s_w}. Further studies are needed to elaborate on this point, and in the absence of any data, caution is needed in applying Eq. 1 to any situation other than that for which it was derived. Its usefulness however is not greatly impaired since it is primarily directed towards flume studies which play such an important part in hydraulic engineering.

The analytical expressions developed initially from the data shown in Fig. 1, and given in Eqs. 1–3, are shown to be of considerable practical significance through Figs. 8–11. Assuming that Eq. 1 is reasonably correct then Figs. 8 and 9 allow an investigator to quickly determine the mean wall and bed shear stresses for given values of B/h and k_{s_b}/k_{s_w}. Fig. 8 indicates that the mean wall shear stress is very considerably reduced with increasing k_{s_b}/k_{s_w}. The values of $\bar{\tau}_w/(\rho g h S_f)$ are approximately halved throughout the range $1.5 < B/h < 15$ when k_{s_b}/k_{s_w} is changed from 1–10^4. Fig. 9 indicates that the mean bed shear stresses are considerably higher once the flume bed is roughened, and allows a bed shear velocity to be quickly estimated for given roughness and aspect ratios.

Two Dimensional Flow.—The concept of a 'wide' rectangular channel is a popular one with hydraulicians on account of the additional complexities that arise in three-dimensional flow with two interacting boundary layers. The precise meaning of 'wide' is of course one of definition. Taking the mean wall shear force as a possible criterion, then the limiting values of B/h which give only 5% or 10% $\%SF_w$ values are shown in Fig. 11. As would be expected the limiting value decreases with increasing bed roughness, e.g., B/h = 22.6–12.6 as k_{s_b}/k_{s_w} varies from 1–10^4 for $5\%SF_w$, and B/h = 12.7–6.6 for the corresponding $10\%SF_w$ case.

Range of Validity.—Eq. 1 was obtained under the following conditions: $1.5 < B/h \leq 15$, $1 < k_{s_b}/k_{s_w} < 10^4$, $2.1 \times 10^4 < 4\bar{u}R/\nu < 3.7 \times 10^5$, $0.23 < \bar{u}/\sqrt{(gh)} < 0.57$. The smooth channel results were restricted to the range of $2.9 \times 10^4 < 4\bar{u}R/\nu < 3.6 \times 10^5$, and $0.46 < \bar{u}/\sqrt{(gh)} < 0.57$. The symbols have their usual meaning in that $\bar{u}$ = mean velocity; and ν = kinematic viscosity. The limited number of data points should also be born in mind.

It should be emphasized again that the results were obtained in a flume with smooth walls and smooth or rough bed. It does not necessarily follow therefore that the k_{s_b}/k_{s_w} range covers the rough wall/rough bed case. Under no circumstances should the k_{s_b}/k_{s_w} ratio exceed 10^4 due to the way the hyperbolic function in Eq. 1 has been formulated, i.e., for $k_{s_b}/k_{s_w} = 10^5$, $\gamma = 5$, $\beta = 0$ and $\%SF_w = 0$.

The B/h range is sufficiently wide to define any major changes in the variation of mean boundary shear stress, e.g., Figs. 3, 4, 6, and 7. It may be possible therefore to extrapolate the results outside the given B/h range with some degree of confidence, although once $B/h = 0.5$ it is likely that other effects will play an important part.

Because boundary resistance and shear is Reynolds number dependent, it is likely that Eq. 1 will need some further modification before it can be used in any design problem involving prototype flows.

General Comments.—The equations put forward in this paper are considered to be reasonably representative of flow conditions in small rectangular open channels, although it must be said that the available data is not extensive. Eq. 1 is therefore recognized to be somewhat tentative, and likely to be improved upon as further data becomes available. However, the general trends predicted by Eq. 1 are sufficiently encouraging to believe that it is a reasonable first attempt at analysing this particular problem. Indeed one of the writer's objectives in putting it forward is to encourage other investigators to analyse and publish their data in the same way. It should not be too difficult to investigate the smooth channel case more thoroughly and for the equation for α to be modified accordingly.

In terms of application, the proposed equations are simple and easy to use on account of the separation of the two dependent variables. There are many practical problems involving flows in flumes or rectangular culverts for which it is important to know the bed shear stress or bed shear velocity accurately. The majority of sediment or dispersion formulae utilize such parameters extensively, and at present it is difficult to estimate the likely influence of shape and roughness. Eqs. 1–3 should enable such estimates to be made more confidently.

Conclusions

1. Eq. 1, together with the associated equations for the three coefficients α, β, and γ, give the percentage of the total shear force carried by the walls for flows in smooth and rough channels of rectangular cross section.
2. The range within which Eq. 1 is valid needs to be strictly observed on account of the limited amount of data, and the curve fitting procedures employed.
3. The reduction is $\%SF_w$ with increasing B/h and k_{s_b}/k_{s_w} is shown by both the experimental results and the proposed equation.
4. The mean wall and bed shear stresses may be calculated for different aspect ratios and roughness conditions using Eqs. 2 and 3.
5. The experimental data for the smooth channel case, which defines the equation for α, is shown to be limited and not very satisfactory.
6. Eqs. 1–3 provide a novel way of estimating the mean boundary shear stresses in flumes and small rectangular culverts.
7. Further experimental data is required in order to check the general validity of these equations.

Appendix I.—References

1. Chiu, C. L., Hsiung, D. E., and Lin, H. C., "Three-Dimensional Open Channel Flow,"

Journal of the Hydraulics Division, ASCE, Vol. 104, No. HY8, Proc. Paper 13963, Aug., 1978, pp. 1119–1136.
2. Ghosh, S. N., and Roy, N., "Boundary Shear Distribution in Open Channel Flow," *Journal of the Hydraulics Division,* ASCE, Vol. 96, No. HY4, Proc. Paper 7241, Apr., 1970, pp. 967–994.
3. Knight, D. W., and Macdonald, J. A., "Hydraulic Resistance of Artificial Strip Roughness," *Journal of the Hydraulics Division,* ASCE, Vol. 105, No. HY6, Proc. Paper 14635, June, 1979, pp. 675–690.
4. Knight, D. W., and Macdonald, J. A., "Open Channel Flow with Varying Bed Roughness," *Journal of the Hydraulics Division,* ASCE, Vol. 105, No. HY9, Proc. Paper 14839, Sept., 1979, pp. 1167–1183.
5. Liggett, J. A., Chiu, C. L., and Miao, L. S., "Secondary Currents in a Corner," *Journal of the Hydraulics Division,* ASCE, Vol. 91, No. HY6, Proc. Paper 4538, Nov., 1965, pp. 99–117.
6. Melling, A., and Whitelaw, J. H., "Turbulent Flow in a Rectangular Duct," *Journal of Fluid Mechanics,* Vol. 78, Part 2, London, England, 1976, pp. 289–315.
7. Myers, W. R. C., "Momentum Transfer in a Compound Channel," *Journal of Hydraulic Research,* International Association for Hydraulic Research, Vol. 16, No. 2, 1978, pp. 139–150.
8. Rajaratnam, N., and Ahmadi, R. M., "Interaction between Main Channel and Flood-Plain Flows," *Journal of the Hydraulics Division,* ASCE, Vol. 105, No. HY5, May, 1979, pp. 573–588.
9. Tracy, H. J., "Turbulent Flow in a Three-Dimensional Channel," *Journal of the Hydraulics Division,* ASCE, Vol. 91, No. HY6, Proc. Paper 4530, Nov., 1965, pp. 9–35.

Appendix II.—Notation

The following symbols are used in this paper:

A = cross-sectional area;
B = channel width;
g = gravitational acceleration;
h = channel depth;
k_s = Nikuradse equivalent sand roughness;
P = wetted perimeter;
R = hydraulic radius;
S_f = energy slope;
SF = shear force;
%SF = percentage shear force;
$\bar{u}$ = section mean velocity;
α = coefficient used in Eq. 1;
β = $1 - \gamma/5$ = coefficient used in Eq. 1;
γ = $\log (k_{s_b}/k_{s_w})$ = coefficient used in Eq. 1;
ν = kinematic viscosity;
ρ = density; and
$\bar{\tau}$ = mean shear stress.

Subscripts

w = wall;
b = bed;
o = overall; and
p = perimeter.

IDENTIFICATION OF STREAMFLOW STOCHASTIC MODELS

By Jose D. Salas,[1] M. ASCE, Jayantha T. B. Obeysekera,[2] and Ricardo A. Smith[3]

INTRODUCTION

Several stochastic models have been used for modeling hydrologic time series in general and streamflow time series in particular. They are: (1) Autoregressive models (15,28,34); (2) fractional Gaussian noise models (14,31); (3) autoregressive and moving average models (3,6,18); (4) broken-line models (16,23); shot-noise models (32); (5) disaggregation models (12,30); (6) Markov mixture models (8); (7) ARMA-Markov models (13); and (8) general mixture models (1). Supposedly justification for using these models follows from their ability to reproduce the main statistical characteristics which are observed in actual hydrologic time series.

Unfortunately, the exact mathematical model of a hydrologic time series is never known. The inferred population model is only an approximation. The exact model parameters are also never known in hydrology; they must be estimated from limited data. Identification of models and estimation of their parameters from available data are often referred to in the literature as time series modeling or stochastic modeling of hydrologic series. A systematic approach to hydrologic time series modeling may be composed of six main phases (24): (1) Identification of model composition; (2) identification of model type; (3) identification of model form; (4) estimation of model parameters; (5) testing goodness of fit of the model; and (6) evaluation of uncertainties. The main objective of this paper is to tackle the 2nd and 3rd phases, namely the identification of the model type and the identification of the model form.

The identification of the type of model is aimed at deciding on one among the various alternative models, say AR (autoregressive), ARMA (autoregressive moving average), FGN (fractional Gaussian noise), BL (broken line), SL (shifting level), or any other model that is available in stochastic hydrology. Once the type of model is identified it is necessary to identify the form or order of

[1]Assoc. Prof., Dept. of Civ. Engrg., Colorado State Univ., Fort Collins, Colo. 80523.
[2]Grad. Student, Dept. of Civ. Engrg., Colorado State Univ., Fort Collins, Colo. 80523.
[3]Grad. Student, Dept. of Civ. Engrg., Colorado State Univ., Fort Collins, Colo. 80523.

Note.—Discussion open until December 1, 1981. To extend the closing date one month, a written request must be filed with the Manager of Technical and Professional Publications, ASCE. Manuscript was submitted for review for possible publication on July 25, 1980. This paper is part of the Journal of the Hydraulics Division, Proceedings of the American Society of Civil Engineers, ©ASCE, Vol. 107, No. HY7, July, 1981. ISSN 0044-796X/81/0007-0853/$01.00.

the model. For instance, if ARMA is the type of model selected for a particular case, finding the values of p and q (the number of autoregressive and moving average coefficients, respectively) is the process of identification of the order of the model.

The selection or identification of the type of hydrologic stochastic model generally depends on: (1) The modelers' input such as judgment, experience, and personal preference; (2) the physical basis of the process under study; and (3) the statistical characteristics of a given time series. The approach developed in this paper leans on the second factor, namely, delineating the physical mechanism underlying the streamflow process.

Several studies have been made in the past aimed at setting the physical basis of streamflow stochastic models. A recent state of the art review by Klemes (11) covers most of the work done in the subject. Thomas (29), and Fiering (4) consider a watershed system where the annual precipitation is decomposed into evaporation, infiltration, and surface runoff. Then, using the mass balance equation for the ground-water storage, the autocorrelation function of the annual streamflow was found by induction as a function of the first serial correlation of the precipitation process which was assumed to follow a first order autoregressive model. The streamflow autocorrelation function (ACF) given by Fiering (4, p. 74) is a fairly complex expression. However, for an assumed independent precipitation process such an autocorrelation function (ACF) simplifies to $\rho_k = \rho_1(1 - c)^{k-1}$ in which k = the time lag; and c = a constant. This function being slightly different from the well-known function, $\rho_k = \rho_1^k$, for an AR(1) model (first order autoregressive) led Fiering to believe that it may correspond to a multilag AR model (see also Jackson (7), p. 60). However, Salas and Smith (25) note that the ACF $\rho_k = \rho_1(1 - c)^{k-1}$ has the same form as that of an ARMA(1,1) model and argue that the streamflow process is in fact an ARMA(1,1) process. Thomas and Fiering's conceptual model of a watershed is used herein to identify the type of model for the ground-water storage and streamflow processes given that the precipitation input may be represented in general by an ARMA process.

The identification of the form or the order of the hydrologic stochastic model has been usually made by applying statistical techniques such as spectral analysis and autocorrelation analysis. The books by Jenkins and Watts (9), and Yevjevich (35) describe such techniques in detail. More recently Hipel, et al. (6) examine

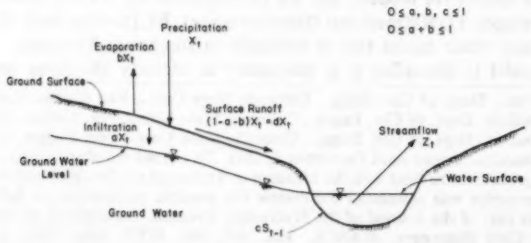

FIG. 1.—Schematic Representation of Precipitation-Storage-Streamflow Processes of Natural Watershed

identification techniques based on the autocorrelation function, partial autocorrelation function, inverse ACF, and inverse partial ACF. However, often such techniques are subjective and do not uniquely identify the order of the model when the model is ARMA. An alternate identification technique is used herein and is based on the R-functions and S-functions proposed by Gray, et al. (5).

In the following section of this paper the problem of identification of the type of stochastic model for annual streamflows, using a conceptual model representation of a watershed is analyzed. Once the type of model is defined, the identification of the order of the model is presented in the third section. An example of model identification is given in the fourth section. The paper ends with a section of summary and conclusions.

Identification of Type of Model

Consider the conceptual representation of a natural watershed as in Fig. 1 in which x_t = the precipitation in the year, t; S_t = the ground-water storage at the end of year, t; and z_t = the streamflow in the year t. Assume that the amount ax_t infiltrates, percolates, and reaches the ground-water storage and the amount bx_t evaporates from the soil, plants, and surface storage. Thus, the amount $(1 - a - b)x_t = dx_t$ represents the surface runoff reaching the stream. Assume further that $c\ S_{t-1}$ is the ground-water contribution to the stream in which S_{t-1} = the ground-water storage at the beginning of year, t. The following conditions are required: $0 \leq a, b, c \leq 1$ and $0 \leq a + b \leq 1$.

The streamflow z_t is made up of the ground-water contribution $c\ S_{t-1}$ and the surface runoff dx_t. Therefore

$$z_t = c\ S_{t-1} + dx_t \quad \ldots \quad (1)$$

The mass balance equation for the ground-water storage is written as

$$S_t = (1 - c)S_{t-1} + a\ x_t \quad \ldots \quad (2)$$

Combining Eqs. 1 and 2 gives

$$z_t = (1 - c)z_{t-1} + dx_t - [d(1 - c) - ac]\ x_{t-1} \quad \ldots \quad (3)$$

Let μ_x, μ_z, and μ_s represent the means of x_t, z_t, and S_t, respectively. From Eq. 2, the expected values μ_s and μ_x are related as $\mu_s = a\ \mu_x/c$. Likewise, from Eq. 3 the expected values μ_z and μ_x are related as $\mu_z = (1 - b)\mu_x$. Furthermore, write $x_t = \mu_x + x'_t$, $z_t = \mu_z + z'_t$, and $S_t = \mu_s + S'_t$, in which x'_t, z'_t, and S'_t = the corresponding residuals with mean zero. Substituting these expressions into Eqs. 2 and 3, it can be shown that

$$S'_t = (1 - c)S'_{t-1} + a\ x'_t \quad \ldots \quad (4)$$

and $$z'_t = (1 - c)z'_{t-1} + dx'_t - [d(1 - c) - ac]\ x'_{t-1} \quad \ldots \quad (5)$$

In the Box-Jenkins notation Eqs. 4 and 5 can be written as

$$(1 - \phi_1 B)S'_t = a\ x'_t \quad \ldots \quad (6)$$

in which $\phi_1 = 1 - c$ and

$$(1 - \phi_1 B)z'_t = d(1 - \theta_1 B)x'_t \quad \ldots \quad (7)$$

in which $\theta_1 = [d(1 - c) - ac]/d$; and B is an operator such that $B^i y_t = y_{t-i}$.

Assume that the precipitation input, $x'_t = x_t - \mu_x$, is represented by the general ARMA (p,q) model

$$\phi'(B)x'_t = \theta'(B)\epsilon'_t \quad \ldots \quad (8)$$

in which $\phi'(B) = 1 - \phi'_1 B - \ldots - \phi'_p B^p$; $\theta'(B) = 1 - \theta'_1 B - \ldots - \theta'_q B^q$; and ϕ'_j and θ'_j = the autoregressive and moving average coefficients, respectively. Combining Eqs. 6 and 8 gives

$$\phi'(B)(1 - \phi_1 B)S'_t = a\,\theta'(B)\epsilon'_t \quad \ldots \quad (9)$$

which is an ARMA $(p + 1, q)$ process. Eq. 9 can be also expressed as

$$\phi''(B)S'_t = \theta'(B)\xi_t \quad \ldots \quad (10)$$

in which $\phi''(B) = \phi'(B)(1 - \phi_1 B)$; and $\xi_t = a\,\epsilon'_t$.

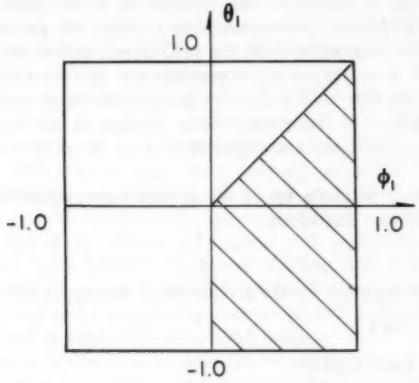

FIG. 2.—Parameter Space for ARMA (1,1) Streamflow Model of Eq. 14

Similarly, combining Eqs. 7 and 8 yields

$$\phi'(B)(1 - \phi_1 B)z'_t = d(1 - \theta_1 B)\theta'(B)\epsilon'_t \quad \ldots \quad (11)$$

which is an ARMA $(p + 1, q + 1)$ process. Eq. 11 can be also expressed as

$$\phi''(B)z'_t = \theta''(B)\eta_t \quad \ldots \quad (12)$$

in which $\theta''(B) = (1 - \theta_1 B)\theta'(B)$; and $\eta_t = d\,\epsilon'_t$.

From the several expressions given in the preceding, particular cases can be readily derived. For instance, if the precipitation input is an independent process, i.e., $p = 0$, and $q = 0$ in Eq. 8, or $x'_t = \epsilon'_t$, then $\phi''(B) = 1 - \phi_1 B$, $\theta'(B) = 1$, and $\theta''(B) = 1 - \theta_1 B$, so Eq. 10 simplifies to

$$(1 - \phi_1 B)S'_t = \xi_t \quad \ldots \quad (13)$$

an AR(1) process with $\phi_1 = 1 - c$. Likewise, Eq. 12 simplifies to

$$(1 - \phi_1 B) z'_t = (1 - \theta_1 B)\eta_t \quad \ldots \quad (14)$$

an ARMA (1,1) process with $\phi_1 = 1 - c$; and $\theta_1 = [d(1 - c) - ac]/d$.

Note that the ARMA processes derived for both the ground-water storage and the streamflow processes are what are called here restricted ARMA processes in the sense that their parameter space is a subspace of that corresponding to the general ARMA models. For instance, for the ARMA (1,1) process of Eq. 14 with $\phi_1 = 1 - c$, and $\theta_1 = 1 - c(1 - b)/(1 - a - b)$, it is required

TABLE 1.—S*-Function for an ARMA (p,q) Model (33)

	n					
k	1	...	p	$p+1$	...	$p+i$
(1)	(2)	(3)	(4)	(5)	(6)	(7)
.	.		.	.		.
.	.		.	.		.
.	.		.	.		.
$-q-3$	.		C_2	u	...	u
$-q-2$	.		C_2	u^a	...	u
$-q-1$	.		C_2	$\pm\infty$	...	$\pm\infty$
$-q$	$S_1^*(-q)$		↑	↑		↑
.	.					
.	.					
.	.					
-1	$S_1^*(-1)$		$2q$			$2q$
0	$S_1^*(0)$		nonconstants			nonconstants
1	$S_1^*(1)$		↓	↓		↓
.	.					
.	.					
.	.					
$q-1$	$S_1^*(q-1)$		↓	↓		↓
q	.		C_1	$-C_1$	...	$(-1)^i C_1$
$q+1$	.		C_1	u	...	u
$q+2$	.		C_1	u	...	u
.	.		.	.		.
.	.		.	.		.
.	.		.	.		.

[a] Undefined.

that $0 \leq \phi_1 \leq 1$, and $\phi_1 \geq \theta_1$ so that the conditions $0 \leq a, b, c \leq 1$, and $0 < a + b \leq 1$ are satisfied. Furthermore, it can be demonstrated that the parameter space of such ARMA (1,1) process is as shown in Fig. 2.

The autocorrelation function of an ARMA (1,1) process is given by (2)

$$\rho_k = \rho_1 \phi_1^{k-1} \quad \ldots \quad (15)$$

$$\text{with} \quad \rho_1 = \frac{(1 - \phi_1\theta_1)(\phi_1 - \theta_1)}{(1 + \theta_1^2 - 2\phi_1\theta_1)} \quad \ldots \quad (16)$$

Note that the sign of ρ_1 is determined by the sign of $\phi_1 - \theta_1$ and since $\phi_1 \geq \theta_1$ for any combination of a, b, and c (within the parameter space as above indicated) ρ_1 will always be positive. Furthermore, since $\phi_1 = 1 - c \geq 0$, the ACF, ρ_k, will also be positive for $k \geq 1$. Thus, ρ_k decays exponentially from the starting positive value ρ_1. This is an important result because a simple conceptual physical model of a watershed with an independent precipitation input leads to an ARMA (1,1) streamflow process whose autocorrelation function is always positive. Note that it is not unusual to obtain negative first serial correlation estimates from historical data of annual streamflows. The foregoing analysis indicates that such negative serial correlations, although statistically possible, are not mathematically justified, given the above physical assumptions.

The main conclusion of this section is that, based on a simple conceptual physical representation of a natural watershed it is demonstrated that the ground-water storage and streamflow processes belong to the general class of ARMA processes. This means that under the linear reservoir assumption the selection of the ARMA models for modeling the ground-water and streamflow time series is justified based on physical grounds.

Identification of Form of Model

Once the type of model is identified, it remains to identify the form of the model. That is, it is necessary to determine the order of the ARMA model

TABLE 2.—Autocorrelation Function, ρ_k, for ARMA (2,1) Model with Parameters, $\phi_1 = 1.0$, $\phi_2 = -0.5$, and $\theta_1 = -0.5$

k (1)	ρ_k (2)	k (3)	ρ_k (4)
−6	−0.0598	0	1.0000
−5	−0.1848	1	0.7391
−4	−0.2500	2	0.2391
−3	−0.1304	3	−0.1304
−2	0.2391	4	−0.2500
−1	0.7391	5	−0.1848

identified in the previous section. This is done following an approach developed recently by Gray, et al. (5).

Definition of R-Functions and S-Functions.—Consider an ARMA (p,q) model as

$$z_t = \sum_{j=1}^{p} \phi_j z_{t-j} + \epsilon_t - \sum_{j=1}^{q} \theta_j \epsilon_{t-j} \quad \ldots \ldots \ldots \ldots \ldots \ldots \ldots \ldots \quad (17)$$

in which z_t = the ARMA dependent variable assumed with mean zero; ϵ_t = the independent variable with zero mean and variance σ_ϵ^2; $\{\phi_1, \ldots, \phi_p\}$ = the set of autoregressive parameters; $\{\theta_1, \ldots, \theta_q\}$ = the set of moving average parameters; and p and q are the number of autoregressive and moving average parameters, respectively.

The R-functions and S-functions are defined by (5)

$$R_n(\rho_k) = \frac{H_n(\rho_k)}{H_n(1,\rho_k)} \quad \ldots\ldots\ldots\ldots\ldots\ldots\ldots\ldots\ldots\ldots\ldots\ldots \quad (18)$$

and $$S_n(\rho_k) = \frac{H_{n+1}(1,\rho_k)}{H_n(\rho_k)} \quad \ldots\ldots\ldots\ldots\ldots\ldots\ldots\ldots\ldots\ldots\ldots\ldots \quad (19)$$

in which ρ_k = the autocorrelation function of the ARMA (p,q) model of Eq.

TABLE 3.—S*-Function for ARMA (2,1) Model with Parameters $\phi_1 = 1.0$, $\phi_2 = -0.5$, and $\theta_1 = -0.5$

	n			
k (1)	1 (2)	2 (3)	3 (4)	4 (5)
−6	2.0910	1.0000	*u*[a]	*u*
−5	0.3530	1.0000	*u*	*u*
−4	−0.4783	1.0000	*u*	*u*
−3	−2.8334	1.0000	*u*	*u*
−2	2.0909	1.0000	∞	−∞
−1	0.3529	0.6461[b]	1.0231[b]	2.4114[b]
0	−0.2609	0.4375[b]	−0.3064[b]	0.3510[b]
1	−0.6765	0.5000	−0.5000	+0.5000
2	−1.5454	0.5000	*u*	*u*
3	0.9167	0.5000	*u*	*u*
4	−0.2609	0.5000	*u*	*u*

[a]Undefined.
[b]Two nonconstants.

17. The functions $H(\cdot)$ are in turn defined as

$$H_n(\rho_k) = \begin{vmatrix} \rho_k & \rho_{k+1} & \cdots & \rho_{k+n-1} \\ \rho_{k+1} & \rho_{k+2} & \cdots & \rho_{k+n} \\ \cdot & \cdot & & \cdot \\ \cdot & \cdot & & \cdot \\ \cdot & \cdot & & \cdot \\ \rho_{k+n-1} & \rho_{k+n} & \cdots & \rho_{k+2n-2} \end{vmatrix} \quad \ldots\ldots\ldots\ldots\ldots\ldots \quad (20)$$

and $$H_{n+1}(1,\rho_k) = \begin{vmatrix} 1 & 1 & \cdots & 1 \\ & & & \rho_{k+n} \\ & H_n(\rho_k) & & \cdot \\ & & & \cdot \\ & & & \cdot \\ & & & \rho_{k+2n-1} \end{vmatrix} \quad \ldots\ldots\ldots\ldots\ldots\ldots \quad (21)$$

in which $H_0(\rho_k) = 1$; k = an integer; and n = a positive integer. Similar expressions are also defined when the ρ_k's in 20 and 21 are replaced by $(-1)^k \rho_k$, in which case the H functions are denoted by $H_n[(-1)^k \rho_k]$, and $H_{n+1}[1, (-1)^k \rho_k]$.

The R-functions and S-functions can be obtained recursively by (21)

$$R_{n+1}(\rho_k) = R_n(\rho_{k+1}) \left[\frac{S_n(\rho_{k+1})}{S_n(\rho_k)} - 1 \right] \quad \ldots\ldots\ldots\ldots\ldots\ldots \quad (22)$$

and $$S_n(\rho_k) = S_{n-1}(\rho_{k+1}) \left[\frac{R_n(\rho_{k+1})}{R_n(\rho_k)} - 1 \right], \quad \ldots\ldots\ldots\ldots\ldots\ldots \quad (23)$$

provided there are no zero divisors. The initial values in Eqs. 22 and 23 are $S_0(\rho_k) = 1$; and $R_1(\rho_k) = \rho_k$. Note that the form of the foregoing functions remains unchanged when the argument is the alternating autocorrelation function, $(-1)^k \rho_k$, instead of ρ_k. It has been shown (33) that the shifted S-function given by

$$S_i^*(\rho_k) = S_i(\rho_{k-i+1}) \quad \ldots\ldots\ldots\ldots\ldots\ldots\ldots\ldots \quad (24)$$

can be used effectively for identifying the order p and q of an ARMA model.

TABLE 4.—Autocorrelation Function, $\hat{\rho}_k$, of Eq. 30 for Annual Flows of Niger River

k (1)	$\hat{\rho}_k$ (2)	k (3)	$\hat{\rho}_k$ (4)
0	1.0000	7	0.0535
1	0.5348	8	−0.1036
2	0.4629	9	−0.2007
3	0.3998	10	−0.3492
4	0.2012	11	−0.4173
5	0.1624	12	−0.4235
6	0.1687	13	−0.3746

For the ARMA (p, q) model of Eq. 17 with $p > 0$, the shifted S*-function has the following properties (33):

1. $S_n^*[(-1)^{kl} \rho_k] = C_1$(constant), $k \geq k_0$ $\ldots\ldots\ldots\ldots\ldots\ldots$ (25)

in which $C_1 = (-1)^p [1 - \sum_{j=1}^{p} (-1)^{jl} \phi_j]$; if $n = p$; and $k_0 = q$.

2. $S_n^*[(-1)^{kl} \rho_k] = C_2$(constant), $k \leq k_1$ $\ldots\ldots\ldots\ldots\ldots\ldots$ (26)

in which $C_2 = (-1)^{pl+1} C_1 / \phi_p$ if $n = p$; and $k_1 = -q - 1$.

3. $S_n^*[(-1)^{kl} \rho_k] \neq C_1$ or C_2, $k_1 + 1 \leq k \leq k_0 - 1$ $\ldots\ldots\ldots$ (27)

if $n = p$.

4. $S_i^*[(-1)^{(-q-1)l} \rho_{-q-1}] = \pm\infty$ $\ldots\ldots\ldots\ldots\ldots\ldots\ldots$ (28)

and $S_i^*[(-1)^{ql} \rho_q] = (-1)^{l-p} C_1$ $\ldots\ldots\ldots\ldots\ldots\ldots\ldots$ (29)

if $i > p$.

in which $l = 0$ for the argument ρ_k and $l = 1$, for the argument $(-1)^k \rho_k$.

The foregoing properties can be better illustrated in a tabular form. Table 1 gives the S*-function of an ARMA (p,q) model. It has a certain pattern that is useful for identifying the order p and q of an ARMA model. For instance, Table 1 shows that precisely at column p there are two constants (C_2 up and C_1 down) around $2q$ nonconstants. The column where this occurs identifies the order, p, of the model. Furthermore, since in this column there are $2q$ nonconstants, this identifies the order, q, of the model. Another feature of the S*-function is that for $n > p$, $S_n^*(\rho_k) = \pm\infty$ for $k = -q - 1$ (S_n^* alternates in sign as n increases), $S_n^*(\rho_k) = (-1)^i C_1$ for $k = p + i$ (S_n^* alternates in sign as n increases), and $S_n^*(\rho_k)$ is undefined for $q + 1 \le k \le -q - 2$. The use of this table is elaborated by an example. Note that the infinite values always occur above the center line in Table 1.

Example.—Consider a particular ARMA (p,q) model as in Eq. 17, with known p and q and known parameters. The autocorrelation function for such a model

TABLE 5.—S*-Function with Argument $(-1)^k \hat{\rho}_k$ for Annual Flows of Niger River

	n				
k	1	2	3	4	5
(1)	(2)	(3)	(4)	(5)	(6)
−6	−1.9622	1.4576	−4.8899	9.8786	15.8900
−5	−2.2390	8.8118	−2.5532	4.1371	−5.9916
−4	−2.9873	−1.9444	−3.6189	2.3996	48.3994
−3	−2.1579	2.1690	−3.7967	−60.9239	15.4122
−2	−2.1552	−665.4361	0.4419	9.5305	−8.3281
−1	−2.8699	−4.6588	−10.6986	9.4689	132.2278
0	−1.5348	1.1545	−1.2941	1.4990	−1.4822
1	−1.8656	1.8576	0.1947	1.5883	11.5954
2	−1.8636	292.9447	−1.6619	1.6741	−1.0344
3	−1.5032	0.7125	−1.7784	−3.0546	−11.8042
4	−1.8071	2.7340	−1.5520	12.3895	−20.6664
5	−2.0393	−3.8043	−4.7433	6.3965	−5.0751

is given in Table 2. It is often difficult to identify the order of a model by visual inspection of the autocorrelation and partial autocorrelation functions, especially for higher order mixed ARMA models. Gray's identification method follows. The S*-function is obtained from Eqs. 22, 23, and 24 and it is given in Table 3. Clearly, in column $n = 2$ two sets of constants appear, the constant $C_1 = 0.5$ for $k \ge 1$ and the constant $C_2 = 1.0$ for $k \le -2$. Since such constants appear in the second column, the order of the autoregressive part is $p = 2$. Furthermore, there are two nonconstants in column 2, that is, $2q = 2$ (see Table 1) or $q = 1$. In effect, the autocorrelation function of Table 2 and the corresponding S*-function of Table 3 were derived from an ARMA (2,1) model with parameters $\phi_1 = 1.0$, $\phi_2 = -0.5$, and $\theta_1 = -0.5$. It is important to note the other features of the S*-function. For instance, the infinity appears for $n > 2$ and $k = -2$. The constant $C_1 = 0.5$ also appears in column 3 and $k = 1$ but with a negative sign. In general the constant 0.5 appears with alternating

sign for $n > 2$ and $q = 1$. On the other hand, undefined values occur for $n > 2$, and $2 \leq k \leq -3$.

Identification of Niger River Annual Flows

Annual flows of the Niger River at Koulicoro, Africa for the period 1906–1957 are used as an example of model identification. Data is in the form of modular coefficients (flows divided by the mean) as appears in Yevjevich (34).

The autocorrelation function, ρ_k, for the annual flows of the Niger River (Table 4) is estimated by

$$\hat{\rho}_k = \frac{\sum_{t=1}^{N-k} (x_t - \bar{x})(x_{t+k} - \bar{x})}{\sum_{t=1}^{N} (x_t - \bar{x})^2} \quad \ldots\ldots\ldots\ldots\ldots\ldots\ldots\ldots\ldots\ldots \quad (30)$$

in which $\bar{x}$ = the sample mean; k = the lag; and N = the sample size.

The S*-function is determined from Eqs. 22, 23, and 24, in which the argument is the alternating autocorrelation function $(-1)^k \hat{\rho}_k$ instead of $\hat{\rho}_k$. Table 5 gives the estimated S*-function for $-6 \leq k \leq 5$, and $1 \leq n \leq 5$. Column 1 of this table shows approximately constant values above the center line as well as below the line. There is no other column where such constant patterns appear as clearly as in column 1. Therefore, it can be concluded that the order of the autoregressive term is one or $p = 1$. It remains to determine the order, q, of the ARMA (p,q) model.

Analyzing Table 5 it should be decided whether there exist nonconstants around the center line. If it is assumed that no nonconstants exist, that is, the constants, C_1 (down) and C_2 (up), would start right at the center line, then the S*-value for $n = 2$ and $k = -1$ would tend to $\pm\infty$. However, $S_2^*(-1) = -4.6588$. On the other hand, the value $S_2^*(-2) = -665.4361$ seems the most likely value to represent $-\infty$ than any other in that second column above the center line. This observation would indicate that two nonconstants should appear in column 1. The values $S_1(-1) = -2.8699$, and $S_1(0) = -1.5348$ would be the two nonconstants. This seems more likely because column 1 shows that $S_1^*(-2) \approx S_1^*(-3) = -2.158$, and $S_1^*(1) \approx S_1^*(2) = -1.864$. Therefore, the constant C_2 above the line (see Table 1) would be about -2.15, and the constant C_1 below the line would be about -1.86. This is supported by the fact that $S_2^*(1) \approx 1.86$ [about the same but with opposite sign as $S_1^*(1)$]. From the foregoing analysis it can be concluded that $2q = 2$ or $q = 1$. Therefore, the model for the annual flows of the Niger River is identified as ARMA (1,1).

Summary and Conclusions

The problem of the identification of streamflow stochastic models has been the main subject of this paper. The identification of the type of stochastic model has been made based on a conceptual physical representation of a natural watershed, and the identification of the form of the model has been made based on the recently developed R-functions and S-functions.

Under certain assumptions, for an ARMA (p,q) precipitation input the ground-water storage is an ARMA $(p+1,q)$ process and the streamflow is an ARMA $(p+1,q+1)$ process. In general such ground-water and streamflow processes belong to the class of restricted ARMA processes in the sense that their parameter space is a subspace of that corresponding to the general ARMA models.

The form or order of the ground-water and streamflow ARMA processes for given historical time series can be uniquely identified by using the R-functions and S-functions. It is expected that such a technique will have a widespread application in modeling of hydrologic time series.

Acknowledgments

The support of the NSF Project ENG-7919300 is acknowledged. Support from CONICIT (Venezuela) for graduate studies of the third writer is also acknowledged. Thanks are due to D. C. Boes for his valuable comments.

Appendix I.—References

1. Boes, D. C., and Salas, J. D., "Nonstationarity in the Mean and the Hurst Phenomenon," *Journal of Water Resources Research*, Vol. 14, No. 1, Washington, D.C., 1978, pp. 135–143.
2. Box, G. E. P., and Jenkins, G., "Time Series Analysis, Forecasting and Control," 1st ed., Holden-Day, San Francisco, Calif., 1970.
3. Carlson, R. F., McCormick, J. A., and Watts, D. G., "Application of Linear Random Models to Four Annual Streamflows Series," *Journal of Water Resources Research*, Vol. 6, No. 4, Washington, D.C., 1970, pp. 1070–1078.
4. Fiering, M. B., "Streamflow Synthesis," Harvard University Press, Cambridge Mass., 135 p., 1967.
5. Gray, H. L., Houston, A. G., and Morgan, F. W., "On G-Spectral Estimation," in *Applied Time Series Analysis*, by D. F. Findley, ed., Academic Press, New York, N.Y., 1978.
6. Hipel, K. W., McLeod, A. I., and Lennox, W. C., "Advances in Box-Jenkins Modeling, 1. Model Construction," *Journal of Water Resources Research*, Vol. 13, No. 3, Washington, D.C., 1977, pp. 567–575.
7. Jackson, B. B., "The Use of Streamflow Models in Planning," *Journal of Water Resources Research*, Vol. 11, No. 1, Washington, D.C., 1975, pp. 54–63.
8. Jackson, B. B., "Markov Mixture Models for Drought Lengths," *Journal of Water Resources Research*, Vol. 11, No. 1, Washington, D.C., 1975, pp. 64–74.
9. Jenkins, G. M., and Watts, D. G., "Spectral Analysis and Its Applications," Holden-Day, San Francisco, Calif., 1969.
10. Klemes, V., "Watershed as Semi-Infinite Storage Reservoir," *Journal of the Irrigation and Drainage Division*, ASCE, Vol. 99, No. IR4, Proc. Paper 10213, 1973, pp. 477–491.
11. Klemes, V., "Physically Based Stochastic Hydrologic Analysis," In *Advances in Hydroscience*, V. T. Chow, ed., Academic Press, New York, N.Y., 1978, pp. 285–352.
12. Lane, W. L., "Applied Stochastic Techniques," Division of Planning Technical Services, U.S.B.R., Denver, Colo., 1979.
13. Lettenmaier, D. P., and Burges, S. J., "Operational Assessment of Hydrologic Models of Long-Term Persistence," *Journal of Water Resources Research*, Vol. 13, No. 1, Washington, D.C., 1979, pp. 113–124.
14. Mandelbrot, B., and Wallis, J., "Noah, Joseph and Operational Hydrology," *Journal of Water Resources Research*, Vol. 4, No. 5, Washington, D.C., 1978, pp. 909–918.
15. Matalas, N. C., "Mathematical Assessment of Synthetic Hydrology," *Journal of Water*

Resources Research, Vol. 3, No. 4, Washington, D.C., 1967, pp. 937–945.
16. Mejia, J. M., "On the Generation of Multivariate Sequences Exhibiting the Hurst Phenomenon and Some Flood Frequency Analyses," thesis presented to Colorado State University, at Fort Collins, Colo., in 1971, in partial fulfillment of the requirements for the degree of Doctor of Philosophy.
17. Moss, M. E., "Serial Correlation Structure of Discretized Streamflow," thesis presented to Colorado State University, at Fort Collins, Colo., in 1972, in partial fulfillment of the requirements for the degree of Doctor of Philosophy.
18. O'Connell, E., "A Simple Stochastic Modeling of Hurst's Law," presented at the 1971, International Symposium on Mathematical Models in Hydrology, held at Warsaw, Poland, pp. 327–358.
19. O'Connor, K. M., "A Discrete Linear Cascade Model for Hydrology," *Journal of Hydrology*, Vol. 29, Amsterdam, Netherlands, 1976, pp. 203–242.
20. Pegram, G. G. S., "Physical Justification of a Continuous Streamflow Model," presented at the June, 1977, Third International Symposium, held at Fort Collins, Colo.
21. Pye, W. C., and Atchison, T. A., "An Algorithm for the Computation of the Higher Order G-Transformation," *SIAM Journal Number*, Analysis, Vol. 10, pp. 1–7.
22. Quimpo, R., "Structural Relation Between Parametric and Stochastic, Hydrology Models," presented at the 1977, International Symposium on Mathematical Models in Hydrology, held at Warsaw, Poland.
23. Rodriquez, I. I., Mejia, J. M., and Dawdy, D. R., "Streamflow Simulation, 1, A New Look at Markovian Models, Fractional Gaussian Noise and Crossing Theory," *Journal of Water Resources Research*, Vol. 8, No. 4, Washington, D.C., 1972, pp. 921–930.
24. Salas, J. D., and Smith, R. A., "Uncertainties in Hydrologic Time Series Analysis," presented at the April, 14–18, 1980 ASCE Spring Convention, held at Portland, Oreg. (Preprint 80-158).
25. Salas, J. D., and Smith, R. A., "Physical Basis of Stochastic Models of Annual Flows," accepted for publication in the *Journal of Water Resources Research*, Washington, D.C., 1981.
26. Selvalingam, S., "ARMA and Linear Tank Models," presented at the June, 1977, Third International Hydrology Symposium held at Fort Collins, Colo.
27. Spolia, S. K., and Chander, S., "Modeling of Surface Runoff Systems by an ARMA Model," *Journal of Hydrology*, Vol. 22, Amsterdam, Netherlands, 1974, pp. 317–332.
28. Thomas, H. A., Fiering, M. B., "Mathematical Synthesis of Streamflow Sequences for the Analysis of River Basins by Simulation," In *Design of Water Resources Systems* by A. Mass, M. M. Hufschmidt, R. Dorfman, H. A. Thomas, S. A. Marglin and G. M. Fair, Harvard University Press, Cambridge, Mass., 1962.
29. Thomas, H. A., Personal Communication to M. B. Fiering, Examination questions for Engineering 250, Harvard University, Cambridge, Mass., 1965.
30. Valencia, D., and Schaake, J. C., "Disaggregation Process in Stochastic Hydrology," *Journal of Water Resources Research*, Vol. 9, No. 3, Washington, D.C., 1973, pp. 580–585.
31. Wallis, J. R., and Matalas, N. C., "Statistical Properties of Multivariate Fractional Noise Processes," *Journal of Water Resources Research*, Vol. 7, No. 6, Washington, D.C., 1971, pp. 1460–1468.
32. Weiss, G., "Filtered Poison Process as Models for Daily Streamflow Data," thesis presented to the Imperial College, at London, England, in 1973, in partial fulfillment of the requirements for the degree of Doctor of Philosophy.
33. Woodward, W. A., and Gray, H. L., "On the Relationship Between the *R* and *S* Arrays and the Box-Jenkins Method of ARMA Model Identification," *Technical Report 134*, Department of Statistics, Southern Methodist University, Dallas, Texas, July, 1979.
34. Yevjevich, V., "Fluctuation of Wet and Dry Years," Part I, Research Data Assembly and Mathematical Models, *Hydrology Paper No. 1*, Colorado State University, Fort Collins, Colo., 1963.
35. Yevjevich, V., "Stochastic Processes in Hydrology," Water Resources Publications, Fort Collins, Colo., 1972.

Appendix II.—Notation

The following symbols are used in this paper:

AR = abbreviation for 'autoregressive';
ARMA = abbreviation for 'autoregressive moving average';
a = fraction of the precipitation reaching ground-water storage;
B = backward shift operator defined by $Bz_t = z_{t-1}$;
b = fraction of precipitation lost by evapotranspiration;
C_1 = constant (down) of pth column of table of S*-function;
C_2 = constant (up) of pth column of table of S*-function;
c = fraction of ground-water storage released as streamflow;
d = $1-a-b$ = fraction of precipitation reaching stream as direct runoff;
$H_n(\cdot)$ = determinants used to define R-functions and S-functions;
N = sample size of annual flows;
p = order of autoregressive component;
q = order of moving average component;
$R_n(\cdot)$ = R-function used in Gray's method of identification;
$S_n(\cdot)$ = S-function used in Gray's method of identification;
$S_t^*(\cdot)$ = shifted S-function used in Gray's method of identification;
S_t = ground-water storage at beginning of year, t;
S_t' = deviation of S_t from its mean, μ_s;
u = symbol used to denote undefined terms in table of S*-function;
x_t = input precipitation to conceptual model of watershed during year, t (Also used as annual streamflow to define autocorrelation function ρ_k);
x_t' = deviation of x_t from its mean, μ_x;
$\bar{x}$ = sample mean of annual streamflows;
z_t = streamflow during year, t;
z_t' = deviation of z_t from its mean, μ_z;
ϵ_t = normally and independently distributed random variable at time, t with zero mean and variance, σ_ϵ^2 (white noise);
ϵ_t' = white noise with zero mean and variance $\sigma_\epsilon'^2$;
η_t = white noise with zero mean and variance $d^2\sigma_\epsilon'^2$;
θ_j = jth moving average parameter of general ARMA model;
θ_j' = jth moving average parameter of ARMA model for input;
$\theta'(B)$ = polynomial in backward shift operator B with coefficients, θ_j'
$\theta''(B)$ = polynomial in backward shift operator B of ARMA model for streamflow;
μ_s = population mean of random variable, S_t;
μ_x = population mean of random variable, x_t;
μ_z = population mean of random variable, z_t;
ξ_t = white noise with zero mean and variance, $a^2\sigma_\epsilon'^2$;
ρ_k = lag-k autocorrelation coefficient;
σ_ϵ^2 = variance of white noise, ϵ_t;
$\sigma_\epsilon'^2$ = variance of white noise, ϵ_t';
ϕ_j = jth autoregressive parameter of general ARMA model;

ϕ'_j = jth autoregressive parameter of ARMA model for input;
$\phi'(B)$ = polynomial in backward shift operator B with coefficients, ϕ'_j; and
$\phi''(B)$ = polynomial in backward shift operator B of ARMA model for streamflow.

PREDICTING LAKE LEVELS BY EXPONENTIAL SMOOTHING

By Sivajogi D. Koppula,[1] A. M. ASCE

INTRODUCTION

Estimating future trends is essential to all planning activities and especially so in water resources management. The need for at least an approximate flood plain mapping is recognized by the United States National Flood insurance program for cases when time and funds do not permit the requisite data gathering (7). Flood plain and land-use management efforts around a large lake are severely handicapped by not having the estimates of future lake levels.

Statistical forecasting is a relatively new application in water resources management and it may provide a way to project and plan for the future. Hydraulic engineers are currently using a variety of methods ranging all the way from subjective intuitive methods to rigorous, cause-effect models such as estimating runoff from rainfall data. The cause-effect models depend wholly on information pertaining to variables which cause, say, lake levels to rise and fall; and are relatively difficult and expensive to develop. Moreover such models may not provide much lead time for the planners to develop preventive measures. There exist, however, mathematical techniques that make use of historical data and project future values. Such techniques have proved to be very useful and often 'accurate' in other disciplines such as economics and marketing.

The purpose of the present study is to utilize a forecasting technique called Exponentially Weighted Moving Average (EWMA) method and forecast water levels of a large lake in Alberta, Canada. The forecasting ability of EWMA is compared with other available results (5).

The lake level study was chosen because: (1) The temporal variations in lake levels due to hydrometeorological and other nonrelated factors are prime causes for floods; (2) the flood-prone lake shore lands require advance planning for rehabilitation measures; (3) the real estate around the lake shore is always in demand for recreational and other development purposes; and (4) the average

[1]Section Head, Design and Construction Div., Alberta Environment, 16403-102 Street, Edmonton, Alberta, T5X 2G9, Canada.

Note.—Discussion open until December 1, 1981. To extend the closing date one month, a written request must be filed with the Manager of Technical and Professional Publications, ASCE. Manuscript was submitted for review for possible publication on September 25, 1980. This paper is part of the Journal of the Hydraulics Division, Proceedings of the American Society of Civil Engineers, ©ASCE, Vol. 107, No. HY7, July, 1981. ISSN 796X/81/0007-0867/$01.00.

monthly data for the years 1913–1977 is readily available for Lesser Slave Lake, Alberta (4).

It has become conventional to classify forecasts as being either ex-post or ex-ante. In the latter case, the true values of exogenous variables are unknown at the time the forecast is made, therefore, they must be estimated. Forecasting errors may, therefore, be due to errors in the estimates of the predetermined variables or incorrect specification of the forecasting model or both. In this study the forecasts presented are of an ex-post nature, which uses actual observations of the predetermined variables to predict values for the endogenous variables; any errors are therefore attributable only to the model.

The monthly data for the period 1913–1972 (see Fig. 1) is used in model building and estimation of the parameters of the model. the predictive ability of the forecasting model is tested by comparing the ex-post forecasts with the 60 actual observations of the period 1973–1977. The predictive accuracy is evaluated by using the mean absolute error, $\Sigma|e|/60$, the mean squared error, $\Sigma e^2/60$, and Mincer-Zarnowitz criterion (6); in which e = the difference between

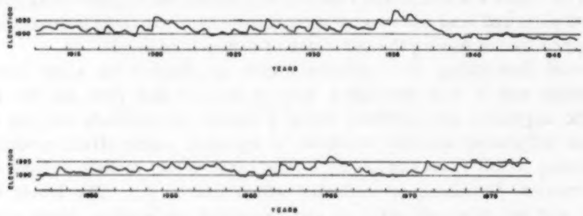

FIG. 1.—Monthly Average Lake Levels, Lesser Slave Lake, 1913–1977

the actual and predicted lake levels. Mincer and Zarnowitz (6) enunciated a definition of forecast accuracy based on

$$A(t) = a_0 + a_1 F(t) \quad \text{. . . . . (1)}$$

in which $A(t)$ = the observation at time, t; $F(t)$ = the corresponding forecast; and a_0 and a_1 = regression coefficients. If $a_0 = 0$ and a_1 tends to unity, the forecast is deemed accurate. the coefficients, a_0 and a_1, are determined by the application of ordinary least squares.

EWMA Method

Let $\{x(1), x(2), \dots \dots \dots, x(t)\}$ be a stationary stochastic series in discrete time and let it be required to predict the value of the series at time, $(t + 1)$. The predictor, $\hat{x}(t + 1)$, may be given as a weighted sum of the past observations

$$\hat{x}(t + 1) = c_0 x(t) + c_1 x(t - 1) + \dots \quad \text{. . . . . (2a)}$$

in which $c_0, c_1, \dots$ = the weights attached to each of the known observations. It seems sensible to attach more weight to recent observations and less weight to observations further in the past. An intuitively appealing set of weights are

those which decrease in geometric progression (2). Eq. 2*a* may then be expressed as

$$\hat{x}(t+1) = \lambda x(t) + \lambda(1-\lambda)x(t-1) + \lambda(1-\lambda)^2 x(t-2) + \ldots \quad (2b)$$

in which λ = a constant such that $0 < \lambda < 1$.

Eq. 2*b* implies an infinite number of past observations that are required to estimate $\hat{x}(t+1)$, however in practice there will only be a finite number. Eq. 2*b* is sometimes written in the form

$$\hat{x}(t+1) = \lambda x(t) + (1-\lambda)\{\lambda x(t-1) + \lambda(1-\lambda)x(t-2) + \ldots\}$$

$$= \lambda x(t) + (1-\lambda)\hat{x}(t) \quad (2c)$$

which is called an exponentially weighted moving average. Thus, for $t = 3$, Eq. 2*c* may be expressed as a series of equations:

$$\hat{x}(4) = \lambda x(3) + (1-\lambda)\hat{x}(3) \quad (2d)$$

$$\hat{x}(3) = \lambda x(2) + (1-\lambda)\hat{x}(2) \quad (2e)$$

$$\hat{x}(2) = \lambda x(1) + (1-\lambda)\hat{x}(1) \quad (2f)$$

in which $\hat{x}(2)$ = the predicted value for period, $t = 2$, made at $t = 1$, at which time the observation $x(1)$ is available. If we set $\hat{x}(1) = x(1)$, i.e., the predicted value of the series at time $t = 1$ equals the actual observation at that time, then $\hat{x}(2) = \lambda x(1) + (1-\lambda)x(1) = x(1)$. This means that the estimated value forecasted for time $t = 2$ of the series is equal to the observation at time $t = 1$. Eq. 2*c* can now be used recursively to compute forecasts at future times. Eq. 2*c* also reduces the amount of arithmetic involved because forecasts may be easily updated using the latest observation and the previous forecast. Eq. 2*c* may be rewritten as

$$\hat{x}(t+1) = \lambda\{x(t) - \hat{x}(t)\} + \hat{x}(t) \quad (2g)$$

$$\text{i.e.,} \quad \hat{x}(t+1) = \lambda e_t + \hat{x}(t) \quad (3)$$

in which $e_t = x(t) - \hat{x}(t)$, the prediction error at time, t. The magnitude of the constant, λ depends on the characteristics of the time series. For an arbitrary chosen λ the following may be calculated:

$$\hat{x}(2) = x(1) \qquad \text{by assumption}$$

$$e_2 = x(2) - \hat{x}(2)$$

$$\hat{x}(3) = \lambda e_2 + \hat{x}(2)$$

$$e_3 = x(3) - \hat{x}(3)$$

and so on.

$$\hat{x}(t) = \lambda e_{t-1} + \hat{x}(t-1)$$

$$e_t = x(t) - \hat{x}(t)$$

and $$\hat{x}(t+1) = \lambda e_t + \hat{x}(t)$$

and the expression $\Sigma_{t=2}^{t} e_t^2$ is computed. This procedure is repeated for various values of λ in the range of 0–1. The value corresponding to the minimum of

the calculated Σe_t^2 is chosen as the optimum λ to be used in computing the forecast at time, $(t + 1)$.

Winters (8) has generalized the foregoing method to deal with time series that contains trend and seasonal variations. Let $M(t)$ denote the estimated current mean of $x(t)$ in period, t; $T(t)$ denote the estimated trend, i.e., the expected change in current mean; and $S(t)$ denote the estimated seasonal factor in period, t. As each new observation becomes available, the three terms $M(t)$, $T(t)$, and $S(t)$ are updated. The seasonal variation in the time series may possess either a multiplicative or an additive effect. Should the amplitude of the seasonal pattern be proportional to the level of the observations a multiplicative, or ratio, seasonal effect is said to exist. However, if the amplitude is independent of the levels then an additive effect should be considered. A graph of the data should be examined to ascertain whether an additive or multiplicative seasonal effect is present. The method may 'blow up' if the wrong seasonal effect is applied. The updating equations for $M(t)$ and $S(t)$ for an additive seasonal effect are

$$M(t) = \alpha\{x(t) - S(t-s)\} + (1-\alpha)\{M(t-1) + T(t-1)\} \quad \ldots\ldots\ldots (4a)$$

$$S(t) = \beta\{x(t) - M(t)\} + (1-\beta)S(t-s) \quad \ldots\ldots\ldots\ldots\ldots\ldots (4b)$$

in which α and β are smoothing constants such that $0 < \alpha$; $\beta < 1$; and s = the seasonal span (e.g., $s = 12$ for monthly data). The current mean and seasonal factors are thus updated by linear superposition of past values. If the seasonal variation is multiplicative the updating equations will be

$$M(t) = \frac{\alpha x(t)}{S(t-s)} + (1-\alpha)\{M(t-1) + T(t-1)\} \quad \ldots\ldots\ldots\ldots (4c)$$

$$S(t) = \frac{\beta x(t)}{M(t)} + (1-\beta)S(t-s) \quad \ldots\ldots\ldots\ldots\ldots\ldots\ldots (4d)$$

in which the current values for $M(t)$ and $S(t)$ are derived through a process of ratio, or division. The updating equation for the current trend term $T(t)$ is

$$T(t) = \gamma\{M(t) - M(t-1)\} + (1-\gamma)T(t-1) \quad 0 < \gamma < 1 \quad \ldots\ldots\ldots (4e)$$

The forecast, $\hat{x}(t + c)$, for time, $(t + c)$, is given by Eq. 5:

$$\hat{x}(t+c) = \{M(t) + cT(t)\}S(t-s+c) \quad c = 1, 2, \ldots, s \quad \ldots\ldots\ldots\ldots (5)$$

Eqs. 4*a*–4*e* are of such a nature that if a state of a time series is specified at some initial time, $t = t_0$, a solution exists for $t > t_0$ and is uniquely determined by Eq. 5. Starting values for $M(t)$, $S(t)$, and $T(t)$ may be approximated from the initial observations in the time series, e.g., for monthly data, the first 24 observations are made use of to calculate

$$M(1) = \sum_{t=1}^{12} \frac{x(t)}{12} \qquad M(2) = \sum_{t=13}^{24} \frac{x(t)}{12}$$

$$T(1) = \frac{M(1) - M(2)}{12}$$

$$S(1) = 0.5\left\{\frac{x(1)}{M(1)} + \frac{x(13)}{M(2)}\right\}$$

$$S(2) = 0.5\left\{\frac{x(2)}{M(1)} + \frac{x(14)}{M(2)}\right\}$$

and so on

$$S(12) = 0.5\left\{\frac{x(12)}{M(1)} + \frac{x(24)}{M(2)}\right\}$$

The three smoothing constants, α, β, and γ, are varied in the range of 0.0–1.0 and the quantity Σe_i^2 is calculated. The set of values for (α, β, γ) corresponding to the minimum of the calculated Σe_i^2 is the optimum for α, β, and γ. The optimum (α, β, γ) is used in updating the equations for $M(t)$, $S(t)$, and $T(t)$; and forecasts are made using Eq. 5 for the horizon of length, c.

Forecast Results and Interpretation

As mentioned in the introduction the first 720 observations in the lake level time series are used to develop the initial values of $M(t)$, $S(t)$, and $T(t)$. The next 60 observations are utilized to test the forecasting model—making a forecast; moving along one period (12 months for monthly lake level data); comparing the forecasts with observed data; absorbing the observed data into the forecasting model; making forecast for the next period; and the cycle is repeated.

A grid of values for the smoothing constants, α, β, and γ, is used to calculate the predicted mean squared error, $\Sigma(\text{actual-forecast})^2/60$. The grid was made up of all possible combinations of 0., 0.2, 0.4, 0.6, 0.8, and 1.0. The values of $\Sigma e^2/60$, in which e = the error between the actual and forecast values, are given in Table 1. Table 2 shows the areas around the minimum $\Sigma e^2/60$ for a finer grid values of α, β, and γ with increments equal to 0.01; as may be seen the value of $\Sigma e^2/60$ is rather flat near its minimum. Perhaps lower values of $\Sigma e^2/60$ could be found, however the benefit gained may not be worth the effort. The lowest calculated value for $\Sigma e^2/60$ is 0.35 at $\alpha = 0.80$, $\beta = 0.64$, and $\gamma = 0.29$ for a multiplicative seasonal model.

Few general comments about the optimal values associated with the smoothing constants can be made. It is possible to imagine a series in which some of the constants are subject to little or no drift; and also a series where there is little random effect. If there is no change in a constant over the series then if the random effect is small, the value associated with that constant would be small, or even zero, because there is no use in changing the original and still accurate estimate of the constant. If the drift in a constant is large over the series, even to the point of abrupt changes in its value from time to time, there are two possibilities: (1) Little random effect would lead to large values weighting current estimates heavily; and (2) a large random effect would yield substantially smaller values depending on the relative importance of the changes in the constant as compared to the random element. These intuitive deductions have been summarized in Ref. 8.

In the case of Lesser Slave Lake level data the smoothing constant, α, is

TABLE 1.—Value of $\Sigma e^2/60$: Grid Results

β	γ = 0.0	0.2	0.4	0.6	0.8	1.0
(1)	(2)	(3)	(4)	(5)	(6)	(7)
			(*a*) $\alpha = 0.0$			
0.0	—[a]	—[a]	—[a]	—[a]	—[a]	55.08
0.2	4.90	4.04	3.18	2.24	1.98	2.24
0.4	1.19	1.03	0.87	0.72	0.70	1.44
0.6	0.99	0.92	0.84	0.77	0.76	1.06
0.8	1.07	1.02	0.97	0.93	0.92	1.05
1.0	1.23	1.21	1.18	1.15	1.14	1.23
			(*b*) $\alpha = 0.2$			
0.0	0.77	2.22	2.18	2.15	4.17	8.93
0.2	0.77	1.74	1.25	1.51	6.65	309.73
0.4	0.79	1.56	0.76	2.33	—[a]	—[a]
0.6	0.81	1.38	0.64	1.78	—[a]	—[a]
0.8	0.84	1.35	1.69	—[a]	—[a]	—[a]
1.0	0.90	1.64	25.90	—[a]	—[a]	—[a]
			(*c*) $\alpha = 0.4$			
0.0	0.70	1.73	3.16	5.41	6.26	6.83
0.2	0.68	0.88	2.48	387.87	—[a]	—[a]
0.4	0.66	0.97	0.65	—[a]	—[a]	—[a]
0.6	0.71	1.58	630.25	—[a]	—[a]	—[a]
0.8	0.78	3.28	—[a]	—[a]	—[a]	—[a]
1.0	0.82	6.00	—[a]	—[a]	—[a]	—[a]
			(*d*) $\alpha = 0.6$			
0.0	0.69	1.83	3.03	3.59	3.54	2.83
0.2	0.65	0.74	2.13	8.33	92.75	158.40
0.4	0.64	1.42	23.01	—[a]	—[a]	338.48
0.6	0.59	2.07	909.72	—[a]	—[a]	—[a]
0.8	0.60	1.54	—[a]	—[a]	—[a]	—[a]
1.0	0.65	0.98	—[a]	—[a]	—[a]	—[a]
			(*e*) $\alpha = 0.8$			
0.0	0.69	1.63	1.94	1.36	0.64	1.19
0.2	0.59	1.11	4.26	6.06	3.15	16.87
0.4	0.65	0.81	1.23	24.54	27.20	226.32
0.6	0.63	0.54[b]	17.09	8.25	127.63	—[a]
0.8	0.63	1.36	6.94	428.39	358.17	—[a]
1.0	0.65	2.98	619.78	—[a]	—[a]	—[a]
			(*f*) $\alpha = 1.0$			
0.0	0.67	1.34	1.22	1.12	3.04	9.08
0.2	0.68	1.45	1.44	1.22	2.69	7.98
0.4	0.67	1.34	1.23	1.12	2.92	8.69
0.6	0.67	1.32	1.19	1.11	3.08	9.22
0.8	0.67	1.35	1.23	1.12	3.04	9.08
1.0	0.67	1.34	1.22	1.12	3.04	9.08

[a]The value is larger than 1×10^3.
[b]Minimum $\Sigma e^2/60$.

large revealing that the effect of earlier observations is quickly attenuated. This generally occurs when the mean of the series changes quickly, and this would seem to be the case for the lake levels. The smoothing constant, β, associated with the seasonal variation is substantially large indicating that seasonal adjust-

TABLE 2.—Value of $\Sigma e^2/60$: Finer Grid Results

	γ				
β	0.28	0.29	0.30	0.31	0.32
(1)	(2)	(3)	(4)	(5)	(6)
			(*a*) α = 0.78		
0.63	1.98	2.08	2.03	1.94	1.71
0.64	2.56	2.77	2.75	2.79	2.58
0.65	3.15	3.49	3.73	3.82	3.69
0.66	3.86	4.44	4.79	5.11	5.15
0.67	4.66	5.40	6.06	6.60	6.89
			(*b*) α = 0.79		
0.63	0.67	0.58	0.49	0.42	0.41
0.64	0.89	0.82	0.72	0.58	0.49
0.65	1.23	1.16	1.04	0.88	0.72
0.66	1.62	1.61	1.53	1.33	1.10
0.67	2.08	2.16	2.10	1.95	1.69
			(*c*) α = 0.80		
0.63	0.37	0.40	0.52	0.73	1.14
0.64	0.36	0.35[a]	0.41	0.59	0.89
0.65	0.39	0.36	0.36	0.45	0.68
0.66	0.48	0.42	0.37	0.38	0.51
0.67	0.63	0.54	0.45	0.40	0.44
			(*d*) α = 0.81		
0.63	0.72	0.94	1.27	1.79	2.36
0.64	0.61	0.79	1.07	1.52	2.20
0.65	0.52	0.66	0.91	1.33	1.93
0.66	0.44	0.56	0.74	1.11	1.66
0.67	0.38	0.46	0.59	0.89	1.41
			(*e*) α = 0.82		
0.63	1.25	1.58	1.99	2.56	3.15
0.64	1.17	1.48	1.89	2.37	3.16
0.65	1.07	1.37	1.76	2.32	3.03
0.66	0.96	1.22	1.62	2.17	2.88
0.67	0.85	1.10	1.47	2.01	2.72

[a]Minimum value of $\Sigma e^2/60$.

ments are quite pronounced in Lesser Slave Lake levels. Finally the trend parameter makes only slight revisions in the smoothing process as is evidenced by a low value for γ. This shows that no abrupt shifts in lake level trends occur. A comparison of the EWMA forecasts with the actual lake level

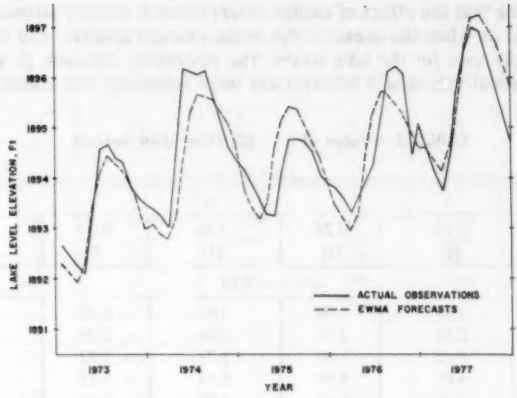

FIG. 2.—Comparison of Forecasts with Lake Level Observations

observations is presented in Fig. 2 for the 60 observations from 1973–1977. A visual inspection of Fig. 2 shows that the forecasts in general follow the trend of the actual observations and the largest deviation appears to be of the order of 1.5 ft (0.45 m).

Comparison with other Forecasting Models

Two other forecasting methods were applied to the lake level data by the writer (5) and the results are used to make a comparison with the results of EWMA. The models were based on Box-Jenkins technique (1) and Harmonic analysis (3). It has been shown in Ref. 5 that a composite model combining the forecasts from Box-Jenkins technique and the Harmonic analysis yields better forecasts than either of the two methods.

The results of these forecasting models together with those from EWMA are given in Table 3. A summary of the comparison between each of the forecasts and the actual observations is presented in Tables 4 and 5. The predicted mean squared error, $\Sigma e^2/60$, for the Harmonic analysis is substantially higher than that of the other three models. The Box-Jenkins and Composite models however are more serious contenders; which in some ways have results similar to those of EWMA for the period being forecast. The Box-Jenkins approach identifies the stochastic components in the time series, i.e., autoregressive (AR) and moving average (MA) components. The Composite model embraces not only the AR and MA stochastic components but also information inherent in harmonic cycles of periodicity greater than 12. On the other hand, EWMA readily incorporates any drifts over time and can filter out substantial random effects in the observations.

Table 4 shows that EWMA is consistently superior in its predictive ability as evidenced by the lowest values of the predicted mean squared error, $\Sigma e^2/60$, and the mean absolute error, $\Sigma|e|/60$. Both these criteria are important because

TABLE 3.—Actual Observations and Forecasts Made over Horizon of Time Periods

Actual observation (1)	EWMA (2)	Forecasts		
		Composite (3)	Box-Jenkins (4)	Harmonic (5)
1,892.68	1,892.31	1,893.62	1,893.58	1,892.86
1,892.48	1,892.08	1,893.62	1,893.61	1,892.78
1,892.28	1,891.92	1,893.49	1,893.43	1,892.91
1,892.12	1,892.26	1,893.33	1,893.16	1,893.21
1,893.21	1,893.29	1,894.12	1,893.80	1,893.59
1,894.59	1,894.11	1,895.25	1,894.80	1,893.94
1,894.68	1,894.47	1,895.38	1,894.86	1,894.15
1,894.44	1,894.33	1,895.14	1,894.62	1,894.15
1,894.34	1,894.16	1,894.61	1,894.17	1,893.93
1,893.90	1,893.90	1,893.92	1,893.63	1,893.53
1,893.63	1,893.55	1,893.35	1,893.23	1,893.06
1,893.50	1,893.01	1,893.08	1,893.13	1,892.62
1,893.41	1,893.09	1,893.73	1,893.89	1,892.32
1,893.26	1,892.89	1,893.74	1,893.93	1,892.23
1,893.06	1,892.79	1,893.61	1,893.75	1,892.36
1,894.23	1,893.16	1,893.45	1,893.48	1,892.67
1,896.21	1,894.36	1,894.22	1,894.11	1,893.05
1,896.13	1,895.33	1,895.37	1,895.12	1,893.41
1,896.09	1,895.67	1,895.50	1,895.17	1,893.63
1,896.14	1,895.62	1,895.26	1,894.93	1,893.64
1,895.58	1,895.56	1,894.75	1,894.49	1,893.44
1,895.09	1,895.36	1,894.06	1,893.94	1,893.06
1,894.64	1,895.13	1,893.50	1,893.55	1,892.61
1,894.38	1,894.71	1,893.24	1,893.45	1,892.20
1,894.19	1,893.82	1,893.90	1,894.21	1,891.93
1,893.91	1,893.45	1,893.91	1,894.24	1,891.86
1,893.63	1,893.19	1,893.79	1,894.06	1,892.02
1,893.29	1,893.53	1,893.64	1,893.79	1,892.36
1,893.25	1,894.59	1,894.43	1,894.42	1,892.77
1,894.12	1,895.16	1,895.58	1,895.43	1,893.16
1,894.78	1,895.43	1,895.73	1,895.48	1,893.41
1,894.80	1,895.37	1,895.51	1,895.24	1,893.45
1,894.75	1,895.07	1,895.00	1,894.80	1,893.28
1,894.54	1,894.76	1,894.32	1,894.25	1,892.94
1,894.10	1,894.41	1,893.77	1,893.86	1,892.52
1,893.90	1,893.91	1,893.53	1,893.76	1,892.14
1,893.82	1,893.47	1,894.20	1,894.52	1,891.89
1,893.61	1,893.16	1,894.23	1,894.56	1,891.86
1,893.37	1,892.97	1,894.12	1,894.38	1,892.04
1,893.61	1,893.32	1,893.98	1,894.11	1,892.40
1,893.92	1,894.43	1,894.78	1,894.74	1,892.84
1,894.25	1,895.31	1,895.94	1,895.75	1,893.25
1,895.22	1,895.72	1,895.37	1,895.08	1,893.51
1,896.14	1,895.68	1,895.87	1,895.56	1,893.57
1,896.23	1,895.50	1,895.37	1,895.12	1,893.42
1,896.09	1,895.27	1,894.70	1,894.57	1,893.08
1,894.47	1,894.98	1,894.15	1,894.18	1,892.67

TABLE 3.—*Continued*

(1)	(2)	(3)	(4)	(5)
1,895.10	1,894.62	1,893.91	1,894.08	1,892.29
1,894.57	1,894.62	1,894.58	1,894.84	1,892.06
1,894.14	1,894.32	1,894.59	1,894.87	1,892.01
1,983.75	1,894.15	1,894.48	1,894.69	1,892.19
1,894.46	1,894.54	1,894.34	1,894.42	1,892.54
1,895.74	1,895.61	1,895.13	1,895.05	1,892.97
1,896.59	1,896.58	1,896.29	1,896.06	1,893.36
1,897.02	1,897.20	1,896.45	1,896.12	1,893.16
1,896.94	1,897.27	1,896.22	1,895.88	1,893.66
1,896.34	1,897.03	1,895.70	1,895.43	1,893.48
1,895.84	1,896.78	1,895.02	1,894.88	1,893.12
1,895.30	1,896.30	1,894.47	1,894.49	1,892.68
1,894.80	1,895.80	1,894.21	1,894.39	1,892.28

TABLE 4.—Comparison of Forecasting Models

Method (1)	$\Sigma\|e\|/60$ (2)	$\Sigma e^2/60$ (3)
EWMA	0.462	0.353
Box-Jenkins	0.712	0.687
Harmonic	1.697	3.674
Composite	0.674	0.628

TABLE 5.—Mincer-Zarnowitz Criterion: Forecast Comparison

Method (1)	Equation (2)	R^2 (3)	Standard error of regression (4)
EWMA	$A(t) = 376.55^a + 0.8012\ E(t)$	0.79	0.54
Box-Jenkins	$A(t) = -254.83^b + 1.1345\ B(t)$	0.51	0.83
Harmonic	$A(t) = 255.27^b + 0.8660\ H(t)$	0.21	1.05
Composite	$A(t) = 0.004^a + 1.0\ C(t)$	0.54	0.81
EWMA	$A(t) = 1.0\ E(t)^c$	0.785	0.54
Composite	$A(t) = 1.0\ C(t)^c$	0.536	0.81

[a]Not significantly different from zero because of the magnitude of standard deviation for the term.
[b]Significantly different from zero.
[c]Equation made to pass through the origin.

it is difficult to determine the consequences of the forecast errors in this particular case study. Whenever the consequences of one large error are more serious than that of several small errors the predicted mean squared error would be a more appropriate criterion for comparing the forecasts made by various methods.

Table 5 contains the regression results obtained utilizing Mincer-Zarnowitz criterion. As is evident only EWMA and Composite forecasts satisfy the criterion.

To further evaluate these two forecasts, the respective regression equations were made to pass through the origin; and the coefficients associated with $E(t)$ and $C(t)$ are found to equal unity and are significant at 0.95 level. The multiple correlation coefficient, R^2, which explains the percentage variation inherent in the actual observations, however is different for the two methods. The EWMA forecasting model explains 78.5% while the Composite model explains only 53.6% of the total variations in the actual observations. Furthermore, the EWMA model possesses a smaller standard error of regression. Thus a complete statistical evaluation reveals that the results from EWMA are significant and are the closest to the actual observations.

Conclusions

The forecasting method presented in this paper provides an easy, convenient, and inexpensive procedure to estimate future lake levels. It must be strongly emphasized that the object is to provide reasonably good estimates for hydraulic and planning engineers who would otherwise may have no flood hazard information at all. Another important application of this paper has been to demonstrate the advantages of the EWMA forecasting model over other methods that use the historical data as the sole input: (1) EWMA requires less information and storage space; (2) EWMA responds more rapidly to sudden shifts in the time series; and (3) EWMA provides routine forecasts without human intervention.

The EWMA method is generally applicable to data which contains a minimum of 50–75 observations taken at regular intervals of time. The larger the number of observations the 'more' accurate will be the forecasts, i.e., the closer will be the forecasts to the actual observations.

By fitting a mathematical model to the historic lake levels it is demonstrated that possible future occurrences of the lake levels can be generated. Furthermore, it is shown that the forecast values are statistically indistinguishable from the historical data. The future lake level(s) is(are) one of the crucial elements in addressing the stormwater management and land use around a lake district.

Appendix I.—References

1. Box, G. E. P., and Jenkins, G. M., "Time Series Analysis, Forecasting, and Control," Holden-Day, San Francisco, Calif., 1976.
2. Cox, D. R., "Prediction by Exponentially Weighted Moving Averages and Related Methods," *Journal of Royal Statistical Society*, Series B, Vol. 23, London, England, 1961, pp. 414–422.
3. Doran, H. E., and Quilkey, J. J., "Harmonic Analysis of Seasonal Data: Some Important Properties," *American Journal of Agricultural Economics*, Vol. 54, Nov., 1972, pp. 646–651.
4. "Lesser Slave Lake Water Levels, 1914–1977," Environment Canada, Water Survey of Canada, Mar., 1978, pp. 1–45.
5. Koppula, S. D., "Forecasting Lake Levels—A Case Study," *Proceedings, National Symposium on Urban Stormwater Management in Coastal Areas*, June, 1980, pp. 280–288.
6. Mincer, J., and Zarnowitz, V., "The Evaluation of Economic Forecasts," *Economic Forecasts and Expectations*, J. Mincer, ed., New York: National Bureau of Economic Research, New York, N.Y., 1969.
7. "Flood Insurance Study Guidelines and Specifications," United States Department of Housing and Urban Development, Federal Insurance Administration, Washington, D.C., Jan., 1975.

8. Winters, P. R., "Forecasting Sales by Exponentially Weighted Moving Averages," *Management Science*, Vol. 6, No. 3, Baltimore, Md., Apr., 1960, pp. 324–342.

APPENDIX II.—NOTATION

The following symbols are used in this paper:

a_0, a_1 = regression coefficients;
$A(t)$ = observation at time, t;
$B(t)$ = Box-Jenkins forecast at time, t;
c = integer;
$c_0, c_1 \ldots$ = constant weights;
$C(t)$ = composite forecast at time, t;
e = error, i.e., actual-forecast;
e_t = error at time, t;
$E(t)$ = EWMA forecast at time, t;
$F(t)$ = forecast at time, t;
$H(t)$ = Harmonic forecast at time, t;
$M(t)$ = mean in period, t;
R^2 = multiple correlation coefficient;
s = seasonal span, e.g., $s = 4$ for quarterly data;
$S(t)$ = seasonal factor in period, t;
$T(t)$ = trend factor in period, t;
t = time;
$x(t)$ = lake level observation at time, t;
$\hat{x}(t)$ = estimate of lake level at time, t;
$\hat{x}(t + c)$ = estimate of lake level at time, $(t + c)$;
α = smoothing constant for $M(t)$;
β = smoothing constant for $S(t)$;
γ = smoothing constant for $T(t)$; and
λ = smoothing constant.

Secondary Flow, Shear Stress and Sediment Transport

By Chao-Lin Chiu,[1] M. ASCE and David E. Hsiung[2]

Introduction

Open channel flow is generally three dimensional, although hydraulic studies mostly deal with one- or two-dimensional analysis and modeling. To treat the flow three dimensionally, "secondary flow" consisting of the vertical and transverse flow components, must be included, along with the "primary flow" (the flow component in the longitudinal direction), in hydraulic studies. It is also necessary to deal with the complex reality that channel cross sections, shear stress (including the boundary shear), velocities of primary and secondary flows, sediment concentration, etc., all vary three dimensionally, and that these hydraulic variables interact each other. A change in one will affect the others.

Earlier papers (2,3) dealt with various other aspects of three-dimensional mathematical modeling of open channel flow; this paper is concerned with relations and interactions among the secondary flow, shear stress, and sediment concentration in alluvial channels. Like those earlier papers, in hydraulic analysis this paper uses the framework of a curvilinear coordinate system consisting of isovels (curves along which the velocity is equal) of primary flow, marked as ξ curves in Fig. 1 and their orthogonal trajectories marked as η curves.

Coordinate System and Basic Flow Equations

In the ξ-η coordinate system the distribution of primary flow velocity can be represented quite well by the following logarithmic equation (Ref. 2, 3, 4):

$$V_1 = \frac{\bar{V}_*}{\kappa} \ln \frac{\xi}{\xi_0} \quad \text{. . . . . (1)}$$

in which a suitable equation for the ξ coordinate, representing a family of primary flow isovels, is

[1] Prof. of Civ. Engrg., Univ. of Pittsburgh, Pittsburgh, Pa.

[2] Engr., General Electric Company, Rockville, Md.; formerly, Research Asst., Dept. of Civ. Engrg., Univ. of Pittsburgh, Pittsburgh, Pa.

Note.—Discussion open until December 1, 1981. To extend the closing date one month, a written request must be filed with the Manager of Technical and Professional Publications, ASCE. Manuscript was submitted for review for possible publication on September 25, 1980. This paper is part of the Journal of the Hydraulics Division, Proceedings of the American Society of Civil Engineers, ©ASCE, Vol. 107, No. HY7, July, 1981. ISSN 0044-796X/81/0007-0879/$01.00.

$$\xi = \left(\frac{x_2}{D}\right)\left[\left(1 - \frac{|x_3|}{B_i}\right) e^{|x_3|/B_i}\right]^{\beta_i} \quad \ldots\ldots\ldots\ldots\ldots\ldots\ldots\ldots\ldots\ldots (2)$$

in Eqs. 1 and 2, V_1 = the point mean velocity of primary flow (in the x_1 direction); $\bar{V}_*$ = the mean shear velocity, evaluated as $\sqrt{gRS}$ at a cross section, in which g = the gravitational acceleration, R = the hydraulic radius, and S = energy or channel slope; D = the water depth at the x_2-axis; B_i for i equal to either 1 or 2 = the transverse distance on the water surface between the x_2-axis and either the left or right bank of a channel cross section; x_3 = the

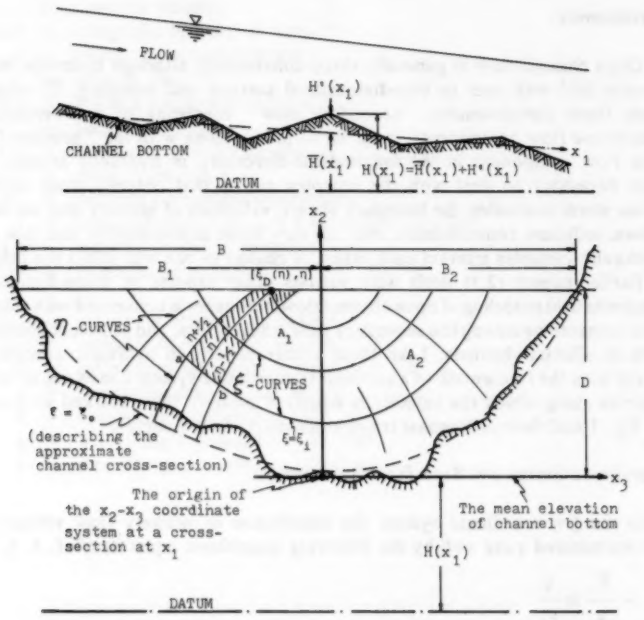

FIG. 1.—x_1-ξ-η Coordinate System

coordinate in the transverse direction; x_2 = the coordinate in the vertical direction (the x_2-axis is selected such that it passes through the point of maximum primary flow velocity); ξ_0 and β_i = empirical coefficients which can be determined according to the variance reducing technique from the linear relation between V_1 and ξ on a semi-log plot. Eq. 1 has the same form as the Prandtl-von Karman universal velocity distribution equation. In addition, κ is a coefficient, actually evaluated with observed data on V_1, which also tends to be equal to about 0.4; thus, if no data are available, 0.4 can be used as a good approximation of κ.

Orthogonal trajectories of ξ curves (isovels of primary flow) can be obtained from Eq. 2 as

$$\eta = \left(\frac{x_2}{D}\right)^2 + \frac{2B_i^2}{D^2\beta_i}\left(\ln\frac{|x_3|}{B_i} - \frac{|x_3|}{B_i}\right) \quad \ldots\ldots\ldots\ldots\ldots\ldots\ldots\ldots (3)$$

Pairing of Eqs. 2 and 3 forms a curvilinear ξ-η coordinate system.

The momentum equation in the x_1 direction (longitudinal direction) in the x_1-ξ-η coordinate system directly gives the ξ component of flow, i.e., the flow component perpendicular to the isovels of primary flow, as:

$$V_\xi = \left(\frac{\rho}{h_\xi}\frac{\partial V_1}{\partial \xi}\right)^{-1}\left[-\rho\frac{\partial V_1}{\partial t} - \rho V_1\frac{\partial V_1}{\partial x_1} - \frac{\partial}{\partial x_1}(\rho g H) + \frac{\partial \sigma_1}{\partial x_1}\right.$$

$$\left. + \frac{1}{h_\xi}\frac{\partial \tau_{\xi 1}}{\partial \xi} + \frac{1}{h_\xi h_\eta}\frac{\partial h_\eta}{\partial \xi}\tau_{\xi 1}\right] \quad \ldots\ldots\ldots\ldots\ldots\ldots\ldots\ldots (4)$$

while the continuity equation gives the η component (the flow component tangent to the isovels of primary flow):

$$V_\eta = -\frac{1}{h_\xi}\int_{\eta^*}^{\eta}\left(h_\xi h_\eta\frac{\partial V_1}{\partial x_1} + h_\eta\frac{\partial V_\xi}{\partial \xi} + V_\xi\frac{\partial h_\eta}{\partial \xi}\right)d\eta + V_\eta\Big|_{\eta=\eta^*} \quad \ldots\ldots (5)$$

In Eqs. 4 and 5, V_ξ and V_η = the ξ and η components of mean secondary flow velocity; h_ξ and h_η = the "scale factors" or the "metric coefficients" on the ξ and η curves; ρ = the fluid density; t = time; g = the gravitational acceleration; H = the mean elevation of the bottom of a transverse cross section of open channel; V_{η^*} = the value of V_η at a boundary point in which $\eta = \eta^*$; $\tau_{\xi 1}$ is the shear stress in the x_1 direction in the plane perpendicular to the ξ direction; and σ_1 = the normal stress in the x_1 direction.

The ξ- and η-components of secondary flow velocity given by Eqs. 4 and 5 are related to the x_2 and x_3 components in the (Cartesian) x_2-x_3 system according to the following standard transformation rule:

$$V_\xi = h_\xi\frac{\partial \xi}{\partial x_2}V_2 + h_\xi\frac{\partial \xi}{\partial x_3}V_3 \quad \ldots\ldots\ldots\ldots\ldots\ldots\ldots\ldots (6)$$

$$V_\eta = h_\eta\frac{\partial \eta}{\partial x_2}V_2 + h_\eta\frac{\partial \eta}{\partial x_3}V_3 \quad \ldots\ldots\ldots\ldots\ldots\ldots\ldots\ldots (7)$$

To compute secondary currents, Eq. 4 can be used first at every grid point of the ξ-η coordinate network to obtain V_ξ. The other component, V_η, can then be obtained by integrating Eq. 5 along each ξ curve starting from a boundary point. The boundary point can be selected on the water surface where the x_2 component of flow, V_2, is equal to zero. This boundary condition, $V_2 = 0$, along with V_ξ from Eq. 4 can be substituted into Eqs. 6 and 7 to determine V_η and the x_3 component, V_3. With Eqs. 4 and 5, along with these boundary conditions, the secondary flow velocities, V_ξ and V_η, can be computed at every grid point in the ξ-η coordinate system, which can then be transformed into V_2 and V_3 in the Cartesian coordinate system by Eqs. 6 and 7.

The scale factors on the ξ and η curves can be derived from Eqs. 2 and 3 as

$$h_\xi = \frac{B_i^2 D}{\left(1 - \frac{|x_3|}{B_i}\right)^{\beta_i - 1} e^{\beta_i |x_3|/B_i} \sqrt{B_i^4 \left(1 - \frac{|x_3|}{B_i}\right)^2 + (\beta_i x_2 |x_3|)^2}} \quad \ldots\ldots (8)$$

$$h_\eta = \frac{\beta_i |x_3| D^2}{2\sqrt{B_i^4 \left(1 - \frac{|x_3|}{B_i}\right)^2 + (\beta_i x_2 |x_3|)^2}} \quad \ldots\ldots (9)$$

Secondary Flow and Shear Stress

As indicated by Eq. 4, the secondary flow interacts with the shear distribution. By definition of ξ coordinate, $\tau_{\eta 1}$ should be zero as the gradient of primary flow velocity in the η direction (tangent to a ξ curve) is zero; then, $\tau_{\xi 1}$ should represent the total shear at a point in a ξ-η plane (x_2-x_3 plane, or a transverse cross section of a channel). Eq. 4 can also be expressed as:

$$\frac{\partial \tau_{\xi 1}}{\partial \xi} + \frac{1}{h_\eta} \frac{\partial h_\eta}{\partial \xi} \tau_{\xi 1} = h_\xi F \quad \ldots\ldots (10)$$

$$\text{in which} \quad F = \rho \left(\frac{\partial V_1}{\partial t} + V_1 \frac{\partial V_1}{\partial x_1} + V_\xi \frac{1}{h_\xi} \frac{\partial V_1}{\partial \xi} \right) + \frac{\partial}{\partial x_1} (\rho g H) - \frac{\partial \sigma_1}{\partial x_1} \quad (11)$$

One can express the solution of Eq. 10 as

$$\tau_{\xi 1}(\xi_i, \eta) = \frac{-1}{h_\eta(\xi_i, \eta)} \int_{\xi_i}^{\xi_D(\eta)} h_\xi(\xi, \eta)\, h_\eta(\xi, \eta)\, F(\xi, \eta)\, d\xi + \tau_{\xi 1}[\xi_D(\eta), \eta] \quad (12)$$

in which $\xi_D(\eta)$ = the value of ξ on the water surface along an η curve, i.e., on each η curve the value of ξ varies from ξ_0 to $\xi_D(\eta)$, which can be calculated once the primary flow isovels and, thus, the ξ-η coordinates are determined; and the last term on the right side is the shear stress at the water surface on an η curve. Eqs. 4 and 10 show the interaction among the secondary flow, shear stress, gravity, hydrostatic pressure, and the variability with time and space of primary flow velocity. For $\xi_i = \xi_0$, Eq. 12 represents the boundary shear stress. If the wind effect is neglected and the shear on the water surface is assumed to be zero, for steady, uniform flow in the x_1 direction, Eq. 12 becomes

$$\tau_{\xi 1}(\xi_i, \eta) = \frac{1}{h_\eta(\xi_i, \eta)} \left[\rho g S \int_{\xi_i}^{\xi_D(\eta)} h_\xi h_\eta\, d\xi - \rho \int_{\xi_i}^{\xi_D(\eta)} h_\eta V_\xi \frac{\partial V_1}{\partial \xi} d\xi \right] \quad \ldots (13)$$

If the primary flow isovels (ξ lines) are horizontal and parallel so that η lines are parallel, vertical lines, e.g., in a "wide channel," h_ξ and h_η along an η line are both constant, independent of ξ. Then, $h_\eta(\xi, \eta) = h_\eta(\xi_0, \eta)$, $h_\xi(\xi, \eta)$

$= h_\eta(\xi_0, \eta) = D$, $\xi_D = 1$, $\xi = x_2/D$, $R = D$, $\tau_{\xi 1} = \tau_{21}$, and $V_\xi = V_2$, so that Eq. 13 becomes

$$\tau_{\xi 1}(\xi, \eta) = \tau_{21}(x_2) = \rho g D S\left(1 - \frac{x_2}{D}\right) - \rho \int_{x_2}^{D} V_2 \frac{\partial V_1}{\partial x_2}\, dx_2 \quad \ldots\ldots\ldots \quad (14)$$

and $$\tau_0 = \rho g D S - \rho \int_0^D V_2 \frac{\partial V_1}{\partial x_2}\, dx_2 \quad \ldots\ldots\ldots\ldots\ldots\ldots \quad (15)$$

If the secondary flow velocity, V_2, is neglected

$$\frac{\tau_{\xi 1}}{\bar{\tau}_0} = 1 - \frac{x_2}{D} \quad \ldots\ldots\ldots\ldots\ldots\ldots\ldots\ldots\ldots\ldots \quad (16)$$

in which $\bar{\tau}_0 = \rho g D S$. Eq. 16 is a shear stress formula commonly used in open channel hydraulics.

The first integral in Eq. 13 is the x_1 component of the weight of water in the volume equal to the shaded area above *ab* (the length of which is h_η) in Fig. 1, multiplied by the unit length of channel in the x_1 direction. If $\xi_i = \xi_0$, the perimeter, *ab*, of length equal to $h_\eta(\xi_0, \eta)$, will be on the channel bed. So, this integral represents the portion of shear stress due to gravity. The second integral represents another portion of shear stress owing to the net momentum transfer above *ab*, in the ξ direction (perpendicular to *ab* and other primary flow isovels above it), by V_ξ (the secondary flow velocity in the ξ direction). The direction of V_ξ may change, positive or negative, i.e., upward or downward. If the net momentum transfer is in the negative ξ direction, i.e., downward and perpendicular to the perimenter, *ab*, so that the integral is a negative quantity, this portion of shear stress contributed by the secondary flow is to increase the total shear, $\tau_{\xi 1}(\xi, \eta)$. The algebraic sum of the two integrals divided by $h_\eta(\xi, \eta)$, which represents the length of *ab*, gives the resultant shear stress under a steady, uniform flow condition. If the flow is unsteady or nonuniform, or both, the remaining terms in F (defined by Eq. 11), other than the gravity and secondary flow terms, will also affect the total shear stress.

To use Eq. 12 or 13 to evaluate the shear stress, one needs the secondary flow velocity V_ξ; however, one must know the shear stress to estimate V_ξ. Both the shear stress and secondary flow are difficult to measure; therefore, it is desirable to develop formulas to estimate them. It seems to be much easier to derive a formula for the shear stress than to derive one for the secondary flow, since the shear stress has a close relationship with the distribution of primary flow velocity, as indicated by existing formulas for the viscous and turbulent shear stresses in fluid mechanics. A shear stress estimated by a formula can then be used in Eqs. 4 and 5 to calculate the secondary flow.

Based on Eq. 12 or 13, $\tau_{\xi 1}(\xi, \eta)$ is a function of ξ and η, which varies with the difference, $\xi_D(\eta) - \xi$, on an η curve. It is, therefore, reasonable to expand the solution of Eq. 10 into the form of a polynomial in $[\xi_D(\eta) - \xi]$, such as

$$\tau_{\xi 1}(\xi, \eta) = \alpha_0 + \alpha_1 [\xi_D(\eta) - \xi] + \alpha_2 [\xi_D(\eta) - \xi]^2 \quad \ldots\ldots\ldots\ldots \quad (17)$$

in which $0 \leq [\xi_D(\eta) - \xi] < 1$; and α_0, α_1, α_2 = coefficients. The selection of Eq. 17 to be a polynomial of degree two, rather than a higher degree, is

mainly based on the number of available boundary conditions of the shear and secondary flow needed to determine the coefficients, and the desirability of a simple formula.

At the water surface on an η curve, $\xi = \xi_D(\eta)$, so that

$$\alpha_0 = \tau_{\xi l}\,[\xi_D(\eta), \eta] \quad \ldots \ldots \ldots \ldots \ldots \ldots \ldots \ldots \ldots \ldots \quad (18)$$

If the wind effect is neglected the shear stress on the water surface can be assumed to be equal to zero everywhere, even at the banks, for a trapezoidal channel; a rectangular channel tends to have nonzero boundary shear at intersections of two banks with the water surface (6). Alluvial channels have cross sections which in general are approximately trapezoidal and, thus, the assumption of zero shear stress everywhere on the water surface should be reasonable if the wind effect is negligible. The assumption implies $\alpha_0 = 0$ everywhere. If the wind effect is not negligible, α_0 will represent the nonzero shear stress on the water surface.

With the boundary conditions $V_2 = 0$ and $\tau_{\xi l} = 0$, along with the derivative of $\tau_{\xi l}$ with respect to ξ on the water surface, which can be obtained by differentiating Eq. 17 and letting $\xi = \xi_D(\eta)$, Eqs. 6 and 10 (or 4) give V_ξ on the water surface as

$$V_\xi = \left(h_\xi \frac{\partial \xi}{\partial x_3}\right) V_3 = \frac{1}{\dfrac{\rho}{h_\xi}\dfrac{\partial V_1}{\partial \xi}}\left[-F_0 - \frac{\alpha_1}{h_\xi}\right] = \frac{\kappa \xi \Delta}{\rho \bar{V}_*} \quad \ldots \ldots \ldots \ldots \quad (19)$$

in which $\Delta = -(h_\xi F_0 + \alpha_1)$ $\ldots \ldots \ldots \ldots \ldots \ldots \ldots \ldots \ldots \ldots \quad (20)$

and F_0 denotes F defined by Eq. 11 with $V_\xi = 0$.

At the point $(x_2 = D, x_3 = 0)$ where the water surface intersects with the x_2-axis, $V_\xi = V_2 = 0$. With this boundary condition, Eq. 19 gives

$$\alpha_1 = -(h_\xi F_0)_{x_2 = D,\, x_3 = 0} \quad \ldots \ldots \ldots \ldots \ldots \ldots \ldots \ldots \ldots \ldots \quad (21)$$

Eq. 19 also gives V_3 and, thus, explains the mechanism that generates the transverse flow on the water surface of an open channel. The transverse flow V_3 is zero at the x_2-axis in which $\Delta = 0$; it also vanishes at the banks where $\xi = \xi_0 \approx 0$. Between the x_2-axis and the two banks the transverse flow on the water surface occurs whose magnitude depends on all factors shown by Eq. 19 while the direction depends on the signs, positive or negative, of Δ and $\partial \xi / \partial x_3$. In addition, $\partial \xi / \partial x_3$ has the positive sign on the left side of x_2-axis, and the negative sign on the right. Thus, if Δ is positive, the transverse flow is directed towards the x_2-axis (the center) from the banks on the both sides, as often seen on the water surface of open channel flow.

On the channel bed (bottom and walls) in which $\xi = \xi_0$, $V_\xi = 0$, i.e., the flow velocity perpendicular to the boundary is zero, so that Eq. 10 becomes

$$\frac{\partial \tau_{\xi l}}{\partial \xi} + \frac{1}{h_\eta}\frac{\partial h_\eta}{\partial \xi}\tau_{\xi l} = h_\xi F_0 \quad \ldots \ldots \ldots \ldots \ldots \ldots \ldots \ldots \ldots \quad (22)$$

With $\tau_{\xi l}$ from Eq. 17 and its derivative with respect to ξ, Eq. 22 gives

$$\alpha_2(\eta) = \frac{-h_\xi F_0 - \alpha_1 \left\{ 1 - \dfrac{1}{h_\eta} \dfrac{\partial h_\eta}{\partial \xi} [\xi_D(\eta) - \xi_0] \right\}}{[\xi_D(\eta) - \xi_0] \left\{ 2 - \dfrac{1}{h_\eta} \dfrac{\partial h_\eta}{\partial \xi} [\xi_D(\eta) - \xi_0] \right\}} \quad \ldots\ldots\ldots\ldots \quad (23)$$

in which F_0, h_ξ, h_η and its derivative are evaluated at each point (ξ_0, η) on the channel bed, so that α_2 is a function only η. In computing α_1 and α_2 by Eqs. 21 and 23, the x_1 gradient of normal stress $(\partial\sigma_1)/(\partial x_1)$ will be needed which may be approximated as equal to the gradient of hydrostatic pressure per unit area, $-(\partial P)/(\partial x_1)$, which arises owing to the variation of channel cross section in the x_1 direction, as other terms are usually relatively small. It may even be approximated to be zero for a fairly uniform, open channel flow. For a steady uniform flow, Eq. 21 becomes

$$\alpha_1 = \rho g D s \quad \ldots\ldots\ldots\ldots\ldots\ldots\ldots\ldots\ldots\ldots\ldots\ldots \quad (24)$$

so that $\Delta = \rho g S(h_\xi - D) \geq 0$ (which steadily decreases to zero from the bank towards the x_2-axis), and

$$\alpha_2(\eta) = \frac{\rho g S h_\xi}{[\xi_D(\eta) - \xi_0]} \frac{1 - \dfrac{D}{h_\xi} \left\{ 1 - \dfrac{1}{h_\eta} \dfrac{\partial h_\eta}{\partial \xi} [\xi_D(\eta) - \xi_0] \right\}}{2 - \dfrac{1}{h_\eta} \dfrac{\partial h_\eta}{\partial \xi} [\xi_D(\eta) - \xi_0]} \quad \ldots\ldots\ldots \quad (25)$$

With all the coefficients determined, Eq. 17 can be used to compute the shear stress in the flow and along the channel bed, that includes among other things the effect of secondary flow. If the flow is steady and uniform, the difference between the shear stress computed by Eq. 17 and the first term on the right side of Eq. 13 should give the portion of shear stress owing to the momentum transfer by secondary flow.

The mean boundary shear along the wetted perimeter of a channel cross section can be evaluated as

$$\bar{\tau}_0 = \frac{1}{\text{w.p.}} \int_{\text{w.p.}} \tau_0(\eta)\, h_\eta(\xi_0, \eta)\, d\eta \quad \ldots\ldots\ldots\ldots\ldots\ldots\ldots\ldots \quad (26)$$

in which w.p. = the wetted perimeter; and $\tau_0(\eta)$ = the boundary shear given by Eq. 17 with $\xi = \xi_0$.

Fig. 2 shows the computed distribution of shear stress [including that in the flow and along the boundary, along with corresponding primary flow velocities distribution (measured)] and the computed secondary flow directions in a cross section (Section No. 255) of Rio Grande Conveyance Channel, near Bernardo, N.M. (5). The shear distribution is expressed in terms of the ratio of local shear to the mean boundary shear. The cross section generally has a trapezoidal shape, although the side slopes appear very steep because of two different scales used for the vertical and horizontal dimensions in the Fig. 2. The boundary shear distribution on the channel bed has two peaks near the two corners of the cross section, which look much sharper than actual because of the exaggerated vertical scale. There are also two peaks of boundary shear distributions on

the two sides of the section. Such a pattern of boundary shear distribution is supported quite well by results of direct measurements in trapezoidal channels (6) as shown in Fig. 3. Fig. 3 also shows results from using two indirect methods of estimating the boundary shear (one by Preston tube, and the other from

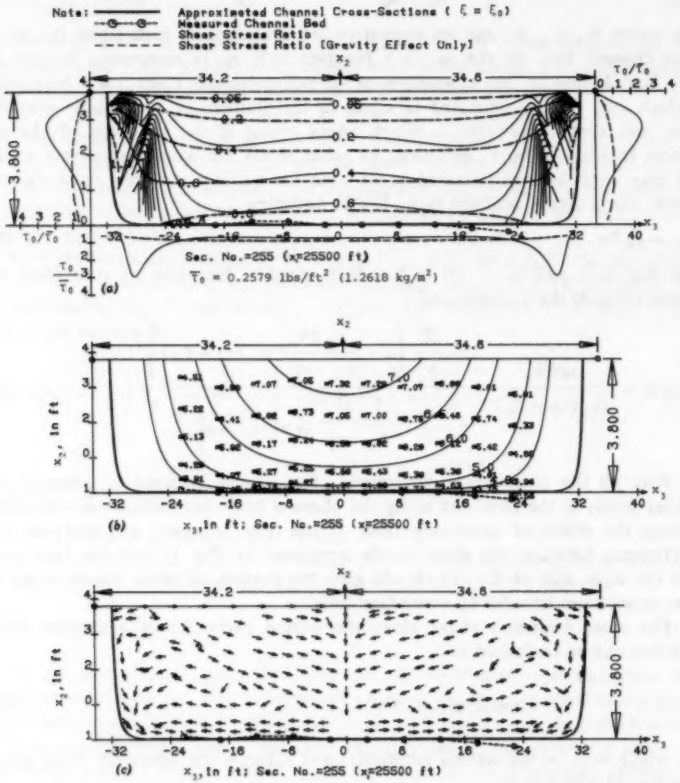

FIG. 2.—Shear Stress, Primary Flow Velocity, and Secondary Flow [Section No. 255, Rio Grande Conveyance Channel (5); Q = 1,280 cfs; 1 cfs = 0.3 mm/s; 1 ft = 0.3 m]: (*a*) Computed Distribution of Shear Stress in Flow and Along Boundary; (*b*) Distribution of Primary Flow Velocity (Measured and Computed); and (*c*) Computed Direction of Secondary Flow

the distribution of primary flow velocity near the boundary). It shows that without using the direct method of measurement, the peak value of boundary shear that tends to occur near the corner on the channel bed cannot be detected. The indirect method, using the velocity distribution of primary flow near the boundary, which is popular and commonly used in the field, tends to give

boundary shear decreasing continuously from the center to the side wall. In alluvial channels, or even in laboratory flumes, as long as the channel is not smooth the boundary shear is not distributed as indicated (misled) by such an indirect method. Direct measurements, even in laboratory flumes, is very difficult especially near the side walls; thus, enhancing the value of a mathematical model of shear stress such as Eq. 17 and the associated computational technique. Fig. 2(*a*) also shows the shear stress distribution including only the first term of Eq. 13 which represents only the portion of shear stress owing to the gravity force. A comparison of shear stress distributions with and without secondary flow indicates that the effect of secondary currents is very pronounced near the side walls.

The secondary flow velocity, V_ξ, is not very great in magnitude, generally less than 10% of cross-sectional average of primary flow velocity, but its effect on shear stress near the side walls is not small (not secondary). The reason

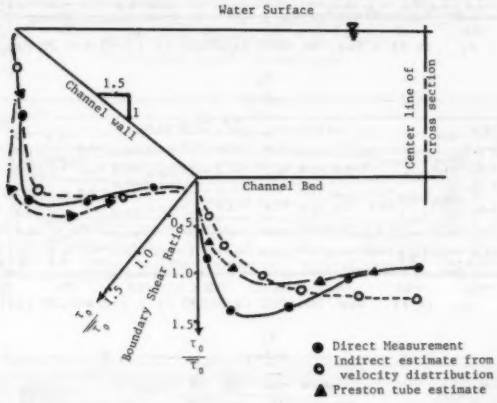

FIG. 3.—Distribution of Boundary Shear in Trapezoidal Channel (Ref. 6)

is that, as shown by the second integral term or the right side of Eq. 13, the contribution of secondary flow to the shear stress at a point is cumulative or net momentum transfer in the ξ direction, along an η curve between the point and the water surface, and that near the side walls the secondary flow is mostly directed toward the channel bed (including the bottom and side walls), as shown in Fig. 2(*c*), so that V_ξ carries the negative sign in Eq. 13 and, thus, its effect is to increase the shear. The magnitude of h_η, one of the metric coefficients, also has effect on the contribution of secondary flow to the shear as shown by Eq. 13. It is relatively large near the side walls and approaches zero near the x_2-axis. Near the x_2-axis, both V_ξ and h_η are very small so that the effect of secondary flow to the shear stress on or near the x_2-axis is relatively small. The shear stress shown in Fig. 2(*a*) also includes the effect of flow being nonuniform, i.e., $\partial V_1/\partial x_1 \neq 0$ as indicated by Eq. 12 which shows that the shear stress could be affected by every term of F defined by Eq. 11.

In a study of bank erosion problem, an equation such as Eq. 17, rather than Eq. 16, should be used to determine the peak values of boundary shear (drag force) that tend to occur on the side walls and on the channel bottom

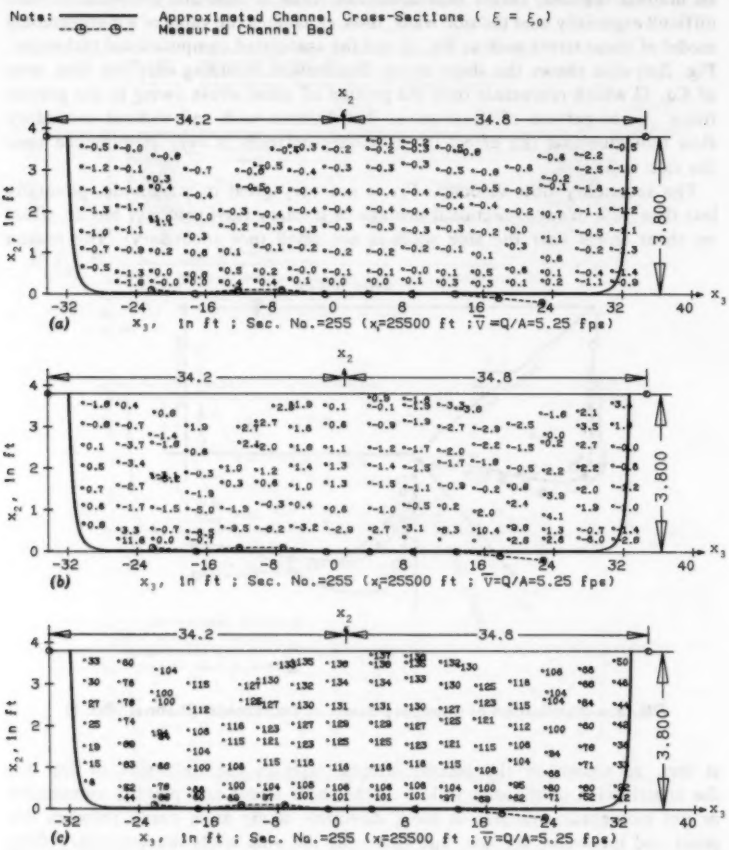

FIG. 4.—Secondary Flow and Total Flow Velocities [Section No. 255, Rio Grande Conveyance Channel (5); Q = 1,280 cfs; 1 cfs = 0.3 mm/s; 1 ft = 0.3 m]: (*a*) Computed x_2 Component of Secondary Flow Velocity (V_2); (*b*) Computed x_3 Component of Secondary Flow Velocity (V_3); and (*c*) Computed Total Flow Velocity ($V_1 + V_2 + V_3$)

near the side walls. Peak boundary shear along with the convection by secondary flow near the side walls should be a major mechanism responsible for bank and bed erosion of alluvial channels. Figs. 4(*a*), and 4(*b*), show computed

secondary flow velocities V_2 and V_3, respectively, in percentages of cross-sectional average of primary flow velocity. Fig. 4(*c*) shows the distribution of total velocity, i.e., the vector sum of primary and secondary flow velocities, which is also expressed in percentage of cross-sectional average of primary flow velocity.

Fig. 5 shows the distribution of computed shear stress at three consecutive sections (Section Nos. 240, 250, and 260), facing downstream and separated

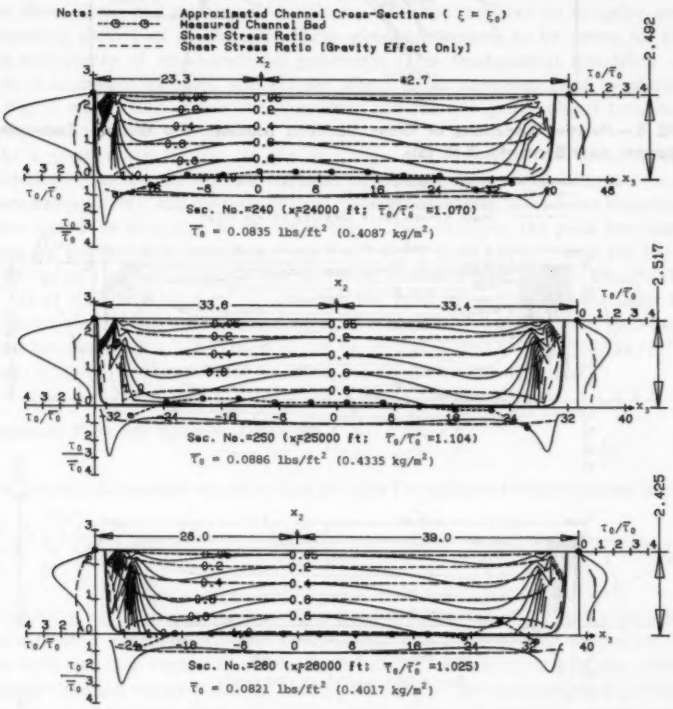

FIG. 5.—Three-Dimensional Shear Stress Distribution [Rio Grande Conveyance Channel (5) Q = 630 cfs; 1 cfs = 0.3 mm/s; 1 ft = 0.3 m]

by 1,000 ft (300 m), in a straight portion of the Rio Grande Conveyance Channel (5), under a steady flow of 630 cfs (18 m^3/s). In Fig. 5 the values of $\bar{\tau}_0$ and $\bar{\tau}_0/\bar{\tau}_0'$ (ratio of mean boundary shear stress to ρgRS) are shown; and the shear distributions are again expressed in terms of the ratio of local shear to the mean boundary shear. It is not surprising to see that the shear distribution, like the primary flow velocity distribution, varies from cross section to cross section. The peak values of boundary shear on the channel bottom and side

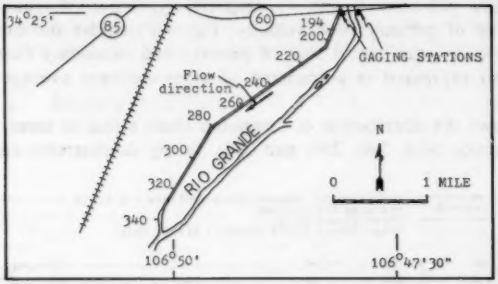

FIG. 6.—Relative Locations of Cross Sections Studied [Rio Grande Conveyance Channel, near Bernardo, N.M. (5)]

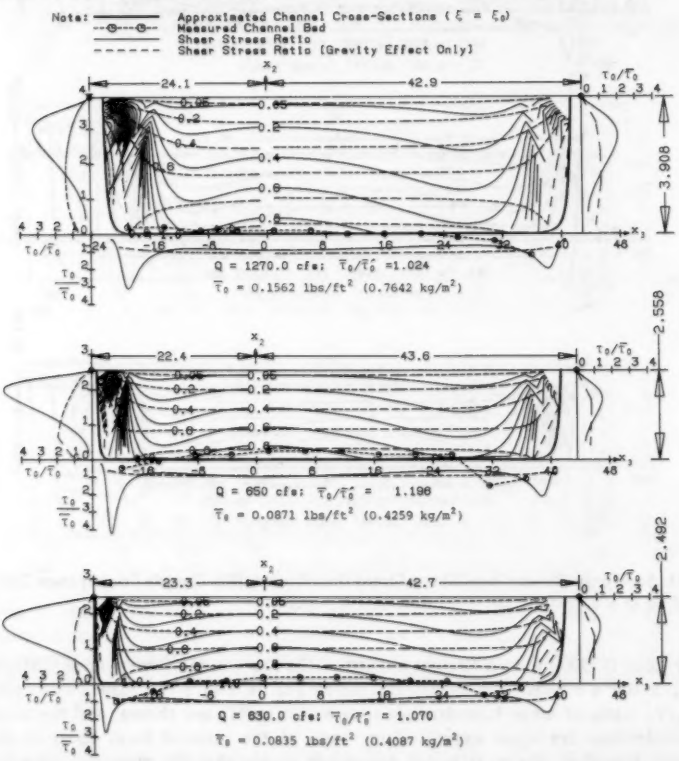

FIG. 7.—Variation of Shear Stress with Discharge Rate [Section No. 240, Rio Grande Conveyance Channel (5); 1 cfs = 0.3 mm/s; 1 ft = 0.3 m]

walls in these sections are different but their locations of occurrence seem to be similar. Probably the most striking finding from observing Fig. 5 is that the geometrical shape of actually measured channel bottom is very similar to the distribution of boundary shear on the channel bottom. The two deepest locations of channel bottom that occur near the side walls coincide with those of peak boundary shear. The two peak values of boundary shear (one on the channel bottom and one on the side wall) on the left side of x_2-axis in each of these cross sections are greater than corresponding values on the right side. The shear stress and primary flow velocity distributions have an irregular and alternating pattern of asymmetry. These phenomena seem to be owing to: (1) The asymmetry of cross-sectional geometry; (2) a fundamental instability of flow in a straight channel; and (3) the effect of an upstream bend as shown in Fig. 6 which also shows the alignment and relative geographical locations of the channel cross sections.

At a given cross section, as the discharge rate increases, the shear stress generally increases although the general pattern of shear distribution does not change appreciably, and the ratio of local (point) shear stress to the mean boundary shear may even decrease, as shown in Fig. 7. For example, the peak boundary shear on the left side increased from 0.417 lb/ft (2.04 kg/m^2) to 0.499 lb/ft (2.44 kg/m^2) as the discharge rate increased (about doubled) from 630 cfs (18 m^3/s) to 1,270 cfs (35.6 m^3/s) although the ratio of peak boundary shear to the mean boundary shear actually decreased from about 5–3.2. The mean boundary shear increased from 0.0835 lb/ft (0.409 kg/m^2) to 0.1562 lb/ft (0.7642 kg/m^2), about doubled, as the increase (doubling) in discharge rate occurred.

Secondary Flow and Sediment Transport

A general differential equation that governs the sediment concentration is:

$$\frac{\partial C}{\partial t} = \sum_{j=1}^{3} \left\{ \epsilon_j \frac{\partial^2 C}{\partial x_j^2} + \left(\frac{\partial \epsilon_j}{\partial x_j} - u_j \right) \frac{\partial C}{\partial x_j} \right\} \quad \ldots\ldots\ldots\ldots\ldots\ldots \quad (27)$$

in which C = the concentration of suspended sediment; t = time; ϵ_j denotes the diffusion coefficient in the x_j direction; and u_j = the x_j component of the total velocity vector U of sediment particle, which in turn is the vector sum of the fluid velocity and the settling velocity of the representative particle, e.g., d_{50}, under the effect of gravity. Both C and U (and its components) are time-averaged quantities without including instantaneous random fluctuations. Then, u_1 is equal to the primary-flow velocity, V_1; u_2 is equal to the sum of the x_2 component of the secondary-flow-velocity, V_2, and the settling velocity, $-V_s$, of the representative sediment particle, or $u_2 = V_2 - V_s$; and u_3 is equal to the x_3 component of the secondary-flow velocity, V_3. For a steady and nearly uniform flow in which

$$\frac{\partial ( )}{\partial x_1} \approx 0 \quad \ldots\ldots\ldots\ldots\ldots\ldots\ldots\ldots\ldots\ldots\ldots\ldots \quad (28)$$

in which ( ) represents C or ϵ_j, Eq. 27 can be approximated as

$$\sum_{j=2}^{3}\left\{\epsilon_j\frac{\partial^2 C}{\partial x_j^2}+\left(\frac{\partial\epsilon_j}{\partial x_i}-u_j\right)\frac{\partial C}{\partial x_j}\right\}=0 \quad \ldots\ldots\ldots\ldots\ldots\ldots\ldots\ldots \quad (29)$$

which can be solved numerically with boundary values of C. If the secondary flow is neglected, Eq. 29 becomes

$$\sum_{j=2}^{3}\left(\epsilon_j\frac{\partial^2 C}{\partial x_j^2}+\frac{\partial\epsilon_j}{\partial x_j}\frac{\partial C}{\partial x_j}\right)+V_s\frac{\partial C}{\partial x_2}=0 \quad \ldots\ldots\ldots\ldots\ldots\ldots\ldots\ldots \quad (30)$$

To use Eqs. 29 and 30, the components ϵ_2 and ϵ_3 of the diffusion coefficient (ϵ) for sediment are needed. In terms of the coefficient for momentum transfer, (ϵ_m), ϵ can be expressed as

$$\epsilon=\gamma\,\epsilon_m \quad \ldots\ldots\ldots\ldots\ldots\ldots\ldots\ldots\ldots\ldots\ldots\ldots\ldots\ldots \quad (31)$$

in which γ = the proportionality constant. It has been reported (1,7,8) that $\gamma\approx 1$ for fine sediment particles, e.g., smaller than 0.1 mm in diameter; and $\gamma<1$ for coarse sediments. For $j=2$ and 3, ϵ_j can be obtained from

$$\epsilon_\xi=h_\xi\frac{\partial\xi}{\partial x_2}\epsilon_2+h_\xi\frac{\partial\xi}{\partial x_3}\epsilon_3 \quad \ldots\ldots\ldots\ldots\ldots\ldots\ldots\ldots\ldots\ldots \quad (32)$$

$$\epsilon_\eta=h_\eta\frac{\partial\eta}{\partial x_2}\epsilon_2+h_\eta\frac{\partial\eta}{\partial x_3}\epsilon_3 \quad \ldots\ldots\ldots\ldots\ldots\ldots\ldots\ldots\ldots\ldots \quad (33)$$

in which ϵ_ξ and ϵ_η = the ξ and η components of ϵ, the diffusion coefficient for sediment transport. The η component of momentum transfer coefficient, ϵ_m, in Eq. 31 should be zero as the η direction is perpendicular to the gradient of primary flow velocity and, thus, the momentum transfer in that direction is zero. The ξ component of ϵ_m can be defined by

$$\tau_{\xi 1}=\rho(\epsilon_m)_\xi\frac{1}{h_\xi}\frac{\partial V_1}{\partial\xi} \quad \ldots\ldots\ldots\ldots\ldots\ldots\ldots\ldots\ldots\ldots \quad (34)$$

in which $(\epsilon_m)_\xi$ can be determined through estimating $\partial V_1/\partial\xi$ and $\tau_{\xi 1}$, for instance, by Eqs. 1 and 17, respectively. A similar expression of $\tau_{\eta 1}$ and consideration of $(\epsilon_m)_\eta$ being proportional to $\partial V_1/\partial\eta$, e.g., according to the Prandtl's turbulent shear formula, it would be reasonable to make $(\epsilon_m)_\eta$ equal to zero as $\partial V_1/\partial\eta = 0$. In using Eqs. 1 and 17 together in Eq. 34 to compute $(\epsilon_m)_\xi$, or in Eq. 4 to compute V_ξ, Eq. 1 should be considered only as an empirical equation which is often found to be quite good from statistical analysis of actual data of primary flow velocity. If other equations of different forms are found from data analysis to be better, they should be used instead of Eq. 1. In any case, it is not even implied here that Eq. 1 can be derived analytically from the shear stress equation such as Eq. 17, although the Prandtl-von Karman universal velocity distribution formula, which has the logarithmic form, was derived from the Prandtl's turbulent shear formula.

The evaluation of the effect of secondary currents on sediment concentration can be accomplished essentially by comparing the sediment concentration estimated by solving the aforementioned equations with or without secondary currents. The effect may vary from point to point within a channel cross section,

as the direction and magnitude of secondary flow tend to vary from point to point.

Fig. 8 is for the same cross section (No. 255) as the one shown in Fig. 2 of Rio Grande Conveyance Channel near Bernardo, N.M., but this figure shows the suspended sediment concentration in the section measured by the United States Geological Survey (5) along with the boundaries of a region in which computations for sediment concentrations using Eqs. 29 and 30 were performed to study the effect of secondary flow. The size and location of the study region were restricted and determined by the measured data available. The data had to be used as references to determine the accuracy of computed results; some of the data were also needed as boundary values in numerical computations. The measured primary flow velocity distribution along with computed shear stress and secondary flow properties, corresponding to the sediment distribution shown in Fig. 8, have been presented in Figs. 2 and 4 which were used in computing sediment concentration.

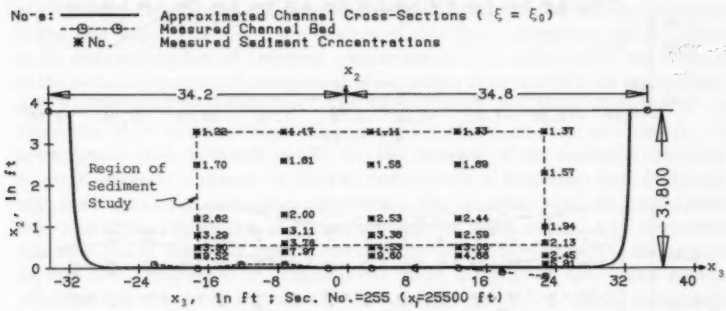

FIG. 8.—Distribution of Sediment Concentration, in grams per liter [Rio Grande Conveyance Channel, New Mexico: $\kappa = 0.4451$; $Q = 1{,}280$ cfs; 1 cfs = 0.03 mm/s; 1 ft = 0.3 m]

While properties of flow and channel are indicated in Figs. 2 and 4, suspended sediment particles in the cross section have the median size, d_{50}, of about 0.12 mm, for which the settling velocity, V_s, at the water temperature of 20° C is 1.1 cm/s (0.04 fps). The value of γ in Eq. 31 was made equal to unity in computations of sediment concentration, in absence of a precise estimate of it and also because of the sediment particles being fairly small.

In Figs. 9(*a*) and 9(*b*) the values of sediment concentration inside the study region, computed with Eqs. 29 and 30, respectively, are compared with the measured. The difference between computed concentration in Fig. 9(*a*) and that in Fig. 9(*b*) represents the effect of secondary flow, as the former included the secondary flow in computation while the latter did not. The sediment concentrations on the boundaries of the study region are not shown in Figs. 9(*a*) and 9(*b*) since they were the measured values (with some interpolation between measuring points) used as the boundary conditions, as shown in Fig. 8. In general, computations with Eq. 30, which does not include the convection

by secondary flow, tend to overestimate the sediment concentration at a point in the region. Computations with Eq. 29 that includes secondary flow generally

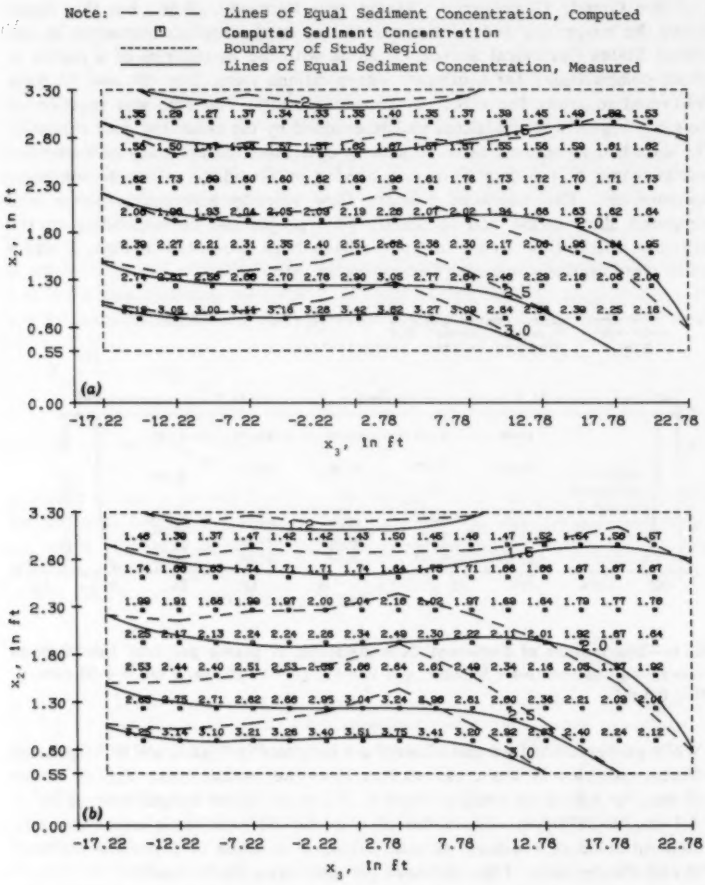

FIG. 9.—Distribution of Sediment Concentration, in gallons per liter [Rio Grande Conveyance Channel Section No. 255 (5); $\kappa = 0.4451$; $Q = 1{,}280$ cfs; 1 cfs = 0.3 mm/s; 1 ft = 0.3 m]: (*a*) Computation Including Secondary Currents (Eq. 29); and (*b*) Computation without Secondary Currents (Eq. 30)

gives very good results. The vertical component of secondary flow velocity, V_2, in the study region, which is located in the central portion of the cross section, is weak but consistently downward in the same direction as gravity,

as shown in Fig. 4(*a*). It means that more downward sediment transport than that by gravity alone exists in the region. This is more so at upper levels of the region where the downward V_2 is stronger than those at lower levels. As shown in Fig. 4(*a*), V_2 approaches zero toward the lower boundary of the region near x_2-axis; it even becomes upward (carrying the positive sign) at lower levels of the region, relatively far from the x_2-axis. Therefore, errors in computed sediment concentrations owing to neglecting the vertical (downward) sediment transport by secondary flow are relatively large at upper levels, and seemingly small or negligible at lower levels. The relatively large discrepancy between the computed sediment distribution and the measured at lower levels, shown in Fig. 9(*b*), is mainly owing to neglecting the sediment transport by secondary flow in the transverse direction. The sediment transport in the transverse direction in the study region is mainly accomplished by secondary flow, as the gradient of sediment concentration in the transverse direction is very small as shown by Fig. 8 or 9 and, thus, the sediment transport by diffusion should also be very small. As shown by Fig. 4(*b*), at upper levels the transverse component of secondary flow carries sediment into the study region from sediment sources at the two sides. Therefore, the neglect of this flow component should result in an underestimation of sediment concentration at a point, while the neglect of the vertical (downward) component of secondary flow results in an overestimation of sediment concentration. The exclusion of the both components of secondary flow in computing sediment concentration, as done customarily, at upper levels of flow should not be too bad because of the mutually canceling effect of sediment transport by the two components of secondary flow (although they may not cancel each other completely). On the other hand, at lower levels the transverse component of secondary flow is quite strong, and transports sediment out of the study region, towards the two sides. Therefore, the neglect of this flow component in computations tends to result in an overestimation of sediment concentration at lower levels. As stated earlier, the vertical component of secondary flow at lower levels is generally weak (quite negligible); and, thus, the neglect of this component cannot offset the effect of neglecting the transverse flow component. The main portion of sediment transport in the longitudinal direction through a transverse cross section of an alluvial channel is achieved through lower levels of the cross section because of the large sediment concentration. Therefore, the role that the secondary flow plays in transporting sediment, especially in the transverse direction, should not be ignored. Also, wherever primary flow isovels have significant curvatures, e.g., under side-wall effect, the role of diffusion in the transverse (x_3-) direction (a component of diffusion in the ξ direction) should be included in sediment transport studies.

Summary and Conclusion

Under the mathematical modeling technique used herein, explicit links have been established among interacting variables in open channel flows, such as the distribution of primary flow velocity, channel cross section, discharge rate, secondary flow, shear stress distribution, and sediment concentration. The accuracy of numerical computations and simulation depends on that of primary flow velocity distribution used as the basis of forming the coordinate system.

Eqs. 1 and 2, used to represent isovels and velocity distribution of primary flow, were developed from statistical analysis of United States Geological Survey data from Rio Grande Conveyance Channel (5), and appear quite adequate. However, some adjustments will be necessary to cope with primary flow velocity distributions significantly different from that indicated by the Rio Grande data. For instance, in many open channels, isovels of primary flow near the water surface tend to curve toward x_2-axis (center) and the maximum velocity occurs below the water surface. An approach to such a situation is to use a separate coordinate system near the water surface. Regardless of adjustments that may be necessary, the basic framework of technique and procedure presented herein will remain valid.

A formula (Eq. 17) has been developed that can be used to calculate the shear stress in the flow and along the bottom and side walls of alluvial channels. A polynomial of degree two, the formula has coefficients determined from a basic hydrodynamic equation (Eq. 10) and boundary conditions of both the secondary flow and the shear stress. No data on shear is required. It is capable of including the effects of gravity, primary and secondary flows, and nonuniformity of flow, etc. Such a formula is essential to hydraulic studies in alluvial channels, especially near the corners and side walls where no other existing formulas work. The shear formula gives peak values of boundary shear, on the channel bottom near the corner or side walls and also on the side walls between the channel bottom and the water surface.

The geometrical shape of boundary shear distribution computed along the channel bottom is found to be similar to that of actual (measured) channel bottom; the deepest locations of channel bottom that tend to occur near the corners and side walls almost coincide with the locations of peak boundary shear, indicating a direct correlation between the boundary shear and the erosion or scour on the channel bed. The distribution of boundary shear, as well as the pattern of secondary flow that moves into the corner from above and out of the corner along the channel bed as shown in Fig. 2(*c*), is clearly a main mechanism responsible for the erosion and scour of channel bed and banks. Such knowledge and the computational technique presented herein for computer simulation of secondary flow and boundary shear distribution should, therefore, be an effective tool for studying and selecting better designs for protecting channel beds and banks from the scour and erosion.

The secondary flow affects the shear stress which in turn affects the diffusion process. Therefore, the secondary flow affects sediment transport both directly (convection) and indirectly (diffusion, through its interaction with the shear stress). At upper levels of the main region of a channel cross section, not including the near-walls area, the secondary flow transports sediment into the region from the sources on the two sides, and helps the gravity force to bring sediment downward. At lower levels, it transports sediment out of the region in the transverse direction, towards the two sides. The upward transport of sediment transport is done by diffusion. The downward secondary flow component is much weaker than the transverse component. The main parts of mechanism governing the sediment concentration is, therefore, the gravity, diffusion, and secondary flow. The traditional analysis considers only the first two; therefore, the inclusion of the third component should receive an emphasis in future studies of sediment transport. A main problem with using Eq. 29 in computing the

sediment concentration, which is capable of including both the diffusion and convection with secondary flow, is the need for data on all boundaries of a study region. An accurate estimation of γ in Eq. 31 for computing the diffusion coefficient for sediment to be used in Eq. 29 also represents a problem to be solved in the future.

At present, there are no directly measured data on shear stress in alluvial channels. There are also shortages of boundary shear data on laboratory flumes, especially near the corners and side walls; data available were mostly measured in the central portion of channel bed. This indicates, therefore, a great need for data collections in both the field and laboratories, to check and, if necessary, improve a shear stress formula such as Eq. 17. An improved shear stress formula can improve the accuracy of secondary flow computations, and accurate secondary flow measurements can in turn check and improve a shear stress formula. A close interaction and coordination between mathematical modeling and data collection is clearly essential in the future.

Acknowledgments

Roscow C. H. Lin and G. F. Lin, Research Assistants, Department of Civil Engineering, University of Pittsburgh, assisted in computations for development of a portion of results presented herein.

This paper is based upon work supported by the National Science Foundation under Grant No. ENG77-25650.

Appendix I.—References

1. *Sedimentation Engineering Manual No. 54*, by ASCE Task Committee for the Preparation of the Manual on Sedimentation, ASCE, Manuals and Reports on Engineering Practice, 1975, p. 82.
2. Chiu, C.-L., Lin, H. C., and Mizumura, K., "Simulation of Hydraulic Processes in Open Channels," *Journal of the Hydraulics Division*, ASCE, Vol. 102, No. HY2, Proc. Paper 11905, Feb., 1976, pp. 185–206.
3. Chiu, C.-L., Hsiung, D. E., and Lin, H. C., "Three-Dimensional Open Channel Flow," *Journal of the Hydraulics Division*, ASCE, Vol. 104, No. HY8, Proc. Paper 13963, Aug., 1978, pp. 1119–1136.
4. Chiu, C.-L., Hsiung, D. E., and Lin, R. C., "Secondary Currents under Turbulence in Open Channels of Various Geometrical Shapes," *Proceedings of the XVIIIth Congress of the International Association for Hydraulic Research*, Sept., 1979, pp. 10–14.
5. Culbertson, J. K., Scott, C. H., and Bennett, J. P., "Summary of Alluvial-Channel Data from Rio Grande Conveyance Channel, New Mexico, 1956–69," Open File Report, United States Geological Survey, Water Resources Division, Aug., 1971.
6. Ghosh, S. N., and Roy, N., "Boundary Shear Distribution in Open Channel Flow," *Journal of the Hydraulics Division*, ASCE, No. HY4, Proc. Paper 7241, Apr., 1970, pp. 967–993.
7. Graf, W. H., *Hydraulics of Sediment Transport*, McGraw-Hill Book Co., Inc., New York, N.Y., 1971.
8. Sayre, W. W., "Dispersion of Mass in Open Channel Flow," *Hydraulics Papers*, No. 3, Colorado State University, Fort Collins, Colo., Feb., 1968.

Appendix II.—Notation

The following symbols are used in this paper:

A = cross-sectional area;
A_i = cross-sectional area on one side of x_2-axis;
B = top width of cross section;
B_i = top width of cross section on one side of x_2-axis;
C = concentration of suspended sediment;
D = water depth along x_2-axis at cross section;
d_{50} = median diameter of sediment particles;
g = gravitational acceleration;
H = mean elevation of channel bottom at x_1;
h_ξ, h_η = scale factors in coordinate transformation;
i = index, denoting either left or right side of x_2-axis;
p = pressure;
Q = volume rate of flow;
S = energy or channel slope;
t = time;
U = total velocity vector of sediment particle;
u_j = x_j component of velocity of sediment particle;
V_j = x_j-component of flow velocity;
$\bar{V}$ = cross-sectional average of primary flow velocity;
$\bar{V}_*$ = mean shear velocity at cross section;
V_ξ, V_η = ξ and η components of secondary flow velocity, respectively;
V_s = settling velocity of sediment particle;
x_1, x_2, x_3 = Cartesian coordinates in longitudinal, vertical and transverse directions of channel flow, respectively;
$\alpha_0, \alpha_1, \alpha_2$ = coefficients in shear distribution formula;
β_i = constant in velocity distribution equation;
κ = constant in logarithmic velocity distribution equation;
ϵ_j = diffusion coefficient in x_j direction;
$\epsilon_\xi, \epsilon_\eta$ = ξ- and η- component of diffusion coefficient;
ϵ_m = momentum transfer coefficient;
$(\epsilon_m)_\eta, (\epsilon_m)_\xi$ = ξ and η components of ϵ_m;
ξ, η = curvilinear coordinates based on isovels of primary flow;
ξ_0 = value of ξ for which $V_1 = 0$;
ξ_D = value of ξ on along η-curve on water surface;
ρ = density of water;
$\tau_{\xi 1}$ = shear stress in x_1 direction in plane perpendicular to ξ direction;
$\bar{\tau}_0$ = mean boundary shear at cross section;
$\bar{\tau}_0' = \rho g R S$; and
τ_0 = boundary shear at point on channel bed at cross section.

FLOW RESISTANCE IN COARSE GRAVEL BED RIVERS

By George A. Griffiths[1]

INTRODUCTION

Quantitative prediction of the resistance to fully turbulent flow in natural open channels is a problem of central importance in hydraulic and sedimentation engineering. Flow resistance or hydraulic roughness coefficients are used principally to derive depth-discharge relations necessary, e.g., in waterway design and in the computation of sediment transport rates.

Leopold, et al. (30) classified the hydraulic roughness of natural channels into three elements: (1) Skin; (2) internal distortion; and (3) spill resistance. Skin friction is a function of the roughness of surficial material; internal distortion resistance is caused by particular boundary features such as discrete boulders, bends, bars and bed undulations that create eddies, and secondary circulations; spill resistance is associated with flow accelerations and decelerations. The relationships between these various forms of roughness and flow variables, are complex and poorly understood. Spill resistance is probably negligible in the more-or-less clean, straight, symmetrical, coarse gravel bed river reaches under fully turbulent, near uniform, subcritical water flows considered herein (33), and is therefore not examined further.

Two sediment transport regimes are studied herein: (1) The bedload transport rate is vanishingly small and the channel boundary is rigid; and (2) the bedload transport rate is finite and the channel boundary deforms. With the former regime, possibly the chief contributors to hydraulic roughness (for the given reach specifications) are grain roughness and internal distortion or form resistance generated by relict or remnant bedforms of previous floods. (With the latter regime, reactivated or developed bedforms probably are responsible for most of the hydraulic roughness.) In contrast to sand bed rivers, which can have a variety of bedforms (35), apparently only dunes or bars develop under subcritical flows on the channel bottoms of gravel bed rivers (13,14). Indeed, Hill (23) has observed the persistence of dune forms, moving downstream under supercritical flows, in a laboratory channel with a gravel bed; whereas for a sand

[1]Scientist, Water and Soil Division, Ministry of Works and Development, P.O. Box 1479 Christchurch, New Zealand.

Note.—Discussion open until December 1, 1981. To extend the closing date one month, a written request must be filed with the Manager of Technical and Professional Publications, ASCE. Manuscript was submitted for review for possible publication on July 23, 1980. This paper is part of the Journal of the Hydraulics Division, Proceedings of the American Society of Civil Engineers, ©ASCE, Vol. 107, No. HY7, July, 1981. ISSN 0044-796X/81/0007-0899/$01.00.

TABLE 1.—New Zealand Gravel Bed

Sequence number (1)	Reach number (2)	River name (3)	Discharge, Q, in cubic meters per second (4)	Mean velocity, V, in meters per second (5)	Water surface width, B, in meters (6)
1	1	Ashburton	4.59	1.08	11.0
2	2		0.34	0.260	5.50
3	3		6.99	1.19	11.9
4	4		7.90	1.12	15.8
5	5	Awatere	6.09	0.790	19.2
6	6	Buller	1.78	0.23	19.8
7	7	Eves	0.054	0.16	2.90
8	8	Gowan	80.1	1.17	36.0
9	8		15.9	0.390	32.0
10	8		9.94	0.280	29.0
11	8		64.3	1.01	35.2
12	8		24.2	0.560	31.1
13	8		34.4	0.740	32.3
14	9	Hangatahua	8.04	0.96	13.4
15	10	Haparapara	18.3	0.44	25.9
16	11	Jacobs	145	1.28	64.0
17	12	Karamea	256	1.09	123.0
18	12		190	0.73	121.0
19	13	Makarora	10.9	0.65	54.9
20	14	Manawatu	5.52	0.27	44.5
21	15		5.55	0.53	25.6
22	15		10.4	0.69	18.3
23	16		2.89	0.23	38.4
24	17	Mohaka	34.4	0.98	59.1
25	17		315	2.07	61.3
26	17		88.3	1.43	60.0
27	17		392	2.14	65.5
28	17		213	1.73	59.7
29	17		179	1.83	60.0
30	17		80.4	1.28	57.0
31	18	Moutere	0.433	0.22	11.3
32	19	Ongarue	50.1	1.09	38.4
33	20	Opihi	2.29	0.34	35.4
34	21		1.93	0.61	12.5
35	22	Pahaoa	0.76	0.25	20.1
36	23	Pororari	113	1.52	56.1
37	24	Rakaia	129	1.53	79.6
38	25	Rangitikei	693	3.32	76.2
39	26		20.4	0.88	29.0
40	27		85.5	1.28	58.5
41	28	Ruamahanga	5.97	0.66	19.2
42	28		1.64	0.48	6.7
43	29		63.1	0.77	51.2
44	29		27.0	0.43	46.6

River Data for Rigid Bed Channels

Wetted perimeter, P, in meters (7)	Hydraulic radius, R, in meters (8)	Maximum depth, Y, in meters (9)	Water surface slope, S (10)	Median size of surface bed material, d_{50}, in meters (11)	Water temperature, T, in degrees celsius (12)
11.3	0.380	0.480	0.00865	0.051	13.3
5.60	0.230	0.340	0.00125	0.051	18.9
12.1	0.480	0.610	0.00490	0.102	16.7
16.2	0.440	0.700	0.0110	0.152	14.4
19.5	0.400	0.580	0.0036	0.102	19.5
21.6	0.39	0.88	0.00035	0.076	10.6
2.96	0.12	0.21	0.00042	0.015	—
36.9	1.86	3.20	0.00140	0.102	12.8
33.0	1.23	2.35	0.00016	0.102	12.8
29.6	1.18	2.13	0.00017	0.102	17.2
36.1	1.76	3.05	0.00102	0.102	6.7
31.7	1.37	2.47	0.00039	0.102	6.7
32.9	1.41	2.59	0.00060	0.102	12.8
14.2	0.59	0.88	0.0109	0.152	15.6
26.9	1.56	2.44	0.000095	0.025	13.3
66.4	1.70	2.07	0.00088	0.102	8.9
125	1.89	3.32	0.000344	0.025	11.7
122	1.68	3.32	0.000336	0.025	11.7
55.8	0.26	0.52	0.0019	0.019	—
45.0	0.45	0.71	0.00017	0.051	17.8
25.8	0.39	0.61	0.00073	0.025	14.4
18.8	0.80	1.34	0.00063	0.025	14.4
38.4	0.34	0.58	0.00081	0.051	15.0
59.7	0.590	1.10	0.00108	0.051	19.4
65.6	2.33	3.17	0.00140	0.051	8.9
61.7	1.00	1.58	0.00119	0.051	7.8
67.5	2.72	3.44	0.00109	0.051	—
62.2	1.98	2.59	0.0010	0.051	8.9
61.0	1.60	2.01	0.0012	0.051	15.0
59.4	1.06	1.89	0.00111	0.051	9.4
11.3	0.17	0.24	0.0011	0.015	11.3
39.9	1.15	1.65	0.00082	0.025	10.0
35.7	0.20	0.50	0.00167	0.051	13.3
12.8	0.26	0.40	0.00250	0.051	18.3
20.1	0.15	0.24	0.00022	0.013	9.4
57.6	1.29	1.55	0.0014	0.025	—
79.9	1.05	1.58	0.00285	0.051	14.4
77.4	2.70	5.12	0.00181	0.051	15.6
29.3	0.79	1.49	0.00071	0.051	21.7
59.4	1.12	2.07	0.00215	0.051	8.9
19.8	0.45	0.70	0.0016	0.025	9.4
7.3	0.48	0.76	0.00092	0.025	—
53.0	1.63	3.17	0.00037	0.038	—
48.2	1.31	2.87	0.00027	0.038	12.2

TABLE 1.—

(1)	(2)	(3)	(4)	(5)	(6)
45	30	Sawyers	3.97	0.77	8.2
46	30		1.86	0.50	8.5
47	30		0.950	0.35	8.4
48	30		0.700	0.30	8.8
49	31	Takaka	10.1	0.31	62.5
50	32		4.22	0.39	29.3
51	33		217	3.16	26.2
52	34		94.8	1.70	31.7
53	35	Tongariro	58.5	1.43	47.2
54	36		50.5	1.30	47.9
55	37	Tukituki	39.5	0.58	72.8
56	38		1.44	0.37	9.8
57	39		18.9	0.84	35.7
58	40	Uawa	32.6	0.86	22.3
59	40		6.17	0.63	14.6
60	41	Waiapu	1.95	0.69	10.4
61	42		24.2	0.89	35.1
62	43	Waiarohia	32.9	2.28	13.4
63	44	Waiau	50.7	0.95	36.0
64	45	Waimea	0.069	0.091	5.20
65	46	Waipaoa	85.7	1.25	77.1
66	47		73.6	0.98	93.3
67	48		2.75	0.50	6.4
68	48		1.61	0.38	6.1
69	49		8.44	1.08	11.6
70	50	Wairoa	84.4	1.31	71.0
71	51	Wanganui	73.4	0.99	56.1
72	52		942	1.89	91.4
73	52		387	1.28	93
74	52		1471	1.94	101
75	52		879	1.71	91.4
76	52		1540	2.08	113
77	53		18.2	0.41	57.6
78	53		15.3	0.39	54.9
79	54		24.4	0.49	36.6
80	55		46.2	0.43	91.4
81	56		80.1	1.14	61.9
82	57	Whangaehu	3.82	0.44	11.9
83	58	Whangaparoa	6.29	0.43	29.3
84	59	Wharehika	4.93	0.62	21.9

bed under these conditions, antidunes moving upstream would occur (28).

The purpose of this study was to derive gravel bed river flow resistance prediction equations suitable for use in engineering design and fluvial studies. Theoretical considerations are employed to assess functional relationships established by a dimensional analysis which is calibrated empirically by linear, multiple regression. The large field data set listed is also useful for research and practical studies of gravel bed river hydraulics and sediment transport.

Continued

(7)	(8)	(9)	(10)	(11)	(12)
8.7	0.59	0.91	0.00548	0.152	—
9.1	0.41	0.52	0.00468	0.152	—
8.4	0.33	0.43	0.00400	0.152	—
7.7	0.27	0.35	0.00380	0.152	—
63.1	0.52	0.76	0.000458	0.127	—
29.4	0.37	0.49	0.00135	0.152	—
31.5	2.17	2.73	0.00200	0.152	13.9
33.5	1.66	2.07	0.00121	0.102	—
47.8	0.86	1.10	0.00530	0.127	12.8
48.0	0.81	1.01	0.00314	0.063	10.6
73.5	0.93	1.55	0.00040	0.076	6.7
10.5	0.43	0.49	0.00062	0.025	10.6
36.0	0.62	1.25	0.00175	0.051	9.4
23.2	1.63	3.08	0.00043	0.019	13.3
15.6	0.62	1.22	0.00057	0.019	13.9
10.7	0.27	0.55	0.0017	0.025	18.9
35.3	0.77	0.94	0.00134	0.102	13.3
15.3	0.94	1.52	0.00682	0.046	—
37.0	1.45	1.68	0.000431	0.025	12.8
5.27	0.14	0.24	0.00062	0.021	—
77.1	0.87	1.58	0.00124	0.013	11.1
93.6	0.80	1.19	0.00077	0.013	17.8
7.5	0.73	1.19	0.00099	0.038	12.8
7.2	0.60	0.85	0.00097	0.038	16.7
12.5	0.63	0.79	0.00182	0.051	13.9
71.2	0.91	1.16	0.0031	0.152	11.7
57.2	1.29	1.62	0.00166	0.025	10.6
98.8	5.04	6.19	0.000345	0.038	15.6
95.0	3.17	3.90	0.000399	0.038	9.4
110	6.89	8.44	0.000338	0.038	9.4
98.6	5.22	6.34	0.000268	0.038	9.4
116	6.42	8.99	0.000314	0.038	—
58.2	0.76	0.91	0.00047	0.076	10.0
55.8	0.70	1.04	0.00036	0.076	11.1
37.2	1.33	2.01	0.00038	0.076	11.1
91.7	1.19	1.52	0.000085	0.019	17.8
62.5	1.12	1.43	0.0009	0.038	11.1
12.2	0.72	1.13	0.00206	0.301	12.2
29.3	0.50	0.79	0.0006	0.013	14.4
22.0	0.36	0.61	0.0012	0.025	18.9

Data Collection and Specification

The 136 field data sets used in this study were obtained from 72 reaches on 46 New Zealand gravel bed rivers (Tables 1 and 2); and were collected mainly by the Ministry of Works and Development and Catchment Authorities as part of their routine water flow gaging programs. The following selection criteria were adopted in the compilation of the data set: (1) Straight channel

TABLE 2.—New Zealand Gravel Bed

Sequence number (1)	Reach number (2)	River name (3)	Discharge, Q, in cubic meters per second (4)	Mean velocity, V, in meters per second (5)	Water surface width, B, in meters (6)
1	1	Acheron	246	3.04	43.9
2	2	Hurunui	186	2.88	43.7
3			180	2.80	43.6
4	2		152	2.68	43.0
5	2		472	2.98	44.7
6	2		88.9	2.29	36.8
7	2		48.3	1.77	33.2
8	2		96.2	2.30	41.6
9	2		107	2.27	43.0
10	2		230	3.06	43.5
11	2		282	2.69	44.5
12	3	Motu	436	3.27	40.2
13	3		328	2.75	39.6
14	4		2,409	3.96	153.4
15	5	Ngarururo	617	2.80	108.0
16	5		625	2.90	108.0
17	6	Shotover	11.4	0.94	33.0
18	6		14.3	1.11	33.1
19	6		12.3	1.08	33.1
20	6		18.3	1.20	33.7
21	6		94.6	2.14	32.0
22	6		23.8	1.53	30.0
23	6		103	2.38	33.5
24	7		388	2.67	52.0
25	7		537	3.11	52.2
26	7		75.8	1.68	35.0
27	7		501	3.50	52.5
28	7		23.7	0.86	29.0
29	8	Waiarohia	33.0	2.28	13.4
30	9	Waimana	575	2.71	73.2
31	9		453	2.41	67.4
32	9		357	2.26	61.9
33	9		300	2.01	60.0
34	9		245	1.99	59.1
35	9		396	2.07	68.4
36	10	Waimea	98.0	1.31	45.1
37	11	Waioeka	309	2.65	38.7
38	11		518	3.34	42.1
39	11		382	3.13	39.3
40	11		354	3.22	42.3
41	11		328	2.93	40.5
42	12	Wairau	100	2.44	30.8
43	12		60.0	1.96	29.3
44	12		47.0	1.77	29.3

River Data for Mobile Bed Channels

Wetted perimeter, P, in meters (7)	Hydraulic radius, R, in meters (8)	Maximum depth, Y, in meters (9)	Water surface slope, S (10)	Median size of surface bed material, d_{50}, in meters (11)	Water temperature, T, in degrees celsius (12)
45.0	1.80	2.90	0.00330	0.038	—
47.4	1.36	2.32	0.00467	0.045	7.8
46.9	1.37	2.23	0.00461	0.045	7.8
45.4	1.25	1.98	0.00490	0.045	10.0
54.8	2.89	4.79	0.00200	0.045	—
40.4	0.96	1.46	0.00517	0.045	7.2
34.7	0.90	1.13	0.00502	0.045	12.8
44.5	0.97	1.62	0.00449	0.045	—
45.7	1.03	1.67	0.00481	0.045	8.9
48.9	1.53	2.62	0.00489	0.045	8.3
51.6	2.03	3.29	0.00351	0.045	—
46.6	2.86	4.72	0.00563	0.051	12.2
48.5	2.48	4.36	0.00612	0.051	12.2
159.7	3.82	6.86	0.00349	0.019	15.0
112.5	1.96	3.78	0.00427	0.051	12.7
111.3	1.94	3.51	0.00388	0.051	12.7
33.4	0.37	0.56	0.00339	0.017	6.2
33.5	0.38	0.66	0.00376	0.017	9.7
33.4	0.34	0.60	0.00370	0.017	5.7
34.2	0.45	0.70	0.00390	0.017	14.6
32.9	1.34	1.93	0.00440	0.017	3.3
30.5	0.51	0.85	0.00420	0.017	—
34.4	1.25	1.70	0.00500	0.017	5.5
53.4	2.72	4.28	0.00250	0.012	13.1
58.0	2.97	4.66	0.00250	0.012	10.0
36.7	1.23	1.82	0.00160	0.012	5.2
57.1	2.51	3.88	0.00240	0.012	4.9
30.1	0.92	1.30	0.00120	0.012	3.0
15.2	0.95	1.52	0.00682	0.046	—
74.4	2.85	4.21	0.00249	0.025	14.4
69.2	2.72	4.54	0.00218	0.025	14.4
63.7	2.47	4.24	0.00185	0.025	16.1
61.6	2.42	4.14	0.00124	0.025	14.0
60.0	2.05	4.01	0.00121	0.025	14.0
71.0	2.70	4.36	0.00119	0.025	14.0
46.0	1.63	2.19	0.00083	0.013	—
42.1	2.77	3.87	0.00131	0.038	13.0
48.5	3.24	5.27	0.00197	0.038	10.5
43.6	2.79	3.57	0.00202	0.038	10.0
42.4	2.60	3.66	0.00247	0.038	10.5
44.8	2.51	3.81	0.00206	0.038	10.0
32.0	1.28	1.71	0.00651	0.038	7.8
30.2	1.00	1.46	0.00649	0.038	9.4
30.2	0.89	1.31	0.00651	0.038	9.4

TABLE 2.—

(1)	(2)	(3)	(4)	(5)	(6)
45	12		185	3.25	30.8
46	12		327	4.29	31.1
47	12		288	4.31	31.1
48	12		159	3.14	31.1
49	12		95.0	2.53	29.3
50	12		19.0	1.03	29.3
51	12		107	2.60	29.3
52	13	Wairoa	182	1.44	39.3

alinement and a more-or-less constant width; (2) little vegetation on the channel bed and banks; (3) stable banks and bed devoid of major irregularities; and (4) relatively wide channel having a simple trapezoidal geometry that contains the entire water discharge without overbank flow. This prescription is similar to that adopted by Limerinos (31).

Standard field and computation procedures were used in the derivation of the Darcy-Weisbach friction factor, f, defined by

$$f = \frac{8gRS}{V^2} \quad \text{(1)}$$

in which g = the gravitational acceleration; R = the hydraulic radius; S = the average longitudinal water surface slope, assumed equal to average energy slope; and V = the mean velocity of flow. Direct measurements and soundings were utilized to determine water surface width, B, wetted perimeter, P, maximum depth, y, and cross section area, A. From this information hydraulic radius, R, was computed, and in conjunction with current meter measurements of point velocities, mean velocity, V, and water discharge, Q, were deduced. Details of these procedures are given by Buchanan and Somers (5). Three staff gages or a surveyor's level and staff were employed to estimate water surface slope, S, determined over a relatively long length of channel as described by Dalrymple and Benson (8); and water temperature, T, was measured with a standard mercury thermometer. All the hydraulic variables were determined at a single cross section during conditions of reasonably uniform flow, i.e., at or near flood crests or at low flows. The Froude Number ($V/\sqrt{gR}$) was always less than 1.0 and therefore flows were subcritical. Median size of surface bedmaterial, d_{50}, was determined using the method of Wolman (39) or variants thereof (27), or by sieving of surface material at reaches with fine gravels.

Flow Resistance in Rigid Boundary Channels

The criterion employed to distinguish rigid boundary (vanishingly small rates of bedload transport) from mobile boundary conditions was Shields Entrainment Function, F_s, which for fully turbulent flows is given by (20)

$$F_s = \frac{RS}{(S_s - 1)\, d_{50}} = \text{constant} \quad \text{(2)}$$

Continued

(7)	(8)	(9)	(10)	(11)	(12)
32.6	1.75	2.38	0.00652	0.038	—
33.5	2.29	3.11	0.00690	0.038	—
33.5	2.01	2.68	0.00714	0.038	—
32.3	1.56	2.13	0.00661	0.038	—
31.1	1.20	1.65	0.00646	0.038	—
29.6	0.63	1.16	0.00653	0.038	7.2
31.4	1.31	1.74	0.00654	0.038	—
41.5	3.05	4.45	0.00125	0.038	14.4

in which $u_* \frac{d_{50}}{\nu} > 400$ . . . . . (3)

in which S_s = specific gravity of bed particles ($S_s = 2.65$ throughout this paper); u_* = average shear velocity; and ν = kinematic viscosity of water. Following Henderson (20) Shields' original value of $F_s = 0.056$ was adopted. With $\nu < 1.60 \times 10^{-6}$ m^2/s Eqs. 2 and 3 yield

$d_{50} > 0.008$ m . . . . . (4)

which is easily satisfied by the data of Tables 1 and 2. Thus, rigid boundary conditions are assumed if, from Eq. 2 and the aforementioned

$d_{50} \geq 11RS$ . . . . . (5)

Data satisfying this criterion are listed in Table 1.

Dimensional Analysis.—Since only water discharges in clean, straight, uniform channels are being considered it can be assumed that friction factors for subcritical flows, satisfying Eq. 5, are a function of V, R, P, y, d_{50}, g, ρ = density of water; and μ = dynamic viscosity of water. Dimensional analysis then yields

$$f = fn\left(\frac{VR}{\nu}, \frac{V}{\sqrt{gR}}, \frac{R}{d_{50}}, \frac{R}{P}, \frac{R}{y}\right) \quad \ldots\ldots (6)$$

or equivalently

$$f = fn\left(\frac{Vd_{50}}{\nu}, \frac{V}{\sqrt{gd_{50}}}, \frac{R}{d_{50}}, \frac{R}{P}, \frac{R}{y}\right) \quad \ldots\ldots (7)$$

in which $\nu = \mu/\rho$, and fn is some function.

The independent variables, P, y are included because, with the exception of mirror images, the set R, P, y uniquely defines cross section shape (21). Because of a lack of other bedmaterial data, it is assumed that the surface bedmaterial or bed pavement is adequately described by the median grain diameter, d_{50} [based on intermediate particle axis (31)]. Choice of median, as opposed to other values in the bed pavement particle size distribution, is supported by Bray (4) who showed that no significant difference obtains, with best fit equations for roughness estimation, using several other measures of particle size.

Theoretical Considerations.—Keulegan (29) employed the Prandtl-von Karman velocity distribution law to derive an equation for the mean velocity of turbulent flow in rough, rigid bed channels:

$$\frac{V}{u_*} = E + \left(\frac{1}{\kappa}\right) \ln\left(\frac{R}{k_s}\right) \quad \ldots\ldots\ldots\ldots\ldots\ldots\ldots\ldots\ldots\ldots\ldots\ldots (8)$$

in which E = a coefficient; κ = von Karman's constant of turbulent exchange; and k_s is the roughness height of the bed surface. Eq. 8 may be written (22) in general terms as

$$\frac{1}{\sqrt{f}} = c \log_{10}\left(\frac{aR}{k_s}\right) \quad \ldots\ldots\ldots\ldots\ldots\ldots\ldots\ldots\ldots\ldots\ldots\ldots (9)$$

in which a = antilog $(E\kappa/2.30)$; and $c = 2.30/(\kappa/\sqrt{8})$. If, as is generally accepted, $\kappa = 0.400$, then $c = 2.03$ and, a, varies with E. The parameter,

TABLE 3.—Correlation Matrix for Logarithms of Dimensionless Variables Computed from Rigid Boundary Data of Table 1

Perimeters (1)	$1/\sqrt{f}$ (2)	R/d_{50} (3)	P/R (4)	y/R (5)	Vd_{50}/ν (6)	VR/ν (7)	$V/\sqrt{gR}$ (8)	$V/\sqrt{gd_{50}}$ (9)
$1/\sqrt{f}$	1.00							
R/d_{50}	0.770	1.00						
P/R	0.038	−0.164	1.00					
y/R	−0.037	−0.067	0.206	1.00				
Vd_{50}/ν	0.113	−0.095	−0.314	−0.309	1.00			
VR/ν	0.653	0.663	−0.347	−0.267	0.674	1.00		
$V/\sqrt{gR}$	0.365	0.088	−0.027	−0.211	0.596	0.517	1.00	
$V/\sqrt{gd_{50}}$	0.643	0.631	0.025	−0.162	0.287	0.678	0.664	1.00

a, is dependent on the shape of the channel and Hey (22) has shown from Keulegan's analysis (29) that for $c = 2.03$

$$a = fn\left(\frac{R}{y}\right) \quad \ldots\ldots\ldots\ldots\ldots\ldots\ldots\ldots\ldots\ldots\ldots\ldots (10)$$

provided flow width/depth ratios are not very small. For the data of Table 1, in which the cross sections are reasonably trapezoidal and mostly very wide, Hey's (22) plotted function (Eq. 10) yields

$$11.6 < a < 13.5$$

This small range for the parameter, a, suggests that the influence of wide channel cross section shape on friction factors is minor. The analysis of Kazemipour and Apelt (25) also indicates similar independence for the data of Table 1. Moreover the Boundary Reynolds Number (VR/ν) and the Froude Number $(V/\sqrt{gR})$ may be neglected because viscosity effects are likely to be unimportant in fully turbulent flows over rough boundaries; and energy losses due to surface waves can be discounted (21). It may be inferred from the preceding that Eq.

6 reduces to

$$f = fn\left(\frac{R}{d_{50}}\right) \quad \text{(11)}$$

for friction factors of reaches and hydraulic conditions specified in this study.

Statistical Analysis.—The seven dimensionless variables of Eqs. 6 and 7 were computed for the data of Table 1. Where water temperature had not been measured, an average value, determined during other flow gaugings at the relevant reach, was used. As the dimensionless variables were found to be approximately log-normally distributed, statistical analyses were made with their logarithms. In order to examine intercorrelations a correlation matrix of their logarithms (Table 3) was computed; and then a linear stepwise regression technique was applied in which the intercorrelations evident in Table 3 were eliminated as

TABLE 4.—Friction Factor Relationships Based on Power Form of Equation

Channel boundary state (1)	Equation (2)	Equation number (3)	Coefficient of determination (4)	Standard error in log units (5)	F-ratio (6)
Rigid	$1/\sqrt{f} = 1.25\,(R/d_{50})^{0.287}\,(V/\sqrt{gR})^{0.241}\,(P/R)^{0.105}$	12	0.710	0.093	65.6
(n = 84)	$1/\sqrt{f} = 0.886\,(R/d_{50})^{0.297}\,(P/R)^{0.103}$	14	0.621	0.107	66.2
	$1/\sqrt{f} = 1.33\,(R/d_{50})^{0.287}$	15	0.591	0.110	119
	$1/\sqrt{f} = 2.22\,(VR/\nu)^{0.185}$	16	0.427	0.132	61.0
Mobile	$1/\sqrt{f} = 2.21\,(V/\sqrt{gd_{50}})^{0.340}$	36	0.384	0.066	31.1
(n = 52)	$1/\sqrt{f} = 2.17\,(R/d_{50})^{0.129}$	37	0.216	0.074	13.8
	$1/\sqrt{f} = 2.15\,(V/\sqrt{gd_{50}})^{0.321}\,(R/d_{50})^{0.129}$	38	0.385	0.066	15.3

far as possible (9). A level of significance corresponding to a Students t value of 2.00 or greater was selected for the inclusion of a dimensionless variable in the interpretation of regression output. The multiple regression result (Eq. 12, Table 4)

$$\frac{1}{\sqrt{f}} = 1.25\left(\frac{R}{d_{50}}\right)^{0.287}\left(\frac{V}{\sqrt{gR}}\right)^{0.241}\left(\frac{P}{R}\right)^{0.105} \quad \text{(12)}$$

explained 71% of the friction factor variance inherent in Table 1: specifically relative roughness (R/d_{50}) explained 59%; Froude Number ($V/\sqrt{gR}$), 9%; and shape factor (P/R), 3%. Eq. 12, and indeed all equations in Table 4 involve a degree of spurious correlation (3) in that all dimensionless variables contain parameters in common with the friction factor, f. In view of the theoretical

preceding considerations, the fact that the relation

$$\left[\frac{1}{\sqrt{f}} = \frac{\left(\frac{V}{\sqrt{gR}}\right)}{(\sqrt{8S})}\right] \text{ versus } \left[\left(\frac{V}{\sqrt{gR}}\right)\right] \quad \ldots\ldots\ldots\ldots\ldots\ldots \quad (13)$$

is involved in the regression, and the low degree of variance explanation, the Froude Number ($V/\sqrt{gR}$) was discounted from Eq. 12. The regression equation for the two remaining dimensionless variables (Eq. 14, Table 4) shows that only a marginal improvement in logarithmic standard error results between Eq. 14 and Eq. 15, which is solely a function of relative roughness (R/d_{50}). Also

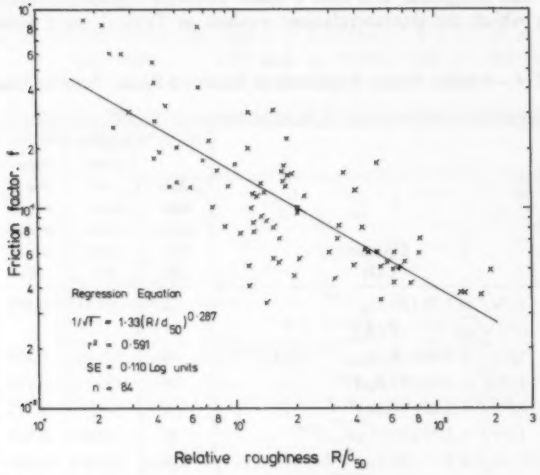

FIG. 1.—Friction Factor vs Relative Roughness for Rigid Boundary Conditions in Coarse Gravel Bed Rivers

the spurious correlation between friction factor parameter, $(1/\sqrt{f})$ and shape factor (P/R) may contribute significantly to the 3% of variance explained by P/R. On these grounds the accepted result of the statistical analysis is (Fig. 1)

$$\frac{1}{\sqrt{f}} = 1.33\left(\frac{R}{d_{50}}\right)^{0.287} \quad \ldots\ldots\ldots\ldots\ldots\ldots\ldots\ldots \quad (15)$$

in accord with Eq. 11.

Using data from 67 Canadian gravel bed river reaches, Bray (4) obtained a significant ($r^2 = 0.472$, $F = 60$) statistical relationship

$$\frac{1}{\sqrt{f}} = 0.0519\left(\frac{VR}{\nu}\right)^{0.294} \quad \ldots\ldots\ldots\ldots\ldots\ldots\ldots\ldots \quad (17)$$

which should be compared with Eq. 16 (Table 4). Bray states that his finding is at variance with the expected result ($1/\sqrt{f}$ a function of R/d_{50} only) based on widely accepted ideas related to the simplified case of two-dimensional flow over a hydrodynamically rough boundary. But since

$$\frac{VR}{\nu} = \left(\frac{Vd_{50}}{\nu}\right) \cdot \left(\frac{R}{d_{50}}\right) \quad \ldots\ldots\ldots\ldots\ldots\ldots\ldots\ldots\ldots\ldots \quad (18)$$

and given: (1) The statistics of Eq. 15 (Table 4); (2) the high correlation between Boundary Reynolds Number (VR/ν); and relative roughness (R/d_{50}) (Table 3); and (3) the low correlations between Particle Reynolds Number (Vd_{50}/ν) and both friction factor parameter ($1/\sqrt{f}$) and relative roughness (R/d_{50}); a conclusion for the data of Table 1 is that the statistical significance of Eq. 16 is probably spurious.

Resistance Equation for Rigid Gravel Bed Channels

The results of the foregoing analysis indicate that, for the given reach conditions and selection of descriptive parameters, the friction factor is given by (Eq. 11)

$$f = fn\left(\frac{R}{d_{50}}\right)$$

in agreement with earlier work with gravel rivers by Leopold, et al., (30), Kellerhals (26), Limerinos (31), and Griffiths (19) amongst others. Contributions to the scatter of Fig. 1 are thought to result from: (1) Inadequate description of relevant reach and hydraulic variables, notably the representation of the surface bedmaterial only by the median size; (2) inconsistencies, errors, and inadequacies in data collection procedures; (3) irregularities in channel alinements and cross sections; and (4) rugged bed topography. Of these the last is qualitatively considered as the most pronounced for the New Zealand data (Table 1). At most reaches, residual or relict bars were present to provide significant internal distortion resistance.

In the estimation of friction factors for river works, the aforementioned theoretically based, empirically calibrated equations (26), (30), and (31) of Keulegan form (Eq. 9) give reasonable predictions for straight regular gravel reaches (4,6). Eq. 15, the result of the statistical analysis, is not however recommended, in addition to the equations previously referenced, for use in natural channel design; instead the use of a more comprehensive equation, calibrated by 186 data sets including data from Table 1 and elsewhere (1, 2, 11, 24, and 40), is advocated. The equation is (19)

$$\frac{1}{\sqrt{f}} = 0.760 + 1.98 \log_{10}\left(\frac{R}{d_{50}}\right) \quad \ldots\ldots\ldots\ldots\ldots\ldots\ldots\ldots\ldots\ldots \quad (19)$$

in which $1 \leq R/d_{50} \leq 200$. For low values of relative roughness ($R/d_{50} < 5$), or where large discrete elements are present in a reach, special studies calibrated by field data (2, 24, 36, and 37) should be consulted.

Mobile boundary conditions, occurring when the bedload transport rate is nonzero, were defined from Eqs. 2, 3, and 4 by

$$d_{50} < 11RS \quad \ldots \quad (20)$$

Data satisfying Eq. 20 are listed in Table 2. Most of the data sets correspond to vigorous bed conditions as the mean value of the Froude Number ($V/\sqrt{gR}$) is 0.606 with a standard deviation of 0.154. Except at Shotover River reaches (Table 2), dune bedforms were not observed directly as suspended sediment almost invariably clouds the water at high flow rates; but residual or relict bedforms are commonly apparent subsequent to flood conditions. A qualitative description of various bedforms in a New Zealand gravel bed river is given by Griffiths (18).

Veiga da Cunha (7) analyzed mobile bed data from the fine gravel bed Mondego River in Portugal. He employed the method of Einstein and Barbarossa (10) and divided the friction factor, f, into two components, namely

$$f = f' + f'' \quad \ldots \quad (21)$$

in which f' = friction factor due to grain roughness; and f'' = friction factor due to form roughness produced by bedforms and other channel irregularities. This separation (Eq. 21) may be of conceptual use; nevertheless it is arbitrary. Moreover there is doubt (38) concerning the ability of the plane bed resistance relations, used to evaluate f', to predict the grain roughness of a gravel bed covered with undulations. Laboratory studies with coarse bedmaterial (32,34) have generally conformed Cunha's results. Furthermore, Gladki (15) has shown that the flow resistance relations derived by the previously mentioned workers (7, 32, and 34) fit data from the coarse gravel bed Raba River, moderately well.

Theoretical Considerations.—Einstein and Barbarossa (10) argued that form resistance contribution to the friction factor must be dependent on the topography of the bed configuration which, in turn, is a function of the sediment transport rate along the channel bed. According to them the bedload transport rate depends solely on the dimensionless variable, ψ:

$$\psi = (S_s - 1)\frac{d_{35}}{RS} = g(S_s - 1)\frac{d_{35}}{u_*^2} \quad \ldots \quad (22)$$

in which d_{35} = size of which 35% of the bedmaterial is finer. In more specific terms it can be argued that for a mobile gravel bed with developed bedforms, flow resistance is mainly due to form drag with minor contributions, given the high Boundary Reynolds Numbers (VR/ν) observed in natural rivers, from grain roughness. Neglecting skin friction, the profile drag, F_D, of a bed undulation of height, h, length, L, and of unit width (wide reaches) may have the form

$$F_D = \frac{1}{2} C_D \rho h V^2 \quad \ldots \quad (23)$$

in which C_D = coefficient of profile drag.

The average resistive stress, τ, is from Eq. 23

$$\tau = \frac{\frac{1}{2} C_D \rho h V^2}{L} \quad (24)$$

But for the reach conditions considered in this paper we have (20)

$$\tau = \rho g R S \quad (25)$$

Combination of Eqs. 1, 24, and 25 yields

$$f = 4C_D \frac{h}{L} \quad (26)$$

In experiments with sand-coated two dimensional triangular roughness elements, simulating ripples and dunes, Vittal, et al., (38) deduced an empirical equation for the form drag coefficient, C_f:

$$C_f = m \left(\frac{R}{h}\right)^{0.375} \quad (27)$$

in which m = a function of h/L.

From the foregoing, $C_f \sim C_D$ and Eqs. 26 and 27 imply

$$f = fn\left(\frac{h}{L}, \frac{h}{R}\right) \quad (28)$$

Interestingly Engelund (12) found, using a pipe expansion analogy, that

$$f'' = \left(\frac{h}{R}\right)\left(\frac{h}{L}\right) \quad (29)$$

Yalin and Emin (41) state that

$$L \sim 2\pi R \quad (30)$$

and present a graphical relation of the form

$$\frac{h}{L} = f_n\left(\frac{\tau}{\tau_c}, \frac{R}{d_{50}}\right) \quad (31)$$

in which τ_c = average bed shear stress at critical conditions of bedload transport. Eq. 31 applies to sand dunes, but the range of R/d_{50} (38) is commensurate with that of Table 2 ($17 \leq R/d_{50} \leq 247$).

Assuming that Eqs. 30 and 31 apply to gravel dunes or bars, then Eqs. 28, 30, and 31 give

$$f = fn\left(\frac{\tau}{\tau_c}, \frac{R}{d_{50}}\right) \quad (32)$$

From Eqs. 2, 22, and 25 we deduce

$$\frac{\tau}{\tau_c} = \frac{u_*^2 F_s}{g(S_s - 1) d_{50}} \sim \frac{1}{\psi} \quad (33)$$

with F_S constant (Eq. 2).

Kennedy (28) has demonstrated however, for sediment of constant specific gravity, the rough proportionality:

$$\psi \sim \frac{gd_{50}}{V^2} \quad \text{(34)}$$

The mobility parameter defined by the RHS (right hand side) of Eq. 34 is preferred in this study as average shear velocity, u_*, may be rather insensitive (28) and mean velocity, V, is more accurately determined than u_* in the field. These several arguments, together with Eqs. 33 and 34 and the neglect of grain roughness effects (Eq. 23), that is, R/d_{50} is assumed to be unimportant, imply that Eq. 32 becomes

$$f = fn\left(\frac{V}{\sqrt{gd_{50}}}\right) \quad \text{(35)}$$

for friction factors of wide reaches with mobile gravel beds. Eq. 35 takes implicit account of grain roughness effects, given Eq. 34 and the relative roughness term (R/d_{35}) in Eq. 22.

TABLE 5.—Correlation Matrix for Logarithms of Dimensionless Variables Computed from Mobile Boundary Data of Table 2

Perimeters (1)	$1/\sqrt{f}$ (2)	R/D_{50} (3)	P/R (4)	y/R (5)	Vd_{50}/ν (6)	VR/ν (7)	$V/\sqrt{gR}$ (8)	$V/\sqrt{gd_{50}}$ (9)
$1/\sqrt{f}$	1.00							
R/d_{50}	0.465	1.00						
P/R	−0.260	−0.514	1.00					
y/R	−0.003	−0.046	0.409	1.00				
Vd_{50}/ν	0.273	−0.095	−0.466	0.063	1.00			
VR/ν	0.497	0.558	−0.786	−0.057	0.704	1.00		
$V/\sqrt{gR}$	0.242	−0.304	0.025	−0.014	0.544	0.197	1.00	
$V/\sqrt{gd_{50}}$	0.620	0.714	−0.505	−0.126	0.306	0.660	0.374	1.00

Statistical Analysis.—The statistical analysis detailed previously was repeated for the data of Table 2. A correlation matrix for the seven dimensionless variables (Eqs. 6 and 7) is given in Table 5 which should be compared with the markedly different Table 3. Linear stepwise regression indicated that only the mobility parameter, $V/\sqrt{gd_{50}}$, was significant: the result was (Eq. 36, Table 4, and Fig. 2)

$$\frac{1}{\sqrt{f}} = 2.21\left(\frac{V}{\sqrt{gd_{50}}}\right)^{0.340} \quad \text{(36)}$$

which is in accord with Eq. 35 and supports earlier work (7, 15, 32, and 34) based on the Einstein and Barbarossa (10) parameter, ψ (Eq. 22). Note that the relative roughness relation (Eq. 37, Table 4) is different from that for rigid boundary channels (Eq. 15, Table 4). The low value of the exponent of Eq. 37 together with its statistics (Table 4) indicate that the friction factor parameter $(1/\sqrt{f})$, is only slightly dependent upon relative roughness (R/d_{50}). Comparison of statistical data (Table 4) for Eqs. 36 and 38 supports this contention.

Resistance Equation for Mobile Gravel Bed Channels.—The foregoing analysis indicates, that for the reach conditions and parameter selection adopted herein, the friction factor is given by (Eq. 35): $f = fn\ (V/\sqrt{gd_{50}})$, and the regression result (Eq. 36) is $1/\sqrt{f} = 2.21\ (V/\sqrt{gd_{50}})^{0.340}$, will be less useful, for flow resistance prediction in gravel bed rivers, than its rigid boundary counterparts (Eqs. 15 and 19) owing to the inferior statistics (Table 4). The main reasons for the scatter evident in Fig. 2 are probably an inadequate description of bedform shape, and the lack of account of bedform dynamics in the predictive model (Eq. 35). In particular, hysteresis effects caused mainly by dune development

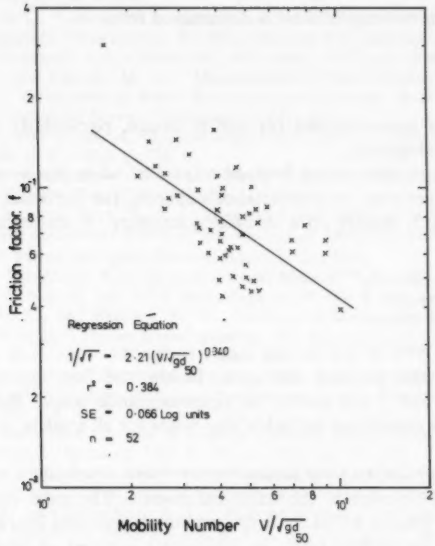

FIG. 2.—Friction Factor vs Mobility Number for Mobile Boundary Conditions in Coarse Gravel Bed Rivers

persisting on the falling stage of a flood, together with the dependence of dune size on flood wave steepness (16 and 17) are likely to provide important scatter contributions.

Conclusions

1. When the channel boundary is rigid, the resistance to fully turbulent flow in straight, regular reaches of coarse gravel bed rivers is dependent, largely, on the relative roughness, provided that bed and bank roughness are not distinguished and surface bedmaterial is described by the median size. A statistical model of this form, namely

$$\frac{1}{\sqrt{f}} = 1.33 \left(\frac{R}{d_{50}}\right)^{0.287}$$

explains nearly 60% of the friction factor variance inherent in a large field data set from New Zealand gravel bed rivers.

2. A theoretically based equation, calibrated by a more comprehensive data set (including that of Conclusion 1), applicable to rigid beds and defined by

$$\frac{1}{\sqrt{f}} = 0.760 + 1.98 \log_{10} \left(\frac{R}{d_{50}}\right)$$

where the mean velocity of flow is determined from

$$f = \frac{8gRS}{V^2}$$

is consequently recommended for use in design, particularly in reaches with a rugged bed topography.

3. For channels with active bedload transport, when the boundary is mobile and bedforms develop, flow resistance depends, for the reach and parameter specification of 1, mainly on a mobility parameter. A statistical model of this form:

$$\frac{1}{\sqrt{f}} = 2.21 \left(\frac{V}{\sqrt{gd_{50}}}\right)^{0.340}$$

explains nearly 40% of the friction factor variance.

4. With the New Zealand data given herein, the flow resistance models of Conclusions 1 and 3 are useful for reconnaissance work, that is for coarse prediction. This conclusion probably also holds for all models of the form given in 2.

5. Other factors, apart from measurement errors, are thought to be responsible for the residual variance in the statistical models. The main contributor in the rigid boundary state is probably form roughness provided by relict or remnant bedforms; and for mobile beds, an inadequate account of bedform geometry and dynamics.

Acknowledgments

The writer recognises and appreciates the contribution to river engineering and fluvial geomorphology made by those who collect field data, under frequently difficult and hazardous conditions. For assistance with the compilation of this paper the writer thanks A. Alderidge, H. Freestone, D. Hewson, M. Hicks, A. Sutherland, A. Tomlinson and, particularly, M. McSaveney, for his guidance and encouragement.

Appendix.—References

1. Barnes, H. H., "Roughness Characteristics of Natural Channels," *Water Supply Paper 1849*, United States Geological Survey, Washington, D.C., 1967.
2. Bathurst, J. C., "Flow Resistance of Large-Scale Roughness," *Journal of the Hydraulics*

Division, ASCE, Vol. 104, No. HY12, Proc. Paper 14239, Dec., 1978, pp. 1587–1603.
3. Benson, M. A., "Spurious Correlation in Hydraulics and Hydrology," *Journal of the Hydraulics Division*, ASCE, Vol. 91, No. HY4, Proc. Paper 4393, July, 1965, pp. 35–42.
4. Bray, D. I., "Estimating Average Velocity in Gravel-Bed Rivers," *Journal of the Hydraulics Division*, ASCE, Vol. 105, No. HY9, Proc. Paper 14810, Sept., 1979, pp. 1103–1122.
5. Buchanan, T. J., and Somers, W. P., "Discharge Measurements at Gauging Stations," *Techniques of Water Resources Investigations*, Book 3, Chapter A11, United States Geological Survey, Washington, D.C., 1969.
6. Burkham, D. E., and Dawdy, D. R., "Resistance Equation for Alluvial Channel Flow," *Journal of the Hydraulics Division*, ASCE, Vol. 102, No. HY10, Proc. Paper 12462, Oct., 1976, pp. 1479–1489.
7. Cunha, Veiga da L., "About the Roughness in Alluvial Channels with Comparatively Coarse Bed Materials," *Proceedings*, Twelfth Congress of the International Association for Hydraulic Research, Vol. 1, Paper No. A10, Sept., 1967, pp. 76–84.
8. Dalrymple, T., and Benson, M. A., "Measurement of Peak Discharge by the Slope Area Method," *Techniques of Water Resources Investigations*, Book 3, Chapter A2, United States Geological Survey, Washington, D.C., 1967.
9. Draper, N. R., and Smith, H., *Applied Regression Analysis*, John Wiley and Sons, Inc., New York, N.Y., 1966, p. 171.
10. Einstein, H. A., and Barbarossa, N. L., "River Channel Roughness," *Transactions*, ASCE, Vol. 117, Paper No. 2528, 1952, pp. 1121–1146.
11. Emmett, W. W., and Seitz, H. R., "Suspended and Bedload Sediment Transport in the Snake and Clearwater Rivers in the Vicinity of Lewiston, Idaho," *Basic-Data Report*, United States Geological Survey, Boise, Idaho, 1974.
12. Engelund, F., "Hydraulic Resistance of Alluvial Streams," *Journal of the Hydraulics Division*, ASCE, Vol. 92, No. HY2, Proc. Paper 4739, Mar., 1966, pp. 315–327.
13. Fahnestock, R. K., and Bradley, W. C., "Knik and Matanuska Rivers, Alaska: a Contrast in Braiding," *Fluvial Geomorphology*, M. Morisawa, ed., State University of New York, New York, 1973, pp. 221–250.
14. Galay, V. J., "Observed Forms of Bed Roughness in an Unstable Gravel River," *Proceedings*, Twelfth Congress of the International Association for Hydraulic Research, Vol. 1, Paper No. A11, Sept., 1967, pp. 85–94.
15. Gladki, H., "Resistance to Flow in Alluvial Channels with Coarse Bed Materials," *Journal of Hydraulic Research*, Vol. 17, No. 2, 1979, pp. 121–128.
16. Griffiths, G. A., "Transport of Bedload by Translation Waves in an Alluvial Channel," *Research Report 76-1*, University of Canterbury, Christchurch, New Zealand, 1976.
17. Griffiths, G. A., and Sutherland, A. J., "Bedload Transport by Translation Waves," *Journal of the Hydraulics Division*, ASCE, Vol. 103, No. HY11, Proc. Paper 13363, Nov., 1977, pp. 1279–1291.
18. Griffiths, G. A., "Recent Sedimentation History of the Waimakariri River, New Zealand," *Journal of Hydrology*, New Zealand, Vol. 18, No. 1, 1979, pp. 6–28.
19. Griffiths, G. A., "Rigid Boundary Flow Resistance of Gravel Rivers," *Report WS 127*, Ministry of Works and Development, Christchurch, New Zealand, 1979.
20. Henderson, F. M., *Open Channel Flow*, The MacMillan Company, Inc., New York, N.Y., 1966.
21. Hey, R. D., "Determinate Hydraulic Geometry of River Channels," *Journal of the Hydraulics Division*, ASCE, Vol. 104, HY6, Proc. Paper 13830, June, 1978, pp. 869–885.
22. Hey, R. D., "Flow Resistance in Gravel-Bed Rivers," *Journal of the Hydraulics Division*, ASCE, Vol. 105, No. HY9, Apr., 1979, pp. 365–379.
23. Hill, I. K., "Fluvial Sediment Transport at a Large Bed Shear Stress," thesis presented to the University of Canterbury, at Christchurch, New Zealand, in 1967, in partial fulfillment of the requirements for the degree of Doctor of Philosophy.
24. Judd, H. E., and Peterson, D. F., "Hydraulics of Large Bed Element Channels," *Report No. PRWG 17-6*, Utah Water Research Laboratory, Utah State University, Logan, Utah, 1969.
25. Kazemipour, A. K., and Apelt, C. J., "Shape Effects on Resistance to Uniform Flow in Open Channels," *Journal of Hydraulic Research*, Vol. 17, No. 2, 1979, pp. 129–147.

26. Kellerhals, R., "Stable Channels with Gravel-Paved Bed," *Journal of the Waterways and Harbors Division*, ASCE, Vol. 93, No. WW1, Proc. Paper 5091, Feb., 1967, pp. 63–84.
27. Kellerhals, R., and Bray, D. I., "Sampling Procedures for Coarse Fluvial Sediments," *Journal of the Hydraulics Division*, ASCE, Vol. 97, No. HY8, Proc. Paper 8279, Aug., 1971, pp. 1165–1180.
28. Kennedy, J. F., "Hydraulic Relations for Alluvial Streams," *Sedimentation Engineering*, V. Vanoni, ed., ASCE, New York, N.Y., 1975, pp. 114–154.
29. Keulegan, G. H., "Laws of Turbulent Flow in Open Channels," *Journal of Research of the National Bureau of Standards*, Vol. 21, Research Paper 1151, Dec., 1938, pp. 707–741.
30. Leopold, L. B., Wolman, M. G., and Miller, J. P., *Fluvial Processes in Geomorphology*, W. H. Freeman and Co., Inc., San Francisco, Calif., 1964.
31. Limerinos, J. T., "Determination of Manning Coefficient for Measured Bed Roughness in Natural Channels," *Water Supply Paper 1898-B*, United States Geological Survey, Washington, D.C., 1970.
32. Raudkivi, A. J., "Analyses of Resistance in Fluvial Channels," *Journal of the Hydraulics Division*, ASCE, Vol. 93, No. HY5, Proc. Paper 5426, Sept., 1967, pp. 73–84.
33. Rouse, H., "Critical Analysis of Open Channel Resistance," *Journal of the Hydraulics Division*, ASCE, Vol. 91, No. HY4, Proc. Paper 4387, July, 1965, pp. 1–25.
34. Shen, H. W., "Development of Bed Roughness in Alluvial Channels," *Journal of the Hydraulics Division*, ASCE, Vol. 88, No. HY3, Proc. Paper 3113, May, 1962, pp. 45–58.
35. Simons, D. B., and Richardson, E. V., "Resistance to Flow in Alluvial Channels," *Professional Paper 422-J*, United States Geological Survey, Washington, D.C., 1966.
36. Simons, D. B., Khalid, S., Al-Shaik-Ali, and Ruh-Ming Li., "Flow Resistance in Cobble and Boulder Riverbeds," *Journal of the Hydraulics Division*, ASCE, Vol. 105, No. HY5, Proc. Paper 14576, June, 1979, pp. 477–488.
37. Thompson, S. M., and Campbell, P. L., "Hydraulics of a Large Channel Paved with Boulders," *Journal of Hydraulic Research*, Vol. 17, No. 4, 1979, pp. 341–354.
38. Vittal, N., Ranga Raju, K. G., and Garde, R. J., "Resistance of Two Dimensional Triangular Roughness," *Journal of Hydraulic Research*, Vol. 15, No. 1, 1977, pp. 19–36.
39. Wolman, M. G., "A Method of Sampling Coarse River-Bed Material," *Transactions*, American Geophysical Union, Vol. 35, No. 6, Part 1, Dec., 1954, pp. 951–956.
40. Wolman, M. G., "The Natural Channel of Brandywine Creek," *Professional Paper 271*, United States Geological Survey, Washington, D.C., 1957.
41. Yalin, M. S., and Emin, K., "Steepness of Sedimentary Dunes," *Journal of the Hydraulics Division*, ASCE, Vol. 105, No. HY4, Proc. Paper 14502, Apr., 1979, pp. 381–392.

STANDARDS FOR COMPUTER-BASED DESIGN STUDIES

By William James,[1] M. ASCE and Mark A. Robinson[2]

INTRODUCTION

This paper examines some special requirements of computer-based studies. These requirements are supplemental to those relating to the specifics of a particular study. The purpose of these additional requirements is to guarantee credibility and confidence in the computer modeling. It is suggested that these special computer-modeling requirements could be set out in the initial study specifications or request for proposals. If these requirements are excluded therefrom, it is suggested that consultants submitting study proposals recommend inclusion of these items to their clients. The suggested additional specifications are summarized at the end of this paper.

In acquiring design services from a reputable engineer, the client expects that the study will be carried out properly, as indeed is almost always the case. The activities listed herein, then, apply more to those cases in which the programs used are complex or not well-known. Most engineers familiar with modeling will normally carry out these activities automatically. The ideas are not entirely new; in a sense they have been applied to undergraduate laboratory studies for generations.

Many programs are capable of describing civil engineering systems to a high level of internal system detail. An example is the Stormwater Management Model (SWMM) (7) used for urban hydrology and drainage hydraulics. Its strength lies in the ability to take into account the interaction of a reasonable number of processes and to report on the status of certain important variables within these processes throughout the simulation. Of course, there would be little point in using such a program if the system under study was simple enough to be modeled with the use of less expensive calculating machines than the main frames still commonly used. The main benefit in using such a complex model therefore appears to be that many, if not all, of the relevant processes and their interactions can be sufficiently accurately investigated, at a large number

[1]Prof., Dept. of Civ. Engrg. and Engrg. Mech., McMaster Univ., 1280 Main Street West, Hamilton, Ontario, Canada, L8S 4L7.

[2]Research Engr., Dept. of Civ. Engrg. and Engrg. Mech., McMaster Univ., 1280 Main Street West, Hamilton, Ontario, Canada, L8S 4L7.

Note.—Discussion open until December 1, 1981. To extend the closing date one month, a written request must be filed with the Manager of Technical and Professional Publications, ASCE. Manuscript was submitted for review for possible publication on October 17, 1980. This paper is part of the Journal of the Hydraulics Division, Proceedings of the American Society of Civil Engineers, ©ASCE, Vol. 107, No. HY7, July, 1981. ISSN 0044-796X/81/0007-0919/$01.00.

of points in the study area, and the system ultimately sufficiently well-understood by the engineers responsible for the design. Thus, programs requiring main-frame support should provide a thorough evaluation of reasonable alternative designs for complex systems.

A difficulty that arises is that the person responsible for devising and coding the original program is usually not available for interpreting the performance of the program in every application. Also, the engineers responsible for the computer simulation, often on a considerably modified version of the original program, are frequently remote from the interpretation of the design and ultimate presentation of the results to the public. Whereas the original author of the program and the engineer responsible for submitting the computer runs may be highly confident of the reliability of his particular computer program, the client, e.g., local authority or municipal engineers, and the people responsible for budgeting and supervising the ultimate project, may not have the same confidence in the computer methods. Indeed, they may be wise to be sceptical until the results are proven to be sound.

This paper attempts to establish controls that ensure that the best model and program are used correctly. Many of these control measures coincide with guidelines for using computer programs published by the Association of Professional Engineers of Ontario (APEO) (2). The aim of these measures is to ensure that credibility and confidence in the results are created and transmitted sequentially from the design office to the client, e.g., from the junior engineers to the project engineer, perhaps in the consultant's office, and thereafter to the municipal engineers responsible for supervising the study, and ultimately through the engineering committees and other political bodies to the beneficiaries, frequently the public. The process is depicted schematically in Fig. 1. In other words, it is not sufficient that the computer model represents all relevant physical processes of the study accurately enough, or that the results are correct or sufficiently accurate. It is important to assure that the study be carried out in such a way that there is little chance of using a wrong model, or using wrong data, or wrongly interpreting the results, or simply of not understanding the model or its relationship to the design objectives.

The writers argue herein that certain precautions be taken at the outset of a study. It is recommended that the study specifications include, among other things, a minimum number of standard tests for model verification, sensitivity analysis, and output interpretation.

More Complex Computer-Based Design Environment

Several factors have increased the complexity of computer-based urban drainage studies over the years: (1) More and more programs are becoming available; (2) the models are including more processes; (3) the variety of computing hardware is increasing; (4) the cost of computing is decreasing; (5) software capabilities, especially of the smaller computers, are becoming more sophisticated; (6) computer communication between design offices and remote main frames is becoming easier; and (7) there is a professional drive within most engineers to improve their understanding of computer modeling, despite the longer learning times associated with this methodology, and higher salaries and related costs (and a tendency for some experts not to divulge the mechanics of key packages).

These developments increase the pressure on regulatory agencies to approve sophisticated design technology which they may not have had time to study fully themselves. Some of these factors are further described subsequently.

Computer Models.—It is evident that the next decade will see an explosion in software development, especially applications programs. Recent studies (3,6,8), e.g., list several hundred computer programs currently available for solving problems associated with water resources development. In fact, it seems that every university and consulting engineering office is bent on developing their own computer programs for the solution of civil engineering problems. Moreover, while most of the popular programs are being enhanced to better describe constituent processes, or to include more process, other programs describe some

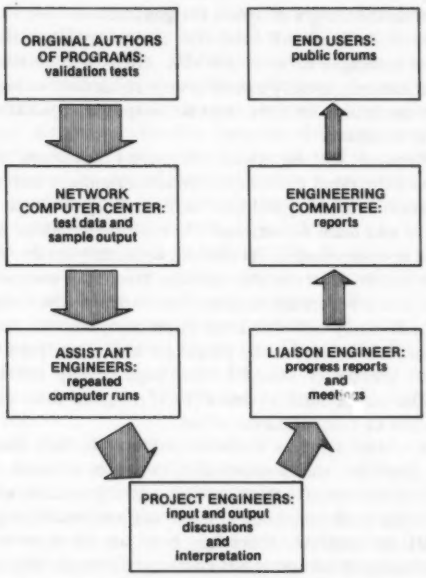

FIG. 1.—Flow of Model Credibility

of these constituent processes in greater details. Thus, the problem that now arises is the selection of the correct sequence of systems and process models to be used in a study. Similarly, if a program adopted is very complex, it may not be clear which processes may be safely ignored, or that the data set used is the best of many possibilities. At some point in the study it may be better to use a sequence of process models than to use one of the system models taking into account similar processes, but doing so inaccurately. Evidently few guidelines exist for this model selection process. On the other hand, as a client organization gains experience with one model, there is a strong tendency to prefer studies based on the same model. Problems such as these which occur

in the municipal drainage area were reviewed in a recent paper (12).

Most tried-and-tested programs are considerably enhanced each year. The latest versions of SWMM, the Illinois Urban Drainage Area Simulation (14), and the Hydrological Simulation Program—FORTRAN (11) may operate in continuous mode, including water quality processes. Since these programs have been under development for 10 yr or more, the precise stage of the evolution of the program must be correctly identified when the program is used. Program documentation seldom matches the capabilities of the program at any point in time; consequently it becomes important that the actual program capabilities are accurately and carefully recorded. In their guidelines for standards of use for computer programs, the APEO recommends appropriate documentation of versions, theory, and software (2). These should be met, as a minimum, by any organization distributing a program for general use.

Many consultants and network computer centers maintain their own versions of large program packages such as SWMM. Often these versions incorporate substantial modifications, usually aimed at core reduction, improved turnaround, simplified data preparation, or more relevant output interpretation. Again proper documentation is necessary.

Hardware.—Readers will be aware of recent advances in programmable calculators (5), and the rapid evolution of microcomputers with their bewildering range of configurations and capabilities. Similar situations exist within the range of minicomputers and main frames and the machines that lie between all these classes. The cost of computing is decreasing, especially on the smaller machines. Increasingly, in order to offer a relatively large amount of computing for available computing dollars, it is becoming necessary to distribute the computational effort involved in any one study between local microcomputers or minicomputers and remote main frames. Already, many programs have been modified so that their solution methods are better suited to the large, cheap memories and small, bit words available on the small systems (13,15). Again, there are few guidelines for this distribution of computational effort.

Systems Ware.—New systems software products include local disc-operating systems, local graphics, and sophisticated word processors. These products considerably aid both output interpretation and input data editing. These, in turn, have benefitted from enhanced communication speeds (e.g., dial-up speeds to 1,200 BAUD). In addition, there has been an increase in the number of national and international computer networks available, so that the smaller design offices may easily access the largest computers. These trends help smaller consulting engineering offices to gain remote job entry into the large programs maintained by various vendors. With the skills of a recent graduate or post-graduate engineer and an inexpensive terminal, any office has immediate access to the largest computers and the most sophisticated programs on the continent without the burden of maintaining or updating the packages.

Computer Modeling Aspects of Study Review

Individual studies often differ greatly in their objectives and available resources. Consultants usually review the complete study problem and available study resources at the outset in order to establish a mutually agreed upon scope and basis for the model study. The problem review should not only be done

in a general descriptive way, but should be directed so as to purposefully list all those characteristics of the study problem that will aid in the selection of computer programs. It should attempt to list specific problems that ought to be considered in any model study undertaken. If hydraulic jumps or energy dissipation at manholes are important in a drainage study, e.g., or if diversion structures are present, these should be identified. Few, if any, programs adequately describe these phenomena.

The study objectives and relevant objective functions should be listed and related. All questions to be answered must be written down in order to explain how the numbers generated by the computer model will relate to the general objectives of the study. Urban runoff computer models, e.g., often produce only hydrographs and pollutographs resulting from a certain limited hydrologic time series. Simple parameters based on these response functions (hydrographs) include: peak values, time-to-peak, and total runoff or loadings. On the other hand, the study objectives often require a least-cost alternative to a specific flooding or drainage problem, such as the production of toxic or other harmful pollutants as a result of a certain hydrometeorological time series. This concise explanation of the logical relationship between the model study results, and the objectives of the design is important for the rest of the study.

To many observers, the model produces only a sequence of numbers. It is advisable to describe early in the study how these numbers may best be compared between several computer runs. It is difficult, e.g., to compare whole response surfaces and curves such as hydrographs. In other words, the performance criteria for assessing the various design proposals must be carefully explained. In some cases it may be sufficient to estimate the total annual loadings, whereas in another case the peak response is more important; perhaps a correlation between whole response surfaces is necessary. The criteria for the performance of one design against another should not be vague or appear to vary. It should be settled initially, a point established and agreed on by both the client and the design engineer.

Accuracy is of overriding importance. If the required accuracy can be established early in the study, it would make the selection of the models and the level of discretization for the model study an easier task. In a sense, the accuracy level predetermines the type of model to be used. There seems to be a mismatch between the accuracy of the results demanded from the computer and those obtainable from field observation or laboratory analysis. Both the systematic and the random sources of error should be investigated for both the model (input data, concepts, solution methods, computational accuracy, etc.) and the field equipment. There is little point in producing simulation results for validation that are many times more accurate than the observations which are used to validate the model. Consider, e.g., the accuracy of rain-gage sampling of moving storms, and the whole question of design storms. In any case, high accuracy may not be necessary in view of the often tenuous relationship between the study objectives and the performance criteria. It would be useful to automatically plot the spread of results rather than a thin response line such as a hydrograph (or a smudge instead of a pollutograph)!

Model Selection Criteria.—There is much published literature and data on the structure and performance of various models. In water resources, see, e.g., Refs. 4, 6, and 8. Hopefully, a simple review of the documentation will indicate

the accuracy with which selected, required important processes are modeled. In their published guidelines (2), the APEO has stressed the fact that program documentation should provide this information to any prospective users. The engineers conducting the study should attempt to show why selected models are deficient or sufficiently accurate for their purposes in the light of problem review and special hydrologic and hydraulic processes required for their particular study. The purpose here is to show how models may be used to support one another, or to establish a reasonable sequence of model use in the study. No model selection should be undertaken prior to this stage; firstly review all available data and available study resources including the models, then establish the criteria for selecting the models and thereafter, select the relevant models. Concurrence between client and designer should be sought at each stage. Finally specify the sequence of model use.

This attempt to show where the selected models are sufficient or deficient for the design study is a central point of this paper. Adherence to this fundamental approach to model selection should naturally bring to light all the points considered herein as guidelines. Assuming that the design engineer has the specific skills (e.g., in hydraulics, hydrology, water quality) these familiar, basic, and fundamental engineering principles lead automatically to the considerations of model pertinence listed in this paper.

A certain amount of time should be invested in searching out existing data. It is much simpler to seek out and review the available data than to collect new data from scratch. In two Canadian studies currently in progress, e.g., several years of sewer water level records, as well as rainfall records were surprising finds. Such data could form part of the model selection criteria; to make maximum use of available data the study should not be constrained to use a model unsuited to these (unknown) existing data. Water levels, e.g., could be directly computed and plotted rather than tediously converted to hydrographs.

The study resources are limited to the available manpower, time, and money; the management of a study is an attempt to maximize the level of detail subject to these manpower, time, and money constraints. Collection of field data is a primary drain on these resources. The field program must be dovetailed to complement the modeling effort. The key is sensitivity analysis.

Model selection criteria should be clearly stated in the study report. It is easy to criticize a study at a later date for not using a model which would describe processes to a much higher level of system detail if it is not made clear that the simpler model was used because of too little expertise, time, or money to meet the effort for higher accuracy or detail. Other criteria include availability of the model, availability of supporting advice, experience with similar or alternative models, availability of data, special costs related to proprietary versions of the models, and the professional interests and jealousies of the engineers involved in the mechanics of the program. This could mitigate against the use of proprietary programs, for instance.

Special Steps to Establish Model Credibility

A series of verification, validation, and sensitivity tests can be designed to produce sufficient information to answer a wide range of questions about the

model's performance. Evidently, such tests will not materially increase the workload for the consultant, nor will it greatly increase the cost of the study. The tests should also help to detect certain types of error.

Verification Tests.—Verification tests use some specific conditions for which the model response can be exactly predicted to check if indeed the model is structured and coded as intended. Verification tests are not conducted by comparison of model responses with those of the actual system to be modeled; rather comparisons between model responses and theoretically anticipated results are made in as many cases as possible. The input data need not be physically reasonable.

Of course it will not normally be necessary for the design group to verify the same model in the same way for every design study. Summary information will normally be sufficient for subsequent studies involving essentially the same model and the same processes. But it must be done at least once on receipt of the model ahead of the first design application.

It would be useful to create a standard input file for verification tests. For stormwater models, e.g., a hypothetical system comprising two simple, square subcatchments, of e.g., 1 acre each would be suitable. The subcatchments could be joined by a pipe of standard diameter and simple form. The hydrograph from the first subcatchment is attenuated in the pipe. At the downstream end of this pipe the hydrographs from both subcatchments are superimposed. At the outlet of the pipe, the combined hydrograph is routed through a simple, standard, perhaps rectangular, storage tank. The purpose of such a verification data set would be simply to test the algorithms for: (1) The generation of the overland flow hydrograph; (2) routing in the pipes; (3) the addition of two hydrographs; and (4) storage routing in storage tanks.

As a further example, we have used the following tests in our stormwater runoff programs: (1) Zero rain to ensure that no runoff is generated; (2) very steep catchments to ensure that the hydrographs generated are very similar to the input hyetograph; (3) light rain and high infiltration rates on low percent impervious areas to ensure that no runoff hydrographs are generated; (4) completely impervious catchments to ensure that the total volume of runoff is equal to the total volume of rainfall; (5) low continuous infiltration rates and high continuous rainfall to ensure that the correct amount of infiltration is subtracted; (6) very flat pipe gradients to check the surcharge calculation; (7) similar tests with small-diameter pipes and high pipe roughness; (8) high and low initial abstractions; and (9) tests on the storage-routing parameters, namely, the outlet rating curve and the storage curve.

In all verification tests particular attention is paid to the quantitative summary output: e.g., total precipitation, total gutter flow, total snowmelt, total infiltration, etc. This is an essential check that the numbers generated by the computer are sensible. The user must check the numbers by hand and categorically state that the results are accurate enough.

Perhaps a special algorithm and data file should be built into the program. When the appropriate "auto-verify" button is pushed, the model automatically carries out a series of verification tests. In our instructional applications, e.g., undergraduate classes, the following verification data are normally used prior to any stormwater drainage analysis: (1) Low imperviousness—5%; (2) high imperviousness—95%; (3) high detention storage—0.62 in.–1.84 in. (15.7 mm–46.7

mm); (4) low detention storage—0.01 in.–0.1 in. (.254 mm–2.54 mm); (5) impervious area with zero detention (High), as a percentage 95%; (6) impervious area with zero detention (Low), as a percentage 5%; (7) high continuous rain—10 in./h (254 mm/h); (8) low continuous rain—0.1 in./h (2.54 mm/h); (9) high continuous infiltration—2 in./h (50.8 mm/h); and (10) low continuous infiltration—0.1 in./h (2.54 mm/h).

Calibration and Validation Tests.—Calibration implies the comparison of model simulation results to field measurements, to another model known to be accurate, or to some other adequate criteria to ensure that the model of the system is producing accurate data. If these comparisons indicate that the model results are not sufficiently accurate, then the model of the system is altered, usually by adjusting one or more program parameters, and the procedure is repeated. This process generally involves several iterations before a satisfactory confidence level is achieved. Techniques used in calibration include: (1) Comparison of results against field observations; (2) cross-correlation of continuous model results with those of another proved, usually discrete event, or process model equivalently initialized, and (3) some combination of field observations and modeling.

Validation implies testing the model of the system with a data set not used in the calibration procedure. The most accurate method of validation is the comparison of output from the calibrated model against corresponding sets of independent field measurements.

The calibration and validation process should be limited to the most important or sensitive parameters, and to the range of parameter values applicable to the normal operating conditions of the system. First, acceptable tolerances must be established. They should be related to achievable field observations and the accuracy of the field equipment. Then, emphasis should be placed upon those critical parameters that have the greatest effect on the performance of the system. Reasonable assumptions may be satisfactory for less critical parameters. Thus, calibration tests are closely related to sensitivity analysis, examined subsequently.

Once verified, calibrated, and validated, the model can be applied with confidence to the evaluation of the real system. A recent paper describes the process for combined quantity and quality modeling (10). Spatially-averaged input quantities that cannot be analytically measured may be considered to be empirical parameters. Following this approach, important empirical parameters in discrete event urban rainfall-runoff models are: (1) Width of subcatchments; (2) ground slope; (3) initial infiltration rate; (4) final infiltration rate; (5) Manning's roughness for overland flow; (6) depression storage for both pervious and impervious areas; and (7) infiltration decay rate.

Whether or not an input quantity should be considered an empirical parameter, initial condition, or a field-determined characteristic, depends on the user's opinions of the basic modeling concepts. For example, the SWMM models subspaces as a single rectangular plane, for the purpose of converting a hyetograph into a hydrograph of overland flow. Lumping the hydrological characteristics of all surfaces in the real subspace into an equivalent rectangle is widely known as "parameterization." The equivalent width of the rectangle cannot be determined analytically in the field. It could be considered a quasi-empirical subspace parameter. Again, another user may not support the basic Horton-infiltration approach used in the SWMM and consider such infiltration input, at least for

discrete-event models, a rough approximation or empirical parameter to be carefully determined, rather than a deterministic initial condition.

Level of Discretization.—The procedure for systematic disaggregation has been described in an earlier paper (9). Disaggregation implies modeling more subspaces of smaller size using a finer time step. For coupling the time increment to the size of the subspatial elements, the concept of an impulse response function is useful, e.g., an instantaneous unit hydrograph. It may be accurate enough for our purposes to represent this response function by a time vector of 20 elements. This effectively sets the time step to 1/20 of the time base of the impulse response functions. Sensitivity tests in which the time step is systematically changed may also be appropriate. In practice, disaggregation and sensitivity analysis proceed simultaneously (9). Often, careful disaggregation and appropriate selection of the time step will produce better results than extensive optimization of empirical factors such as Manning's roughness for pipes and overland flow. A recent paper provides some guidelines (1).

There is an obvious conflict in the selection of the level of discretization. Consultants' costs increase rather rapidly with an increasing number of subspaces. More data have to be abstracted and prepared, and more expensive computer runs will result. On the other hand, the client will usually prefer to have a high level of discretization for the agreed upon fixed study price. It is useful to have, at the outset of a study, an indication of the desirable level. As a guide, it is important to identify all significant elements in the system. These represent locations for which it is necessary to generate a response surface, such as hydrographs, e.g., at all diversion structures and outfalls in hydrologic studies. If these elements can be identified at the time the terms of reference are set out, consultants will have a better idea of the scope of the work. It makes sense to face this possible conflict squarely at the beginning of the study.

Sensitivity Analysis.—Sensitivity analysis proceeds by holding all parameters but one constant at their expected values, and perturbing that parameter within reasonable expected limits such that the variation of the objective function can be examined. If apparently small perturbations of the parameter produce large changes in the objective function, the system is said to be sensitive to that parameter. The user must obtain a measure of how accurate that parameter must be represented in his model. If the objective function is not sensitive to the pertubated parameter, then the parameter need not be accurately represented. If the system is insensitive to the pertubated parameter, the parameter and its associated process is redundant and the process should be deleted. The tests are done using the full design problem input data set. It must be stressed that the actual values of the constant parameters may affect the sensitivity analysis, and so, their values should be typical of the conditions being modeled.

Here again, algorithms should be available that permit the user to easily conduct a sensitivity analysis. Another special button within the program is desirable. When this "auto-sensitivity" button is pushed, the computer requests the user to identify the parameter whose sensitivity is to be tested, and the range of perturbated values. The data file is then automatically rebuilt and the tests carried out. All output response functions, such as hydrographs, should be plotted on the same family of curves in order to present the impact immediately to the user.

Two essential components of the response function are peak response and

total integrated loading, such as the peak flow and runoff volume in a runoff hydrograph. Following the general approach to parameter determination examined earlier, the runoff parameters which affect each of these components are as follows:

1. A: Peak Flow: slopes (pipe and land), Manning's n, subcatchment width, and pipe length.
2. B: Volume: imperviousness, as a percentage, infiltration, surface retention, and percentage impervious area with zero detention.

It is critically important to rank environmental parameters that affect the important components of your response function for your model in this way.

Control of Errors.—Having carried out the required verification, calibration, validation, and sensitivity analyses at various levels of discretization, the results have to be presented in the report in a way which ensures that the purposes of the tests have been achieved. The author of the report must explain or interpret the results carefully for readers who cannot submit the computer runs. The verification tests must be shown to produce expected results. The calibration and validation results must be shown to be reasonably accurate. The trends resulting from the sensitivity analysis must be shown to make sense in the light of the actual design problem. The purpose of this is to provide irrefutable evidence that the model is indeed performing properly: (1) The verification tests demonstrate that there are no serious errors in the coding of the model, (2) the calibration and validation tests at a simple level of discretization, say one or two subcatchments and pipes, demonstrate that the model is being used in a reasonable way, (3) the validation tests on the full data set, i.e., for all of the subcatchments acting together as a complete system, indicate whether serious blunders have been made in preparing the input data set, and (4) the sensitivity analyses will indicate whether the level of effort put into estimating the individual parameters is appropriate based on their significance in affecting model results.

The required output interpretation provides the argument that proves that the results in fact make sense, and helps to ensure that the study authors have not misinterpreted the model results. All of these points are summarized in the following logical sequence.

Conclusions

This paper suggests that the following topics should be included in any computer-based study. It is appropriate to specify them in the initial study specifications or request them for proposals.

Problem Review.—The problem review should identify all significant elements in the study area so that the model selected can be shown to include all relevant processes, and to be disaggregated to the correct degree.

Study Objectives.—The study objectives should be reviewed to show how the objective functions, such as pollutographs, or hydrographs, or both, relate to the design alternatives. New problems may become apparent during the study

so it must be possible to redefine the objectives and all subsequent deductions.

Performance Criteria.—The performance criteria for the comparison of one design alternative against another include peak response, total loadings, time to peak, cross-correlations, etc., and must be correctly identified so that the simplest modeling can be justifiably used to select the best design alternative.

Requisite Accuracy.—Accuracy of field measurements for validation should be carefully reviewed in order to ensure that the model runs are not inordinately expensive. Systematic and random errors should be defined.

Review of Available Programs.—Several programs should be suggested or selected for review. The review should consider process models, as well as system models, and an appropriate sequence of models.

Study Resources.—Study resources include time, manpower, money, and information, and these, in turn, will determine which of the models may be selected.

Model Selection Criteria.—All available data must be reviewed. Models should be selected where expertise is available and ample data easily collected considering the limited study resources available.

Model Verification.—Verification tests should be required on a specified simple data set consisting of simplified elements chosen to test each process of interest. The verification tests should check the summary output and demonstrate that the coding is performing as intended.

Model Calibration and Validation.—Calibration tests should be carried out on one of the subspatial data sets using specified parameters to demonstrate that the model is being correctly used. Validation tests should be carried out on an independent data set to demonstrate that the input data are reasonable.

Minimum Level of Discretization.—The smallest number of subspaces required for modeling the system should be selected commensurate with the objectives of achieving the best design at a reasonable cost. These minimum levels should correspond to the disaggregation necessary to identify response surfaces at all significant elements in the system, which should be specified at the outset, so far as possible.

Sensitivity Analysis.—Sensitivity analyses should be carried out on a minimum number of parameters, e.g., infiltration parameters, roughness values, widths of subcatchments, etc., to identify which are of most significance, and to justify the effort put into their estimation.

Data Preparation and Output Interpretation.—All input and output should be interpreted to demonstrate that the model is performing in a logical way. The magnitude and direction of errors should be estimated.

Documentation.—The version of the program actually used in the study should be identified and appropriate documentation sources listed in the report. In addition, the machine readable input and output files should be listed and archived for future use.

The delivery of computer-based engineering design services could be improved by enlightened study specifications and attentive control by the responsible municipal or local authority engineers. The suggestions in this paper should reduce the chances of inexperienced engineers using an inappropriate model, inappropriately using an otherwise suitable model, through erroneous data preparation or output interpretation, and remaining ignorant of the model even when the results are acceptable. Credibility would thus be improved.

Acknowledgment

The work reported herein is based on the experience gained in the joint study on the Chedoke Creek between McMaster University and the Hamilton-Wentworth Regional Engineering Department. Assistance from the latter is gratefully acknowledged.

Appendix.—References

1. Alley, W. M., and Veenhuis, J. E., "Determination of Basin Characteristics for an Urban Distributed Routing Rainfall-Runoff Model," *Proceedings, Stormwater Management Model Users' Meeting*, United States Environmental Protection Agency, May, 1979, pp. 1–27.
2. "Guidelines to Standards of Practice for the Use of Computer Programs in Engineering," Association of Professional Engineers of Ontario, Toronto, Ontario, Apr., 1977.
3. Chung, S. C., and Bowers, C. E., "Computer Programs in Water Resources," *Bulletin 97*, Water Resources Research Center, University of Minnesota, Minneapolis, Minn., Nov., 1977.
4. Colyer, P. J., and Pethick, R. W., "Storm Drainage Design Methods," *INT 54*, 4th ed., Hydraulics Research Station, Wallingford, England, Sept., 1977.
5. Croley, T. E., *Hydrologic and Hydraulic Computations on Small Programmable Calculators*, Iowa Institute of Hydraulic Research, University of Iowa, Iowa City, Iowa, 1977.
6. Hinson, M. D., and Basta, D. J., "Analysing Recieving Water Systems," *Analysis for Residuals—Environmental Quality Management: Analyzing Natural Systems*, D. J. Basta and B. T. Bower, eds., Resources for the Future, Office of Research and Development, United States Enviornmental Protection Agency, Cincinnati, Ohio, Dec., 1979.
7. Huber, W. C., et al., *Storm Water Management Model User's Manual Version II*, United States Environmental Protection Agency, Cincinnati, Ohio, Mar., 1975.
8. Huber, W. C., and Heaney, J. P., "Analyzing Residuals Generation and Discharges From Urban and Nonurban Land Surfaces," *Analysis for Residuals—Environmental Quality Management: Analyzing Natural Systems*, D. J. Basta and B. T. Bower, eds., Resources for the Future, Office of Research and Development, United States Environmental Protection Agency, Cincinnati, Ohio, Dec., 1979.
9. James, W., "Developing Simulation Models," *Journal of Water Resources Research*, Vol. 8, No. 6, Dec., 1972. pp. 1590–1592.
10. Jewell, T. K., et al., "Methodology for Calibrating Stormwater Models," *Proceedings*, Stormwater Management Model Users' Meeting, United States Environmental Protection Agency, May, 1978, pp. 125–173.
11. Johanson, R. C., et al., *Users Manual for Hydrological Simulation Program—FORTRAN (HSPF)*, United States Environmental Protection Agency, Athens, Ga., Apr., 1980.
12. McPherson, M. B., "Overview of Urban Runoff Tools of Analysis," *EP79-R-20, GREMU-79/01*, Ecole Polytechnique de Montreal, Montreal, Quebec, Canada, 1979.
13. Patry, G., et al., "Description and Application of an Interactive Minicomputer Version of the ILLUDAS Model," *Proceedings*, Stormwater Management Model Users' Group Meeting, United States Environmental Protection Agency, May, 1979, pp. 252–274.
14. Terstriep, M. L., and Stall, J. B., "The Illinois Urban Drainage Area Simulator ILLUDAS," *Bulletin 58*, Illinois State Water Survey, Urbana, Ill., 1974.
15. Thompson, L., and Sykes, J., "Development and Implementation of an Urban-Rural Sub-Catchment Hydrologic Model (SUBHYD) for Discrete and Continuous Simulation on a Micro-Computer," *Proceedings*, Stormwater Management Model Users' Group Meeting, United States Environmental Protection Agency, May, 1979, pp. 320–361.

DISCUSSION

Note.—This paper is part of the Journal of the Hydraulics Division, Proceedings of the American Society of Civil Engineers, ©ASCE, Vol. 107, No. HY7, July, 1981. ISSN 0044-796X/81/0007-0933/$01.00.

Discussions

Discussions may be submitted on any Proceedings paper or technical note published in any *Journal* or on any paper presented at any Specialty Conference or other meeting, the *Proceedings* of which have been published by ASCE. Discussion of a paper/technical note is open to anyone who has significant comments or questions regarding the content of the paper/technical note. Discussions are accepted for a period of 4 months following the date of publication of a paper/technical note and they should be sent to the Manager of Technical and Professional Publications, ASCE, 345 East 47th Street, New York, N.Y. 10017. The discussion period may be extended by a written request from a discusser.

The original and three copies of the Discussion should be submitted on 8-1/2-in. (220-mm) by 11-in. (280-mm) white bond paper, typed double-spaced with wide margins. The length of a Discussion is restricted to two *Journal* pages (about four typewritten double-spaced pages of manuscript including figures and tables); the editors will delete matter extraneous to the subject under discussion. If a Discussion is over two pages long it will be returned for shortening. All Discussions will be reviewed by the editors and the Division's or Council's Publications Committees. In some cases, Discussions will be returned to discussers for rewriting, or they may be encouraged to submit a paper or technical note rather than a Discussion.

Standards for Discussions are the same as those for Proceedings Papers. A Discussion is subject to rejection if it contains matter readily found elsewhere, advocates special interests, is carelessly prepared, controverts established fact, is purely speculative, introduces personalities, or is foreign to the purposes of the Society. All Discussions should be written in the third person, and the discusser should use the term "the writer" when referring to himself. The author of the original paper/technical note is referred to as "the author."

Discussions have a specific format. The title of the original paper/technical note appears at the top of the first page with a superscript that corresponds to a footnote indicating the month, year, author(s), and number of the original paper/technical note. The discusser's full name should be indicated below the title (see Discussions herein as an example) together with his ASCE membership grade (if applicable).

The discusser's title, company affiliation, and business address should appear on the first page of the manuscript, along with the *Proceedings* paper number of the original paper/technical note, the date and name of the *Journal* in which it appeared, and the original author's name.

Note that the discusser's identification footnote should follow consecutively from the original paper/technical note. If the paper/technical note under discussion contained footnote numbers 1 and 2, the first Discussion would begin with footnote 3, and subsequent Discussions would continue in sequence.

Figures supplied by the discusser should be designated by letters, starting with A. This also applies separately to tables and references. In referring to a figure, table, or reference that appeared in the original paper/technical note use the same number used in the original.

It is suggested that potential discussers request a copy of the *ASCE Authors' Guide to the Publications of ASCE* for more detailed information on preparation and submission of manuscripts.

DIFFRACTION OF WAVES BY SHORE-CONNECTED BREAKWATER[a]

Closure by Volker W. Harms,[3] M. ASCE

The writer would like to thank Memos for his valuable comments. In his discussion, Memos focuses principally upon the problem and probable cause of the wave-height nonuniformity encountered. As described in the original paper, it had been found that regular waves of very-nearly sinusoidal form could be generated in deep water ($d/L = 0.39$ and $H/L = 0.43$), but that the resulting three-dimensional wave field was certainly not of uniform height. Wave heights varied both in the direction of wave motion (but not monotonically, i.e., no evidence of significant viscous dissipation) and laterally along the wave-crest line, but at every location the wave record was regular and did not vary significantly with time. If this in itself was not surprising, the degree of wave-height variability was. For some wave conditions, the ratio of extreme wave heights, ϵ, exceeded a value of 2.5; here ϵ is the ratio of largest to smallest wave height recorded within the wave-tank test area, i.e., at 520 points, with regular waves of constant height at each location (as in Fig. 6). This finding raised serious questions about the results of diffraction studies in which the incident wave height was measured at only a single fixed position along the wave-crest line; depending upon the spatial wave-height distribution that happens to prevail (see, e.g., Fig. 5), this measured incident wave height could vary by a factor of 2.5 depending upon the position chosen!

Upon recognizing the seriousness of this problem, it was first ascertained that it was not unique to our wave tank or wave generator. Thereupon, a trial-and-error search for wave conditions (d, H/L, d/L) that would minimize the problem was initiated. This search for that elusive "most nearly two-dimensional wave field" was undertaken recognizing that some wave conditions are more likely to be troublesome than others, and therefore are to be avoided if possible. Among those to be shunned were: (1) Wave-generator cut-off frequencies—to prevent "wave-sloshing modes" (transverse waves), as predicted by linear wave-generator theory; (2) lateral basin-resonance conditions—to avoid the generation of standing waves between basin walls; (3) substantial Benjamin-Feir-type amplitude modulations—to ensure that wave heights remain reasonably constant with time (e.g., $\epsilon < 1.1$) at each wave-gage position, no matter how far from the generator; (4) cross waves—since they are not only standing waves but are also of lesser frequency than the primary waves being generated; and (5) highly-reflective basin boundaries—since these reflect energy back into the test area and produce standing-wave effects throughout the basin, i.e., wave heights may be locally constant but vary spatially. Recognizing the existence

[a]December, 1979, by Volker W. Harms (Proc. Paper 15075).

[3]Staff Scientist, Univ. of California, Lawrence Berkeley Lab., Berkeley, Calif. 94720.

of such potential problem areas was certainly important but did not provide a practical basis for selecting the sought-after "most nearly uniform wave conditions." The following criteria were finally chosen as the most practical and important for the selection process: (1) The surface time history at any location in the basin must indicate a nearly sinusoidal shape that is invariant with time; (2) wave attenuation should be negligible over the length of the basin; (3) the variation in wave height across the tank should be as small as practically attainable; and (4) the wave-crest lines must be parallel throughout the testing area and well-alined when breaking upon the beach.

The discusser concludes that irregularities in the wave generator contributed to the spatial wave-height nonuniformity, (as, e.g., stroke variations along the length of the paddle), as did reflections from the wave-tank boundaries which, though perhaps very low, can never be totally eliminated in the continuous-operating mode. The writer shares this conclusion, but would like to clarify a misunderstanding that emerges from the discusser's arguments supporting this position. From the near-center line wave-height distribution shown in Fig. 3, which were obtained with a variety of models in the basin (and correspond to ϵ values from 1.29–1.45), and the statement in the original paper that without any wave obstruction in the basin, ϵ was typically 1.6 for the whole basin, it must not be inferred that the lowering of ϵ was caused by the presence of the model (and might therefore lead one to conclude that strong reflections from the main beach were being blocked). Instead, the difference in ϵ values should be attributed principally to the difference in sampling spaces: $\epsilon = 1.6$ is the largest value that was encountered upon surveying the whole basin (wave records at 520 points), whereas the lower values of ϵ shown in Fig. 3 are for a much smaller data subset acquired near the basin center line (see Fig. 5 for representative wave-height distributions).

The discusser also feels that basin-resonance conditions contributed to the wave-height nonuniformity, particularly since the wave length of $L = 0.69$ m (that was finally adopted for the test program) is close to one of the natural modes of oscillation of the wave tank, albeit the 56th mode, with $L = 0.700$ m. The writer was never able to detect any influence of this "closeness" to a basin-resonant mode or to one of the wave-generator cut-off frequencies, and wonders whether such high basin-oscillation modes can actually be excited, and whether linear wave-generator theory can be meaningfully applied to such wide basins (the wave maker extended across a tank 28 L wide). It should be noted that resonant wavelengths could hardly be avoided during our exploratory tests since, for our test condition, they are so very-closely spaced, e.g., lateral basin-oscillation modes numbers 55, 56, 57 correspond for resonant wavelengths of $L = 0.709$ m, 0.700 m, and 0.685 m, respectively. Even small frequency variations in the wave-generator electric motor, due to line-voltage fluctuations, e.g., would probably generate variations as great as this.

The discusser considers Benjamin-Feir modulation instabilities (1) to have been present because the adopted test conditions fall within a range that makes the evolution of these instabilities possible ($d/L > 0.22$), and for which limited laboratory experiments have shown them to be detectable ($H/L > 0.03$). If they were present, then at such a low level that, in the opinion of the writer, the question becomes somewhat academic; serious cases of Benjamin-Feir instabilities could easily be avoided by simply ensuring that the wave record

for each gage on the carriage remained reasonably regular, e.g., ϵ less than 1.1 (as in Figs. 6, 8, 9). When such wave-height stability is evident at each wave gage, in our case over a distance of 21 m (70 ft), then the influence of Benjamin-Feir-type modulation instabilities can be ruled out as an important contributor to the problem. Recent findings from research in the area of deep-water wave instabilities (28,29) indicate that the Benjamin-Feir analysis is valid only for the initial growth period and that, in the long-time evolution, unstable modulations typically grow to a maximum, subside, and then repeat themselves in a series of modulation and demodulation cycles, without reaching a state of complete breakdown of the wave train. The presence of this so-called Fermi-Pasta-Ulam recurrence phenomenon could not be detected at any time, nor could significant levels of Benjamin-Feir instabilities.

Memos points out that some disagreement exists between the findings of Putnam and Arthur's 1948 study (16) which indicated that "diffraction theory is conservative," and the present investigation, in which diffraction theory was not found to be conservative; in fact, at large distances in the shadow zone, measured wave heights consistently exceed theoretical values. This is indeed so and, in the opinion of the writer, is principally a result of the far more limited laboratory data base available to Putnam and Arthur at the time (some 30 yr earlier!); wave heights were generally measured at only four locations in the shadow zone, as opposed to 50 in our study, the incident wave was obtained from only one fixed wave recorder, measurements were not performed as far from the structure, etc. This in no way detracts from Putnam and Arthur's very substantial contribution: that their results are still being used is tribute in itself. Instead, the present results are intended to augment and complement their findings and in so doing, establish an experimental data base adequate for a comprehensive understanding of the diffraction process.

The discusser suggests that errors in the measurement of wave height may be responsible for the relatively high values of K' at large distances in the shadow zone (compared to theory); a given measurement error would have a greater impact since wave heights are relatively small in that region. This argument is initially appealing but, upon inspection, demands that distant wave gages (see Figs. 7*f*–7*h*) have larger measurement errors than other gages, otherwise the agreement between measurement and theory that is evident close to the breakwater (see Figs. 7*b*–7*e*) even for small K', could not be explained. In fact, all gages were similar in construction, had very nearly the same calibration factors, and were similarly operated, and would therefore be subject to wave-height error bands of the same magnitude. The initial supposition is therefore most probably incorrect.

The discusser has apparently conducted diffraction experiments on shore-connected breakwaters under very similar conditions. The results from these studies will hopefully become available to us in the near future and perhaps shed more light on some of the questions that have been raised.

With regards to experimental procedure, it should be clarified that the "15-min waiting period between transverses" (p. 1514) of the instrument carriage, refers to the continuous data-acquisition mode and not, as understood by the discusser, to the intermittent mode. Each traverse of the instrument carriage-generated analog wave traces such as those shown for wave-gages numbers 11, 2, 4, and 6 in Fig. 9.

APPENDIX.—REFERENCES

28. Yuen, H. C., and Lake, B. M., "Instabilities of Waves on Deep Water," *Annual Review of Fluid Mechanics*, Vol. 12, 1980, pp. 303–334.
29. Lake, B. M., Yuen, H. C., Rungaldier, H., and Ferguson, W. E., "Nonlinear Deep-Water Waves: Theory and Experiment: Part 2, Evolution of a Continuous Wave Train," *Journal of Fluid Mechanics*, London, England, Vol. 83, Part 1, 1977, pp. 49–74.

LONGITUDINAL DISPERSION IN RIVERS[a]

Closure by Spyridon Beltaos[3]

The writer thanks Gögüs, for his comments and interest in the paper. The discusser has expressed two concerns, namely how is α evaluated and why are inconsistent results obtained upon application of the writer's model to Fischer's test data of series 2800, 2900, and 3100.

To determine the value of α, one may proceed as indicated by the discusser. A slightly simpler method has been used by the writer: this method starts with Eq. 25 and requires that $f(\tau) = 1$ and $df/d\tau = 0$ at $t = t_p$. The coefficient α can then be determined by trial-and-error for different values of β, as summarized in Table 2 (for $\beta = 0$, a limit analysis was performed, resulting in $\alpha = 8 \ln 2 = 5.545$). Table 2 shows that $\alpha \simeq 5.55$ for $\beta \leq 0.1$. For $\beta > 0.1$, α increases slightly, being equal to 5.763 at $\beta = 0.5$. When preparing the paper, the writer did not suspect that values of β exceeding 0.1 could be encountered (see Fig. 7), and thus suggested that α be a constant equal to 5.55. Recently, however, the writer found values of β as large as 0.28 for dispersion in a pool-fall sequence (the information is contained in an unpublished report by the writer). Where β exceeds 0.1, Table 2 should be taken into account. To find β from Eq. 27, plot $\alpha\beta$ versus β, based on Table 2; enter graph at $\alpha\beta = (Vd\Delta T/dx)^2$ and determine corresponding values of β. Apply a similar procedure when evaluating β from Eq. 31.

The fact that β may exceed 0.1 introduces an additional consideration. It may be recalled that Eq. 15 is an approximate version of Eq. 14. The term which has been neglected from Eq. 14 may become significant when $\beta > 0.1$ and x/L is small. It can be shown from Eq. 14 that, for small x/L, the right-hand side of Eq. 16 should be multiplied by $\sqrt{1+\beta}$. This implies that, for small values of x/L, the definition of α should read:

---

[a]January, 1980, by Spyridon Beltaos (Proc. Paper 15118).

[3]Research Scientist, Environmental Hydr. Section, Hydr. Div., National Water Research Inst., Canada Centre for Inland Waters, P.O. Box 5050, Burlington, Ontario, Canada L7R 4A6; formerly, Research Officer, Water Research Council, Edmonton, Canada.

$$\alpha \equiv (1 + \beta)\left(\frac{\Delta T}{\bar{\sigma}_t}\right)^2; \quad \frac{x}{L} \lesssim 0.5 \ldots\ldots\ldots\ldots\ldots\ldots\ldots\ldots\ldots\ldots (39)$$

for which numerical values of α are given in Table 2. For $0.5 \lesssim x/L \lesssim 3.0$, the multiplier of $(\Delta T/\bar{\sigma}_t)^2$ on the right-hand side of Eq. 39 will be less than $1 + \beta$, becoming $\simeq 1.0$ when $x/L \geq 3.0$ even if β is as large as 0.5. When $\beta \lesssim 0.1$, Eq. 39 reduces approximately to the definition given in Eq. 30, regardless of the value of x/L.

TABLE 2.—Evaluation of α

β (1)	α (2)
0	5.545
0.00001	5.545
0.0001	5.546
0.001	5.547
0.005	5.548
0.010	5.550
0.020	5.555
0.050	5.566
0.100	5.588
0.200	5.633
0.500	5.763
1.000	5.986

Regarding comparison of ΔT with $\bar{\sigma}_t$ using experimental results, the writer has carried out a comprehensive analysis which has resulted in the following:

1. For any one test, ΔT and $\bar{\sigma}_t$ are related linearly as predicted by Eq. 30 (or by Eq. 39).

2. For the tests analyzed in the paper, $\Delta T/\bar{\sigma}_t$ varied from 0.60–2.11 and had an average value of 1.64. The second lowest and highest values of $\Delta T/\bar{\sigma}_t$ were 1.08 and 2.06, respectively. The theoretical value of $\Delta T/\bar{\sigma}_t$ is equal to $\sqrt{5.55} = 2.36$, which is some 44% larger than the "observed" average value. In terms of $(\Delta T/\bar{\sigma}_t)^2$, this deviation should be doubled to 88%. This result may be interpreted as a flaw of the theory or simply as a reflection of the error associated with "observed" values of $\bar{\sigma}_t$. The writer's view coincides with the latter interpretation, based on his experience with $\bar{\sigma}_t$ computations from experimental $\bar{C}$-t curves. (Note that, in addition to $\bar{\sigma}_t$ being very sensitive to the tail region of a $\bar{C}$-t curve, as suggested by the discusser, the tail region is the least accurately defined; the prevailing $\bar{C}$ are very small and usually comparable to the lower detectability limit of the instrumentation used.) Additional support for this interpretation is provided in the following item.

3. According to Eqs. 28 and 30, the value of $\Delta T\bar{C}_p/(M/Q)$ should be equal to $(\Delta T/\bar{\sigma}_t)/\sqrt{2\pi}$. For $\Delta T/\bar{\sigma}_t = 2.36$ $(= \sqrt{5.55})$, this works out to be 0.94. "Observed" values of $\Delta T\bar{C}_p/(M/Q)$ were calculated by substituting $\int_0^\infty \bar{C}dt$ in place of M/Q (to account for tracer losses), and compared with both 0.94

and the value of "observed" $(\Delta T/\bar{\sigma}_t)/\sqrt{2\pi}$. "Observed" values of $\Delta T\bar{C}_p / \int_0^\infty \bar{C}\,dt$ ranged from 0.69–1.04 with an average of 0.86. This is much closer to 0.94 (predicted by the theory) than to 0.65 which is obtained using the average "observed" value of $\Delta T/\bar{\sigma}_t (0.65 = 1.64/\sqrt{2\pi})$. Moreover, of the 51 tests considered, only on three occasions did the latter approach give better estimates of $\Delta T\bar{C}_p / \int_0^\infty \bar{C}dt$ than the theoretical approach.

The next concern of the discusser is the failure of the model to produce consistent results when applied to Fischer's test data of series 2800, 2900, and

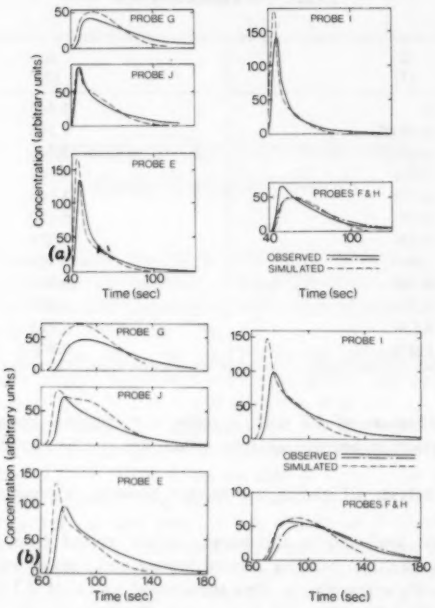

FIG. 11.—Concentration-Time Variations Observed at Different Lateral Positions; Series 2800, by Fischer (13); Example Reproduced from Ref. 33: (*a*) x = 16.07 m; (*b*) x = 26.11 m (1 m = 3.28 ft)

3100. The discusser states: "Fischer's experiments (15) conducted in laboratory flumes should nearly satisfy the condition of one-dimensionality required for the application of the author's model." The writer has carefully examined the detailed results of these test series and found that he must disagree with the discusser's premise (note that Ref. 15 gives only cross-sectional average parameters; detailed data are given in Ref. 13). Considering, e.g., series 2800, Fig. 11 shows C-t curves (solid lines) observed at different lateral positions within the same cross section for two cross sections located at x_1 and x_2 (also see Table 1). The curves of Fig. 11 can hardly be considered to indicate "one-dimen-

sional" dispersion as defined in the paper, not even approximately. (In fact, these results were considered sufficiently representative of two-dimensional mixing and were thus utilized to test a pertinent numerical simulation algorithm, described in Ref. 33—the broken lines in Fig. 11 are simulated results.)

Similar considerations apply to series 2900 and 3100, which the discusser may wish to verify directly using Ref. 13. For the present closure, it is considered sufficient to provide Table 3, in which certain characteristics of the pertinent *C-t* curves are summarized. It is seen that, at $x = x_1$, there is a threefold variation of C_p (across the channel) and a fivefold variation of ΔT; these figures are reduced to twofold and two and a half-fold, respectively at $x = x_2$. It may now be recalled that the writer's definition of one-dimensionality calls for nearly identical *C-t* curves across any one value of x (though shifted in time). This implies that, to apply the model, corresponding values of C_p and ΔT should not vary excessively across the channel. It is therefore concluded that the data used by the discusser are not representative of one-dimensional

TABLE 3.—Selected Dispersion Characteristics of Fischer's Series 2800, 2900, and 3100[a]

Test series (1)	Range of C_p (arbitrary units) as Indicated from *C-t* Curves at Six Lateral Positions		Range of ΔT (in seconds) as Indicated from *C-t* Curves at Six Lateral Positions	
	at $x = x_1$[b] (2)	at $x = x_2$[c] (3)	at $x = x_1$[b] (4)	$x = x_2$[c] (5)
2800	42–138	46–99	8–39	20–51
2900	29–99	36–75	4–21	12–30
3100	31–84	36–54	5–23	21–34

[a]Data from Ref. 13.
[b]x_1 = 16.1 m, 16.1 m, and 17.5 m for series 2800, 2900, and 3100, respectively.
[c]x_2 = 26.1 m, 26.1 m, and 29.5 m for series 2800, 2900, and 3100, respectively.
Note: 1 m = 3.28 ft.

dispersion. As such, these data cannot provide reliable estimates of β and L. Concerning the latter, it could safely be stated that it should exceed the value of x_2 and L_T should exceed $3x_2$.

Errata.—The following corrections should be made to the original paper:

Page 158, paragraph 1, line 8: Should read "by a small time interval" instead of "by small time interval"

Page 160, Eq. 17: Should read "$\bar{\sigma}_t^2 \simeq \dfrac{2\beta L^2}{V^2}\left(\dfrac{x}{L} - 1\right); \quad \dfrac{d\bar{\sigma}_t^2}{dx} = \text{constant}$"

instead of "$\bar{\sigma}_t^2 \simeq \dfrac{2\beta L^2}{V^2}\left(\dfrac{x}{L} - 1\right); \quad \dfrac{d\sigma_t^2}{dx} = \text{constant}$"

Page 161, line 1: Should read "(as will be shown" instead of "(as well be shown"

Page 165, line 1: Should read "t_p" instead of "tp"

Page 165, paragraph 4, item 2, line 2: Should read "ϵ_z (= transverse mixing coefficient) αRV_*" instead of "$\epsilon_z \alpha RV_*$"

Page 166, Fig. 6(*a*), The label of the ordinate: Should read "$\sqrt{\overline{u'^2}}/V^2$" rather than "$\sqrt{\overline{u'^2}}/V$"

APPENDIX.—REFERENCE

33. Beltaos, S., "Transverse Mixing in Natural Streams," *Report SWE 78-1*, Transportation and Surface Water Engineering Division, Alberta Research Council, Edmonton, Canada, 1978, 99 pp.

OPTIMIZATION OF UNIT HYDROGRAPH DETERMINATION[a]

Closure by Larry W. Mays[8] and Lynn Coles[9]

The comments, suggestions, and additions presented by Ford, Meredith and Byrnes, Wormleaton, and Diskin are pertinent and of interest to the writers. Ford commented that practical applications of the model seemed unlikely because it requires the user to know rainfall excess. This is true of any unit hydrograph procedure. Then Ford goes on to present a modified form of the model that includes an initial loss volume and a loss rate. The modified form of the model is then solved by geometric programming. Basically, all this does is to include the simple operations that can be done by hand in a model that is much more difficult to solve, especially for large problems, with several multiperiod storms. Ford did not state how baseflow separation was handled. The writers feel that Ford complicated a simple problem with no advantages presented at all. As stated by Wormleaton, the computational simplicity of the linear programming (LP) approach and the ease with which it can be applied make it a very attractive method for practical purposes.

The writers agree with Ford and Meredith and Byrnes that weights should have been used in the objective function. In fact, the first version of this paper incorporated the following objective function:

$$\text{Min } Z_o = \sum_{i=1}^{I_i} \sum_{n=1}^{N_n} W_{i,n}(Z_{i,v} + V_{i,n}) \quad \ldots \ldots \ldots \ldots \ldots \ldots \ldots \ldots \quad (21)$$

in which $W_{i,n}$ refers to the weight given to the nth ordinate of the ith observed runoff hydrograph. The reviewers felt that the idea of weights should be deleted from the paper. Meredith's suggestion of using the weighting factor, of Eq. 20 from Ref. 24, would be satisfactory.

---

[a]January, 1980, by Larry W. Mays and Lynn Coles (Proc. Paper 15129).

[8]Asst. Prof. of Civ. Engrg., Coll. of Engrg., Environmental Health and Water Resources Planning, Ernest Cockrell, Jr., Hall 8.600, Univ. of Texas, Austin, Tex. 78712.

[9]Planner, Texas Dept. of Water Resources, Austin, Tex.

Meredith and Byrnes, Wormleaton, and Diskin each commented on the choice of M, which defines the time base of the derived unit hydrograph. Wormleaton suggested using the maximum of the respective M_i values of Eq. 25 and adding constraints to relate runoff to rainfall in those storms in which $M_i < M_{max}$. Meredith and Byrnes suggested using an M somewhat larger than that indicated by the data results in the model determining the optimal number of unit hydrograph ordinates, which is simply the number of nonzero unit hydrograph ordinates. This also is a good suggestion to enhance the capability of the model.

Wormleaton suggested that a disadvantage of the LP method is that an initial guess is required for the solution (i.e., unit hydrograph solution). This is not true because most LP codes do not require an initial basic feasible solution (initial guess); in fact, only the more sophisticated codes can handle a user inputted initial basic feasible solution.

The writers disagree with Wormleaton's comment that the most significant drawback of the LP method is that the number of decision variables increases with the number of storm events considered. This is a disadvantage; however LP codes do exist that can handle hundreds and even thousands of constraints and decisions variables, and, in addition, specialized decomposition techniques exist such as Dantzig-Wolf decomposition and Bender decompositions. The writers doubt that there are few, if any, watersheds that have more reliable existing data in excess of what can be handled by an existing LP method.

Meredith and Byrnes' comparison of the LP approach and the least-squares and weighted least-squares approaches was interesting. From their preliminary analysis the least-squares models may be more accurate. However, the writers agree that further study should be done to evaluate the different models.

The writers do agree with Diskin that the LP approach to the multistorm optimization has advantages in comparison to the least-squares solution.

Diskin's comments concerning the compacted forms of the matrix and other suggestions concerning reduction of the problem size are applicable.

Meredith and Byrnes suggested formulating models that could determine the optimal unit hydrograph for several multiperiod storms when the input data are observed precipitation and total runoff hydrograph ordinates. Such a model is presently being developed at the University of Texas by the first writer. This model is basically an extension of the previous model so that the rainfall excess and consequently, the rainfall losses are considered as unknowns. This model results in a large nonlinear programming problem with both linear and nonlinear constraints. The model solution requires the use of the large-scale generalized reduced gradient technique by Lasdon and Waren (25).

APPENDIX.—REFERENCE

25. Lasdon, L. S., and Waren, A. D., "Generalized Reduced Gradient Software for Linearly and Nonlinearly Constrained Problems," *Working Paper 77-85*, Graduate School of Business, University of Texas, Tex., Oct., 1977.

TIDAL HYDRAULICS IN ESTUARINE CHANNELS[a]

Closure by Robert M. Snyder,[3] M. ASCE

The writer appreciates the recognition of Kundzewicz and looks forward to studying his Ref. 10 when it is published.

With respect to the discusser's issue of "intuition," the writer must point out that while the "analogy may be proved by comparing the mathematical equations describing certain electrical and hydraulic systems," the discovery, if indeed there has been one, came not from excursions into pasigraphy but, rather, from a recollection of familiar phenomena. Arguing *Cantorian antinomies* (12), however, would more properly be carried out elsewhere.

The writer agrees that flow transformation along an estuarine channel is more properly represented by a distributed circuit analogy. This has been previously pointed out in detail in a personal communication between the writer and Price, and was mentioned briefly by the writer in the full version of the paper as originally submitted. Because of the other nonlinearities associated with tidal flow that are not directly analogous to the transmission line theory, the writer felt it best to introduce the concepts of hydraulic capacitance, hydraulic inductance, and their related reactances in the simplified form of ordinary differential equations. This was considered important since most hydraulic engineers are not familiar with radio electronics. As pointed out by Ref. 13, breaking with pure empiricism can lead to closer ties with physical analysis which is still unlimited in its possibilities. It is hoped that the discusser's referenced work is just a beginning of the physical analysis of flow based on the fundamental equation of forced hydraulic motion of which "steady" or "dc" flow is a special case. For further discussion of hydraulic analogs, see Ref. 14.

APPENDIX.—REFERENCES

12. Poincaré, H., *Science and Method*, Dover Publications, Inc., New York, N.Y., 1952, p. 145.
13. "History of Hydraulics," Rouse, Hunter and Simon Inc., Iowa Institute of Hydraulic Research, The University of Iowa, Iowa City, Iowa, 1957, p. 249.
14. Snyder, R. M., Christensen, B. A., and Walton, R., "Use of Electrical Analogs As a Design Tool for Tidal Canals," *Proceedings*, of the Urban Stormwater Management In Coastal Areas, ASCE, June, 1980.

[a]February, 1980, by Robert M. Snyder (Proc. Paper 15202).
[3]Pres., Snyder Oceanography Services, Inc., 95 Lighthouse Drive, Jupiter, Fla. 33458.

Design Hyetographs for Small Drainage Structures[a]

Discussion by Richard H. French[3]

The authors are to be congratulated on their careful and important research regarding the feasibility of using triangular hyetographs to approximate the geometry of local rainstorm hyetographs for small drainage systems. However, the authors neglect to discuss some aspects of their work which are relevant to storms which occur in the southern Nevada area.

TABLE 6.—Mean Values of a° for Nondimensional Triangular Hyetographs at Well 5B, Nevada Test Site

Season, in months of year (1)	All Durations		DURATIONS					
			$2 < t_d < 4$		$4 < t_d < 10$		$10 < t_d$	
	Case I (2)	Case II (3)	Case I (4)	Case II (5)	Case I (6)	Case II (7)	Case I (8)	Case II (9)
6–8	(12)	(15)	(8)	(9)	(3)	(5)	(1)	(1)
	0.41	0.30	0.35	0.30	0.41	0.19	0.86	0.86
5–9	(23)	(29)	(16)	(18)	(6)	(10)	(1)	(1)
	0.49	0.41	0.49	0.50	0.43	0.26	0.86	0.86
3–4	(19)	(20)	(9)	(9)	(9)	(9)	(1)	(2)
	0.54	0.57	0.49	0.49	0.61	0.61	0.37	0.75
10–11	(22)	(24)	(13)	(14)	(7)	(8)	(2)	(2)
	0.46	0.51	0.43	0.49	0.55	0.61	0.27	0.27
12–2	(45)	(54)	(14)	(18)	(15)	(18)	(16)	(18)
	0.50	0.51	0.52	0.59	0.48	0.47	0.50	0.43

Note: Numbers in parentheses indicate number of storms in given category.

First, no consideration is given to storms whose hyetographs yield negative estimates of the parameters a and b. This situation may arise when a storm hyetograph does not have a rising leg; i.e., the maximum storm intensity occurs at time $t = 0$. Using the authors' definitions, the writer has examined 345 storm records from a weighing bucket gage located at well 5B on the Nevada test site. The time scale of the gage records was such that for storms of 2 h or less in duration an accurate hyetograph could not be constructed. Thus, of the 345 storms considered, only 127 could be analyzed by the authors' methods. Of these 127 storms, 18 resulted in negative estimates or either a or b and subsequently a° and b°. In Table 6 the results of this study are summarized. In this table, Case I denotes that storms resulting in negative estimates of either

[a]June, 1980, by Ben Chie Yen and Ven Te Chow (Proc. Paper 15452).

[3]Assoc. Research Prof., Desert Research Inst., Water Resources Center, Univ. of Nevada System, 4582 Maryland Parkway, Las Vegas, Nev. 89109.

a° or b° were not considered while Case II denotes that all storms constituting 127 sample data base were considered. The numbers in parentheses indicate the number of storms in a given category.

Although the sample size is small, the results indicate that the effect of considering hyetographs which result in negative estimates of a° or b° can be significant; e.g., storms occurring in months 5–9 with durations greater than 4 h but less than 10 h. It is further noted that hyetographs having this characteristic composed 14% of the total sample at this site.

Second, the authors evaluate the validity of their hypothesis by comparing the measured and computed hydrographs for several experiments. Although this method of verification has merit, it does not provide detailed information regarding the validity of the triangular hyetograph hypothesis. In a number of cases at the well 5B site, the authors' triangular hyetograph hypothesis yields a very poor estimate of the measured hyetograph. The hyetograph in Fig. 10 cannot

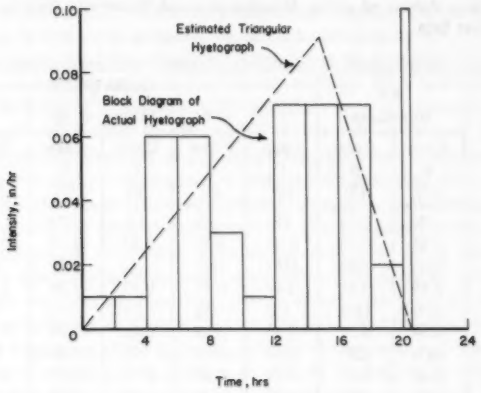

FIG. 10.—Comparison of Actual and Estimated Hyetographs for Storm of February 8, 1976 at Site Well 5B

be accurately approximated by the authors' hypothesis. Although the use of additional moments might resolve this problem, the authors' primary objective would be defeated. This situation usually arises in the case of large winter storms with relatively long durations. It is hypothesized that some consideration must be given to the size of the storm relative to the size of the drainage basin. If a single storm approximately as large as the drainage basin is located over the basin, then a very simple hyetograph might result but in the case of large storms, large relative to the basin, composed of many storm cells then additional factors must be considered.

Acknowledgment.—The work described in this discussion was sponsored by the U.S. Department of Energy under Contract DE-AC08-76DP01253.

Closure by Ben Chie Yen[4] and Ven Te Chow,[5] Fellows, ASCE

French's thoughtful discussion is appreciated. Concerning the first of his two comments, namely on the negative values of the triangular hyetograph parameters a and b (Fig. 2), the effect was previously evaluated and reported in pp. 208–211 of Ref. 20. However, because of the length limitation of the paper, this as well as many other data problems was not elaborated in the paper. In fact, these problems, as they have not appeared in the literature (although many researchers must have encountered and overcome them) deserve their own right to be presented in a separate paper.

The anomaly of negative values of a and b indeed occurs for some rainstorms, especially when the time interval of the data is large, such as $2h$ used in Table 6. To avoid the anomaly, rainstorms having negative values of a or b can be disregarded as suggested by French, resulting in a significant increase in the mean value of a^o and decrease in the mean value of b^o. Alternatively, one may arbitrarily set the values of a or b to zero for those rainstorms having negative a or b and include them in the statistics instead of disregarding them.

TABLE 7.—Comparison of Mean Values of a^o, Nevada Test Site, June–August

	DURATIONS, in hours					
	All Durations		$2 < t_d \leq 4$		$4 < t_d \leq 10$	
Case (1)	a^o (2)	Number of storms (3)	a^o (4)	Number of storms (5)	a^o (6)	Number of storms (7)
1. $a^o \geq 0$	0.41	12	0.35	8	0.41	3
2. $a^o \geq -\infty$	0.30	15	0.30	9	0.19	5
3. $a^o \geq 0$	0.33	15	0.31	9	0.25	3

The result is a slightly increased mean values of a^o and decreased mean value of b^o from the case allowing negative values, as shown in Case 3 for a^o in Table 7. These a^o values are computed from the June–August data given in Table 6 by French assuming that the three disregarded rainstorms all have negative a^o. Values of a^o for Cases 1 and 2 given by French are also listed in Table 7 for comparison. The statistics given in the writers' paper were obtained by setting negative a and b to zero.

Considerably more rainstorm statistics have been obtained, using 5-min and hourly rainfall data, since the publication of the paper. It has been found that in order to obtain reasonably reliable values of the nondimensional hyetograph parameters, the sample size must not be small; normally there should be more than 100 rainstorms in each class. As the sample size becomes large, the effect of not allowing negative a and b becomes relatively small and insignificant, as shown in Table 8 for the data of 469 rainstorms for the months of June–August, from 1959–1972, at Urbana, Ill. (20).

[4]Prof. of Civ. Engrg., Univ. of Illinois at Urbana-Champaign, Urbana, Ill. 61801.
[5]Prof. of Civ. and Hydrosystems Engrg., Univ. of Illinois at Urbana-Champaign, Urbana, Ill. 61801.

Concerning French's second comment on comparing the triangular hyetograph to that of a particular rainstorm, one should realize that the triangular hyetograph based on the statistical mean values is an estimate of the expected hyetograph in the future. It would not fit perfectly with any rainstorm of the past or future; this is analogous to the case that no American family actually has 2.2 children although this is the statistically expected number of children in an American family. As no two hyetographs are identical, obviously a synthetic hyetograph that would precisely fit one actual hyetograph would not fit any other hyetograph. The purpose of the synthetic hyetographs is to give a reasonable estimate of the future that has not yet happened and could be in any of the infinite number of shapes. Recently, particularly in the field of urban hydrology, too much

TABLE 8.—Effect of Negative Values of a and b, Urbana, Ill., June–August, 1959–1972 (469 Rainstorms)

Case (1)	a, in hours (2)	b, in hours (3)	a^o (4)	b^o (5)
2. $a, b, > -\infty$	0.95	1.50	0.42	0.58
3. $a, b \geq 0$	1.00	1.46	0.43	0.57

attention has been given to trying to duplicate what has happened in the past at the expenses of searching for a good prediction for the unknown future.

Some Paradoxes in the History of Hydraulics[a]

Closure by Hunter Rouse,[3] Hon. M. ASCE

Following his kind words about the paper, my sole discusser remarked that I now had the "right and privilege" (i.e., obligation) to keep certain additional paradoxes from becoming perpetuated. So be it!

As recounted in my bicentennial story of American hydraulics (3), Shields' work on sediment movement was first brought to the profession's attention by several of my early papers on the subject, but the notion that it was he who introduced the critical tractive into the literature is new to me. The chapter in *Engineering Hydraulics* to which Professor Gill refers (1) specifically recognized Du Boys' original contribution. Although Shields inserted his own numerical values into Du Boys' transportation equation, Shields' real accomplishment was

[a]June, 1980, by Hunter Rouse (Proc. Paper 15475).

[3]Carver Prof. Emeritus, The Univ. of Iowa, Iowa City, Iowa 52242; also Visiting Prof., Colorado State Univ., Fort Collins, Colo. 80523.

that of correlating the initial stages of movement with the grain Reynolds number, as Gill correctly concluded. I am not aware of any paradox in this regard. Until the discussion appeared, moreover, I had never seen Brown's name or mine mentioned in connection with the Einstein and Kalinske formulations.

While bringing several chapters of *Engineering Hydraulics* to completion in time for the Fourth Hydraulics Conference, I took frequent advantage of my editorial prerogatives. For example, the work of one author was subjected to considerable last-moment revision, and another was completely replaced. The late Carl Brown, on the other hand, had consented to serve as author of the sediment chapter only if he received help with a few of the sections. This, several of us undertook to provide (albeit more extensively than I had anticipated), as acknowledged at the end of the chapter. In the bed-load section, I made a special effort to present the Shields, Einstein, and Kalinske relationships in a comparable manner; the underlying analyses, however, remained their own, and association of either Brown's name or mine with theirs is hardly justified. I thus agree fully with the discusser's implication that there are already enough paradoxes in the literature.

Appendix.—Reference

3. Rouse, H., *Hydraulics in the United States, 1776–1976*, Iowa Institute of Hydraulic Research, Iowa City, Iowa, 1976.

Reciprocal-Distance Estimate of Point Rainfall[a]

Discussion by Ismael Pagán-Trinidad,[3] A. M. ASCE and Ben C. Yen,[4] F. ASCE

The authors presented an interesting study on handling missing point rainfall record. It has long been known that the inverse-distance estimate of point rainfall is superior to the standard National Weather Service methods (5). In fact, the inverse-distance method has been taught in the undergraduate hydrosystems engineering course at the University of Illinois at Urbana-Champaign, Ill., since 1975. The authors' result, which is based on one of the possible inverse-distance methods, further supports the advantage of this method.

The writers have conducted an extensive study of spatial and temporal rainfall variabilities for engineering applications. The evaluation of different weighting methods to estimate missing precipitation records is a part of the research.

[a]July, 1980, by John R. Simanton and Herbert B. Osborn (Proc. Paper 15516).

[3]Prof. Dept. of Civ. Engrg., Mayagüez Campus, Univ. of Puerto Rico, Mayagüez, Puerto Rico; currently Grad. Student, Dept. of Civ. Engrg., Univ. of Illinois at Urbana-Champaign, Urbana, Ill. 61801.

[4]Prof., Dept. of Civ. Engrg., Univ. of Illinois at Urbana-Champaign, Urbana, Ill. 61801.

The techniques investigated included not only the weighted inverse-distance techniques but also weighted subscribing-area and other techniques. An example of another inverse-distance technique is

$$\frac{R}{\overline{D^b}} = \frac{1}{n} \sum \left(\frac{P_i}{D_i^b} \right) \qquad (3)$$

in which $\overline{D^b}$ = the mean of D_i^b. Since the complete results will appear in a paper, suffice it to mention here that the selection of the preference technique depends on a number of factors, including the error measurement criteria, the type of rainfall record (i.e., storm event, daily, monthly, etc.), the geometry of the raingage network arrangement, and the physical constraints. The writers have used over 300 rainfall events from a 12-yr record data collected at the East Central Illinois Raingage Network by the Illinois State Water Survey. The writers' results show that the inverse-distance technique used by the authors is indeed a superior method under similar conditions, namely, single heavy rainstorm events and hydrometeorologically relative homogeneous areas. They also show that Eq. 3 does not apply for large values of b. Nevertheless, it should be pointed out that in all cases the isohyetal method gives equal or better results than any of the weighting methods evaluated, because the rainfall directional gradient effect can be more realistically represented. However, the isohyetal method is also more complicated and time-consuming than any of the weighting methods.

As mentioned previously, the judgment on the goodness of a method depends on the criteria of error measurement. The correlation coefficient is not necessarily the most suitable error criterion because it measures only the degree of linear dependence between the two variates. Moreover, the correlation coefficient is a function not only of the distance between rain gages as shown in Fig. 1, but also of the orientation, synoptic pattern, type of event, and duration of rainstorms (6). It would be helpful if the authors can give the equation they used to compute the correlation coefficient. Also, the writers assume that Eq. 1, as printed, is in error, but the results presented in Tables 1 and 2 and Fig. 1 are correct.

Appendix.—References

5. Gilman, C. S., "Rainfall," *Handbook of Applied Hydrology*, V. T. Chow, ed., McGraw-Hill Book Co., Inc., New York, N.Y., 1964, p. 9.28.
6. Huff, F. A., "Spatial and Temporal Correlation of Precipitation in Illinois," *Circular 141*, Illinois Institute of Natural Resources, Illinois State Water Survey, Urbana, Ill., 1979.

Force on Sill of Forced Jump[a]

Discussion by Karam S. Karki[3] and Shantanu K. Mishra[4]

The authors are to be commended for presenting some valuable data regarding the force experienced by a sill under various forced jump conditions. The writers would like to make a few comments and add some interesting results on the basis of authors' experimental data.

The writers would like to know the authors' observation about the deflection of the supercritical jet and the surface profile near the sill under flow condition I. When the downstream conditions do not affect the upstream flow, the writers have observed that the jet partly splashes-over and partly over turns to form an intense roller very close to the sill under the conditions $4 \geq (h/y_1) \geq 1.25$ and $F > 3.5$. It has been also reported that the authors could not identify flow condition I for $(h/y_1) = 3$. The writers feel that it would have been easier to understand this identification if it was explained in terms of surface profile/jet deflection.

The coefficient of drag under flow condition I has been reported to be constant with a value approximately equal to 0.45. In this connection, the writers do not agree with the authors' remark, "Although this 'nonsplashing-over' behavior does not exactly describe the flow condition I of the present investigations, the *Cd* value and the fact that it is a constant are consistent." The writers are of the opinion that the "nonsplashing-over" condition for $4 \geq (h/y_1) \geq 1.25$ and $F > 3.5$, as described in the first writer's paper (4) is the same as that of flow condition I. At the same time, it is not very correct to designate the drag coefficient under this condition of flow as the maximum drag coefficient, Cd_m, of forced jump, since there is no jump at all. Under no jump condition, the maximum drag experienced by the sill occurs under the "splashing over" condition (4); the writers would prefer to call it the drag coefficient under flow condition I. Under this condition of flow, a knowledge of drag experienced by the sill is not sufficient. It has been observed by the writers that substantial negative pressures do occur on the downstream face of the sill. It is needless to mention that these negative pressures are of great importance in designing the sill.

The authors' second conclusion states that "the maximum drag coefficient varies from 0.45–0.3 depending on the relative sill height," whereas their Fig. 6 shows that this variation depends on the Froude number and not on the relative sill height.

The writers tried to predict the drag coefficient of the sill at transition from

[a]July, 1980, by Rangaswami Narayanan and Loizois S. Schizas (Proc. Paper 15552).

[3]Reader, Dept. of Civ. Engrg., Inst. of Tech., Banaras Hindu Univ., Varanasi, 221005, India.

[4]Reader, Dept. of Civ. Engrg., Inst. of Tech., Banaras Hindu Univ., Varanasi, 221005, India.

flow condition I to flow condition II by using the momentum principle. The results obtained on the basis of the data shown in Fig. 3 do not compare well with the experimentally-observed values. This may be due to the fact that the demarcation lines, distinguishing flow condition I from flow condition II are not sharp, as has also been reported by the authors.

It is of interest to note that the drag coefficient at transition, predicted from the data of flow condition II, as shown in Fig. 4, through the momentum equation compares well with the experimental observations. In Fig. 4, this transition may be seen as the beginning of flow condition II with $(X_6/y_1) = 0$, although this flow transition is difficult to establish but may be visualized as the transition—the very first beginning of flow condition II. The following equation due to Rajaratnam (7) is used for prediction:

$$Cd = \frac{(\alpha - 1)[2F_r^2 - \alpha(1 + \alpha)]}{F_r^2 \alpha\beta} \quad \text{(9)}$$

in which $\alpha = y_2/y_1$ and $\beta = h/y_1$.

TABLE 1.—Results of Calculations

(h/y_1) (1)	F (2)	(y_2/y_1) (3)	Cd (4)
1	3.99	4.5	0.282
	5.11	6.1	0.298
	6.54	8	0.275
	7.64	9.5	0.261
	8.37	10.5	0.251
	9.09	11.5	0.243
2	3.99	1.7	0.352
	5.11	5	0.342
	6.54	6.7	0.334
	7.64	8.6	0.258
	8.37	9.7	0.233
	9.09	10.5	0.238

The values of y_2/y_1 used for calculations are obtained by carefully extending back the various experimental curves of Fig. 4 for different Froude numbers up to the y-axis, i.e., where $(X_0/y_1) = 0$. Table 1 shows the results of these calculations. From this table, it is seen that the drag coefficients of the sill at the transition remains approximately constant with an average value of 0.28. This compares well with the experimentally-observed value of 0.3.

Finally, the writers would like to point out that for almost all the observations of flow condition II, the depth ratio, y_2/y_1, is always higher than the corresponding sequence depth ratio of a free jump. This observation is contrary to all previous observations (2, 5, 12, 15, 16, 17, and the writers' unpublished experimental data). An explanation to this effect is very much required.

Appendix.—References

15. "Energy Dissipators for Spillways and Outlet Works," by the Task Force on Energy

Dissipators for Spillways and Outlet Works Committee on Hydraulic Structures, R. H. Berryhill, Chmn., *Journal of the Hydraulics Division*, ASCE, Vol. 90, No. HY1, Proc. Paper 3762, Jan., 1964, pp. 121–147.
16. Pillai, N. N., and Unny, T. E., "Shapes for Appurtenances in Stilling Basins," *Journal of the Hydraulics Division*, ASCE, Vol. 90, No. HY3, Proc. Paper 3888, May, 1964, pp. 1–21.
17. Weide, L., "The Effects of the Size and Spacing of Floor Blocks in the Control of the Hydraulic Jump," thesis presented to Colorado A. and M., at Colorado, in 1951, in partial fulfillment of the requirements for the degree of Master of Science.

Turbulence Measurements in Simulated Tidal Flow[a]

Discussion by Robert Booij[3]

The authors have succeeded in measuring Reynolds shear stress profiles in an accelerating and decelerating flow in a flume as a simulation of a tidal flow. They got around the contamination problems of hot-film anemometers by using a small electromagnetic current meter. Important conclusions concern the difference between the magnitude of the Reynolds shear stresses and their profiles in accelerating and decelerating flow, and a hysteresis effect of these stresses with respect to the mean velocity. The data, however, do not seem to be entirely consistent as regards these aspects.

In Fig. 8 the hysteresis effect of the Reynolds stresses is significant, especially in the more strongly accelerated and decelerated flows. If accelerated flows and decelerated flows are considered separately, this hysteresis effect must be perceptible in the difference between them. In fact, the data for $T = 550$ sec in Fig. 8 are based on such separate measurements. Rearranging the data of Fig. 6 by plotting the nondimensional Reynolds stress against $\bar{U}/\bar{U}_R$ instead of against y/D yields Fig. 12. The hysteresis effect in Fig. 12 is much smaller (if apparent at all) than in Fig. 8, although for $T = 550$ sec the measurements are the same or analogous in both cases. For $T = 200$ sec the time between the accelerating and the decelerating phase is too short in the case of Fig. 8 to create a steady state in between. There is no reason, however, to expect an important influence of this absence of a steady state on account of Fig. 12. After all, the Reynolds stresses at the end of the accelerating phase in Fig. 12 are comparable to the stresses at the beginning of the decelerating phase or, because of the steady state in between, to the Reynolds stresses in the steady state. So, the decelerating phase should also behave in accordance with Fig. 12, and little or none hysteresis should be measured.

The data in Fig. 6 demonstrate, in conformity with some measurements in a tidal flow by Bowden, et al. (20), that the location of the maximum Reynolds

[a]August, 1980, by Habib O. Anwar and Roy Atkins (Proc. Paper 15609).

[3]Sr. Scientific Officer, Fluid Mech. Group, Dept. of Civ. Engrg., Delft Univ. of Tech., Stevinweg 4, Delft, The Netherlands.

shear stress in decelerating flow occurs at a larger distance from the bed than, e.g., in uniform flow. This decreasing Reynolds stress near the bed does not agree with the bed shear stress obtained from Preston tube measurements. The data in Fig. 6, replotted in Fig. 12 suggest, instead of the strong hysteresis effect in Fig. 8, a (small) reversed effect at $y/D = 0.11$.

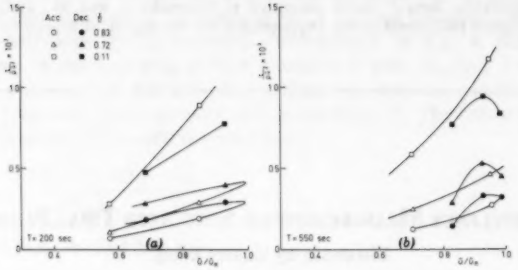

FIG. 12.—Hysteresis of Reynolds Stress at Various Nondimensional Depths (y/D) as Deduced from Fig. 6: (*a*) $T = 550$ sec; (*b*) $T = 200$ sec

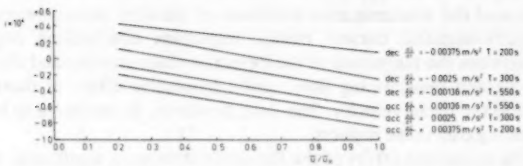

FIG. 13.—Variation of Surface Slope, i, with Dimensionless Velocity $\bar{U}/\bar{U}_R$

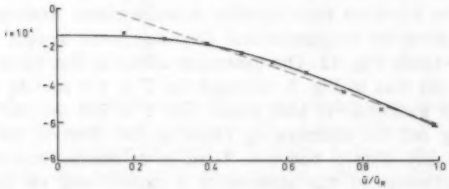

FIG. 14.—Quadratic Versus Linear Variation of Surface Slope with Dimensionless Velocity, $\bar{U}/\bar{U}_R$, for $T = 550$ sec (Acceleration)

As stronger decelerations are connected with less favorable slopes, the observation that the slope for $T = 200$ sec remains favorable through the measurements, does not seem correct. This is probably caused by a possible sign error in Fig. 10. After this correction the parts of Fig. 10 may be combined to give Fig. 13.

Contrary to the sixth conclusion in the original paper, the relation between

slope i and time or $\bar{U}/\bar{U}_R$ in Fig. 10 may be better described by a quadratic than by a linear relation, as shown in Fig. 14. As quadratic friction is likely to dominate, this would be more acceptable (see also Eq. 5).

In Fig. 5 data by Gordon, et al. (7), found from measurements in a tidal estuary are plotted. However, the maximum accelerations in this estuary were about a factor 100 smaller than 0.37 cm/s^2, which means that the results of the flume and those of the prototype cannot be directly compared. Therefore, the eighth conclusion of the original paper seems somewhat premature.

Appendix.—Reference

20. Bowden, K. F., Fairbairn, L. A., and Hughes, P., "The Distribution of Shearing Stresses in a Tidal Current," *Geophysical Journal of the Royal Astronomical Society*, Vol. 2, 1959, pp. 288–305.

Empirical Investigation of Curve Number Technique[a]

Discussion by Richard H. Hawkins,[4] M. ASCE

Hjelmfelt has made a useful contribution to applied hydrology by demonstrating a defensible procedure for determining curve numbers from data. His method satisfies the frequency-related assumptions in applying the curve number method to peak flow calculations.

An alternate acceptable method also exists, i.e., that of Rallison and Cronshey (10), which has the relative advantage of not requiring a lengthy record. Its application has been demonstrated by Springer, et al. (11). A useful investigation would be a comparison of the two methods. Also, the "visual fit" to the curve number frequency data tempts the suggestion of a statistically-correct fitting or a data analysis routine. Such could perhaps require satisfying a least-squares criterion for the runoff data estimated by the moment fit rainfall frequency data. That is, what CN (or S) creates the best fit line to the observed runoff frequency data using Eq. 2 with the rainfall frequency fit line estimates as rainfall inputs?

Much of the power of the CN method lies in its adjustment to land conditions. Thus, it is of interest to consider the land condition of the five studied basins. In particular, was it consistent throughout the sampling period, or in systems terms, was stationarity present? This is less of a problem with the large basins studied than smaller basins, where a single act of random or designed land use (urbanization, fire, or agriculture) could disrupt the entire hydrologic regimen.

[a]September, 1980, by Allen T. Hjelmfelt, Jr. (Proc. Paper 15693).

[4]Prof., Dept. of Forestry and Outdoor Recreation (Watershed Sci. Unit); also Prof., Dept. of Civ. and Environmental Engrg., Utah State Univ., Logan, Utah 84322.

The Sonoita Creek results clearly do not affirm the curve number runoff equation (i.e., Eq. 2). The parallel rainfall and runoff data in a logarithmic scale indicate a runoff function of the structure

$$Q = CP \tag{4}$$

and for the Sonoita Creek data, a c value of about 0.05 seems to fit. This relationship, an alternate form of the deeply-entrenched "rational equation" has been found by the writer for other western watersheds (9), though its emergence for this particular basin is surprising. Under these conditions, a relatively small consistent source area may be hypothesized, a fraction, C (from Eq. 4), of the watershed area. As shown in Ref. 9, this causes the observed curve number (as determined from storm P and Q observations) to decrease with increasing storm size.

In the case of Sonoita Creek, assuming CN = 74 to be a statistically-correct fitting and scaling P values from the fit line in Fig. 5, the analysis of errors in overprediction and underprediction, as presented in Table 2, would result.

From the design safety standpoint, as with flood accommodating structures, it is comforting to have the CN method *over*estimate for extreme large events.

TABLE 2.—Rainfall and Runoff for Sonoita Creek

Probability, as a percentage (1)	P, in inches (2)	Q, in inches CN = 74 (3)	Q, in inches C = 0.05 (4)	Error, as a percentage (5)
2	5.2	2.525	0.26	870
5	4.0	1.596	0.20	698
10	3.2	1.038	0.16	548
50	1.5	0.147	0.07	110
80	0.7	0	0.035	−100

It is of less solace to consider the effects on project expenditures from overdesign, or to contemplate decisions made in other situations where overestimating of runoff volume is not on the side of safety. An example of the latter might be flood insurance studies, where a true best estimate of reality would be needed.

Appendix.—References

9. Hawkins, R. H., "Runoff Curve Numbers from Partial Area Watersheds," *Journal of the Irrigation and Drainage Division*, ASCE, Vol. 105, No. IR4, Proc. Paper 15024, Dec., 1979, pp. 375–389.
10. Rallison, R. E., and Cronshey, R. G., discussion of "Runoff Curve Numbers with Varying Site Moisture," by Richard H. Hawkins, *Journal of the Irrigation and Drainage Division*, ASCE, Vol. 105, No. IR4, Proc. Paper 15010, Dec., 1979, pp. 439–441.
11. Springer, E. P., McGurk, B. J., Hawkins, R. H., and Coltharp, G. B., "Curve Numbers from Watershed Data," *Proceedings of the Symposium on Watershed Management*, ASCE, 1980, pp. 938–950.

Entrained Air in Linearly Accelerated Water Flow[a]

Discussion by Maurice J. Kenn[2]

Abdin Salih will doubtless be pleased to know that his important studies at Imperial College have now been extended to include work on entrained air in decelerating water flows (separately with constant, linear, and nonlinear pressure gradients) (13).

These latter tests have not only confirmed that the decelerated bubbles move (in these cases) more slowly than the water stream, but that they can also be severely shattered by the overtaking host stream.

This more recent knowledge has been effectively applied at Bolarque Dam, in Spain, where small quantities of air have been successfully injected *into the decelerating water stream* of the water-turbine draught tubes, in order to suppress cavitation, cavitating vortices, associated water hammer (at a frequency of 3.9 Hz) with draught-tube vibrations, and the resonating vibrations of the 30-m high concrete dam, with an estimated first-mode rocking frequency also at 3.9 Hz (14).

Appendix.—References

13. Stafanakos, J. P., "Entrained Air in Decelerating Water Flows," thesis presented to the University of London, at London, England, in 1979, in partial fulfillment of the requirements for the degree of Doctor of Philosophy.
14. Kenn, M. J., Cassell, A. C., and Grootenhuis, P., "Vibrations at the Bolarque Dam," *Symposium on Practical Experiences with Flow-Induced Vibrations*, International Association for Hydraulic Research/International Union of Theoretical and Applied Mechanics, 1980.

[a]October, 1980, by Abdin M. A. Salih (Proc. Paper 15728).
[2]Acting Head, Hydr. Section, Civ. Engrg. Dept., Imperial College, London, SW7 2BU, England.

Hydraulic Transients Following Valve Closure[a]

Discussion by Alan E. Vardy[4]

The finite element technique has justifiably gained wide acceptance in the engineering world. However, considerable difficulty has been experienced in adapting it to the conditions pertaining in hyperbolic problems. It is to be hoped that work will continue towards this end.

In support of their conclusion that "both the method of characteristics and the finite element method are shown to give an accurate simulation of pressure surges produced through rapid valve closure," the authors draw specific attention to Fig. 5 of their paper. For reasons given in the following, the writer feels very uneasy with this interpretation of their results.

1. The term "rapid" is misleading because the valve closure time of about 1 sec greatly exceeds the pipe period. As a result, the type of pressure wave activity normally associated with water hammer is not strongly in evidence until after about $t = 0.9$ sec.

2. When the authors presented these results at a recent conference (9), several discussers drew attention to the marked differences between the magnitudes of the measured and predicted pressures when $t > 0.9$ sec. Significantly better agreement would be expected if the closure was more sudden, and so the writer suspects that the descrepancy is due more to the simulation of the valve as a boundary condition than to the simulation of the flows in the pipe. The likelihood of this possibility is strengthened by the existence of significant discrepancies between theory and experiment even during the preceding period of slowly varying flow. As the discussion to the earlier paper has not been published, the writer would like to ask again whether the authors have considered using the measured pressure history just upstream of the valve as the downstream boundary condition for the theoretical analyses. Although a simulation of real valves is clearly advantageous in a practical environment, the elimination of this source of error would be highly desirable for the purpose of verifying the authors' theoretical technique.

The results presented in Fig. 5 can be interpreted from another viewpoint which encourages me to believe that the authors' finite element technique is much better than the disappointing comparison which the experiment suggests. There is good reason to suppose that the method of characteristics (MOC) is capable of predicting water hammer behavior very closely. Therefore, the validity of any new theoretical approach can be evaluated relatively cheaply by comparing its predictions with those of the MOC. Large differences indicate errors in the new approach; small differences represent open questions that

[a]October, 1980, by C. S. Watt, J. M. Hobbs, and A. P. Boldy (Proc. Paper 15740).
[4]Prof., Dept. of Civ. Engrg., Univ. of Dundee, Dundee DD1 4HN Scotland.

must be answered by precise experiments. The writer could take issue with the authors on some of the limitations that they unreasonably attribute to the MOC, but this would be quibbling. The point is that the agreement shown between the MOC and the authors' finite element approach is quite close. Their analysis is therefore proceeding along the right lines and is well worth extending to more complex networks.

Appendix.—Reference

9. Watt, C. S., Boldy, A. P., and Hobbs, J. M., "Combination of Finite Difference and Finite Element Techniques in Hydraulic Transient Problems," *Proceedings*, Third International Conference on Pressure Surges, Mar., 1980.

Fall Velocity of Shells as Coastal Sediment[a]

Discussion by Walter H. Graf[4]

In the authors' summary an important conclusion is that "shells in stable mode of settling have comparatively lower drag coefficients than those settling in the unstable mode"; this is clearly evident if Figs. 8 and 9 are compared.

To judge the significance of this difference, it would be important to have a clear definition of the fall velocity, W, since it enters into the definition of C_D; see Eq. 7. Was the fall velocity, W, obtained with the true path length or the "projected" path length; how was it measured and with what accuracy?

Furthermore, an attempt should be made to quantify the difference between stable and unstable modes of settling. In this way it might be helpful to explore the use of a dimensionless "stability criterion," such as a Strouhal number. This might turn out to be a difficult task, if not the entire particle's path was recorded.

While it is certainly appreciated that the shell geometries are compared with shape factors, it appears that something could be learned from a comparison with freely-falling disk data. A rather valuable summary of data for disks is given in Ref. 14; interestingly enough the data of the unstable settling mode, as given in Fig. 9, show the same trend as freely-falling disks. In this context, it would be also worthwhile to regard the concept of "pitching frequency" as put forward by Marchillon, et al. (13).

Appendix.—References

13. Marchillon, E. K., Clamen, A., and Gauvin, W. H., "Oscillatory Motion of Freely

[a]November, 1980, by Ashish J. Mehta, Jieh Lee, and Bent A. Christensen (Proc. Paper 15795).

[4]Prof., Laboratoire d'Hydraulique, Ecole Polytechnique Fédérale, CH-1015, Lausanne, Switzerland.

Falling Disks," *Physics of Fluids*, Vol. 7, No. 12, Dec., 1964.
14. Schiller, L., "Fallversuche mit Kugeln und Scheiben," *Handbuch der Experimentalphysik*, Vol. IV/2, Akad, Verlagsges, Leipzig, Germany, 1932, pp. 376–379.

SCOUR AROUND BRIDGE PIERS AT HIGH FLOW VELOCITIES[a]

Discussion by Fred W. Blaisdell,[3] F. ASCE and Clayton L. Anderson,[4] M. ASCE

This paper is exceptionally well-written, easy to read and comprehend, and complete within the scope of the research reported. The writers thank the authors of this paper for their efforts on behalf of the reader.

Since 1966, the writers have been studying local scour that has several points of similarity to the work of the authors. The writers' research is on scour produced in uniform-sized sand beds by the clear-water efflux from a cantilevered pipe. The pipe invert is positioned from $2D$ below to $8D$ above the tailwater surface (D = the pipe diameter). The surface of the bed is $0.5D$ above the tailwater level. A channel is formed in the bed downstream of the pipe exit. The discharge parameter, differing from the Froude number only by a constant multiplier but more appropriate for quantifying closed-conduit flow, is $Q/\sqrt{gD^5}$, in which Q = the discharge; and g = the acceleration due to gravity. The range of $Q/\sqrt{gD^5}$ tested is from 0.5–5. Unlike the work of Jain and Fischer, here there is no flow over the bed to transport bed material from upstream into the scour hole. All tests are three-dimensional, and most of them involve three-phase flow—air, water, and sand. Time is an additional variable. The five sands used, described after Jain and Fischer, have the properties:

D_{50}	0.46	0.90	1.84	3.92	7.65
σ_g	1.24	1.24	1.22	1.23	1.26

Three groups of tests were made.

For the first group of tests, the scoured material deposited in and completely filled the channel. The scoured material deposited because the channel was stable and the velocities were insufficient to transport the scoured material. As a result, this procedure was abandoned and a test method devised for keeping the downstream channel clear of deposited sediment.

[a]November, 1980, by Subhash C. Jain and Edward E. Fischer (Proc. Paper 15845).

[3]Research Hydr. Engr., United States Dept. of Agr., Sci. and Education Administration, Agricultural Research, St. Anthony Falls Hydr. Lab., Third Avenue Southeast at Mississippi River, Minneapolis, Minn. 55414.

[4]Hydr. Engr., United States Dept. of Agr., Sci. and Education Administration, Agricultural Research, St. Anthony Falls Hydr. Lab., Third Avenue Southeast at Mississippi River, Minneapolis, Minn. 55414.

For the second test group, a "suction dredge" in the form of a pipe oscillating longitudinally along a short length of the excavated channel just downstream of the scour hole kept the channel clean of the scoured material deposited in the channel. This procedure proved to be satisfactory.

To quote the authors' statement at the top of p. 1828—i.e., to adapt the authors' explanation of scour at bridge piers to the writers' scour at cantilevered pipe outlets—explains what the writers observed during the second group of tests:

> Experimental observations show that the side slopes of the scour hole . . . are approximately equal to the natural angle of repose of the bed material. This indicates that the scour mechanism is in the immediate vicinity of the [point where the plunging jet impinges on the sand bed], and that the sediment slides in toward the base before it is removed. . . . visual observation of the scour process . . . shows that a dynamic equilibrium exists between the scour hole and . . . streamflow which is not apparent when the flow is stopped; the flow field near the [point of jet impingement on the bed] is strong enough to support the sides of the scour hole at angles greater than the angle of repose of the sediment. The wall periodically collapses and dumps sediment into the hole . . . as the fluid forces supporting it become unstable. The maximum scour depth under such unstable conditions cannot be measured . . . after stopping the flow.

The authors also describe and picture this action on p. 1840.

Like Jain and Fischer, the writers were interested in determining the maximum extent of the scour by the jet. Two methods were used to accomplish this objective.

The first method used the data obtained from the second group of tests. The logarithm of dimensionless rate of scour (dimensionless scour depth divided by dimensionless time) was plotted against the logarithm of dimensionless time. A rectangular hyperbola was fitted to the data as described in Ref. 14. The ultimate scour depth was computed from the asymptote of the hyperbola.

The second method required a third group of tests to provide data to determine the maximum depth of scour. In these tests the maximum scour depth was determined by actual measurement as described in the following. But first, a description of the scour at the end of the time-dependent tests is in order.

At the conclusion of the time-dependent scour tests, sediment was still suspended by the jet turbulence. This is shown in the authors' Fig. 9. Just upstream of the authors' pier there is a relatively wide dark line indicating movement of bottom material toward the periphery of the scour hole. The dark line curves upward and toward the pier and there is a cap of suspended material directed toward the upstream angle-of-repose slope of the scour hole. This plume of suspended material is typical of conditions at the end of the writers' time-dependent cantilevered outlet scour tests, which usually were terminated at an elapsed time of 10,000 min—seven days. Energy from the jet supported this suspended material—energy that otherwise would be available to further scour the bed.

For the writers' third group of tests, the "dredge" suction was extended

into the plume of material suspended within the hole. Removal of the suspended material made available the energy previously used to suspend material to further scour the bed. The sides became unstable and sluffed into the base of the hole where the sediment was suspended and "dredged" out. This process greatly increased all scour hole dimensions. Turbulent bursts continued to move material around intermittently at the base of the scour hole even at the termination of the third group of tests, but the side slopes extended along a smooth line to the bottom of the hole; the steep face at the base of the slope in the authors' Fig. 9 no longer existed.

Cantilevered outlet scour hole data are still being obtained and analyzed at this writing. Presentation of quantitative data at this time is not appropriate. This discussion is written to emphasize the similarity between the writers' qualitative observations and those of the authors. These two experiences show that, to insure the safety of structures subjected to scour, the scour tests must be thorough.

Appendix.—Reference

14. Blaisdell, F. W., Anderson, C. L., and Hebaus, G. G., "Ultimate Dimensions of Local Scour," *Journal of the Hydraulics Division*, ASCE, Vol. 107, No. HY3, Proc. Paper 16144, Mar., 1981, pp. 327–337.

Technical Papers

Original papers should be submitted in triplicate to the Manager of Technical and Professional Publications, ASCE, 345 East 47th Street, New York, N.Y. 10017. Authors must indicate the Technical Division or Council, Technical Committee, Subcommittee, and Task Committee (if any) to which the paper should be referred. Those who are planning to submit material will expedite the review and publication procedures by complying with the following basic requirements:

1. Titles must have a length not exceeding 50 characters and spaces.

2. The manuscript (an original ribbon copy and two duplicate copies) should be double-spaced on one side of 8-1/2-in. (220-mm) by 11-in. (280-mm) paper. Three copies of all figures and tables must be included.

3. Generally, the maximum length of a paper is 10,000 word-equivalents. As an *approximation*, each full manuscript page of text, tables or figures is the equivalent of 300 words. If a particular subject cannot be adequately presented within the 10,000-word limit, the paper should be accompanied by a rationale for the overlength. This will permit rapid review and approval by the Division or Council Publications and Executive Committees and the Society's Committee on Publications. Valuable contributions to the Society's publications are not intended to be discouraged by this procedure.

4. The author's full name, Society membership grade, and a footnote stating present employment must appear on the first page of the paper. Authors need not be Society members.

5. All mathematics must be typewritten and special symbols must be identified properly. The letter symbols used should be defined where they first appear, in figures, tables, or text, and arranged alphabetically in an appendix at the end of the paper titled Appendix.—Notation.

6. Standard definitions and symbols should be used. Reference should be made to the lists published by the American National Standards Institute and to the *Authors' Guide to the Publications of ASCE*.

7. Figures should be drawn in black ink, at a size that, with a 50% reduction, would have a published width in the *Journals* of from 3 in. (76 mm) to 4-1/2 in. (110 mm). The lettering must be legible at the reduced size. Photographs should be submitted as glossy prints. Explanations and descriptions must be placed in text rather than within the figure.

8. Tables should be typed (an original ribbon copy and two duplicates) on one side of 8-1/2-in. (220-mm) by 11-in. (280-mm) paper. An explanation of each table must appear in the text.

9. References cited in text should be arranged in alphabetical order in an appendix at the end of the paper, or preceding the Appendix.—Notation, as an Appendix.—References.

10. A list of key words and an information retrieval abstract of 175 words should be provided with each paper.

11. A summary of approximately 40 words must accompany the paper.

12. A set of conclusions must end the paper.

13. Dual units, i.e., U.S. Customary followed by SI (International System) units in parentheses, should be used throughout the paper.

14. A practical applications section should be included also, if appropriate.